SHEAR, FLEXURE AND AXIAL TENSION IN REINFORCED CONCRETE MEMBERS

A thesis presented for the
degree of Doctor of Philosophy
in Civil Engineering
in the University of Canterbury,
Christchurch, New Zealand.

by

A. J. O'Leary

1970

ENGINEERING
DEPT'L LIBR.
THESIS
TA
683.5
.B3
.045
copy 2

ABSTRACT

In this project the strength and behaviour of reinforced concrete beams subjected to flexure, shear and axial tension are examined. This combination of actions may be induced by lateral loading in the external column of a multibay frame or in the lower columns of a coupled shear wall. Although the flexural behaviour of such members is well understood little is known about their deformation characteristics and resistance to shear.

Ten beams subjected to eccentric axial tension have been tested. The load was so applied that the axial force to shear force ratio remained approximately constant throughout each test. The major variables examined have been content of web reinforcement and variation in axial load to shear force ratio.

A theoretical method of determining the deformations of flexurally and diagonally cracked beams subjected to axial tension is developed. It is shown that allowance for stirrup anchorage slip must be incorporated in such a theory if it is to predict beam behaviour successfully.

To enable the contribution of dowel action to be evaluated in the test beams concrete cantilever dowel test specimens have been tested, and also dowel shear tests on yielded reinforcement bars, are reported. In this way the dowel shear resistance throughout the loading of the test beams is examined.

It has been found that current code recommendations for the shear resisted by stirrups in members subjected to axial tension are conservative. Diagonal cracks form in similar patterns to those in normal flexural members, and the critical separation diagonal crack forms at an angle of less than 45° to the axis. The presence of diagonal cracks reduces the stiffness of the members in the elastic range of loading. The members are ductile if adequate shear reinforcement is present.

ACKNOWLEDGEMENTS

To Dr. T. Paulay I wish to extend my grateful thanks. Without his continual help, guidance and encouragement the completion of this project would not have been possible. For aiding me in the absence of Dr. Paulay my thanks to Mr F.P.S. Lu.

I acknowledge with gratitude the overall supervision by the Head of the Civil Engineering Department, Professor H. J. Hopkins.

My thanks for the technical assistance and advice given to me by the technical officer, Mr H. T. Watson, and the technical staff who helped me with the experimental work in this project. In particular I would like to sincerely thank Mr K. L. Marrion who built both of the test frames and prepared all the test specimens. To him and Messrs J. N. Byers, H. Crowther, P. Robinson, and N. W. Prebble I wish to extend my thanks for helping with the arduous and exacting task of testing the beams.

I wish to thank my parents for their encouragement and understanding during this project.

Finally my deep gratitude to my wife, Marie, who not only typed this manuscript, but who has also been so forebearing.

TABLE OF CONTENTS

Page

Page

LIST OF SYMBOLS

A_{ev} area of equivalent stirrup in the analogous truss.

A_g the gross area of a section, bt.

A_s area of tension reinforcement, area of steel.

A'_s area of compression reinforcement.

A_{tr} transformed area of concrete.

A_v area of one stirrup.

a shear span, i.e., distance from the point of application of the load to the nearest support point in a simply supported beam, or depth of Whitney equivalent rectangular stress block.

a_1 distance from support point to where a diagonal crack crosses the tension reinforcement (see fig. 2.2).

B_f bond force.

b width of a rectangular beam, web width of a T beam.

b_n the effective width of concrete resisting the tensile stress in the concrete at the level of the reinforcement in a beam.

C compression force in the compression zone of a beam.

C' compression force carried by the concrete in the compression zone of a beam.

C" compression force carried by the compression reinforcement.

c ratio of the depth of the equivalent rectangular stress block to the depth of the intact concrete in the compression zone.

c_o depth of concrete cover measured from the underside of the bottom reinforcement.

D' diameter of compression reinforcement.

D_d dowel diameter.

D_f dowel shear at dowel cracking.

D_k kinking force.

d effective depth of a beam, i.e., depth from the extreme compression fibre to the centroid of the tension reinforcement.

d' depth of compression reinforcement from extreme compression fibre of the concrete.

d_1 a distance defined in fig. 4.1.

d_i distance apart of compression reinforcement and inner layer of tension reinforcement.

d_o distance apart of compression reinforcement and outer layer of tension reinforcement.

E_c 50% secant modulus of concrete.

E_s Young's modulus of steel, also of tension reinforcement.

E'_s Young's modulus of compression reinforcement.

e distance between point of application of dowel shear and the face of the joint.

e' eccentricity of axial tension measured from the centroid of the tension reinforcement.

f_b bearing strength of concrete.

f'_c compressive cylinder strength of the concrete.

f_{cu} concrete cube strength.

f_s steel stress, stress in tension reinforcement.

f'_s stress in compression reinforcement.

f_{sp} splitting tensile strength of concrete.

f_t modulus of rupture of concrete, tensile strength of concrete.

f_u ultimate stress of steel.

f_y yield stress of steel, yield stress of tension reinforcement.

f'_y yield stress of compression reinforcement.

h depth of concrete under a dowel or the minimum distance from the centroid of a dowel to the nearest concrete face.

I_{cr} second moment of area of the cracked transformed section at the maximum moment section.

I_d second moment of area of the composite section made up of a dowel and the concrete cover to the dowel.

I_{eff} effective second moment of area.

J_v transformed second moment of area of the dowel and concrete cover below it (see fig. 2.5).

j ratio of the internal lever arm to the effective depth of a beam.

k, k' ratio of depth of neutral axis to effective depth of a beam.

k_s a constant given in table 8.1

l embedded or effective length of a dowel, or $\sqrt{l_1^2 + d^2}$ in the analysis of the analogous truss.

l_1 length of beam along which the cracks radiating from the critical compression reentry corner cross the tension reinforcement.

l_2 length of beam along which parallel diagonal cracks cross the tension reinforcement.

l_c projected length along the longitudinal axis of a beam of the tapered strut in the analogous truss, or a length used in the definition of equivalent curvature.

l'_c projected length along the longitudinal axis of a beam of all the parallel sided concrete struts in one path through the analogous truss.

l_d length of a tapered concrete strut in the analogous truss.

l'_d length of a parallel sided concrete strut in the analogous truss.

l_k kinked length of a reinforcement bar.

l_t length used in the definition of equivalent curvature.

l_x distance along a tapered concrete strut in the analogous truss.

l_z depth of equivalent stress block in determining dowel bearing stress (see fig. 2.4).

M applied moment.

M_1 a factor used in Eq. (8.19).

M_{max} maximum moment in a beam under working load.

M_{ud} ultimate flexural capacity of a dowel beam.

N applied axial tension.

N_u applied ultimate axial tension.

N^*_u axial tension at conventional Whitney[49] ultimate flexural capacity.

N^{**}_u axial tension at modified theoretical ultimate flexural capacity.

N_y applied axial tension at yield of the tension reinforcement.

N^*_y theoretical axial tension at yield of the tension reinforcement.

n the ratio of Young's modulus of tension reinforcement to the Young's modulus of concrete.

n' ratio of the Young's modulus of compression reinforcement to the Young's modulus of concrete.

n_u nominal axial stress at ultimate load, N_u/bt.

P, P' applied load.

P_k load applied to the kinking apparatus in the kink tests.

P_u^* load at conventional Whitney[49] ultimate flexural capacity.

p ratio of the area of tension reinforcement to the effective area of concrete, A_s/bd.

p' ratio of area of compression reinforcement to the effective area of concrete, A_s'/bd.

p_s stirrup force per unit length along the axis of a beam.

p_v ratio of stirrup area to web area of concrete, A_v/bs.

R, R_1, R_2, R_3 reactions.

s stirrup spacing.

s' crack spacing at the level of the tension reinforcement.

s_c effective crack length.

s_d depth of a dowel test specimen.

s_e length of an elemental cross section of a beam.

T, T_1, T_2 forces in the tension reinforcement.

T_w tension force in one stirrup.

T_x tension reinforcement force at a distance x from the critical flexural section.

T_y yield force in a reinforcement bar or a stirrup.

t total beam depth.

V applied shear.

V_{cs} shear resisted by compression zone concrete.

V_{cz} dowel shear of compression reinforcement.

V_d dowel shear force across tension reinforcement.

V_{dc} applied shear at diagonal cracking.

V_{do} dowel shear resistance of the compression reinforcement.

V_{du} ultimate dowel shear.

V_{dx} dowel shear force in the tension reinforcement at a distance x from the critical flexural section.

V_s shear carried by stirrups across a diagonal crack.

V_{sc} shear in one path through the analogous truss.

v_{ai} shear stress resulting from aggregate interlock.

v_c nominal shear stress carried by the concrete in a beam.

v_{dc} nominal shear stress at diagonal cracking.

v_{flex} nominal shear stress at initial flexural cracking.

v_{inc} increment of nominal shear stress between flexural and diagonal cracking.

v_u nominal shear stress at ultimate load.

v_y nominal shear stress at yield of the tension reinforcement.

w_a a factor defined in Eq. (6.7).

w_h a factor defined in Eq. (6.6).

x distance along the shear span from the support, or from the point of maximum moment in chapter 8, or as shown in fig. 2.6.

x_c length of compression zone which has yielded.

x_t length of tension reinforcement which has yielded.

y distance between where a crack crosses the tension reinforcement and the nearest stirrup on the low moment side of the crack, or depth of intact compression zone in a beam.

z the internal lever arm in a beam.

α angle through which a bar is kinked.

γ a factor used in Eq. (2.12).

Δ deflection.

Δ_c, Δ_s, Δ'_c components of shear deflection of the analogous truss.

Δ_{flex} flexural deflection.

Δ_l, Δ_t rigid body translations.

Δx crack spacing.

δ deflection.

δ_c shortening of a tapered concrete strut in the analogous truss.

δ'_c shortening of a parallel sided concrete strut in the analogous truss.

δT increase of tension in the tension reinforcement across a concrete cantilever.

ε_c concrete strain at the compression face of a beam.

ε_{cu} ultimate unconfined compression strain in concrete.

ε_s steel strain.

ε'_s strain in compression reinforcement.

ε_{sh} strain hardening strain of steel.

ε_{si} strain in inner layer of tension reinforcement.

ε_{so} strain in outer layer of tension reinforcement.

ε_{su} ultimate steel strain.

ε_y yield strain of steel, also of tension reinforcement.

η_d ratio of maximum dowel shear to total applied shear.

η_s ratio of shear taken by the stirrups across the critical separation diagonal crack to the total applied shear.

θ rotation.

θ_e elastic rotation.

θ_p plastic rotation.

θ_u rotation at ultimate load.

θ_y rotation at yield of the tension reinforcement.

φ curvature.

φ_e equivalent curvature.

φ_i curvature calculated from inner layer of tension reinforcement strains.

φ_o curvature calculated from outer layer of tension reinforcement strains.

φ_u equivalent curvature at ultimate load.

φ_y equivalent curvature at yield of the tension reinforcement.

ψ_r rigid body rotation.

REFERENCES

1 Acharya, D. N. and Kemp, K. O., "Significance of Dowel Forces on the Shear Failure of Rectangular Reinforced Concrete Beams Without Web Reinforcement," ACI Journal, Proceedings V. 62, No. 10, Oct. 1965, pp. 1265-1279.

2 ACI-ASCE Committee 326, "Shear and Diagonal Tension," - 3 parts. ACI Journal, Proceedings V. 59, Nos 1, 2, and 3, Jan.-Mar. 1962, pp. 1-30, 277-333, 353-395.

3 ACI Bibliography No. 4, "Shear, Diagonal Tension, and Torsion," 1964.

4 ACI Committee 435, "Deflection of Reinforced Concrete Flexural Members," ACI Journal, Proceedings V. 63, No. 6, June 1966, pp. 637-674.

5 "ACI Standard Building Code Requirements for Reinforced Concrete," (ACI 318-63).

6 Anderson, B. G., "Rigid Frame Failures," ACI Journal, Proceedings V. 53, No. 7, Jan. 1957, pp. 625-636.

7 "Aus Unseren Forschungsarbeiten," Bericht Nr. 80, Materialprufungsamt fur das Bauwesen der Technischen Hochschule Munchen, 1968.

8 Baldwin Jr., J. W., and Viest, I. M., "Effect of Axial Compression on Shear Strength of Reinforced Concrete Frame Members," ACI Journal, Proceedings V. 55, No. 5, Nov. 1958, pp. 635-654.

9 Baron, M. J., "Shear Strength of Reinforced Concrete Beams at Points of Bar Cutoff," ACI Journal, Proceedings V. 63, No. 1, Jan. 1966, pp. 127-134.

10 Baron, M. J., and Siess, C. P., "Effect of Axial Load on the Shear Strength of Reinforced Concrete Beams," Structural Research Series No. 121, Civil Engineering Studies, University of Illinois, June 1956.

11 Base, G. D., "Further Notes on the Demec - a Demountable Mechanical Strain Gauge for Concrete Structures," Magazine of Concrete Research (London), V.7, No. 19, Mar. 1955, pp. 35-38.

12 Baumann, T., "Versuche zum Studium der Verdubelungswirkung der Biegezugbewehrung eines Stahlbetonbalken," Bericht Nr. 77, Materialprufungsamt fur das Bauwesen der Technischen Hochschule Munchen, 1968.

13 "Bestimmungen des Deutschen Ausschusses fur Stahlbeton; A. Bestimmungen fur Ausfuhrung von Bauwerken aus Stahlbeton," DIN 1045, 1960.

14 Blume, J. A., Newmark, N.M., and Corning, L. H., "Design of Multistory Reinforced Concrete Buildings for Earthquake Motions," P.C.A. 1961.

15 Bresler, B., and MacGregor, J. G., "Review of Concrete Beams Failing in Shear," Proceedings, ASCE, V. 93, ST1, Feb. 1967, pp. 343-372.

16 Diaz de Cossio, R., and Siess, C. P., "Behaviour and Strength in Shear of Beams and Frames Without Web Reinforcement," ACI Journal, Proceedings V. 56, No. 8, Feb. 1960, pp. 695-735.

17 Elstener, R. C., and Hognestad, E., "Laboratory Investigation of Rigid Frame Failures," ACI Journal, Proceedings V. 53, No. 7, Jan. 1957, pp. 637-668.

18 Fenwick, R. C., "The Shear Strength of Reinforced Concrete Beams," Ph.D. Thesis, University of Canterbury, Christchurch, New Zealand, 1966.

19 Fenwick, R. C., and Paulay, T., "Mechanisms of Shear Resistance of Concrete Beams," Proceedings, ASCE, V. 94, ST10, Oct. 1968, pp. 2325-2350.

20 Ferguson, P. M., "Some Implications of Recent Diagonal Tension Tests," ACI Journal, Proceedings V. 53, No. 2, Aug. 1956, pp. 157-172.

21 Friberg, B., "Design of Dowels in Transverse Joints of Concrete Pavements," Transactions, ASCE, V. 105, 1940, pp. 1076-1095.

22 Grinter, L., "Design of the Reinforced Concrete Road Slab," Bulletin No. 39, Texas Engrg. Experiment Station, College Station, Texas, 1931, pp. 53-59.

23 Hognestad, E., "What Do We Know About Diagonal Tension and Web Reinforcement in Concrete?" Circular Series No. 64, University of Illinois Engineering Experiment Station, 1952.

24 Jones, R., "The Ultimate Strength of Reinforced Concrete Beams in Shear," Magazine of Concrete Research (London), V.8, No. 23, Aug. 1956, pp. 69-84.

25 Kani, G.N.J., "How Safe are Our Large Reinforced Concrete Beams?" ACI Journal, Proceedings V. 64, No. 3, Mar. 1967, pp. 128-141.

26 Kani, G.N.J., "A Rational Theory for the Function of Web Reinforcement," ACI Journal, Proceedings V. 66, No. 3, Mar. 1969, pp. 185-197.

27 Kani, G.N.J., "The Riddle of Shear Failure and Its Solution," ACI Journal, Proceedings V. 61, No. 4, Apr. 1964, pp. 441-467.

28 Kani, G.N.J., "Was Wissen Wir Heute Über Die Schubbruchsicherheit?" Der Bauingenieur, V. 43, No. 5, May 1968, pp. 167-174.

29 Kent, D. C., "Inelastic Behaviour of Reinforced Concrete Members With Cyclic Loading," Ph.D. Thesis, University of Canterbury, Christchurch, New Zealand, 1969.

30 Kinnunen, S., "Punching of Concrete Slabs with Two-Way Reinforcement - With Special Reference to Dowel Effect and Deviation of Reinforcement from Polar Symmetry," Transactions of the Royal Institute of Technology, Stockholm, Sweden, No. 198, 1963.

31 Krefeld, W. J., and Thurston, C. W., "Contribution of Longitudinal Steel to Shear Resistance of Reinforced Concrete Beams," ACI Journal, Proceedings V. 63, No. 3, Mar. 1966, pp. 325-344.

32 Leonhardt, F., and Walther, R., "The Stuttgart Shear Tests 1961," Translation No. 111, Cement and Concrete Assn., London, England.

33 Lorentsen, M., "Theory for the Combined Action of Bending Moment and Shear in Reinforced and Prestressed Concrete Beams," ACI Journal, Proceedings V. 62, No. 4, Apr. 1965, pp. 403-420.

34 Marcus, H., "Load Carrying Capacity of Dowels at Transverse Pavement Joints," ACI Journal, Proceedings, V. 48, No. 2, Oct. 1951, pp. 169-184.

35 Mattock, A. H., "Diagonal Tension Cracking in Concrete Beams With Axial Forces," Proceedings, ASCE, V. 95, ST9, Sept. 1969, pp. 1887-1900.

36 Mayer, H., "Versuche zum Studium Von Grosse und Verteilung der Bugelkrafte im Stahlbeton-Rechteckbalken," Bericht Nr. 72, Material-frufungsamt fur das Bauwesen der Technischen Hochschule Munchen, 1967.

37 MacGregor, J. G., and Hanson, J. M., "Proposed Changes in Shear Provisions for Reinforced and Prestressed Concrete Beams," ACI Journal, Proceedings, V. 66, No. 4, April 1969, pp. 276-288.

38 Moore, W. P., "An Analytical Study of the Effect of Web Reinforcement on the Strength of Reinforced Concrete Beams Subjected to Combined Flexure and Shear," Ph.D. Thesis, University of Illinios, 1964.

39 Morice, P. B., "The Design and Use of a Demountable Mechanical Gauge for Concrete Structures," Magazine of Concrete Research (London), V. 5, No. 13, Aug. 1953, pp. 37-42.

40 "National Building Code of Canada (1965)," National Research Council, Ottawa, 1965.

41 Park, R., and Paulay, T., "Ultimate Strength Design of Reinforced Concrete Structures," For a Seminar Arranged by Departments of Civil Engineering and Extension Studies, University of Canterbury, Christchurch, New Zealand, 1969.

42 Paulay, T., "The Coupling of Shear Walls," Ph.D. Thesis, University of Canterbury, Christchurch, New Zealand, 1969.

43 Rajagopalan, K. S., and Ferguson, P. M., "Exploratory Shear Tests Exphasizing Percentage of Longitudinal Steel," ACI Journal, Proceedings, V. 65, No. 8, Aug. 1968, pp. 634-638.

44 Regan, P. E., "Shear Tests of Reinforced Concrete Beams," Interim Report, CRIRIA Project No. 91, Aug. 1969.

45 Ritter, W., "Die Bauweise Hennebique," Schweizerische Bauzeitung (Zurich), V. 33, No. 7, Feb. 1899, pp. 59-61.

46 Taylor, R., "A New Method of Proportioning Stirrups in Reinforced Concrete Beams," Magazines of Concrete Research (London), V.15, No. 45, Nov. 1963, pp. 177-181.

47 Taylor, R., "Some Shear Tests on Reinforced Concrete Beams Without Shear Reinforcement," Magazine of Concrete Research (London), V.12, No. 36, Nov. 1960, pp.145-154.

48 Watstein, D., and Mathey, R. G., "Strains in Beams Having Diagonal Cracks," ACI Journal, Proceedings, V. 55, No. 6, Dec. 1958, pp. 717-728.

49 Whitney, C. S., "Plastic Theory of Reinforced Concrete Design," Proceedings ASCE, V. 66, No. 10, Dec. 1940, pp. 1749-1780.

50 Yu, Wei-Wen, and Winter, G., "Instantaneous and Long-Time Deflection of Reinforced Concrete Beams Under Working Loads," ACI Journal, Proceedings, V. 57, No. 1, July 1960, pp. 29-50.

51 Zsutty, T. C., "Beam Shear Strength Prediction by Analysis of Existing Data," ACI Journal, Proceedings V. 65, No. 11, Nov. 1968, pp. 943-951.

THE LIBRARY
UNIVERSITY OF CANTERBURY
CHRISTCHURCH, N.Z.

CHAPTER 1

INTRODUCTION, HISTORICAL REVIEW AND SCOPE OF THE PROJECT

1.1 Introduction

The flexural behaviour of reinforced concrete beams is now well understood but there is still considerable lack of knowledge of their mechanism of shear resistance. More than 500 papers dealing with various aspects of the problem have been published since the beginning of the century but inspite of this it has still not been satisfactorily solved.

Two additional actions superimposed on flexure and shear in concrete beams add to the problem. These are the presence of axial load and torsion. Combinations of biaxial bending, applied shear in two planes, and the actions mentioned above make understanding of the behaviour of reinforced concrete members a very complex problem. Until this desirable state of knowledge is reached each addition to the already large fund of analytical and experimental research findings is of value.

At present the design of reinforced concrete members against failure in shear or torsion is based on semi-empirical or entirely empirical equations relating

nominal shear stress to various physical properties of the member. The nominal shear stress itself is a grossly idealised concept which bears little relationship to the actual shear stress across a section. There have been a number of attempts to make these design recommendations more rational but so far none have been proved entirely successful.

In the case of the resistance of concrete beams to an applied shear force, the understanding of the internal mechanisms of resistance has developed to the stage where reliable design recommendations do exist. However, relatively little research into the effect of axial loads on the shear strength of flexural members has been done. It is known that axial compression increases, and axial tension decreases shear strength, but it is not known to what extent.

This project was undertaken to contribute towards a better understanding of the effect of axial tension on the shear strength of reinforced concrete flexural members. It is one phase of a research programme initiated in the Civil Engineering Department of the University of Canterbury to study the behaviour of coupled shear walls. The first of these projects studied the coupling beams [42].

Shear and eccentric axial tension can occur in the vertical members of a coupled shear wall or in the

external column of a multibay frame subjected to lateral forces resulting from seismic or wind loading. If the lateral force is large, as it can be under seismic loading, the axial tension can be considerably larger than the shear force.

1.2 Historical Review

It is not intended to give a full historical review of the literature published on reinforced concrete beams subjected to shear in this thesis. Fenwick [18] amongst others has summarised the major contributions to the understanding of the mechanism of shear resistance from Ritter [45] in 1899 to Kani [27] in 1964. The development of the ACI Code 318-63 [5] and the German Concrete Code DIN 1045 [13] recommendations for shear design up to 1952 have been reviewed by Hognestad [23]. In 1964 the American Concrete Institute published a bibliography entitled "Shear, Diagonal Tension, and Torsion" [3]. It includes nearly 500 references and summaries of papers published between 1897 and 1961. Bresler and MacGregor [15] have reviewed the work done on shear resistance up to 1967. The paper discusses some of the basic problems such as dowel action and diagonal and flexural crack shapes. Only brief mention is made of aggregate interlock but its importance is not discarded.

1.2.1 Shear Strength of Beams Subjected to Axial Tension

Few papers have been written on the effect of axial tension on the shear strength of reinforced concrete beams. In 1955 portions of some U.S. Air Force rigid frame warehouses collapsed because of shear failures. The general nature of the distress was described by Anderson [6]. He found that the nominal shear stress in the warehouse members at the time of failure, as computed by usual design methods, was well below the shear capacity anticipated by then existing codes. The distress took the form of diagonal cracks at, or near, points of contraflexure. Most of these cracks made an angle of greater than 45^{o} with the longitudinal axis of the member.

Elstner and Hognestad [17] carried out a laboratory investigation of the rigid frame failures. They reported tests of 13 beams, six of which were loaded to failure in combined flexure, shear and axial tension. The beams were loaded in flexure and then loaded in axial tension with the flexural load held constant. Failure of four of the beams was of either the separation or diagonal tension type. The failure crack was inclined at an angle steeper than 45^{o} to the longitudinal axis, and it occurred at the point of contraflexure.

The conclusion drawn from these tests was the inadequacy of the web reinforcement design assumption that the diagonal cracks formed at 45° to the longitudinal axis of the member. A diagonal crack steeper than 45° would need to be crossed by sufficient stirrups to provide full protection against shear failure.

Only two other investigations into the effect of axial tension on the shear strength of reinforced concrete members have been made to the knowledge of the author. Mattock [35] in 1965 tested 40 beams, 14 of which were subjected to axial tension as well as shear. These beams were loaded in axial tension and while this load was held constant the beams were transversly loaded to failure. He found that the nominal shear stress at diagonal cracking of reinforced concrete beams with or without axial load of either sign can be determined by adding to the shear stress at the onset of flexural cracking a positive increment of shear stress given by

$$v_{inc} = \sqrt{f'_c}(1.25 + 5.0\ np) \qquad (1.1)$$

where f'_c = compressive cylinder strength of the concrete

n = the modular ratio

and p = the percentage of longitudinal tension reinforcement.

The effect of the magnitude and sign of the axial load is allowed for in the development of flexural cracks.

It has been found by Regan [44] in tests conducted in 1969 that the shear strength of reinforced beams without web reinforcement is not substantially reduced when axial tension is applied provided that the longitudinal reinforcement is sufficient to prevent a purely tensile failure, i.e., a tension crack across the whole section. This research project also includes an evaluation of dowel action in beams both with and without web reinforcement.

1.2.2 New Advances in the Understanding of Shear Resistance

Since 1964 there have been several notable advances in the understanding of the mechanisms of shear resistance in reinforced members both with and without web reinforcement. Some of those which have been of particular help to the author, or which have revealed some new facet of the problem, will now be briefly discussed.

An analytical approach has been followed by Moore [38]. Using strain energy principles applied to an idealised model of rigid bodies and flexible linkages he has studied the role of web reinforcement in the resistance of beams to combined flexure and shear. Only shear-

compression failures were considered in this study, i.e., the criterion of failure was limiting strain conditions in the compression zone of the beam model. 18 problems for beams without stirrups and 450 problems for beams with stirrups were solved. The 450 beams were divided into five groups of 90 beams each. The only difference in the beams contained in the five groups was the inclination of the stirrups. Many of the conclusions drawn from the analytical study merely reconfirmed conclusions from numerous beam tests. The most notable result was the effect of inclination of the stirrups in the model. It was found that the efficiency of the stirrups increased slightly as the inclination of the stirrups was changed from 90^{o} to 75^{o} or 60^{o}. However, there was a definite loss of efficiency when the angle was lowered to 45^{o} and a large loss at a value of 30^{o}.

Fenwick [18] has documented the results of numerous small scale tests on dowel and aggregate interlock action as well as eight beam tests. He has shown that the concrete cantilevers formed by the blocks of concrete between adjacent cracks in the shear span have a moment acting on them as a result of the change of tension force in the tension reinforcement. This is the bond force on the tension steel. The bond force moment acting on the concrete cantilevers is resisted in the

following approximate proportions in beams without web reinforcement:

(i) 20% by the flexural resistance of the concrete,

(ii) 60% or more by aggregate interlock action, and,

(iii) 20% or less by dowel action of the longitudinal reinforcement.

A full account of beam action and arch action as mechanisms of shear resistance in reinforced concrete beams is given. Fenwick discusses the incompatibility of beam action and arch action working together to resist the applied shear force after diagonal tension cracking. Arch action is shown to develop appreciably only after beam action has broken down. If the shear resistance afforded by the arch is then less than that of beam action before beam action is lost, the beam fails when beam action breaks down.

The effect of cutting off flexural reinforcement was illustrated by Baron [9] in 1966. It was found that critical diagonal tensile stresses develop at cut off points and hence shear strength decreases with increased proportion of cut off bars. In the region of bar cut off it is necessary to provide additional web reinforcement to ensure adequate protection against shear failure.

In 1967 Kani [25] published some results of beam tests to show that there is an absolute scale effect for

beams failing in shear. Large beams are relatively weaker than smaller ones. This is attributed to the crack factor $\Delta x/s_c$, which is the ratio of crack spacing to effective crack length. In a subsequent paper [28] he presented the following conclusions from shear tests he has performed on 700 beams;

(i) concrete strength has negligible influence,

(ii) flexural steel percentage is of major importance; an increase from p = 0.5 to 2.8% results in 100% increase of shear strength,

(iii) strength decreases with increased height of a beam, i.e., depth increase from 6 to 48 inches results in 40% loss of relative strength,

(iv) the shear span to depth ratio is important. With a/d = 1 a strength increase of 1300% was obtained compared to a/d = 2.5.
where a = shear span,
and d = effective depth of a beam.

(v) width of beam has no influence,

(vi) the shear strength of "T" beams is not proportional to the web thickness but is somewhat more favourable. (In a T beam with the ratio of web to flange width of $\frac{1}{3}$, he found that the shear strength was $\frac{1}{2}$ of the shear strength of an equivalent rectangular beam of

width equal to the flange width of the T beam), and

(vii) there is no direct relationship between shear strength and nominal shear stress.

In 1969 a paper was published in which Kani[26] proposed a so called rational theory for the function of web reinforcement. He developed the principle of internal arches and contended that the function of web reinforcement is to provide springings for this system of internal arches. He tried to show that stirrups closer to load and support points than a distance d, provide no additional shear resistance in a beam. This ignores the possibility that the supports and load may be through secondary beams and not idealised laboratory loading plates. Both Ferguson [20] and Taylor [47] have shown that arch action cannot develop if there is no suitable springing for the arch. This paper by Kani is a somewhat different approach to the traditional truss analogy for the action of web reinforcement.

Rajagopalan and Ferguson [43] have shown that present ACI Code [5] recommendations for the shear carried by the concrete in reinforced beams are not conservative for low percentages of longitudinal reinforcement, i.e., p less than approximately 1%. This finding agrees with conclusion (ii) of Kani above.

Dimensional analysis was used by Zsutty [51] in 1968 to derive an equation to predict the diagonal cracking load of beams with shear span to depth ratios greater than 2.5. He found the nominal shear stress at diagonal cracking from the relationship;

$$v_{dc} = 59(f'_c pd/a)^{\frac{1}{3}} \qquad (1.2)$$

The constant, 59, is based on observations on 151 beam tests reported in the literature.

MacGregor and Hanson [37] have reviewed the shear recommendations of the revised (1970) ACI Building Code. The provisions for reinforced concrete beams without axial load have not been changed from the ACI 318-63 Code[5]. However, the shear allowed to be carried by the concrete in beams subjected to significant axial tension is given by

$$v_c = 2(1+0.002N/A_g)\sqrt{f'_c} \qquad (1.3)$$

where N = the axial load, negative for tension

and A_g = the gross area of the section.

This is now identical to the National Building Code of Canada[40] equation (62).

A separate historical review of work done in connection with dowel action is given in chapter 2 of this thesis.

1.3 The Nature of the Mechanism of Shear Resistance in Reinforced Concrete Beams

The mechanism of shear resistance in reinforced concrete beams as it is understood at the present time is described by Fenwick [18], Kani [26, 27], and Bresler and MacGregor[15]. It is not intended to present a full review of this but rather to briefly summarise the fundamental actions associated with the shear strength of beams.

The basic relationship between the external moment M, and the tension reinforcement force T, in the shear span of a reinforced beam is,

$$M = Tz$$

where z = the internal lever arm.

Differentiating this equation with respect to x, the distance along the shear span from the support, gives:

$$\frac{dM}{dx} = V = T\frac{dz}{dx} + z\frac{dT}{dx} \qquad (1.4)$$

1.3.1 Beam Action

If z is constant in Eq. (1.4) the shear is given by

$$V = z\frac{dT}{dx} \qquad (1.5)$$

This equation describes beam action, i.e., the shear is resisted by the change in the tension reinforcement force along the shear span. This change in force is provided by bond forces between the steel and the concrete.

Consider the cracked reinforced concrete beam without web reinforcement shown in fig. 1.1. The free body in part (b) of the figure is the typical block of concrete between two adjacent cracks as shown shaded in part (a). This block of concrete will be referred to as a concrete cantilever. The reinforcement forces T_1 and T_2 give rise to a bond force $B_f = T_2 - T_1$. This produces a moment in the cantilever. The moment is resisted by three sets of forces:

(i) the shears V_d, across the tension reinforcement,

(ii) the forces v_{ai}, which are due to the interlocking of aggregate particles across the crack, and

(iii) the flexural resistance M, of the concrete at the fixed end of the cantilever.

The shear forces V_d, across the tension reinforcement are the forces associated with dowel action. For these shears to develop there must be displacement across the crack at the level of the longitudinal reinforcement.

The aggregate interlock shears v_{ai}, can also develop only if there is displacement across the crack. Aggregate interlock depends on the width of the crack across which it acts, and also on the aggregate properties of the concrete.

The flexural resistance of the concrete at the fixed end of the cantilever is predominantly dependent on the

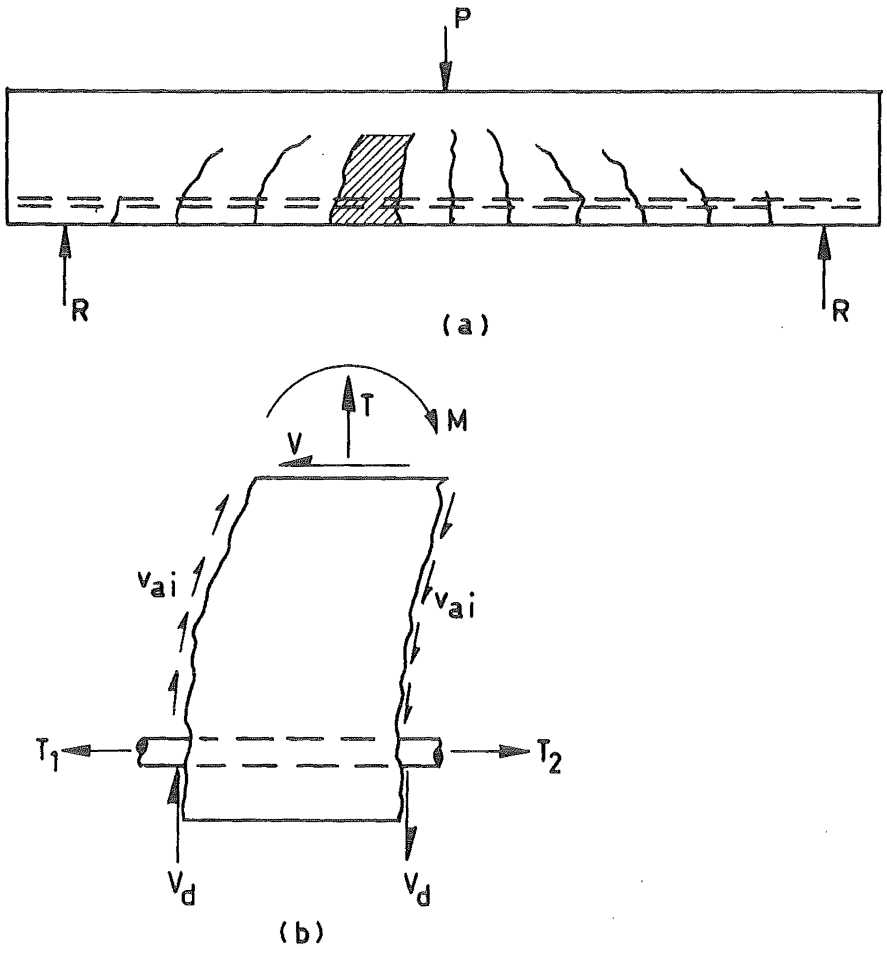

Fig. 1.1 Concrete Cantilever Action

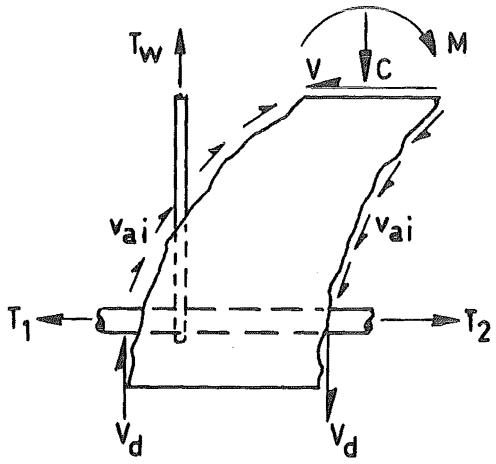

Fig. 1.2 Function of Web Reinforcement

tensile strength of the concrete. It is the cracking of the concrete, as a result of the moment acting on this end of the cantilever, that is responsible for the propagation of the flexural cracks bounding the cantilever as diagonal cracks.

1.3.1.1 The Function of Web Reinforcement

Web reinforcement in the form of either vertical or inclined stirrups, or bent up bars, is used to resist shear once diagonal cracks form in reinforced concrete beams. The traditional function of web reinforcement is to form the tension web members of a truss. The compression web members are formed by concrete struts, and the top and bottom chords of the truss are formed by the compression zone concrete and the tension reinforcement respectively. Various truss mechanisms are illustrated by Bresler and MacGregor[15]. As mentioned previously in this chapter, Kani[26] has extended the truss action of web reinforcement to a system of internal arches.

The function of web reinforcement can also be considered from a somewhat different aspect. Fig. 1.2 shows a concrete cantilever containing a stirrup with a tension T_w. It can be seen that under the bond force moment induced by the bond force $T_2 - T_1$, the concrete cantilever and the stirrup act as a reinforced concrete

cantilever. The cantilever thus has a resultant compression, C, imposed on it which increases its flexural strength. Thus the stirrup enhances beam action by strengthening the concrete cantilever. Additional benefits of the stirrups are to keep cracks which they cross, narrow, thus improving aggregate interlock. Stirrups also increase the efficiency of dowel action by suppressing dowel cracking and supporting the dowel.

1.3.2 Arch Action

Once diagonal cracks form in a reinforced beam without web reinforcement the tension steel force tends to equalise along the whole shear span, i.e., the bond force becomes small. Thus the shear is resisted by a change in internal lever arm, or in other words, inclining of the compression force. This is known as arch action. If T is constant in Eq. (1.4)

$$V = T\frac{dz}{dx} \tag{1.6}$$

which quantitatively describes arch action.

1.4 Scope of the Project

From a review of the rigid frame failures in some U.S. Air Force warehouses[6, 17], it was apparent that the presence of axial tension in a reinforced concrete beam subjected to shear forces could lead to premature shear failure. The critical diagonal cracks in the beams were steeper than the 45° assumed in code recommendations for the design of web reinforcement.

According to the principal stress theory[2] it can be shown that cracks in reinforced concrete beams with axial tension should be inclined at a steeper angle to the longitudinal axis than in beams with no axial tension.

Considering the evidence from both the U.S. warehouse failures and the principal stress theory it was apparent that an investigation into the combined action of shear, flexure and axial tension in reinforced concrete members was essential for fuller understanding of the behaviour of coupled shear walls and external columns of multibay frames subjected to lateral loads.

1.4.1 Beam Tests

The major part of this research project consists of evaluation of the results of tests on ten reinforced concrete beams subjected to flexure, shear and axial tension. Seven of these beams contained web reinforcement. The beams were tested with three combinations of axial load to shear force ratio ranging from 1 to 3. During the tests this ratio was kept sensibly constant as it is believed that this would achieve more realistic results than loading the beams in tension, and then, with the tension constant, loading the beams transversly to failure.

The beams were loaded to approximately 30% of ultimate load and then unloaded. They were then loaded

to failure. The experimental equipment and procedure are described in chapter 3.

The beam test results are discussed in chapters 4 and 5. Numerous diagrams illustrating behaviour are presented as it is believed that it is easier and more instructive to show results in the form of graphs rather than in tables. In these two chapters longitudinal reinforcement strains are reviewed, observed deflection characteristics are discussed, and crack patterns and crack propagation are described. Various mechanisms, e.g. the position of the centre of the compression force in the beams, shear deflections, etc., are derived from the observations made.

The load carrying capacities of the beams are considered in chapter 6. Diagonal cracking loads, loads at yield of the tension reinforcement, and ultimate capacities are included and compared with existing theory. A modification of one of these theories is used to account for large increases in ultimate flexural capacity caused by strain hardening of the tension reinforcement.

In chapter 7 the shear resistance of the test beams is reviewed. Ultimate load carrying capacities in shear are considered. Stirrup behaviour in the beams with web reinforcement is described.

A theory to account for the tension reinforcement strains and deflection characteristics of the beams after

diagonal cracking is developed in chapter 8. Conventional methods of calculating beam deflections, disregarding the effect of diagonal cracks, are compared with results from the theory developed. Shear and flexural deflections are derived separately. The decrease in stiffness of beams after flexural and diagonal cracking is illustrated.

Finally in chapter 9 conclusions are drawn from the beam tests and the theory developed in chapter 8. Because of the small field covered by the tests it is impossible to make any recommendations for design. Consequently the lines along which future research should develop in the field of the combined action of shear, flexure and axial tension are reviewed.

1.4.2 Dowel Tests

At ultimate flexural capacity of reinforced beams there can be little aggregate interlock because the cracks are too wide. It was observed from previous tests [42] that when all stirrups across a diagonal crack have yielded there is sometimes some reserve shear strength provided by another mechanism of shear resistance. After study of the possible mechanisms it was deduced that this additional shear resistance originated largely from dowel action.

Therefore, in chapter 2 tests on small scale concrete specimens and on reinforcement bars, to study dowel action, are described. These tests were designed to study dowel action at all stages of shear resistance of beams with stirrups. In chapter 7 the tests are correlated with the tests of the reinforced beams subjected to axial tension.

CHAPTER 2

DOWEL ACTION

2.1 Introduction

Dowel action has been recognised for some time as a mechanism of shear resistance in reinforced concrete beams. In this chapter various modes of dowel shear resistance will be isolated and tests to verify their actions will be discussed. Some comparison of the dowel tests with previously published test results will be made.

2.2 Definitions

Fig. 2.1 shows crack in the shear span of a reinforced concrete beam. Only dowel shears are included in the figure although aggregate interlock forces act across such a crack. The dowel shear is the result of a relative displacement across the crack at the level of the dowel. The displacement is referred to as the "dowel displacement". The condition of stress in the concrete as a result of dowel shears is indicated on the two faces of the vertical crack.

The term "dowel beam" is used to identify the flexural member made up of the tension reinforcement and the concrete cover situated below a dowel crack.

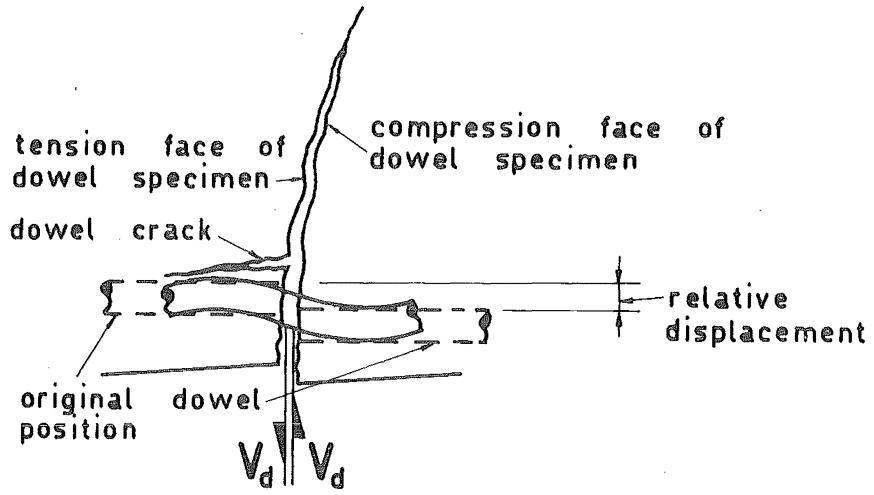

Fig. 2.1 Dowel Displacement at a Crack

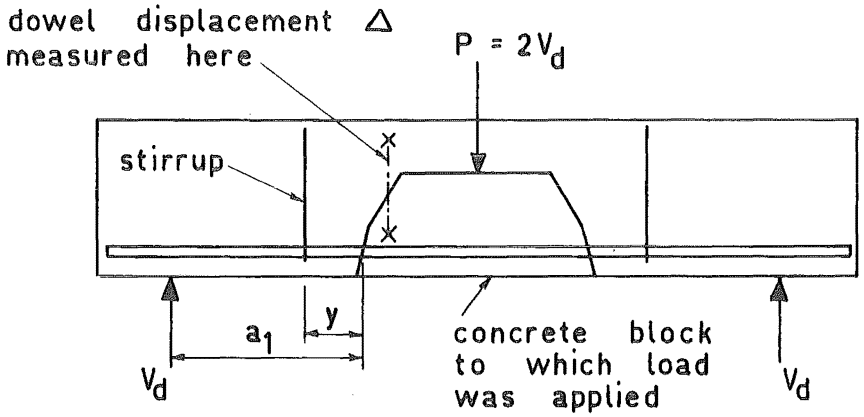

Fig. 2.2 Dowel Test Beams of Baumann[12]

2.3 Historical Review

The first interest in dowel action of reinforcement bars was associated with shear transfer across pavement joints. Grinter [22], as early as 1931, considered the bearing stress under a 4 ft dowel. He approached the problem by considering an elastic beam on an idealised elastic foundation. In a paper published in 1940 Friberg [21] extended the theory proposed by Grinter. He considered shorter dowels of various diameters and at various spacings. Again only bearing stresses were considered, no account being taken of the splitting of the concrete. Presumably this was not critical in pavement design because the bearing of wheel loads suppressed dowel cracking.

Further investigation of the bearing stress at the pavement face end of the dowel was presented by Marcus [34] in 1951. He considered the cracking load caused by excessive bearing stresses to be the failure load of the dowels although they could support some increase in load after this. He found the failure load to be given by

$$D_f = \frac{3D_d(h - D_d)}{2\left(1 + \frac{e}{l}\right)} f_t \qquad (2.1)$$

where D_d = dowel diameter

h = depth of concrete under the dowel

e = distance between the point of application of the load and the face of the joint

l = embedded or effective length of dowel

and f_t = tensile strength of the concrete.

The dowel blocks in the tests were supported on idealised elastic subgrade, viz., timber blocks.

Early work on dowel action in reinforced concrete beams was reported by Jones [24] in 1956. He found the dowel shear sustained before dowel cracking of beams he tested to be given by:

$$D_f = 0.7 f_t (jdI_d)^{\frac{1}{4}} b_n^{\frac{3}{4}} \qquad (2.2)$$

where b_n = the effective width of concrete resisting the tensile stress in the concrete at the level of the reinforcement

j = the ratio of the internal lever arm in the beam to the effective depth

d = the effective depth of the beam

and I_d = the second moment of area of the composite beam consisting of the dowel and concrete cover.

The theoretical grounds for the derivation of Eq. (2.2) were that the tension reinforcement with the concrete below it was equivalent to a beam supported on an elastic foundation. This support was provided by the concrete above the reinforcement. It will be shown later in this chapter that full participation of the dowel and concrete cover as a composite section is

extremely unlikely because of the high bond stresses that would be required to transfer the shear between the steel and concrete. The beams tested by Jones were specially designed to study dowel action. The shear spans were cast with an artifically formed crack crossed only by stirrups and the tension steel. The compression zone was a special device to measure the shear transferred across it.

Watstein and Mathey [48] tested 11 beams without web reinforcement. They determined the shear transferred across the diagonal crack which was attributed to dowel action only. The shear forces calculated for dowel action are in agreement with shear forces that Fenwick [18] found to be resisted by combined dowel action and aggregate interlock action.

In 1963 Kinnunen [30] used the dowel bearing stress equation developed by Marcus [34] to determine the dowel resistance to punching shear in slabs. He indicated that the equation could be used to find the splitting dowel shear if h (see Eq. (2.1))was taken as the minimum distance from the centre of gravity of the dowel cross section to the concrete face.

Taylor [46] made one of the first contributions to the participation of stirrups in resisting dowel shear in a paper published in 1963. He suggested that horizontal splitting is resisted by stirrups and hence

because of dowel action more stirrups resist the shear than cross the diagonal crack.

To evaluate the shear carried by the dowel in reinforced beams Lorentsen [33] designed and tested nine special beams. These beams had a vertical preformed crack in the shear span so that the dowel action of the tension reinforcement only could be studied. He found the relationship between dowel force and dowel displacement to be sensibly constant after formation of dowel cracks or splits. A reasonable valve of the dowel shear that could be carried was found to be given by:

$$D_f = 0.95bt\sqrt{f'_c} \qquad (2.3)$$

where b' = web width of the beam

and t = total beam depth.

This relationship assumes that the dowel diameter has no influence on the splitting shear.

Acharya and Kemp [1] produced evidence from consideration of stresses in the compression zone of reinforced beams failing in shear to show that dowel action was considerable. They neglected aggregate interlock and thus the proportion of shear they attribute to dowel action was too large.

In 1966 Fenwick [18] proposed two pairs of equations for dowel shear in beams without web reinforcement.

$$D_f = 0.174s'bf_t \qquad (2.4a)$$

when $0 < s' < 5.875$

and $D_f = 1.02bf_t$ (2.4b)

when $s' > 5.875$

where s' = the crack spacing at the level of the tension reinforcement.

The numerical factors in this pair of equations are only valid when the dowel is cast near the bottom of the mould so that water gain has minimum influence on the concrete surrounding the dowel. Where water gain seriously effects the properties of the surrounding concrete the numerical constants in Eqs. (2.4a) and (2.4b) were found to change to:

$$D_f = 0.102s'bf_t \quad (2.5a)$$

when $0 < s' < 7.0$

and $D_f = 0.72bf_t$ (2.5b)

when $s' > 7.0$

The relationships were derived from observations on numerous small scale specimens. Concrete strength, position of casting and dowel length were varied. As can be seen from the difference in the factors in the two pairs of equations, the influence of water gain on the dowel shear resistance is considerable.

Krefeld and Thurston [31] proposed the following empirical equation to fit the results of their test beams, designed to study dowel action only.

$$D_f = b\sqrt{f'_c}\left\{1.3\left(1 + \frac{180p}{\sqrt{f'_c}}\right)c_o + d\right\}\frac{1}{\sqrt{\frac{x}{d}}} \qquad (2.6)$$

where c_o = the depth of the concrete cover measured from the underside of the bottom reinforcement

and x = the distance from the support point of the beam to the crack being considered.

The most comprehensive study of dowel action in reinforced concrete beams to date was reported by Baumann [12] in 1968. His main aim was to establish a dowel force dowel displacement relationship both before and after dowel cracking in beams with and without stirrups. Numerous beams were tested in the study. They were similar to those investigated by Krefeld and Thurston [31]. A sketch of the type of test beam used is shown in fig. 2.2. The general dowel shear dowel displacement relationship observed in the tests is reproduced in fig. 2.3. It consists essentially of three separate relationships. No. 1 is the curve before dowel cracking of beams with and without stirrups. After cracking the dowel shear is almost constant in beams without stirrups, viz., No. 2. The relationship after dowel cracking in beams with stirrups is represented by No. 3. The curve shown by the heavy line is the shear displacement relationship of a dowel loaded in an initially uncracked beam with stirrups.

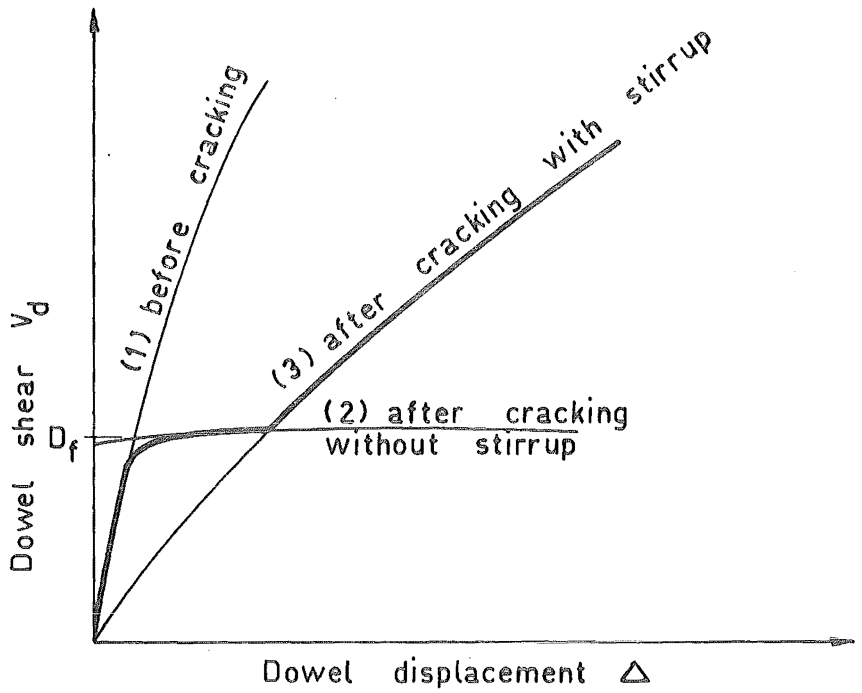

Fig. 2.3 General Dowel Shear – Dowel Displacement Relationship

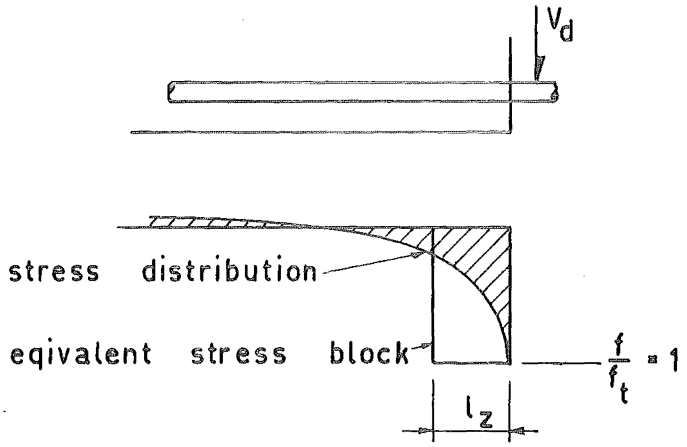

Fig. 2.4 Bearing Stress Distribution Along a Dowel

The analysis of a beam on an elastic foundation was used to find the theoretical dowel cracking shear of the test beams. Fig. 2.4 shows the tensile stress distribution of the concrete surrounding a dowel loaded as indicated. The distribution was replaced by Baumann with an equivalent stress block of length l_z where

$$l_z = \frac{32.9D_d}{\sqrt[3]{f'_c}} \tag{2.7}$$

A summary of Baumann's findings follows:

(a) Up to and including dowel cracking load.

(i) The dowel cracking load can be found using the following relationship

$$D_f = 47b_n D_d \sqrt[3]{f'_c} \tag{2.8}$$

(ii) The relationship between dowel shear and dowel displacement up to dowel cracking is given by:

$$\Delta = .00315\frac{V_d}{D_f} \tag{2.9}$$

(iii) l_z can be found from experiment using the relationship

$$l_z = \frac{D_f}{b_n 0.9 f_{sp}} \tag{2.10}$$

where f_{sp} = the splitting tensile strength of the concrete.

(iv) l_z is independent of the position of the stirrup if $y > 2l_z$ (see fig. 2.2). If the stirrup is closer to the crack, l_z increases with decreasing y.

(v) For two layers of reinforcement l_z is considerably higher than with only one layer, and is given by

$$l_z = 1.6 + 0.52J_v \qquad (2.11)$$

where J_v = the transformed second moment of area of the dowel and concrete cover below it (see fig. 2.5).

(vi) l_z is not influenced to any great extent by cover, width of beam, net width of beam (b_n), height of beam, and span a_1 (see fig. 2.2).

(b) After dowel cracking

(i) The dowel shear dowel displacement relationship, where the longitudinal reinforcement is supported by a stirrup, is

$$\Delta = \gamma V_d^2 \qquad (2.12)$$

where $$\gamma = 0.0056\frac{Y^2}{J_v}$$

and V_d is in kips.

(ii) After dowel cracking in a beam without stirrups the dowel displacement is independent of dowel shear.

(iii) Propagation of a dowel crack is a consequence of incompatability of deformations rather than vertical tensile stress.

(iv) Once a dowel crack has formed concrete quality and beam width have no influence on dowel shear displacement characteristics.

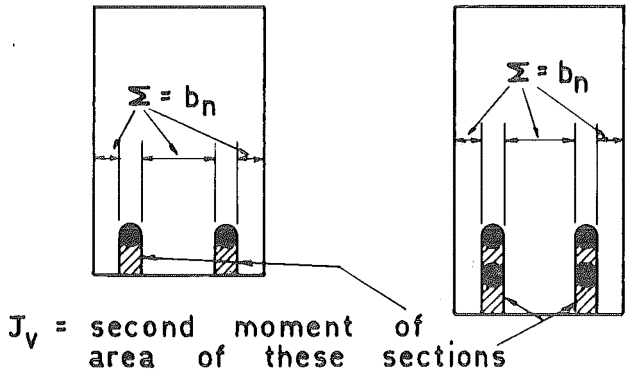

Fig. 2.5 Second Moment of Area of the Dowel Beam

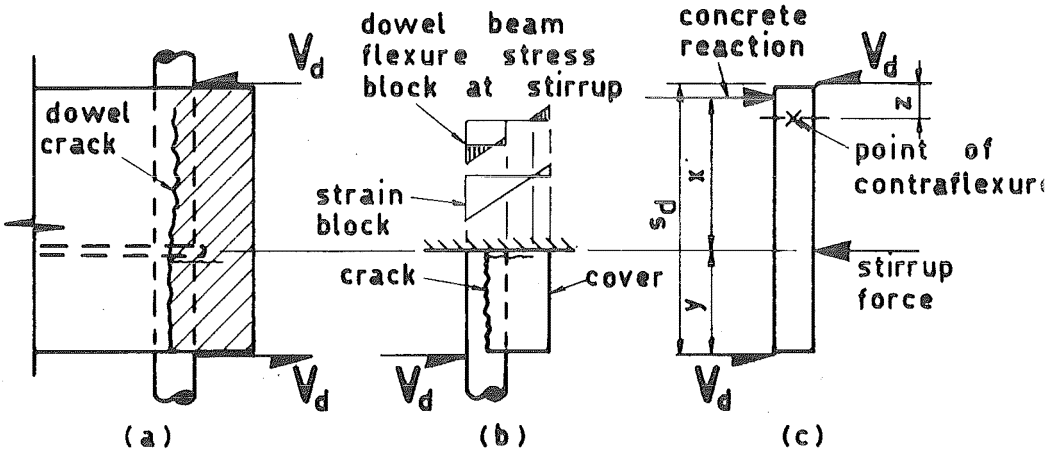

Fig. 2.6 The Dowel Beam

(v) The concrete cover contributes to the dowel shear displacement relationship to only a small extent because of the extremely high shear required between the cover and reinforcement for full composite action.

(vi) Two layers of reinforcement give a large increase in the dowel shear for a given displacement after dowel cracking.

(vii) A second stirrup has little effect on the shear deflection relationship.

Baumann made some observations of a general nature on the results of his tests. In normal beam experiments the maximum width of dowel cracks before failure is of the order of 0.06 inches. The corresponding dowel displacement is therefore of the order of 0.08 inches. Dowel shear dowel displacement relationships are therefore of interest only up to 0.08 inches. Because of shrinkage and creep, etc., the tensile strength of the concrete in dowel shear resistance should be ignored both before and after dowel cracking. In repeated loading, if the dowel shear before unloading is larger than the dowel cracking load, a permanent set of 30% of the total deflection before unloading must be expected at all subsequent loadings.

The most recent work on dowel action has been reported in preliminary form by Regan [44] in 1969. He has found that dowel cracking commences between 0.004 and 0.008 inches dowel deflection. In beams without stirrups the load after dowel cracking except where the beam support is closer than approximately 4 inches to the diagonal crack, is independent of dowel displacement and equals the dowel cracking load. Two layers of tension reinforcement increase dowel action in beams both with and without stirrups. For beams with a low percentage of tension reinforcement the presence of more than one stirrup has little effect. Where the reinforcement percentage is larger two or even three stirrups can help in resisting the dowel shear because of the increased stiffness of the dowel. Hence the dowel action is markedly enhanced.

2.4 The Nature of Dowel Shear Resistance

The loading on the dowel beam defined in section 2.2 is the dowel shear force across a crack in the shear span of a reinforced beam. This load is resisted by flexure and shear in the dowel beam itself, tension stresses in the concrete between the cover and the main body of concrete above the tension reinforcement, and stirrups forces.

2.4.1 Prior to Dowel Cracking

Several investigators [12, 21, 22, 30, 34] have assumed that the dowel beam is equivalent to a beam on an elastic foundation. Dowel cracking is initiated when the tensile stress in the concrete at the face of the dowel block reaches the concrete tensile strength.

2.4.2 After Dowel Cracking

There are four aspects of dowel shear resistance after dowel cracking has developed.

2.4.2.1 Flexural Resistance of the Dowel Beam

Fig. 2.6(a) shows a dowel beam at the end of a concrete cantilever. Because a dowel crack has already formed there is no loading on the dowel beam between the point of application of the dowel shear V_d, and the stirrup. Therefore the moment produced in the dowel beam is a maximum at the stirrup. In part (b) of the figure the stress and strain profiles of the dowel beam at the stirrup are sketched. This mode of dowel shear resistance is limited by the flexural capacity of the dowel beam under the applied moment $V_d y$. Tension in the dowel from flexure of the beam would reduce the dowel beam flexural capacity.

2.4.2.2 Resistance Provided by the Stirrups

The forces shown acting on the dowel beam in fig. 2.6 (c) include the stirrup force. This is dependent on the dowel displacement. If the dowel beam flexural capacity is large enough the stirrup may reach yield before the dowel beam reaches flexural yield. Thus the stirrup capacity may govern the dowel shear resistance.

If the concrete cantilever contains two or more stirrups and the one nearest the tension face of the cantilever yields, the second stirrup and other stirrups may then support additional shear on the dowel.

In fig. 2.6(c) the force in the stirrup is equal to the concrete reaction. The dowel shears at both faces of the concrete cantilever may not be equal but for the purposes of this analysis they are assumed to be equal. It is believed that in a reinforced beam the dowel shears vary only gradually along the shear span. If the stirrup force is known then the distance x can be calculated and thus the maximum bearing stress under the top of the dowel can be found by assuming an equivalent rectangular stress block [12] as shown in fig. 2.4.

2.4.2.3 The Kink Effect

The flexural resistance of the dowel beam decreases to zero when the tension reinforcement in the beam yields in the concrete cantilever under the action of an external moment. At this stage the dowel can resist shear only by the kink effect. Fig. 2.7 illustrates how a bar can sustain shears after it has yielded. The bar carries a constant load $T_y = A_s f_y$, where A_s = area of the bar and f_y = yield stress.

The dowel shears act at a distance l_k apart. From statics

$$V_d = T_y(\sin\alpha)$$

As α is small

$$V_d = T_y \frac{\Delta}{l_k} \qquad (2.13)$$

which gives the dowel shear in terms of displacement. The small component along the reinforcement bar of the kink forces D_k can be taken by bond in the concrete surrounding the dowel. The dowel shears for the kink effect are provided by bearing on the concrete, and by stirrup forces. As with the stirrup resistance for dowel beam action, more than one stirrup may provide the dowel shear for the kink effect.

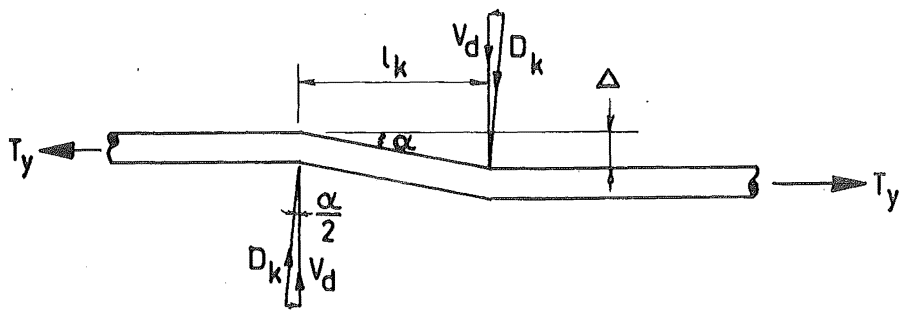

Fig. 2.7 The Kink Effect

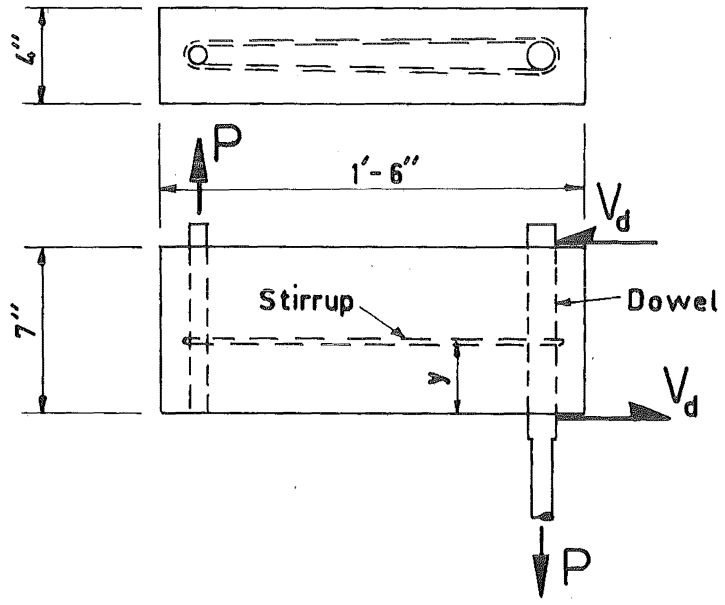

Fig. 2.8 The Dowel Test Specimen

2.4.2.4 The Pure Shear Strength of a Dowel

If very heavy stirrups are provided in the shear span of a reinforced concrete beam it is possible that the dowel shear resistance of the longitudinal reinforcement may be limited by the pure shear strength of the bars. The pure shear strength of the dowel is not included in this study of dowel action as the likelihood of a pure shear failure is small compared with that of a flexural failure of the dowel beam, or the capacity of the stirrup resistance to dowel action being exceeded. The interaction of pure shear and axial stresses in the dowel is also believed to be a second order effect in the dowel tests discussed in this chapter.

2.5 Test Specimens, Apparatus and Procedure

Two series of dowel tests were performed. One was to study the aspects of dowel shear resistance before flexural yield of the tension reinforcement, and the other was to study the kink effect.

2.5.1 Dowel Tests to Study Behaviour Prior to Flexural Yield of the Tension Reinforcement

2.5.1.1 The Test Specimen

The test specimen was an idealised concrete cantilever. It is shown in fig. 2.8. 15 of

these specimens were tested. The two variables were the dowel size and the distance y, of the stirrup from the tension face of the specimen (for definition of tension face see section 2.2). The properties of the dowel specimens are given in table 2.1.

The notation for the dowel test specimens is

pq - rs

where p = depth of specimen in inches (equivalent to crack spacing in the shear span of a beam).

q = nominal dowel size in multiples of eights of an inch.

r = nominal stirrup size in multiples of eights of an inch.

s = distance of stirrup from the tension face of the model in inches (see fig. 2.8).

The dowels in all the specimens were deformed bars and the stirrups were plain reinforcement. The stirrup was a closed hoop tack welded to the dowel and the bar at the opposite end of the specimen.

2.5.1.2 Casting and Curing

The dowel specimens were cast with the dowel in a vertical position. The tension face (see section 2.2 for definition) was uppermost in the mould. The concrete was mixed in the laboratory. Properties of the concrete together with the mix proportions,

Table 2.1 Properties of Dowel Test Specimens

Specimen	Dowel Diameter (in.)	Cover to Dowel (in.)	Stirrup Diameter (in.)	Stirrup Position (in.) (1)	Concrete Mix (2)	Dowel Steel Designation (3)	Stirrup Steel Designation (3)	Age of Specimen (days) (4)
77-21	$\frac{7}{8}$	1.38	$\frac{1}{4}$	1.05	2	B	C	12
77-22	$\frac{7}{8}$	1.38	$\frac{1}{4}$	2.09	2	B	C	11
77-23	$\frac{7}{8}$	1.38	$\frac{1}{4}$	3.00	1	B	A	11
77-23(ii)	$\frac{7}{8}$	1.44	$\frac{1}{4}$	3.00	4	B	C	27
77-24	$\frac{7}{8}$	1.38	$\frac{1}{4}$	4.00	1	B	A	10
77-25	$\frac{7}{8}$	1.38	$\frac{1}{4}$	5.00	2	B	C	12
77-26	$\frac{7}{8}$	1.38	$\frac{1}{4}$	6.00	1	B	A	11
79-21	$1\frac{1}{8}$	1.25	$\frac{1}{4}$	1.03	4	G	C	28
79-22	$1\frac{1}{8}$	1.25	$\frac{1}{4}$	2.05	3	G	C	13
79-23	$1\frac{1}{8}$	1.25	$\frac{1}{4}$	3.00	4	G	C	28
79-24	$1\frac{1}{8}$	1.25	$\frac{1}{4}$	4.01	3	G	C	13
79-26	$1\frac{1}{8}$	1.25	$\frac{1}{4}$	6.02	3	G	C	14
77-00	$\frac{7}{8}$	1.45	–		4	B	–	27
77-00(ii)	$\frac{7}{8}$	1.38	–		4	B	–	28
79-00	$1\frac{1}{8}$	1.34	–		4	G	–	29

(1) Distance of the centre line of the stirrup from the tension face of the specimen (dimension y in fig. 2.8).

(2) Details in table 2.2.

(3) Details in table 3.2.

(4) Age when tested.

are presented in table 2.2.

Table 2.2 Properties of the Concrete Used in the Dowel Tests

(1)	(2)	(3)	(4)		
Concrete Mix	f'_c (psi.)	f_t (psi.)	E_c (psi. x 10^6)	Age tested (days)	Duration moist cured (days)
1	3570	538	3.87	10	9
2	4000	595	-	12	5
3	3840	500	-	13	6
4	4450	657	3.95	29	7

(1) Mixes 1, 2 and 3 had the following properties

water/aggregate = 0.0854

water/cement = 0.63

Aggregate grading	%
3/4" - 3/8"	34.0
3/8" - 3/16"	19.9
3/16"- 7 (B.S.)	6.9
7 - 14 "	6.9
14 - 25 "	11.5
25 - 52 "	11.1
52 -100 "	9.7

For mix 4 see table 3.4

(2) Average of three 6" x 12" cylinders

(3) Average of three 12" x 3" x 3" prisms

(4) 50% secant modulus from one 6" x 12" cylinder.

2.5.1.3 The Test Frame

A photograph of the test frame with a failed specimen in it is shown in fig. 2.9, and fig. 2.10 is a schematic diagram of the frame. In fig. 2.10 A is a jack bearing plate. B is a $\frac{3}{4}$ inch thread screw jack. Between the jack and load cell C, is a smooth bearing ball. The load cell bears on the bearing plate D fixed to the rigid frame H. The hanger E, which is fixed to the jack hangs down both sides of the dowel specimen M, and is smoothly pinned at G to the specimen bearing plate F. K and Q provide the horizontal couple to resist the jacking force. The vertical reaction is provided by the assembly consisting of the knife edge U, rollers S, the bearing plate T, and the nut V on the end of the dowel extension R. K has a knife edge at the end bearing against the dowel and is smoothly pinned at L which is in line with the top end of the dowel specimen. Q is connected through a knife edge assembly P, to a bearing plate N. This bearing plate can be adjusted vertically. The assembly of N and P is shown in detail in fig. 2.11.

2.5.1.4 Instrumentation

All measurements were made with either 8 or 2 inch demec gauges and were duplicated on both sides of the dowel specimens. Details of the operation

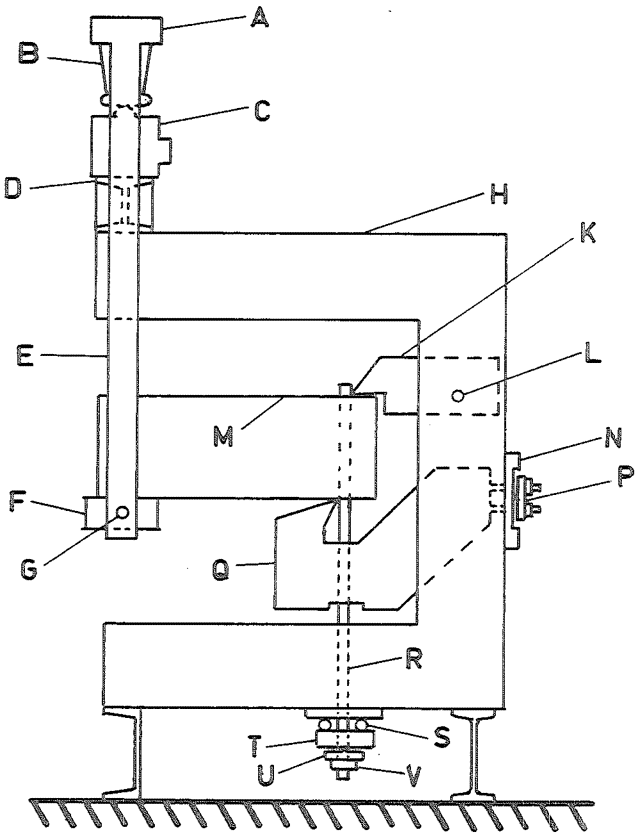

Fig. 2.10 Schematic View of the Loading Frame

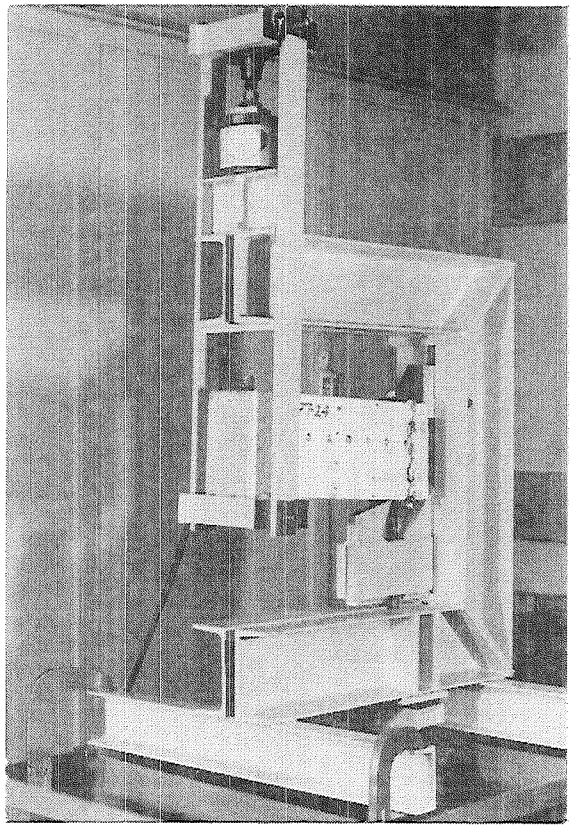

Fig. 2.9 Dowel Test Loading Frame

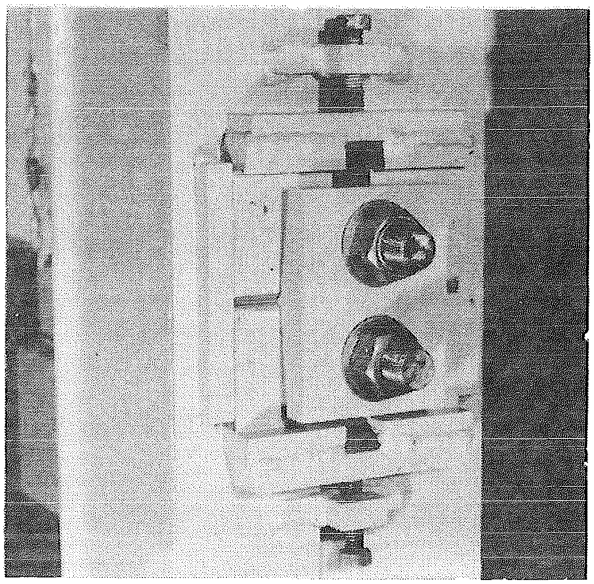

Fig. 2.11 Knife Edge Detail

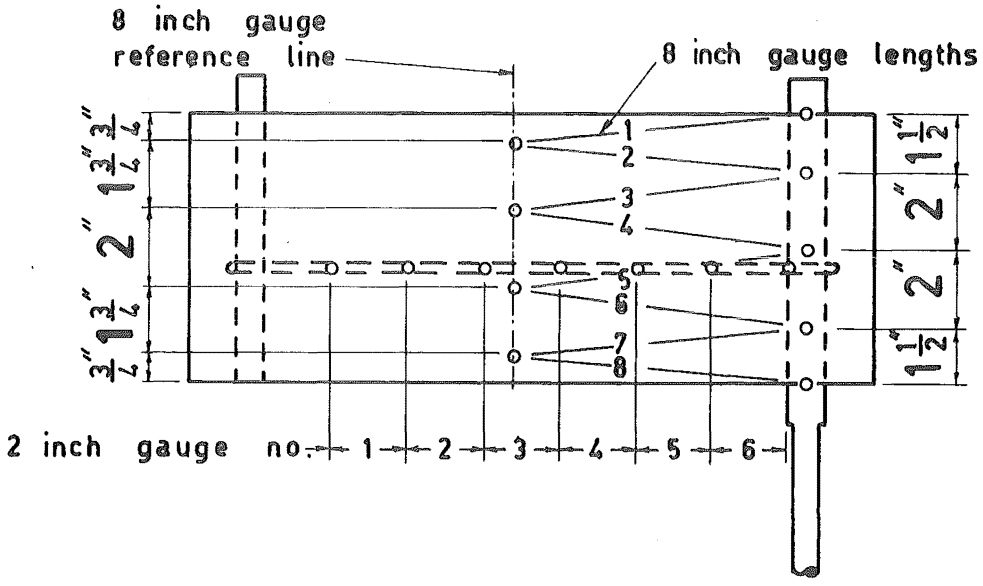

Fig. 2.12 Demec Gauge Lengths on Dowel Specimen

of the demec gauges are discussed in chapter 3. The gauge lengths on the specimens are shown in fig. 2.12. The 8 inch gauge observations were made to find the dowel displacement. The 2 inch gauge lengths were used to find the variation in stirrup strains. To measure the dowel displacement the demec discs were on studs welded to the dowel.

The results plotted in the diagrams in this chapter are the averages of these readings from both sides of the specimen.

2.5.1.5 Testing Procedure

All the dowel specimens, except those made from concrete mix no. 4, (see table 2.1) were tested in a constant temperature environment and hence no temperature corrections to the demec gauge readings were necessary. Corrections were made to those specimens cast from mix no. 4 by making observations on a previously tested dowel specimen. A typical example of the corrections measured for the eight inch demec gauges is shown in fig. 2.13.

The zero readings of all the demec gauges where taken until a tolerance of less than 10 and 25 micro-strains for the 8 and 2 inch gauges respectively was obtained for two successive readings.

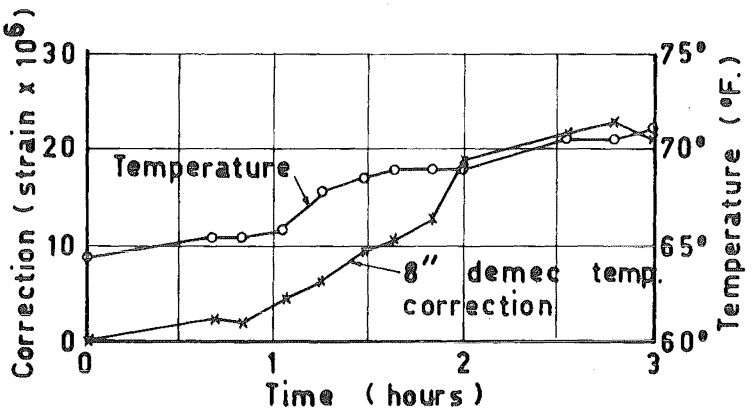

Fig. 2.13 Typical Temperature Corrections

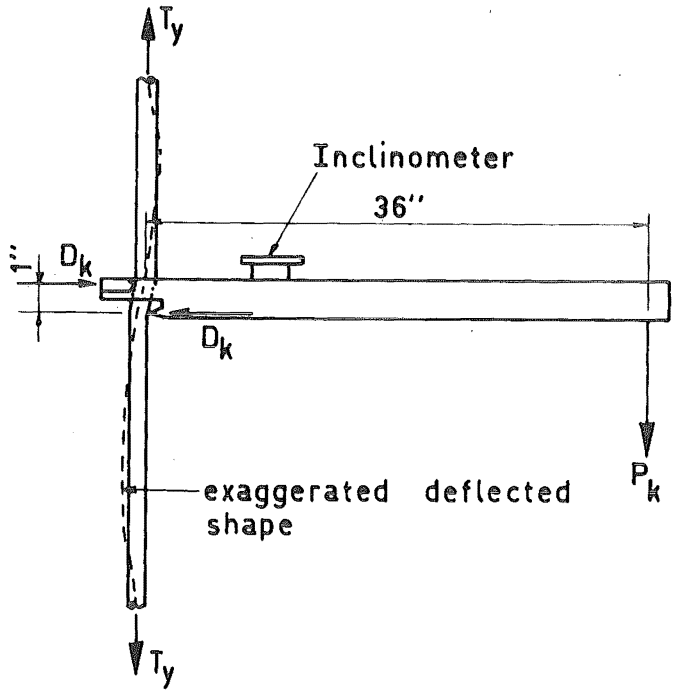

Fig. 2.14 Kink Test Experiment

The following sequence of steps was taken at each load increment of the tests.

(i) The load applied smoothly at the same time being followed on the strain bridge connected to the load cell.

(ii) The load and time were recorded at peak load.

(iii) The specimen was left for a few minutes to allow short term creep to take place and cracks to develop.

(iv) The load and time were recorded again.

(v) The demec gauge corrections (if any) and the gauges on the specimen were read.

(vi) The load and time were recorded again.

The loading of specimens 77-23, 77-24 and 77-26 were an exception to this sequence. For these three tests the load at the start of reading the demec gauges was adjusted to equal the initial peak load recorded in step (ii).

Table A.1 Appendix A gives the loading sequences for all the dowel test specimens.

Where a dowel crack formed suddenly the load was noted and no further displacement of the jack was made until the demec gauges were read. The test on 77-24 did not include this step and hence the maximum load before dowel cracking was not recorded.

2.5.2 The Test Specimen, Equipment and Procedure for Tests to Study the Kink Effect

The test specimen for the kink effect test was $\frac{7}{8}$ inch diameter deformed reinforcement about 5 ft. in length. It was placed in the 250 kip universal testing machine as for a normal tensile test, and loaded in tension to yield.

The transverse shear was provided by hanging dead weights on the end of a horizontal arm which had knife edges bearing on the reinforcement at the other end of the arm. The method of applying the shears is sketched in fig. 2.14. The kinking force is $D_k = 36P_k$ with suitable allowance for the self weight of the arm. The load P_k was a very small fraction of the yield force in the bar so its effect on T_y was neglected.

The displacement Δ (see fig. 2.7) was measured by an inclinometer placed on the horizontal arm. The arm was stiff compared to the dowel but there was some bowing as shown exaggerated by the dashed line in fig. 2.14, as well as the kinking observed in the dowel bar during the tests. Any inaccuracy in Δ as calculated from the inclinometer readings would tend to make the observed deflection larger than the true kinked deflection.

The method of testing the dowel bars involved the following steps:

(i) Yielding the bar in tension.

(ii) Taking the zero reading on the inclinometer.

(iii) Placing the weights on the loading bar for each increment and recording the inclinometer reading.

(iv) Noting the strain in the bar away from the kinked length. This was to check that the dowel did not enter the strain hardening range.

2.5.3 Points of Similarity Between the Dowel Test Specimens and Concrete Cantilevers in Reinforced Concrete Beams

The following points of similarity of the dowel test specimens with the conditions in the shear span of the reinforced concrete beams tested in this project are noted.

(i) The depth of the specimens correspond to the crack spacing in a beam at the level of the tension reinforcement (s_d in fig. 2.6).

(ii) Concrete properties.

(iii) Steel properties including size of stirrup and dowel.

(iv) The distance of the stirrup from the tension face of the dowel specimen corresponds with the distance of the nearest stirrup from the tension face of a concrete cantilever, i.e.,

the stirrup nearest a crack on the low moment side.

(v) Concrete cover to the main reinforcement.

(vi) The dowel displacement between both faces of the test specimens corresponds to the dowel displacement across a crack in a reinforced beam.

2.6 The Test Results

2.6.1 Results of Tests to Study Dowel Action Prior to Yield of the Tension Reinforcement

It is convenient to divide this discussion into sections dealing with behaviour prior to dowel cracking, at cracking, and when dowel cracking is well developed.

2.6.1.1 Behaviour Prior to Dowel Cracking

Fig. 2.15, shows the dowel shear dowel displacement relationships for the dowel test specimens without stirrups. The relationship for the specimens containing $\frac{7}{8}$ inch diameter dowel, and those containing $1\frac{1}{8}$ inch diameter dowel, are shown in figs. 2.16 and 2.17 respectively. Part (a) of each of the three figures gives the relationship up to and including dowel cracking. It is seen to be almost linear but with a

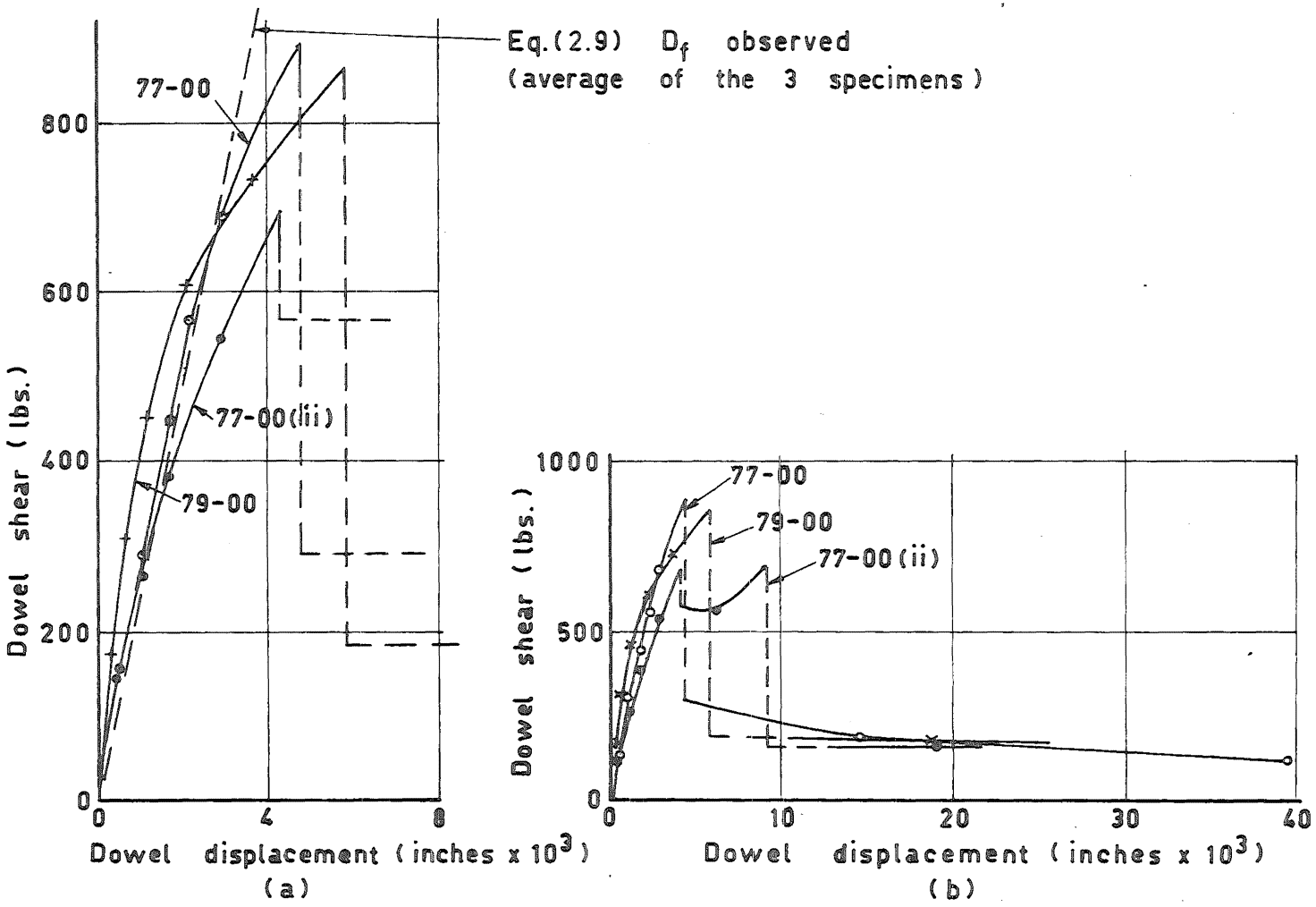

Fig. 2.15 Dowel Shear – Dowel Displacement Relationship for Specimens Without Stirrups

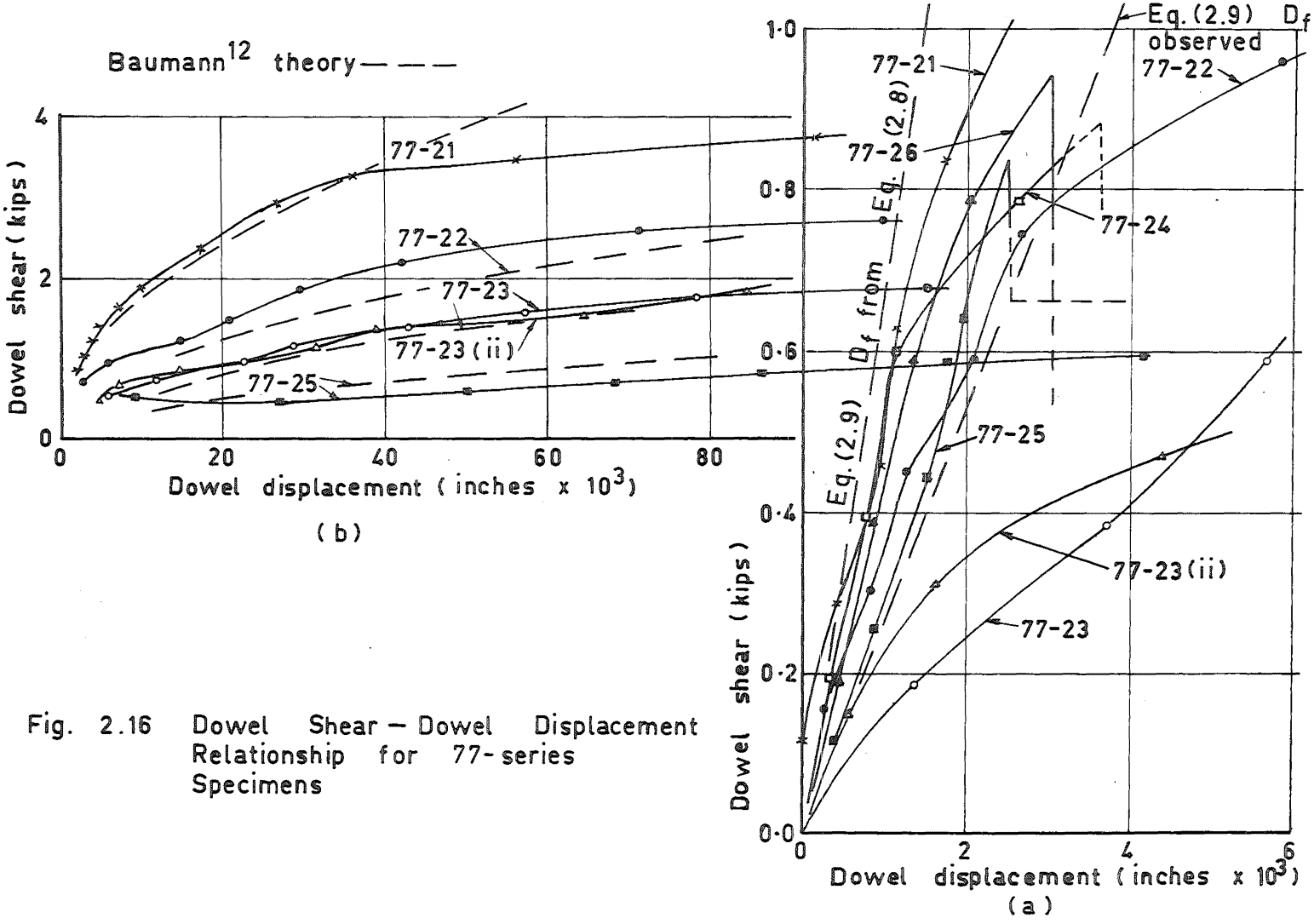

Fig. 2.16 Dowel Shear – Dowel Displacement Relationship for 77-series Specimens

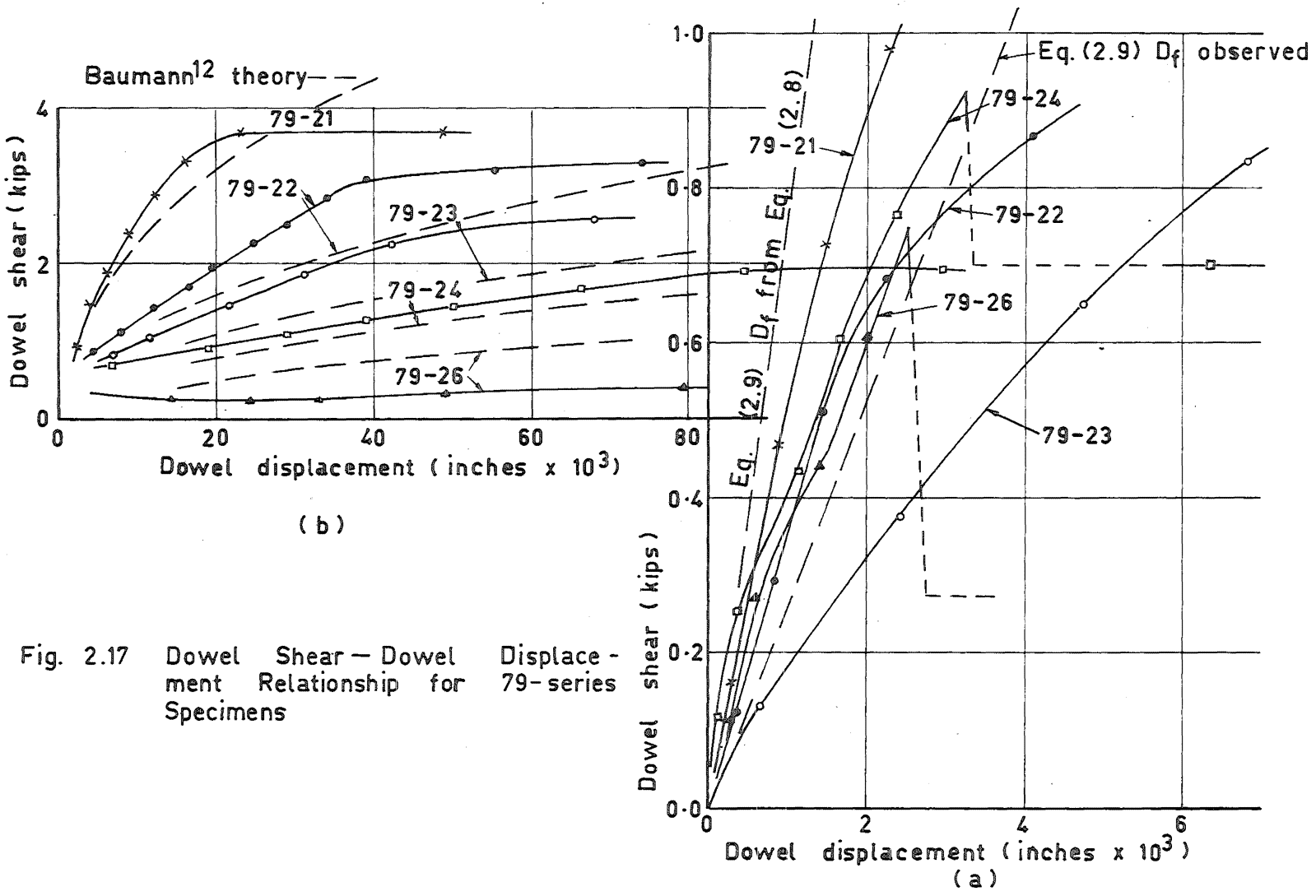

Fig. 2.17 Dowel Shear — Dowel Displacement Relationship for 79-series Specimens

tendency for the displacement to increase more rapidly when the load on the dowel approaches the dowel cracking shear.

The relative deflected shape of the dowels in the three specimens without stirrups are shown in fig. 2.18. The shapes plotted in part (a) are before dowel cracking. Although it is not pronounced the double curvature of the dowels is apparent. The idealised loading on a dowel before dowel cracking is illustrated in fig. 2.19 (a), and part (b) is a sketch of the deflected shape as a result of that loading.

Prior to dowel cracking the maximum tension observed in the stirrups was of the order of 50 micro-strains. The stirrups which were located near the compression face of the specimens tended to be in compression. This is consistent with the flexural behaviour of the test specimens under the applied dowel shears.

2.6.1.2 Dowel Cracking

The dowel cracking loads are presented in table 2.3 which summarises the critical loads on the dowel test specimens. All the cracking loads lie within the range of 697 to 986 lb., i.e., a range of 300 lb. Considering the possible variations in the tensile strength of the concrete from specimen to specimen this

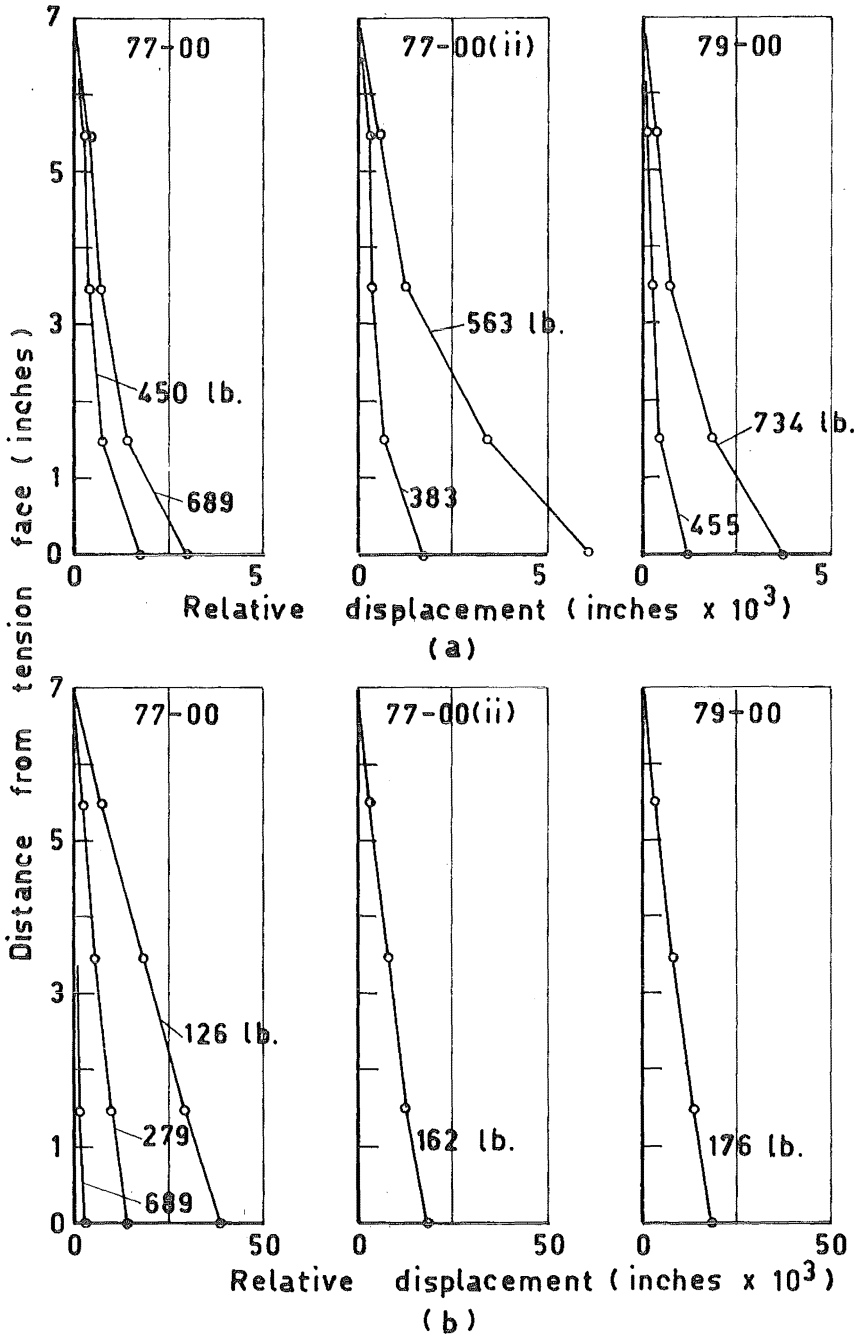

Fig. 2.18 Relative Deflected Shape of Dowel Specimens Without Stirrups

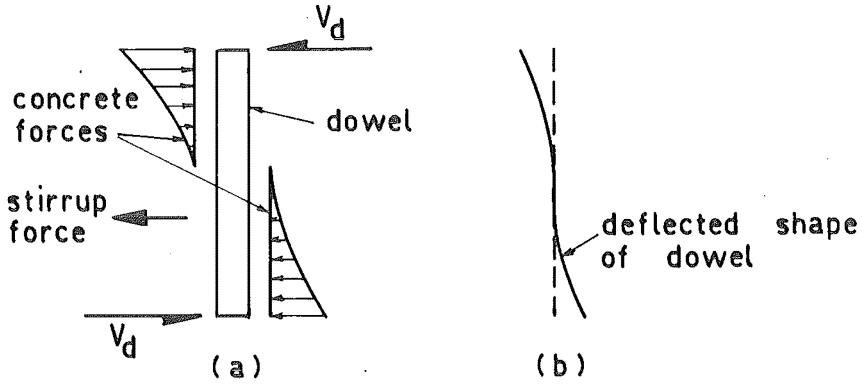

Fig. 2.19 Loading on Dowel in Uncracked Specimen

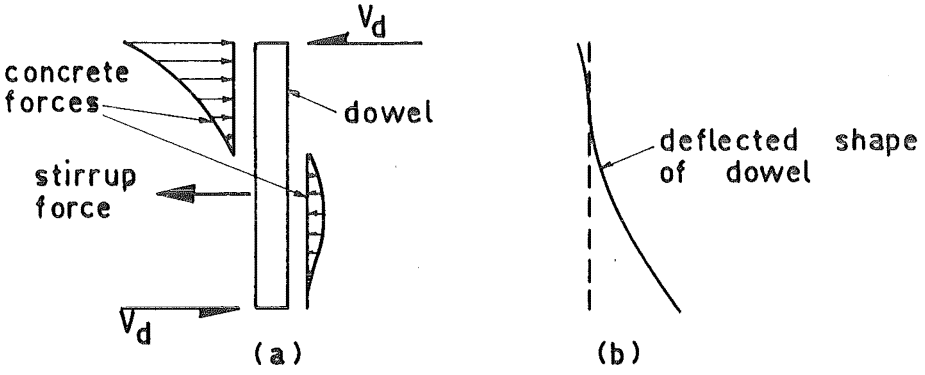

Fig. 2.20 Loading on Dowel in Cracked Specimen

Table 2.3 Critical Shears on Dowel Test Specimens

	(1)	(2)	(3)	(4)	(5)
Specimen	Dowel Cracking Shear (lbs)	Maximum Shear (lbs)	Ultimate Dowel Shear from Eq. (2.15) (lbs)	Ultimate Dowel Shear from Eq. (2.18) (lbs)	$\frac{V_{d_{test}}}{V_{d_{calc.}}}$
77-21		4250*	4600	3960	1.07
77-22		3290*	2310	3240	1.42
77-23		1868	1610	2940	1.16
77-23(ii)		1903	1610	2640	1.18
77-24	786-986	1292	1210	2140	1.07
77-25	816	1192	970	1230	1.23
77-26	940	198	810	530	0.37
79-21		4200	9560	4050	1.04
79-22		3720*	4800	3320	1.12
79-23		2825	3280	2680	1.05
79-24	923	2080	2460	1960	1.06
79-26	743	572	1640	570	1.00
77-00	892	293			
77-00(ii)	697	167			
79-00	865	185			

* These specimens, at failure, had demec studs bearing against the tubing in the concrete. The max. loads given may thus be high.

(1) Shear at dowel cracking if dowel cracking was sudden and followed by a decrease in shear.

(2) Maximum shear during test after cracking.

(3) Theoretical ultimate dowel shear based on the ultimate flexural capacity of the dowel.

(4) Theoretical ultimate dowel shear based on the stirrup capacity and bearing strength of the concrete.

(5) Ratio of the ultimate dowel shear from tests, to the governing dowel shear from theory given in cols. 3 or 4.

is regarded as a reasonable variation. In figs. 2.15 to 2.17 the fall off in load at dowel cracking is shown by the broken lines. The exact path of the dowel shear dowel displacement relationship immediately after dowel cracking is not certain but the general trend is apparent.

The range of dowel displacement at dowel cracking is from 0.0025 to .006 inches.

Once diagonal cracking had been initiated the stirrup strains in the specimens became appreciable.

Dowel cracks propagated slowly where the stirrup was near the tension face. There was no distinct dowel cracking shear. As can be seen in figs. 2.16 and 2.17 the shear deflection curves are smooth for these specimens except for a slight flattening of the curve for 77-22 (fig. 2.16) in the region of the dowel cracking shear.

2.6.1.3 Behaviour After Dowel Cracking

After dowel cracking has developed to a sufficient extent for the stirrup to become effective in resisting the dowel shear the loading on the dowel changes. The idealised load pattern is illustrated in fig. 2.20 (a) and the resulting deflected shape of the dowel is sketched in part (b) of the figure. Some concrete force is shown bearing on the right hand side of the dowel but this is likely to be small. It can be seen that the dowel must still be in double curvature

but the point of contraflexure has risen markedly (compare figs. 2.19 (b) and 2.20 (b)). Figs. 2.21 and 2.22 show the deflected shapes of the dowels in the 77- series and 79- series dowel test specimens with stirrups, respectively. Because of the small number of points at which the deflections were measured the point of contraflexure cannot be seen in these diagrams.

In fig. 2.21 the broken lines represent the likely shape of the dowel near the stirrups. The large bend at the stirrup is a result of the concentrated stirrup load on the dowel beam. This was not apparent in the 79- series specimens because of the greater flexural stiffness of the dowel.

Figs. 2.23 and 2.24 show the strain distribution along the stirrups of the 77- series and 79- series respectively. It can be seen that the dowel shear increases, in some cases substantially after yield of the stirrups. It should be noted that no strain hardening of the stirrups was observed in any of the test specimens.

The dowel beam shown in fig. 2.6 (c) can be used to illustrate how the dowel shear increases after yield of the stirrup. Taking moments about the centre of the concrete bearing force gives

$$V_d = \frac{T_y}{s_d} x \qquad (2.14)$$

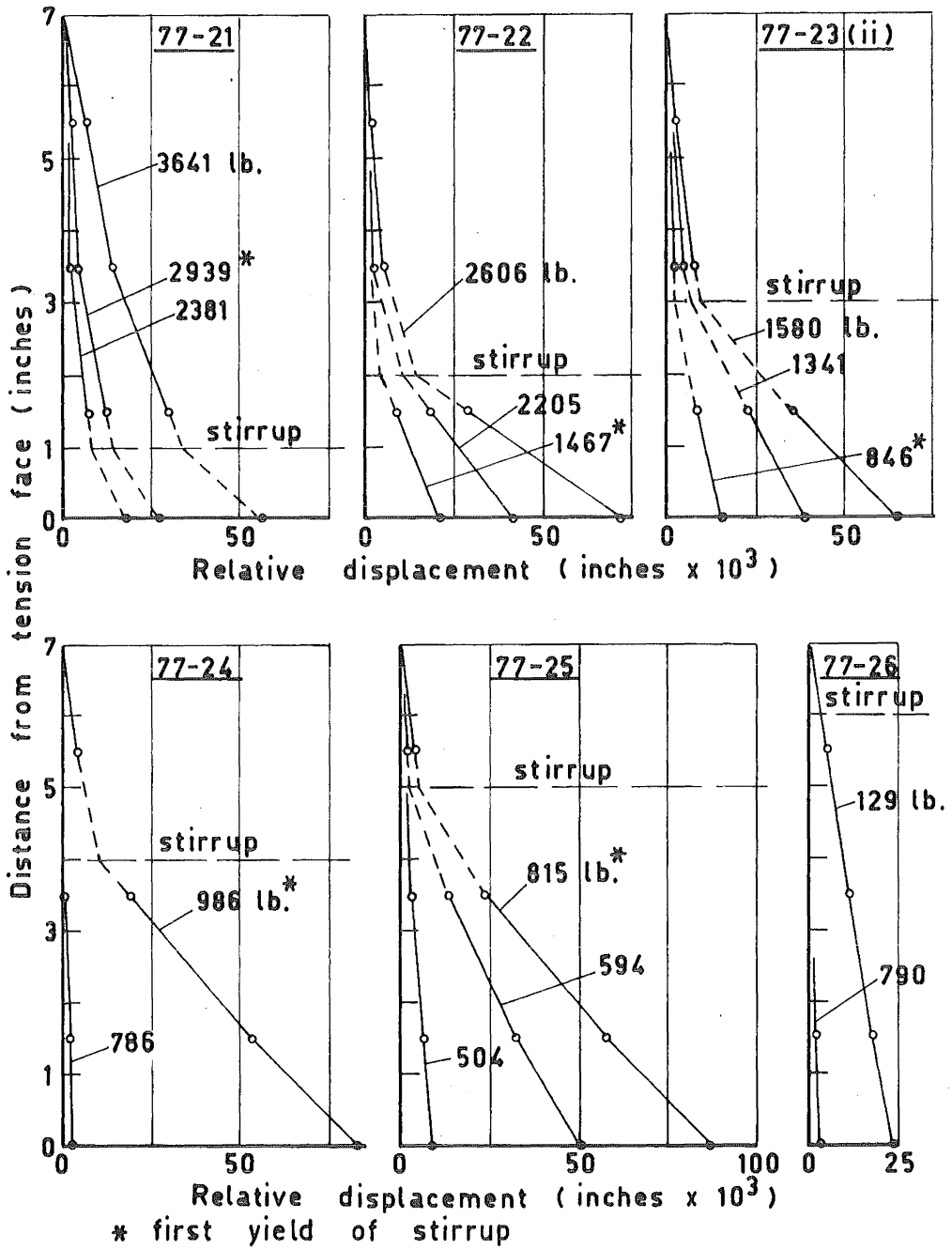

Fig. 2.21 Relative Deflected Shape of Dowels in 77- series Specimens

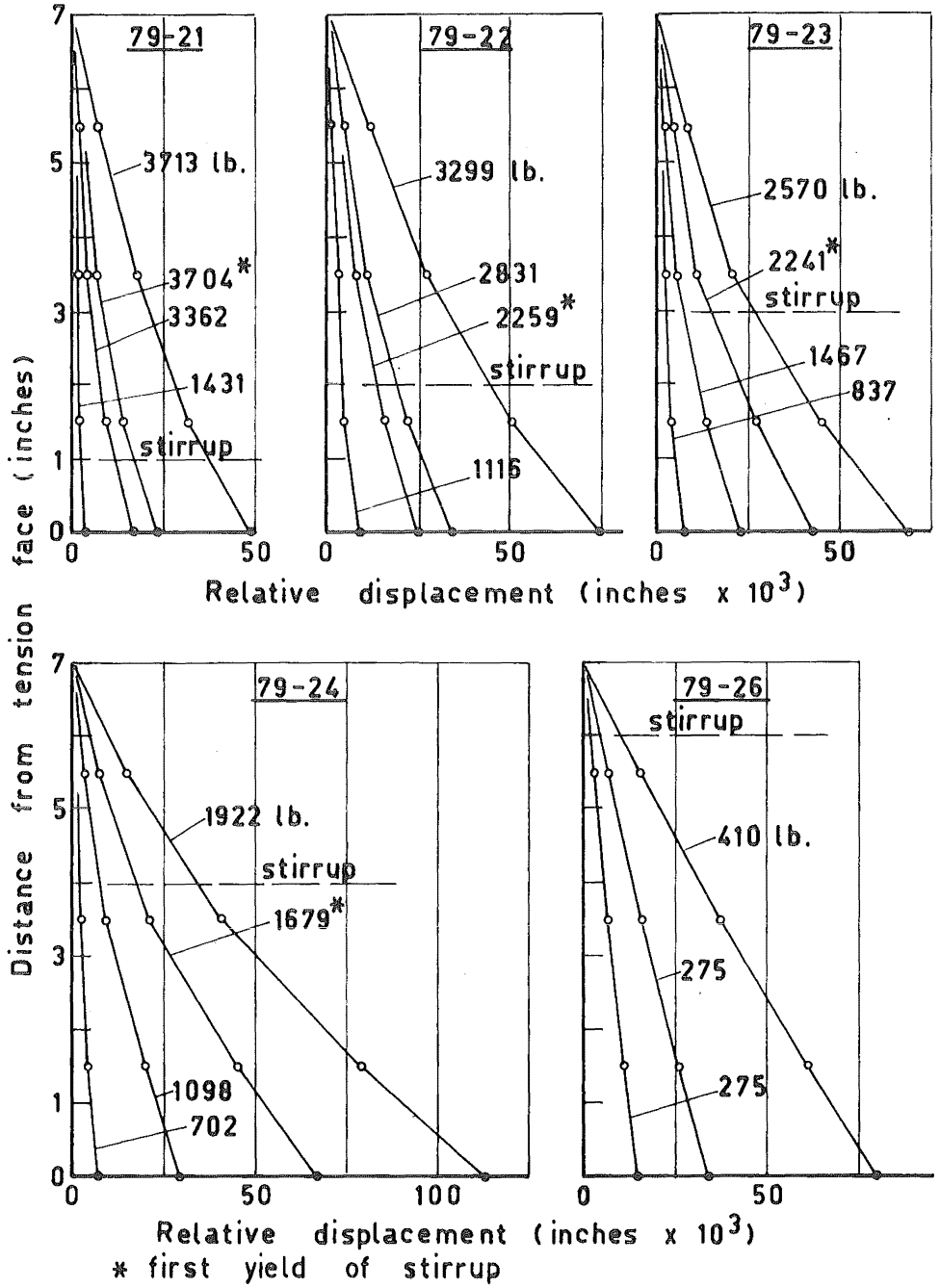

Fig. 2.22 Relative Deflected Shape of Dowels in 79-series Specimens

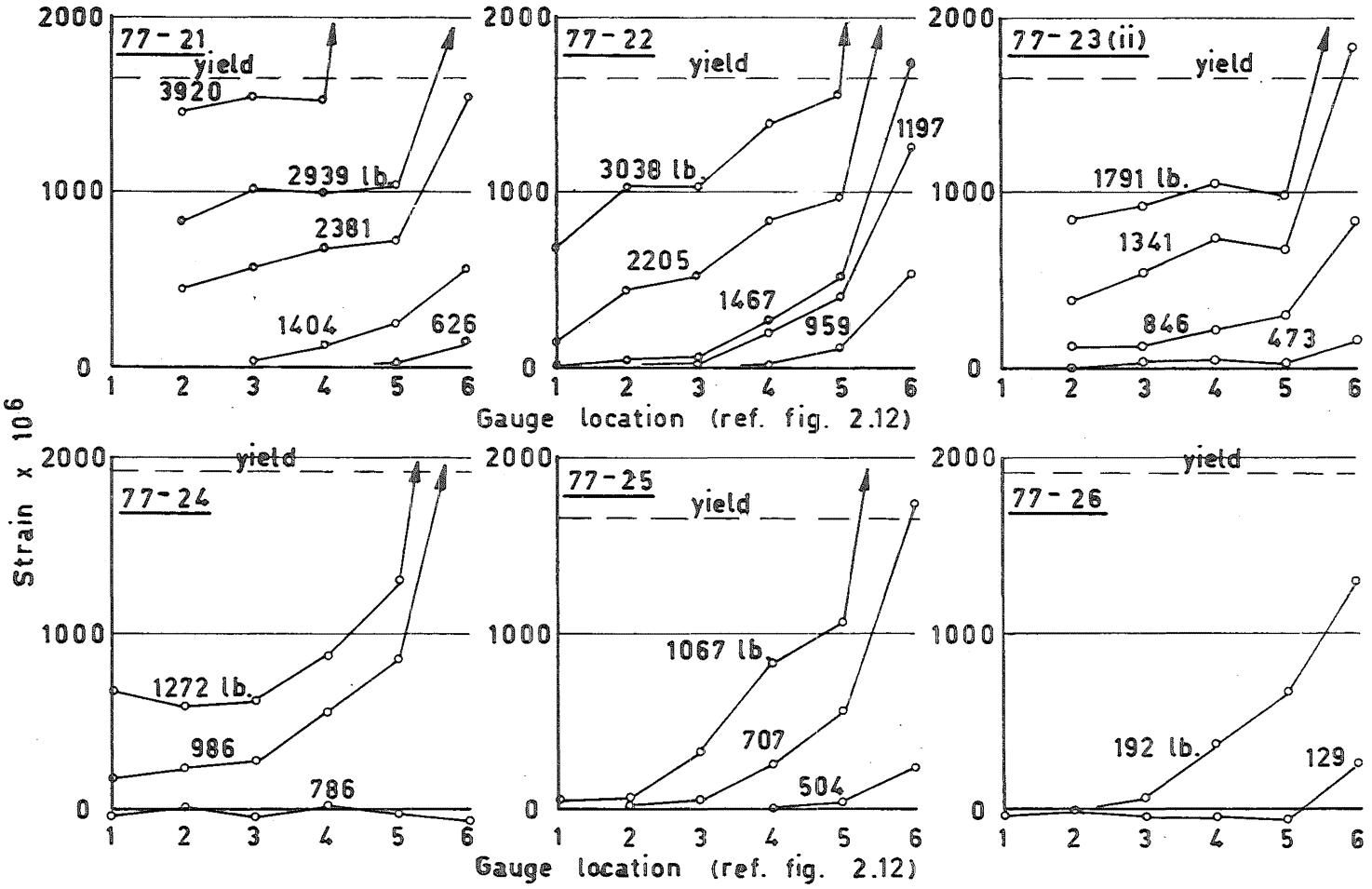

Fig. 2.23 Stirrup Strains in 77- series Specimens

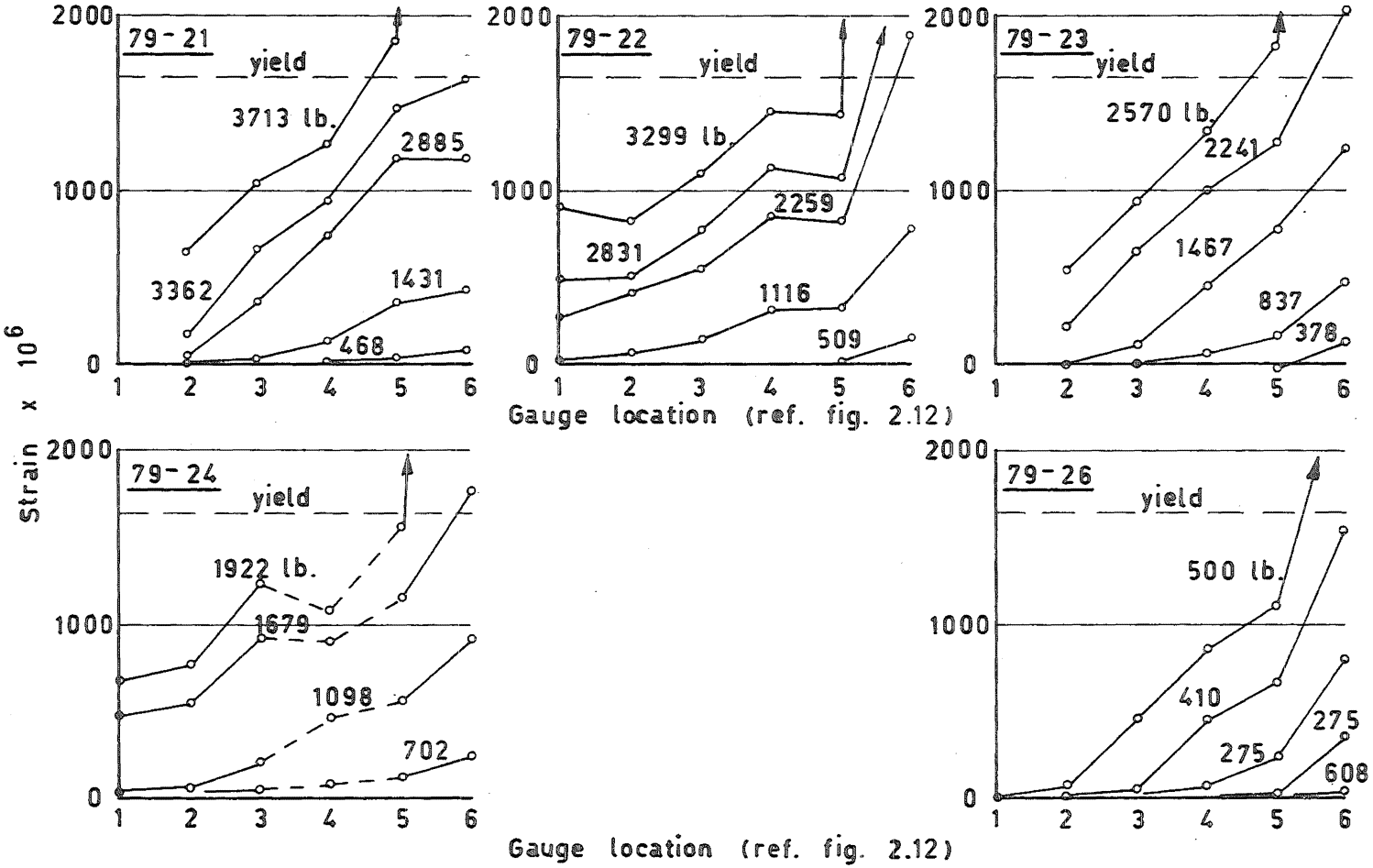

Fig. 2.24 Stirrup Strains in 79-series Specimens

where $T_y = f_y A_v$, i.e., the yield force of the stirrup. This relationship shows that the dowel shear after yield of the stirrups is proportional to the distance between the stirrup and the centre of the concrete bearing force.

From consideration of fig. 2.6 conditions can be formulated for the ultimate dowel shear on the test specimens.

(i) The ultimate flexural capacity of the dowel beam at the stirrup is reached.

$$V_{du} = \frac{M_{ud}}{y} \qquad (2.15)$$

where M_{ud} = the ultimate flexural capacity of the dowel beam.

(ii) The point of application of the concrete bearing force approaches the compression face of the concrete cantilever. From Eq. (2.14)

$$V_{du} = T_y\left(1 - \frac{y}{s_d}\right) \qquad (2.16)$$

which gives the ultimate shear if $x + y = s_d$.

However the dowel shear given by Eq. (2.16) can not be reached because the bearing stress in the concrete under the dowel would be infinite. The bearing stress based on an equivalent rectangular stress block is given by

$$f_b = \frac{T_y}{D_d 2(s_d - x - y)} \qquad (2.17)$$

where D_d = dowel diameter.

Eliminating x from Eqs. (2.14) and (2.17)

$$V_{du} = T_y \left[\left(1 - \frac{y}{s_d}\right) - \frac{T_y}{2 f_b D_d s_d} \right] \qquad (2.18)$$

Column 3 of table 2.3 presents the ultimate dowel shear based on Eq. (2.15). It ignores the composite action of the dowel and concrete cover. In column 4 the ultimate dowel shear based on the yield load in the stirrup and the bearing stress under the dowel is given. The ultimate bearing stress is taken as $2f'_c$. This is considered to be a sufficient approximation as the effect of large variations in f_b in Eq. (2.18) on V_{du} is small.

In column 5 of table 2.3 the maximum dowel shear measured in the tests is compared to the governing ultimate theoretical dowel shear given by Eqs. (2.15) and (2.18). The shear derived from the governing mode of failure is underlined in columns 3 and 4. Where the flexural capacity of the dowel beam governs the observed maximum dowel shear is often substantially larger than the theoretically predicted ultimate load. Composite action of the dowel and concrete cover accounts for this. On the other hand the agreement between the tests and theory is considered to be good

where the stirrup capacity and the bearing strength of the concrete govern the failure mode. The test was not continued to give a displacement large enough for specimen 77-26 to attain its ultimate capacity.

Figs 2.25, 2.26 and 2.27 are photographs of three typical dowel specimens at failure. The horizontal cracks into the concrete cover of specimens 77-26 (fig. 2.25) and 79-23 (fig. 2.26) are a result of flexure of the dowel beam. Many of the specimens including 79-21, did not show signs of horizontal cracking in the concrete cover. If one half of the perimeter of the $1\frac{1}{8}$ inch diameter dowel is effective in resisting the bond force for full composite action of the dowel and concrete cover a bond stress as high as 1600 psi. would be required in specimen 79-21, and a bond stress of 800 psi would be required in 79-24. Stresses of a similar order would be required in the 77- series specimens. It is therefore improbable that full composite action would exist near ultimate dowel capacity.

Figs. 2.28 and 2.29 show the maximum stirrup strain dowel displacement relationship after dowel cracking for the 77- series and 79- series tests respectively. The maximum strain was always observed at demec gauge no. 6 on the stirrup (see fig. 2.12). It can be seen that the relationships are

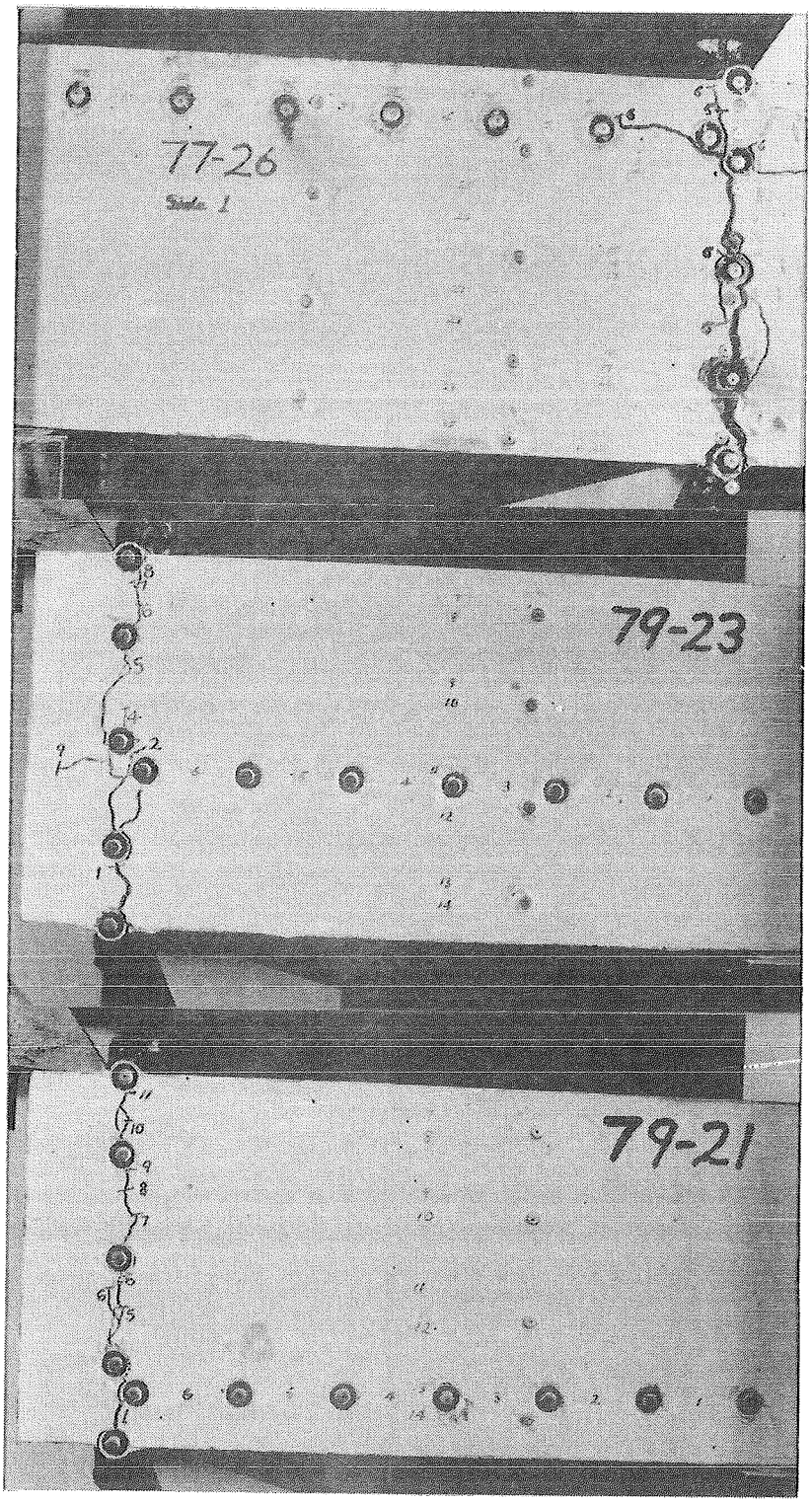

Fig. 2.25
Specimen
77-26

Fig. 2.26
Specimen
79-23

Fig. 2.27
Specimen
79-21

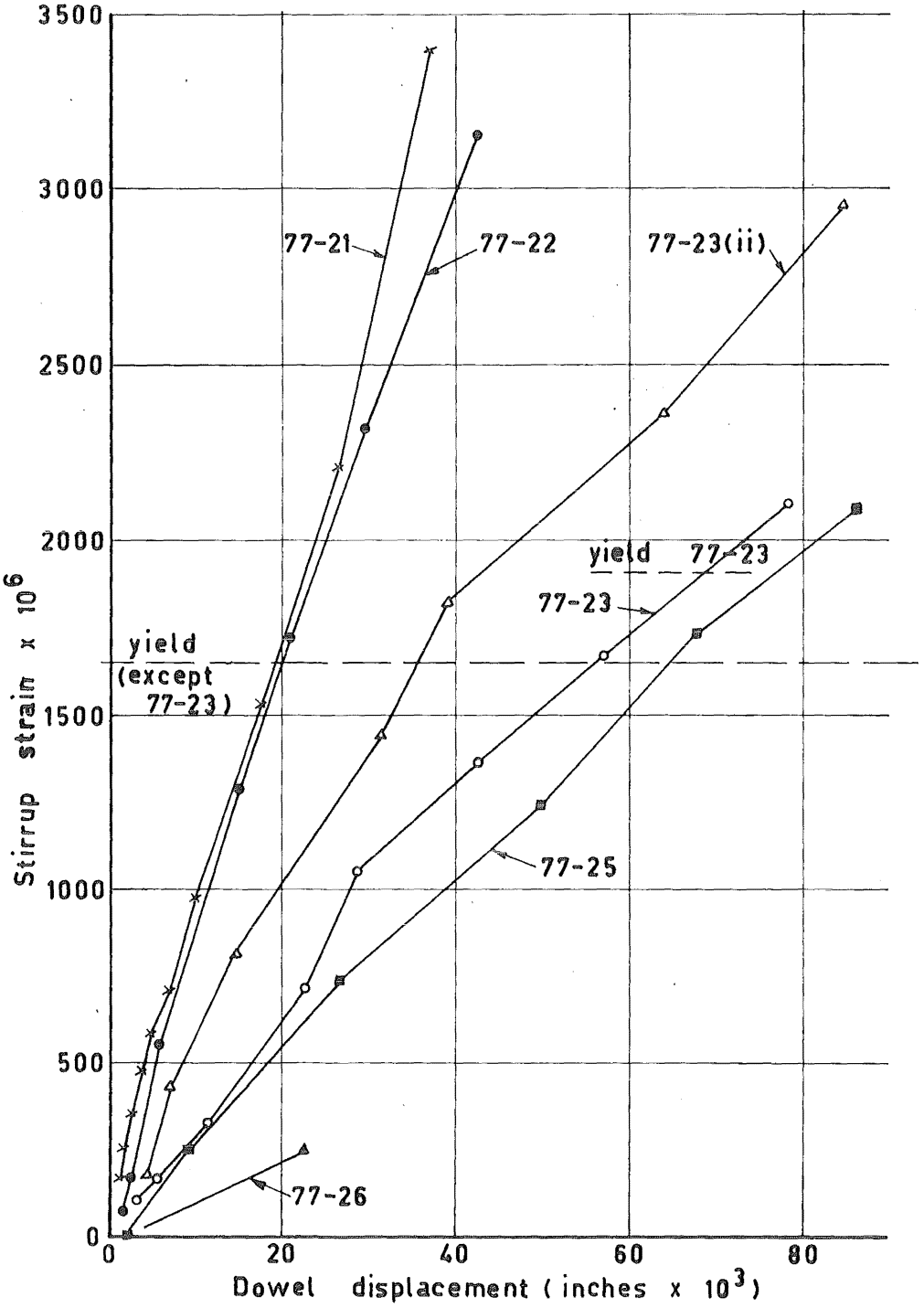

Fig. 2.28 Dowel Displacement – Maximum Stirrup Strain Relationship of 77-series Specimens

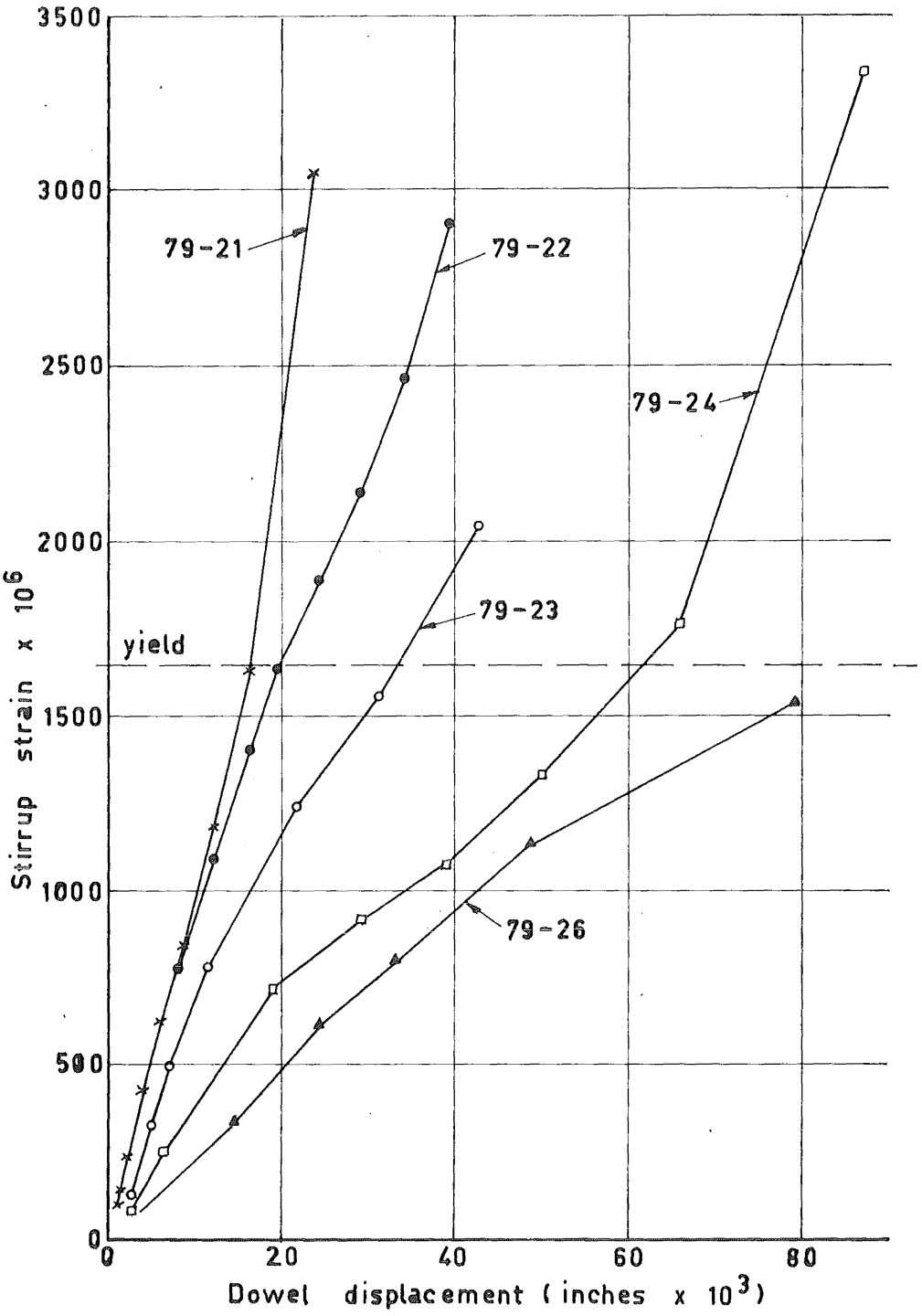

Fig. 2.29 Dowel Displacement - Maximum Stirrup Strain Relationship of 79-series Specimens

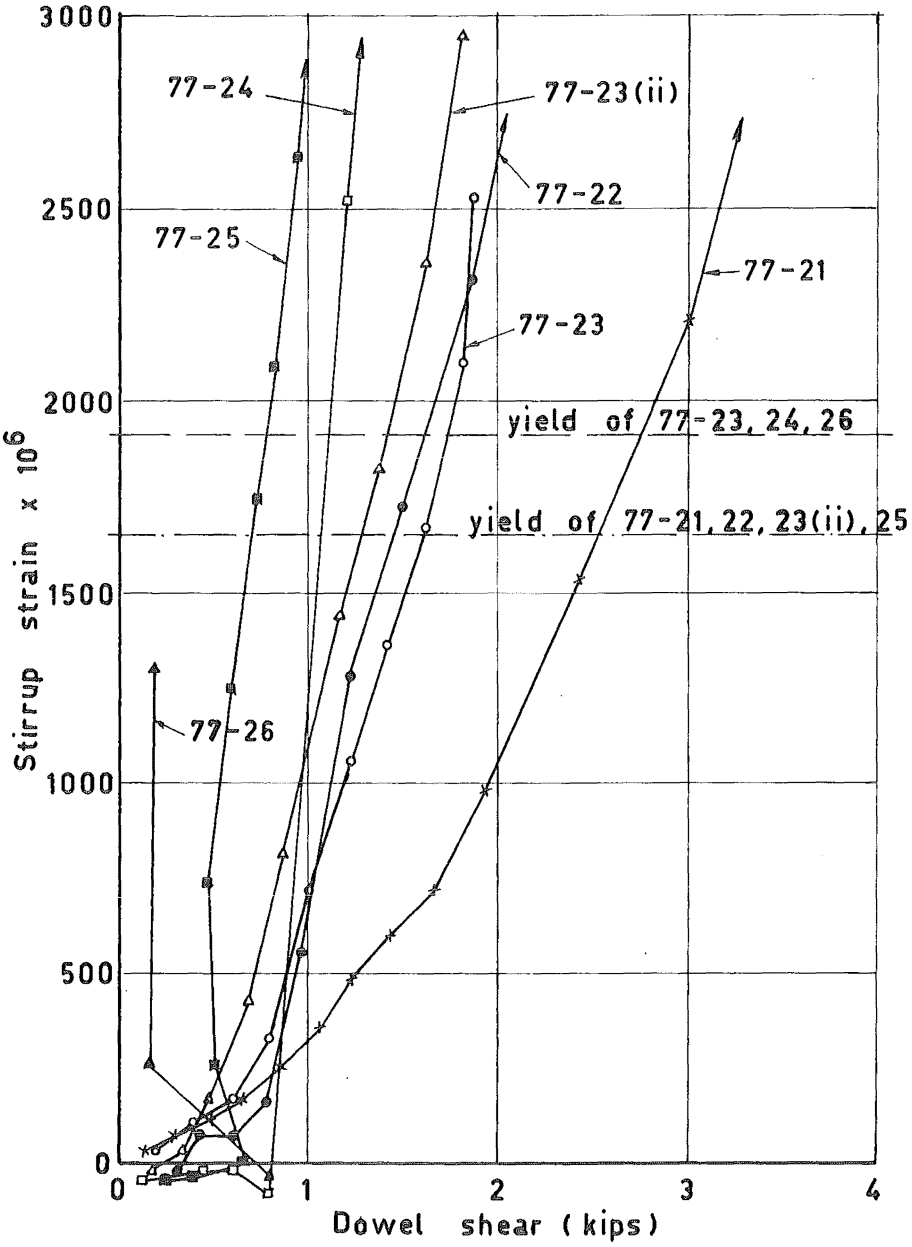

Fig. 2.30 Dowel Shear – Maximum Stirrup Strain Relationship of 77-series Specimens

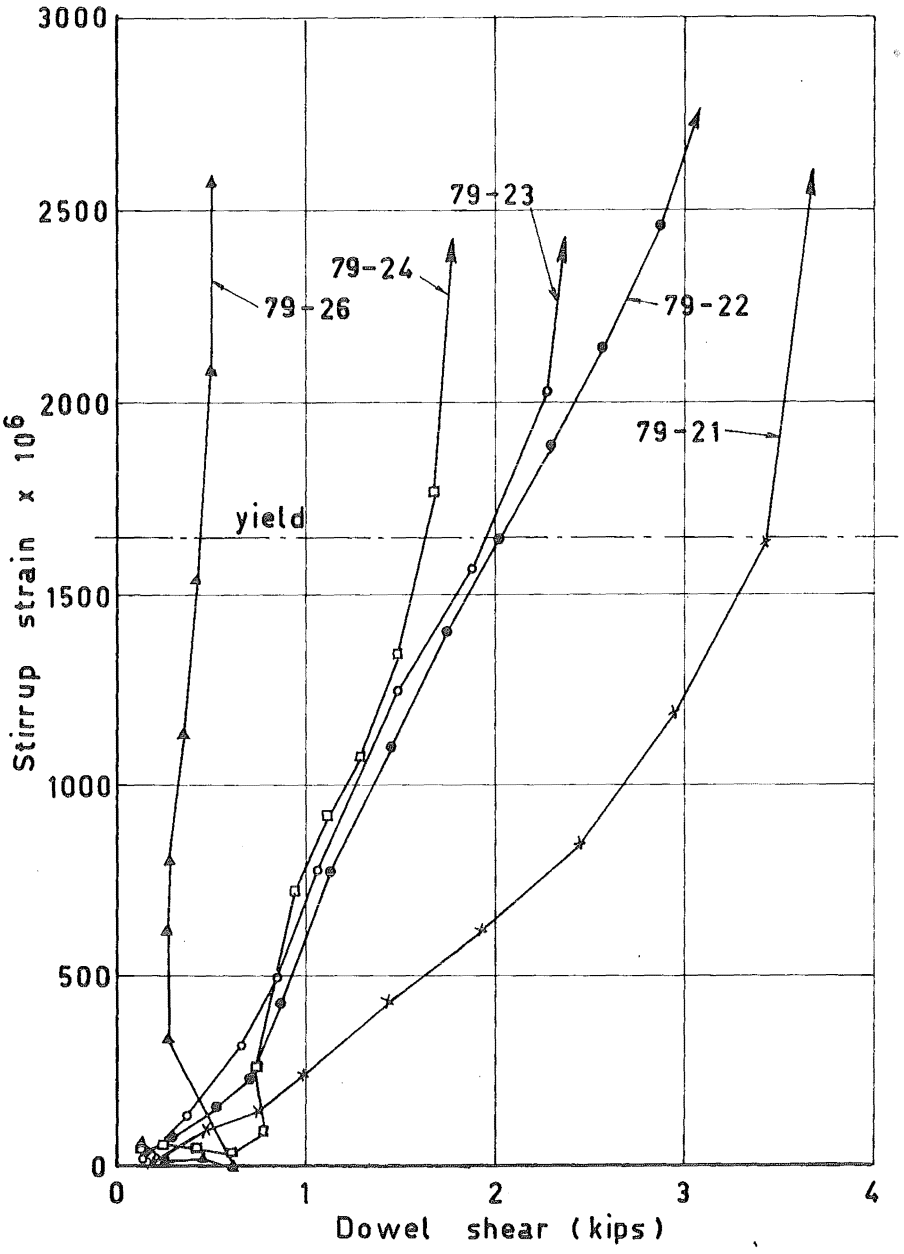

Fig. 2.31 Dowel Shear - Maximum Stirrup Strain Relationship of 79-series Specimens

substantially linear. Figs. 2.30 and 2.31 are plots of maximum stirrup strain versus dowel shear for the two series of tests. Before dowel cracking the stirrup strains are small and somewhat random. After cracking the strain-shear relationships are linear up to yield of the stirrups but after this as expected the strain tends to increase quickly for only small increases in dowel shear.

2.6.2 Results of the Kink Effect Tests

Three tests were performed to study the dowel shear dowel displacement relationship of $\frac{7}{8}$ inch diameter deformed reinforcement bars after yield. The results are plotted in fig. 2.32. The theoretical relationship given by Eq. (2.13) is shown as the dashed line. Also shown is a line representing three times the dowel shear for equal displacement. It can be seen that this second relationship fits the observed dowel shear dowel displacement curves found from the tests very well.

It was observed during the tests that the strain in the dowel was within a few hundred microstrains of strain hardening. It is believed that strain hardening partly contributed to the difference between experiment and theory. It can be shown that under a kinking shear of 4 kips the difference in strain required on the

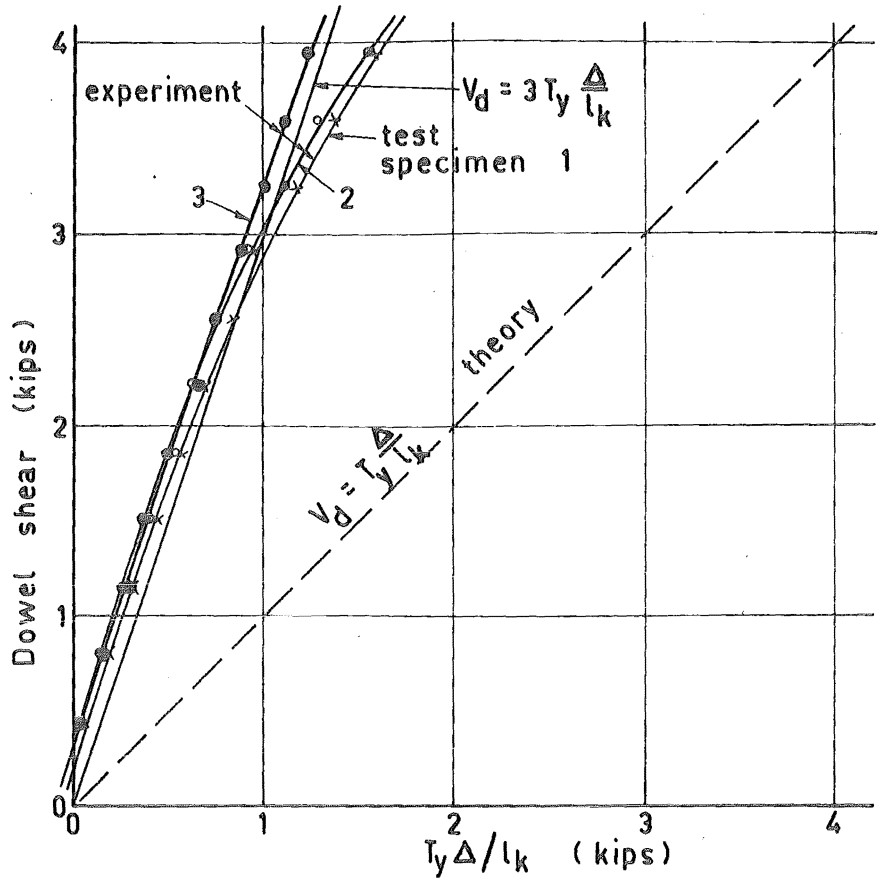

Fig. 2.32 Dowel Shear - Dowel Deflection Relationship for a 7/8 in. Deformed Bar After Yield

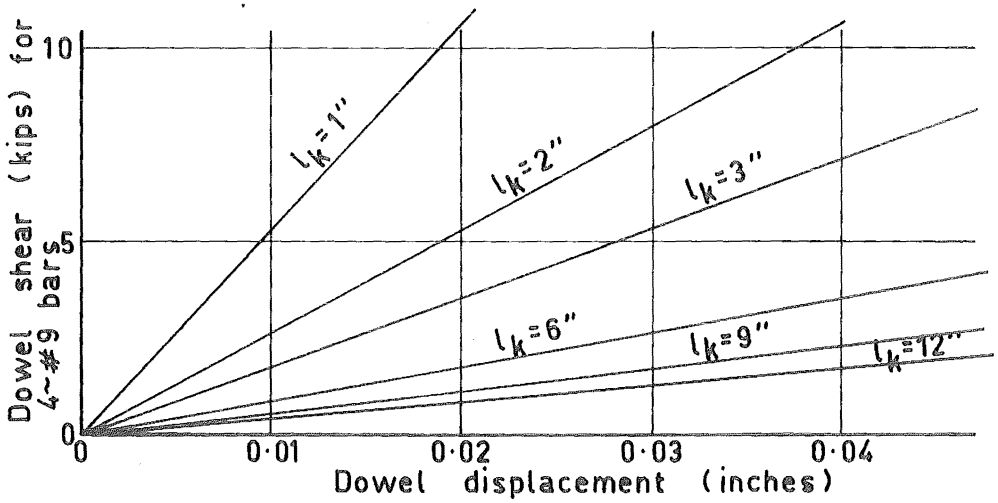

Fig. 2.33 Dowel Shear - Dowel Displacement Relationship for Various Kinked Lengths of 4 $1^1/_8$ in. Deformed Bars After Yield

inside and outside of the curved section of bar to produce sufficient curvature for the observed rotations, is of the order of 4%. The flexural moment in the bar associated with the additional stress resulting from strain hardening may then be as high as 1 kip.inch which is sufficient to support approximately half of the dowel shears by flexure of the bar. No adequate explanation for the rest of the difference between experiment and theory has been found.

The results obtained illustrate that dowel action after yielding of the tension reinforcement in a beam does exist. Assuming the relationship:

$$V_d = 3T_y \frac{\Delta}{l_k} \qquad (2.19)$$

the dowel shear dowel displacement relationship for varying values of l_k have been plotted in fig. 2.33 for four $1\frac{1}{8}$ inch reinforcement bars.

If the capacity of one stirrup is exceeded in the kinking of bars in a reinforced concrete beam additional resistance over a longer kinked length l_k, is afforded by each successive stirrup away from the tension face of the concrete cantilever. Thus more than one stirrup is capable of supplying support to the reinforcement so kinking may develop. It is apparent from fig. 2.33 that the additional support of stirrups further from the tension face of the concrete cantilever decreases

rapidly as the kinked length of bar increases. Thus large dowel displacements would be required for significant increases in dowel shear once the first stirrup has yielded.

2.7 The Dowel Tests as Related to Dowel Action in the Shear Resistance of Reinforced Concrete Beams

If the displacement across a crack in a concrete beam is known the dowel shear across the crack can be found from dowel shear dowel displacement relationships for the particular parameters involved. In this study it has been attempted to reproduce in the dowel test specimens some of these parameters as related to the test beams which will be discussed in subsequent chapters. The major parameters are size and position of stirrups, crack spacing, size and arrangement of the dowels.

Unfortunately it was impossible to cover variations in all these parameters adequately. It is considered that the knowledge gained from the limited tests that were carried out has helped in the evaluation of dowel action in the beams.

2.7.1 Stirrup Strains

The stirrup strain dowel shear relationships shown in figs. 2.30 and 2.31 cannot be directly related to dowel action in reinforced concrete beams. The

strains plotted in these figures are entirely due to dowel shear resistance. On the other hand the stirrup strains observed in reinforced beams are a result of truss action as well as dowel action. The contribution of these mechanisms to the load on a stirrup is difficult to separate and no attempt has been made to do so in this project.

2.7.2 Effect of Axial Stress in the Dowel

It has already been noted that tension in the dowel resulting from flexure of a reinforced beam reduces the flexural capacity of the dowel beam. At yield of the tension steel the flexural strength of the dowel is reduced to zero. The composite action of the dowel and cover is likely to have so severely deteriorated that it can be ignored once a beam has entered the post elastic range.

The kink effect can develop in a beam at any stage of loading. Before yield of the tension reinforcement it is only a secondary effect because the displacements across cracks are small. Hence the dowel shears from kinking would be small because of small displacements and also low tension force in the reinforcement. After yield of the tension steel the dowel displacements become larger especially when stirrups have also yielded. As is shown in fig. 2.33 dowel shears of 10

or more kips could be easily sustained by four $1\frac{1}{8}$ inch diameter bars provided the stirrups are capable of supporting the dowel beam.

2.7.3 Effect of Crack Spacing and Stirrup Position

A variable not included in the dowel specimens tested was the depth s_d. In a reinforced concrete beam this depth corresponds to the crack spacing at the level of the tension reinforcement.

The main influence of crack spacing is on the stirrup resistance to dowel shear. From Eq. (2.18) it is apparent that the ultimate dowel shear that can be sustained by one stirrup on the low moment side of a major flexural or diagonal crack increases with increasing crack spacing.

The stirrup position in relation to a crack in a beam also has considerable influence on the ultimate dowel capacity if stirrup resistance governs. The distance between the tension face of the concrete cantilever and the nearest stirrup in the cantilever is critical, viz., dimension y in fig. 2.6. From Eq. (2.18) it can be seen that as y decreases the dowel shear sustained by stirrup action increases.

Similarly when dowel shear is resisted by the kink effect it is apparent from fig. 2.33 that for

equal dowel displacement the dowel resistance increases with decreasing kinked length. The kinked length is equivalent to y in fig. 2.6.

It can therefore be concluded that the closer the stirrup spacing in a reinforced beam the more efficient dowel shear resistance becomes.

2.7.4 Concrete Strength and Reinforcement Properties

Concrete properties only substantially influence dowel shear resistance up to dowel cracking. It has been assumed by Fenwick [18] that dowel cracking shear is directly proportional to the surrounding concrete tensile strength. In the dowel test specimens the concrete strength was similar or slightly lower than that of the test beams.

Both the tension reinforcement in the test beams and the stirrups had similar properties to the corresponding steel used in the dowel test specimens. On the other hand two layers of tension reinforcement were used in the test beams. From observations made by Baumann [12] the shear resistance of two layers of tension steel is approximately twice that of a single layer as in the dowel test specimens. Also the test beams were 8 inches wide and there were two bars in each layer of steel. To obtain similarity of composite action between the dowel and concrete

cover the dowel specimens contained one bar and were 4 inches wide. The cover to the reinforcement was similar in each case.

2.8 Comparison of Test Results With Previous Work

Only Baumann [12] and Regan [44] have quantitatively studied dowel action in reinforced concrete beams with stirrups, but the latter's report is of a preliminary nature. Several proposals have been made for predicting the dowel cracking load but only Baumann has fully considered post dowel cracking behaviour.

2.8.1 Dowel Cracking Shear

Table 2.4 gives a comparison of the theoretical and experimental dowel cracking shears of two test specimens. The properties of the specimens, and the observed dowel cracking loads are determined from the average of the test specimens that cracked suddenly in each of the two series of tests. In order that the test specimens can be related to the equations proposed by the various investigators the following assumptions have been made:

(i) The effective depth of the corresponding beam is 16.16 inches.

(ii) $j = 7/8$.

Table 2.4 Comparison of Dowel Cracking Shear

Relevant Properties		(1)	(2)
Dowel		$\frac{7}{8}$" dia.	$1\frac{1}{8}$" dia.
D_d (in.)		0.96	1.21
b_n (in.)		3.04	2.79
f'_c psi.		4120	4040
f_t psi.		612	552
E_c psi. x 10^6		3.92	3.95
c_o (in.)		1.40	1.28
h (in.)		1.88	1.88
p		0.0099	0.0153
e (in.)		0	0
$l = s_d$ (in.)		7.13	7.13
		lbs.	lbs.
Experimental Dowel Cracking Shear		836	844
Dowel Cracking Shear from Equations Proposed by Previous Researchers.			
	Equation		
Kinnunen[30] after Marcus[34]	2.1	810	671
Jones[24]	2.2	1650	1510
Fenwick[18]	2.4(a),(b)	1900	1570
"	2.5(a),(b)	1340	1110
Baumann[12]	2.8	2200	2520

(1) Properties of the specimen, and the dowel cracking shear, are the average of specimens 77-25, 77-26, 77-00 and 77-00(ii).

(2) Properties and dowel cracking shear are the average of specimens 79-24, 79-26 and 79-00.

The equations predicting the dowel cracking shear proposed by Jones [24], Lorentsen [33] and Krefeld and Thurston [31] depend to a varying extent on the effective depth of the beam. For the dowel tests discussed in this chapter there was no corresponding effective beam depth. The influence of beam depth on the dowel cracking load of the test specimens is considered negligible. The dowel cracking shears predicted by Lorentsen [33] and Krefeld and Thurston [31] consequently do not give a valid comparison with those observed, and have therefore not been included in the table. The cracking shears from Jones [24] have been included because the influence of d is not as large as in Eqs. (2.3) and (2.6). They are of the same order as those of Fenwick [18] and Baumann [12].

The best agreement between theory and experiment is provided by Kinnunen [30] who interpreted Eq. (2.1) which was proposed by Marcus [34] for dowel bearing capacities across pavement joints, to include dowel action for punching shear in slabs.

The low observed dowel cracking shear in the test specimens is discussed in section 2.8.3.

2.8.2 Dowel Shear Resistance in Beams Without Stirrups After Dowel Cracking

In beams where the dowel is not supported by stirrups Lorentsen [33], Baumann [12] and Regan [44] have found that after dowel cracking the dowel shear is independent of the dowel displacement. In the dowel tests in this project the relationships was not observed. The reason is that these tests considered concrete cantilevers whereas those of all three investigators mentioned above considered the last crack in the shear span of a beam. Fenwick [18] also found a marked drop in load once dowel cracking was initiated in his dowel tests of the concrete cantilever type. On the other hand he observed only approximately 10% drop in dowel shear after dowel cracking in tests on long dowel specimens which represented the last crack in the shear span of a beam.

2.8.3 Comparison of the Test Results With Baumann's [12] Proposals

The length of the equivalent stress block l_z, for the dowel test specimens before dowel cracking has been calculated from Eq. (2.7). The ranges of values for the 77- series and 79- series tests are 1.92-2.06 inches and 2.42-2.54 inches respectively.

The corresponding values of l_z from the relationship

$$l_z = 2.03D_d \qquad (2.20)$$

which was proposed by Baumann to fit his experimental results, are 1.95 inches and 2.46 inches respectively.

If l_z is calculated from Eq. (2.10), taking the splitting tensile strength as the modulus of rupture, values of l_z for the test specimens of only 0.50 inches and 0.61 inches are obtained. The approximation that $f_{sp} = f_t$ is known to be incorrect but a suitable relationship has not been found to the knowledge of the author, between the two methods of determining the tensile strength of concrete. However the conclusion that the dowel cracking shear of the test specimens is low in comparison with those predicted by Baumann still remains. The phenomena is partly explained by consideration of the steel tubing around the demec stud at the tension face of the dowel specimens. This tube was at the top surface of the concrete when cast. Water gain combined with stress concentration around the tubing both contributed to produce conditions for premature cracking in the test specimens. It is believed that shrinkage along the stirrup also contributed to premature dowel cracking.

Figs. 2.26 and 2.27 show cracks which formed at very low dowel shears. The crack propagation in both

these specimens is retarded by the stirrup. It can be seen in fig. 2.17(a) that the dowel beam in specimen 79-23 was initially less stiff than in all the other specimens of the 79- series. The crack propagation is retarded more by the lower stirrup in 79-21 and consequently the dowel beam is as stiff as the specimens that have not cracked. Those that cracked suddenly all had stirrups towards the top of the specimen and consequently shrinkage along the stirrup had little influence. The effect in the 79- series tests was also observed in the 77- series tests (see fig. 2.16(a)).

The relationship given by Eq. (2.9) is plotted in figs. 2.15, 2.16 and 2.17 parts (a). The two dowel cracking shears used are (i) given by Eq. (2.8) and (ii) are the observed average values.

From the figures it can be seen that the dowel deflection in the test specimens is larger than those obtained from Eq. (2.9) using the dowel cracking shear given by Eq. (2.8). On the other hand if the observed cracking shear is used in Eq. (2.9) the majority of the observed dowel displacements are smaller than given by the equation. The important conclusion is that the displacements are of the same order as those observed by Baumann. Discrepancies must be expected because of the different type of tests.

After dowel cracking was well developed the relationships between dowel shear and dowel displacement given by Eq. (2.12) have been plotted as the broken lines in figs. 2.16 and 2.17. The agreement between observation and the relationship proposed by Baumann is good. Except for the specimens where y = 6 inches the theoretical displacements are greater than the corresponding experimental displacements. From this it can be concluded that the recommended value of J_v is conservative. Hence the composite action of the concrete and dowel is of greater benefit than implied by Baumann.

Where the observed dowel shears become independent of displacement in figs. 2.16 and 2.17 the stirrup in the specimens have yielded and the dowel is virtually hinging around a point close to the compression face of the specimen. This is particularly obvious in specimens 77-21 and 79-21.

2.9 Conclusions

Prior to dowel cracking the presence of stirrups in the concrete cantilevers of a reinforced concrete beam has little effect on the dowel shear resisted by the longitudinal reinforcement. The dowel shear dowel displacement relationship is approximately linear.

Dowel cracking occurs when the tensile strength of the concrete at the face of the cantilever is exceeded. Dowel displacements at cracking are of the order of 0.003 to 0.006 inches.

Once dowel cracks develop the important factors in the shear resistance of the dowel are the size and position of stirrups, and the flexural capacity of the dowel and concrete cover working as a composite section. It has been shown that some composite action does exist but full composite action is unlikely, because of high bond stresses involved between the cover and dowel.

Dowel action before flexural yield of the longitudinal reinforcement in a reinforced beam is limited by two modes of resistance.

(i) The flexural capacity of the dowel beam.

(ii) The capacity of the stirrup or stirrups supporting the dowel beam, and the bearing strength of the concrete under the dowel.

More than one stirrup can be effective in supporting the dowel beam but the efficiency of the other stirrups reduces quickly with increased stirrup spacing. The flexural capacity of the dowel beam is reduced as a result of axial tension in the dowel owing to flexure of the concrete beam.

After yield of the reinforcement owing to flexure of the reinforced beam the kink effect of the bars resists dowel shear. This is proportional to the dowel displacement and the change of slope of the dowel as a result of kinking. The kink effect is limited by the support given by the stirrups on the low moment side of the crack across which the bar is kinked. Two or more stirrups can support the bar but their efficiency is reduced rapidly with increasing kinked length.

Dowel action is an effective means of shear resistance in reinforced concrete beams with stirrups. The ultimate dowel shear before yield of the tension reinforcement in a reinforced beam can conveniently be calculated from the flexural capacity of the dowel beam or the capacity of the stirrups supporting the dowel. Concrete properties have little influence on dowel action after dowel cracking.

CHAPTER 3

BEAM TEST APPARATUS, SPECIMENS AND PROCEDURE

3.1 Beam Identification

The general notation for the test beams is

Nx - Syz

where N = a constant symbol used to refer to the beam loading

x = the nominal axial load to shear force ratio

S = a constant symbol used to refer to the web reinforcement in the beam

y = the stirrup spacing in inches

z = the stirrup diameter in multiples of eights of an inch.

In one beam y = 12 but in all other beams with web reinforcement y and z are single digits. A zero following the S indicates no web reinforcement.

During testing the beam sides were referred to as side 1 facing West and side 2 facing East.

3.2 The Test Beam

The dimensions of the test beams are shown in fig. 3.1 Details of the beam test lengths are given in table 3.1.

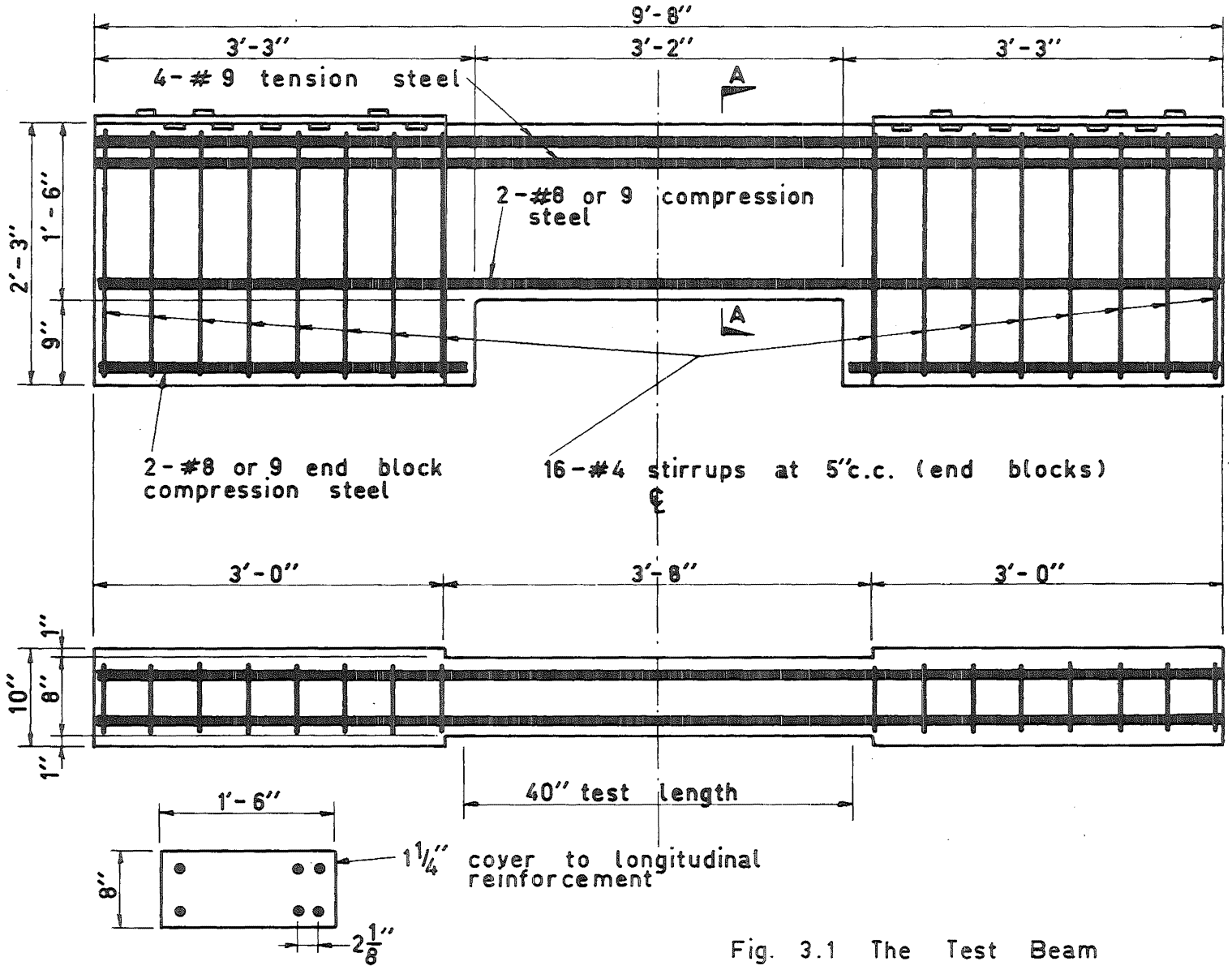

Fig. 3.1 The Test Beam

Table 3.1 Beam Test Section Properties

Beam	t (in)	b (in)	d (in)	d' (in)	Tension Reinforcement		Compression Reinforcement		Web Reinforcement		
					A_s (in^2)	p %	A_s' (in^2)	p' %	A_v (in^2)	s (in)	$p_v=A_v/bs$ %
N1-S0	18.00	8.00	15.09	-	3.956	3.28	-	-	-	-	-
N2-S0	18.00	8.00	15.13	-	3.956	3.26	-	-	-	-	-
N3-S0	17.97	8.00	15.03	-	3.956	3.29	-	-	-	-	-
N1-S62	17.97	8.00	14.97	1.50	3.956	3.30	1.978	1.65	0.0990	6.00	0.206
N1-S32	18.00	8.00	15.02	1.50	3.828	3.18	1.914	1.59	0.0990	3.00	0.412
N1-S63	18.00	8.00	15.00	1.50	3.828	3.19	1.914	1.60	0.226	6.00	0.471
N2-S62	18.00	8.00	15.00	1.50	3.956	3.30	1.494	1.25	0.0990	6.00	0.206
N2-S32	17.97	8.00	15.06	1.47	3.828	3.18	1.914	1.59	0.0990	3.00	0.412
N2-S63	18.00	8.00	15.06	1.56	3.956	3.28	1.978	1.64	0.226	6.00	0.471
N3-S12,4	18.00	7.97	15.06	1.59	3.828	3.19	1.914	1.59	0.3776	12.00	0.395

Table 3.2 Reinforcement Properties *

Designation	Nominal Diameter (in)	Surface	Area A_s (in^2)	Yield Stress f_y (lb/in^2)	Ultimate Stress f_u (lb/in^2)	Youngs Modulus E_s ($lb/in^2 \times 10^6$)	Strain at hardening ε_{sh} (in/in)	$\varepsilon_{sh}/\varepsilon_y$
A	$\frac{1}{4}$"	plain	0.0491	58200	78300	30.5	.0376	19.7
B	$\frac{7}{8}$"	deformed	0.587	46900	68200	30.0	.0291	18.7
C	$\frac{1}{4}$"	plain	0.0495	49900	68500	30.2	.0425	25.8
D	$\frac{3}{8}$"	plain	0.113	46400	70300	29.5	-	-
F	1"	deformed	0.747	44200	70400	30.5	.0235	16.2
G	$1\frac{1}{8}$"	deformed	0.989	44500	66900	30.3	.0245	16.7
H	$\frac{1}{2}$"	deformed	0.1874	45900	68200	30.0	.0350	22.9
I	$1\frac{1}{8}$"	deformed	0.957	44500	71900	31.1	.0190	13.3
J	$\frac{1}{2}$"	deformed	0.1888	45800	67700	31.3	.0290	19.9

* All properties listed are the average of 3 tests except for types A and B, which are the results of tests on only one sample. The Youngs Modulus measured for types F and I are the average of two tests.

3.2.1 Reinforcement Steel

Each batch of reinforcement had tensile tests performed on randomly selected samples before it was used in the test beams. The properties of the steel from each batch are presented in fig. 3.2 and table 3.2. A Baty type extensiometer was used to find the stress-strain relationships for the reinforcement.

The reinforcement batches used in the test beam cages are summarised in table 3.3. It should be noted that the beams without web reinforcement contained no compression steel. Before assembly of the cages $\frac{1}{4}$ inch diameter bright steel studs where welded to the reinforcement upon which demec strain gauge measurements were to be made.

The cages were made up as one unit. Fig. 3.3 shows a cage in the beam mould ready for casting. The four tension bars were welded to a 10 x 4 x $\frac{1}{4}$ inch steel plate at both ends as can be seen in the figure. This was to enable the cage to be assembled more easily and to prevent slip during testing. All the stirrups were tied with wire to each longitudinal bar.

3.2.1.1 Preparation of the Studs for Demec Gauge Measurements

To ensure that the strains measured on the reinforcement were not influenced by the surrounding

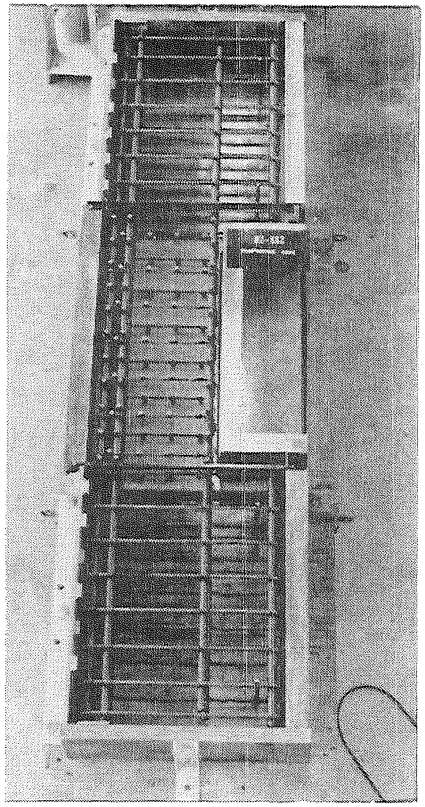

Fig. 3.3 Beam Mould and Reinforcement Cage

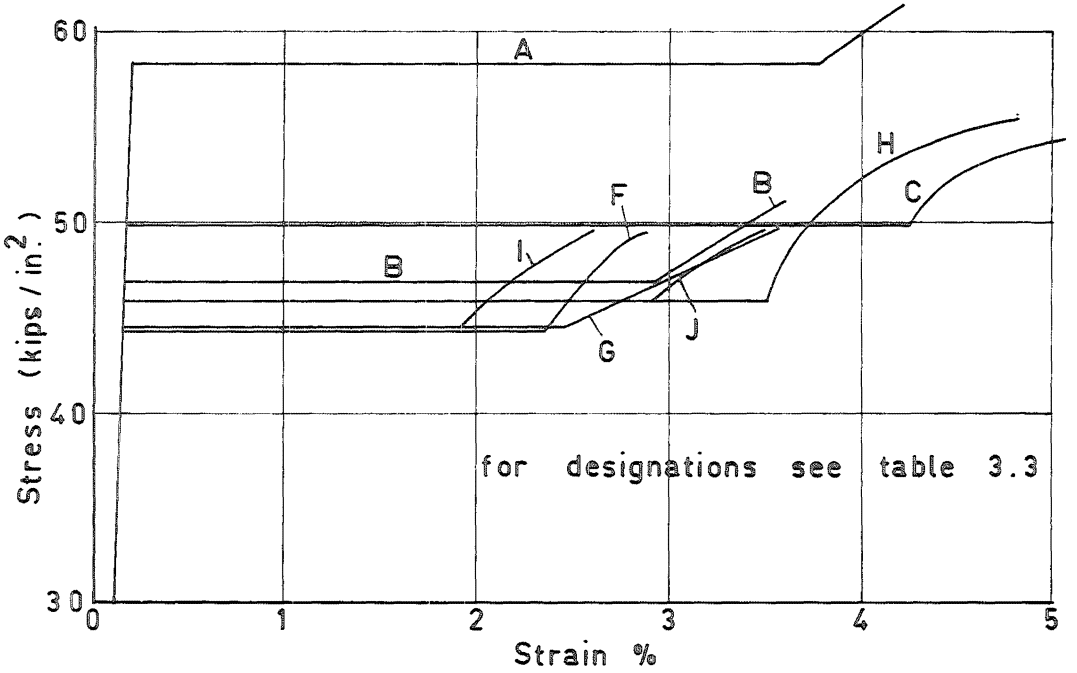

Fig. 3.2 Stress – Strain Relationships of the Reinforcement

Table 3.3 Reinforcement in the Test Beams

Beam	Test Section Reinforcement		End Block Compression Reinforcement	Test Section Stirrups	End Block Stirrups
	Tension	Compression			
N1-S0	G	-	F	-	H
N2-S0	G	-	F	-	H
N3-S0	G	-	F	-	H
N1-S62	G	G	F	C	H
N1-S32	I	I	I	C	J
N1-S63	I	I	I	D	H
N2-S62	G	F	F	C	H
N2-S32	I	I	I	C	J
N2-S63	G	G	G	D	H
N3-S12,4	I	I	I	J	J

For designations see table 3.2

concrete it was necessary to ensure that the steel studs welded to the reinforcement were not in contact with the surrounding concrete. Therefore, before the beams were cast, plastic tubing was placed around the studs and then steel tubing around both. Bituminous putty was used to keep the bottom of the steel tube sealed and then the tube was filled with a low melting point wax. After the concrete was set the wax and plastic tubing were cleaned from inside the steel tubing thus leaving a space between the steel stud and the tubing set in the concrete.

3.2.2 The Beam Mould

The beams were cast on their sides. The mould had a core board base with steel sides and timber ends. The centre section of the base was built up 1 inch with core board finished with perspex. As can be seen in fig. 3.3 the left hand side of both end sections of the mould were cleated plates. These plates were integral parts of the beam and were used to transfer the axial load from the loading frame to the end blocks of the beam.

3.2.3 Concrete

The concrete used in the beams was supplied by "Certified Concrete (Christchurch) Ltd". The mix properties are presented in table 3.4. For each test beam controls consisting of four 6 x 12 inch cylinders,

three 6 inch cubes, and three 12 x 3 x 3 inch prisms were cast and vibrated with an internal vibrator. Table 3.5 gives the properties of the concrete for each beam. The controls were tested on or within three days after the completion date of the beam tests. The standard deviation of all the cylinder, cube and prism tests for the ten beams are listed below:

Cylinder strength	2.5%
Cube strength	2.1%
Modulus of rupture	7.9%

3.2.4 Casting, Curing and Stripping

The concrete was placed in the mould immediately after delivery. It was vibrated with an internal vibrator and screeded. When the surface was sufficiently dry it was finished with a steel trowel, then the controls and beam were covered with wet scrim and a polythene sheet and moist cured for seven days. After curing the beam and controls were stripped and kept in the laboratory until tested.

3.3 The Test Frame

A diagram of the test frame and beam assembly is shown in fig. 3.4, and a photograph of the frame with a beam ready for testing is reproduced in fig. 3.5. The test frame was made of structural steel with welded

Table 3.4 Concrete Mix Properties

Design 28 day strength = 4000 psi. Slump = $2\frac{1}{4}$ inches.		
Aggregate		
Max. Grading	% of Aggregate	State
$\frac{3}{4}$"	34.3	30% crushed
$\frac{1}{2}$"	22.7	30% crushed
Kaiapoi sand	21.8	all natural
Hornby sand	21.2	50% natural
water/cement ratio = .643 water/aggregate ratio = .084		
Additives:- 10 c.c. per yard of Darex AEA 7 fl. ozs per yard of W.R.D.A. (water reducing agent)		
Air content = 4.3%		

connections where possible. The bottom loading frame was bolted to the laboratory strong floor although the floor was not required to provide any reaction to the applied load. The two horizontal members on either side of the top loading frame, that can be seen in fig. 3.5, were to provide lateral support for the beam.

The reaction plates at the left hand end of the three stirrups shown in fig. 3.4 were connected to the loading

Table 3.5 Concrete Properties

Beam	Time to Start of test days	Time of test days	f_c' (1) lb/in^2	f_{cu} (2) lb/in^2	f_t (3) lb/in^2	$\frac{f_c'}{f_{cu}}$	$\sqrt{f_c'}$	$\frac{f_t}{f_c'}$	$\frac{f_t}{\sqrt{f_c'}}$	Density (4) lb/ft^3	E_c (5) $lb/in^2 \times 10^6$	E_c (6) A.C.I. $lb/in^2 \times 10^6$	$\frac{E_c}{E_c \text{ A.C.I.}}$
N1-S0	41	3	4690	5610	652	0.84	68.5	0.139	9.52	148.9	3.82	4.10	0.932
N2-S0	26	3	6005	7340	725	0.82	77.5	0.121	9.35	150.3	4.20	4.71	0.891
N3-S0	48	5	4940	6395	809	0.77	70.2	0.164	11.51	148.2	4.00	4.19	0.955
N1-S62	26	3	4220	5070	559	0.83	65.0	0.132	8.60	146.2	3.51	3.79	0.926
N1-S32	33	3	4000	4450	673	0.90	63.2	0.168	10.64	144.0	3.65	3.60	1.013
N1-S63	81	3	4925	5810	756	0.85	70.1	0.153	10.78	147.4	4.10	4.15	0.988
N2-S62	38	3	4970	6450	691	0.77	70.5	0.139	9.80	147.5	3.42	4.17	0.820
N2-S32	75	3	4860	5390	793	0.90	69.7	0.163	11.38	147.5	4.00	4.12	0.971
N2-S63	40	3	4040	4645	649	0.87	63.5	0.161	10.22	146.5	3.40	3.72	0.914
N3-S12,4	32	3	4635	5625	665	0.82	68.0	0.143	9.78	147.9	3.62	4.04	0.896

1. Average of three 6" x 12" cylinders.
2. " " " 6" cubes.
3. " " " 12" x 3" x 3" prisms.
4. " " cylinders, cubes and prisms.
5. 50% secant modulus from one 6" x 12" cylinder.
6. From ACI 318-63, section 1102.

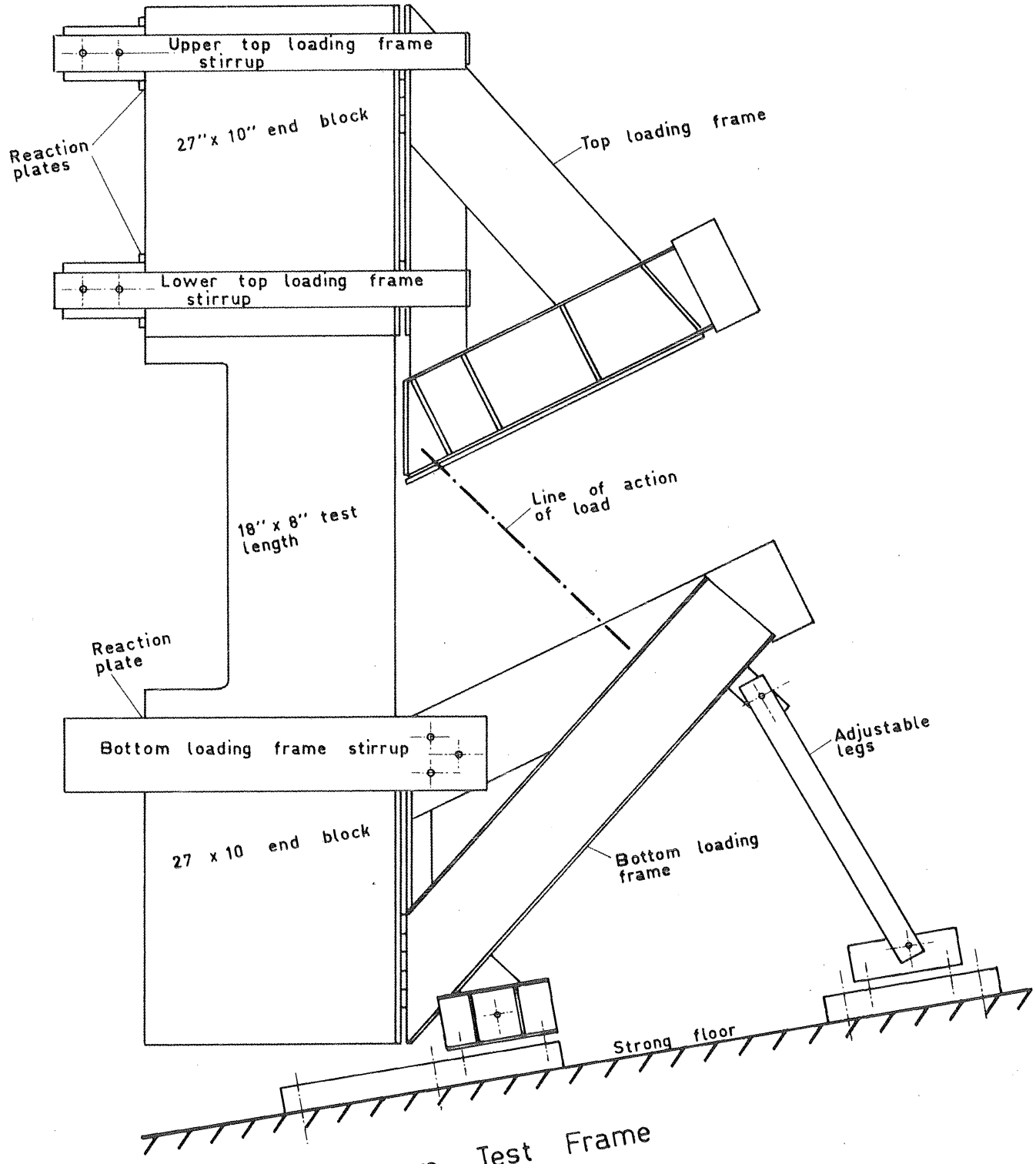

Fig. 3.4 Beam Test Frame

THE LIBRARY
UNIVERSITY OF CANTERBURY
CHRISTCHURCH, N.Z.

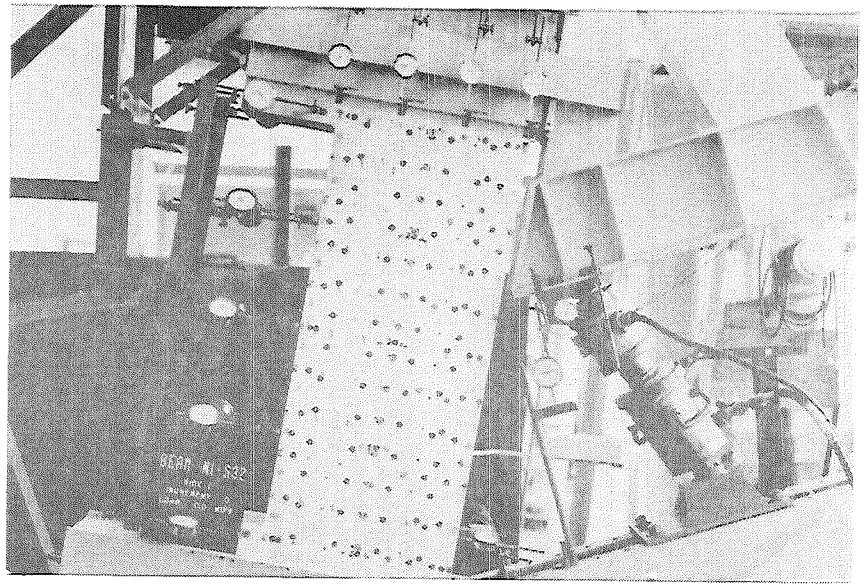

Fig. 3.6 Loading Details

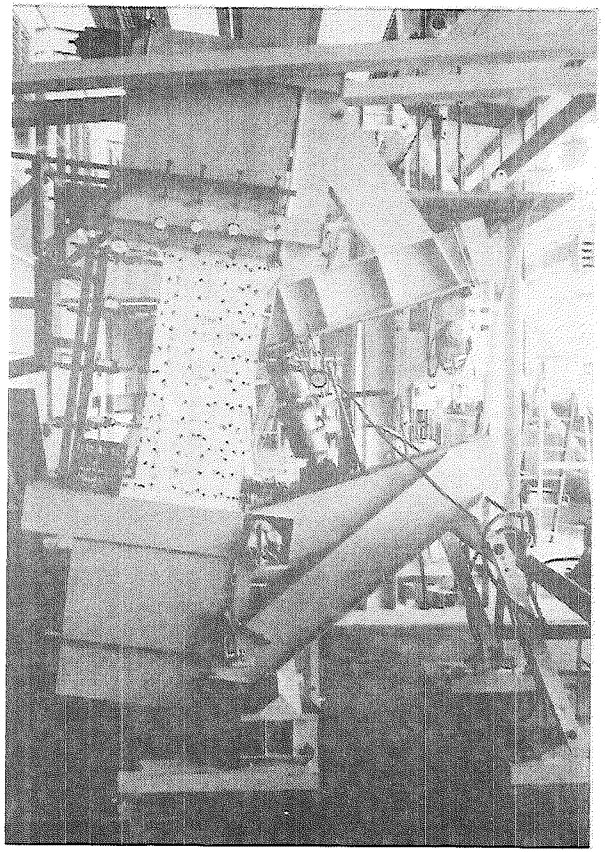

Fig. 3.5 Beam Test Frame

frames by high tensile friction grip bolts. These plates had $\frac{1}{8}$ inch rubber bearing surfaces in contact with the beam. To ensure that the beam was firmly positioned in the test frame the reaction plates were "prestressed" against the beam and then the high tensile bolts were tightened.

The angle of the test beam with the floor could be varied. The original intention was to have the load line vertical for each axial load to shear force ratio but it was found after two tests that it was too difficult to read the demec gauges when the beam was too far from vertical. For the remainder of the tests the beams were kept almost vertical as can be seen in fig. 3.5.

3.3.1 Transfer of Load From the Loading Frame to the Beam

The axial load was transferred from the loading frames to the beam through cleated plates cast into both end blocks of the beam. These plates are shown as part of the beam in fig. 3.1. The cleats on the outside surface of the plates keyed with similar cleated plates welded to the loading frames. It is considered that the axial load was transferred at a sufficient distance from the test length of the beams to have negligible effect on the stress pattern in the test length.

3.3.2 Method of Load Application

The load was applied to the beam by a 60 ton capacity hydraulic jack. A 50 ton capacity load cell was mounted on top of the jack ram. On the top of the load cell and under the base of the jack 2 inch diameter steel balls were mounted. They fitted into smooth spherical cavities in plates attached to the top and bottom loading frames. The two balls ensured that the line of action of the load was known. The load cell and jack assembly can be seen in fig. 3.6. The assembly was lined up on the centre line of the test section of the beams by adjustments in the connections to both the top and bottom loading frames. The strap around the top of the jack was a safety device only and it was not in contact with the jack during testing.

The jack was connected to a pumping system on which a constant pressure could be set. In order to obtain a constant displacement type load a valve was included in the hydraulic line between the jack and the pump. This type of load application is indicated in the beam load sequence tables B.1 to B.10 (see appendix B).

The load on the beam was measured by the load cell and also, if required, from pressure readings on the hydraulic pump. The load cell was calibrated up to a load of 120 kips against one of the laboratory universal testing machines.

3.4 Instrumentation

3.4.1 Demec Gauges

All strains on both the concrete and the reinforcement were measured using demountable mechanical strain gauges (demec gauges). The operation of these gauges is described by Morice [39] and Base [11]. The locating discs required for the demec gauges were attached with sealing wax to the concrete surface and to the steel studs on the reinforcement.

Errors associated with demec gauge reading have been described by Fenwick [18].

3.4.1.1 Demec Gauge Observations

All the demec gauge observations were made on both sides of the beams. 4 and 8 inch gauge lengths were used to measure longitudinal concrete strains over the 40 inch test length of the beams, and 4 inch gauge lengths were used on both the longitudinal reinforcement and over a 12 inch length of the stirrups.

Displacements across cracks were measured by sets of three 2 inch demec gauge lengths. The readings were made along the sides of an equilateral triangle with the base on one side of the crack normal to the beam axis. The apex of the triangle was on the other side of the crack.

3.4.1.2 Corrections to Demec Readings

Temperature control readings were made before each set of demec gauge readings. These were taken on a standard invar bar and on a previously tested beam. It is believed that this procedure eliminated the possible scale effects involved on small temperature control specimens.

The corrections made from the standard bar observations were normally of the order of only 5 or 10 micro-strains.

A typical time temperature correction relationship is shown in fig. 3.7. Also included are the temperature variations in the laboratory. The general trend between the laboratory temperature and the temperature corrections is apparent. The small variations in the corrections are within the limit of accuracy of the demec gauges and hence the reliability of the corrections is small. The 2 inch gauge zero readings were taken at the start of the second day. Consequently the corrections are different from those for the 8 and 4 inch gauges. The corrections as measured were applied to the demec gauge readings but the corrections shown by the broken lines would have been more realistic.

3.4.2 Dial Gauges

Dial gauges were used to find beam deflection characteristics and to trace the variation in the position

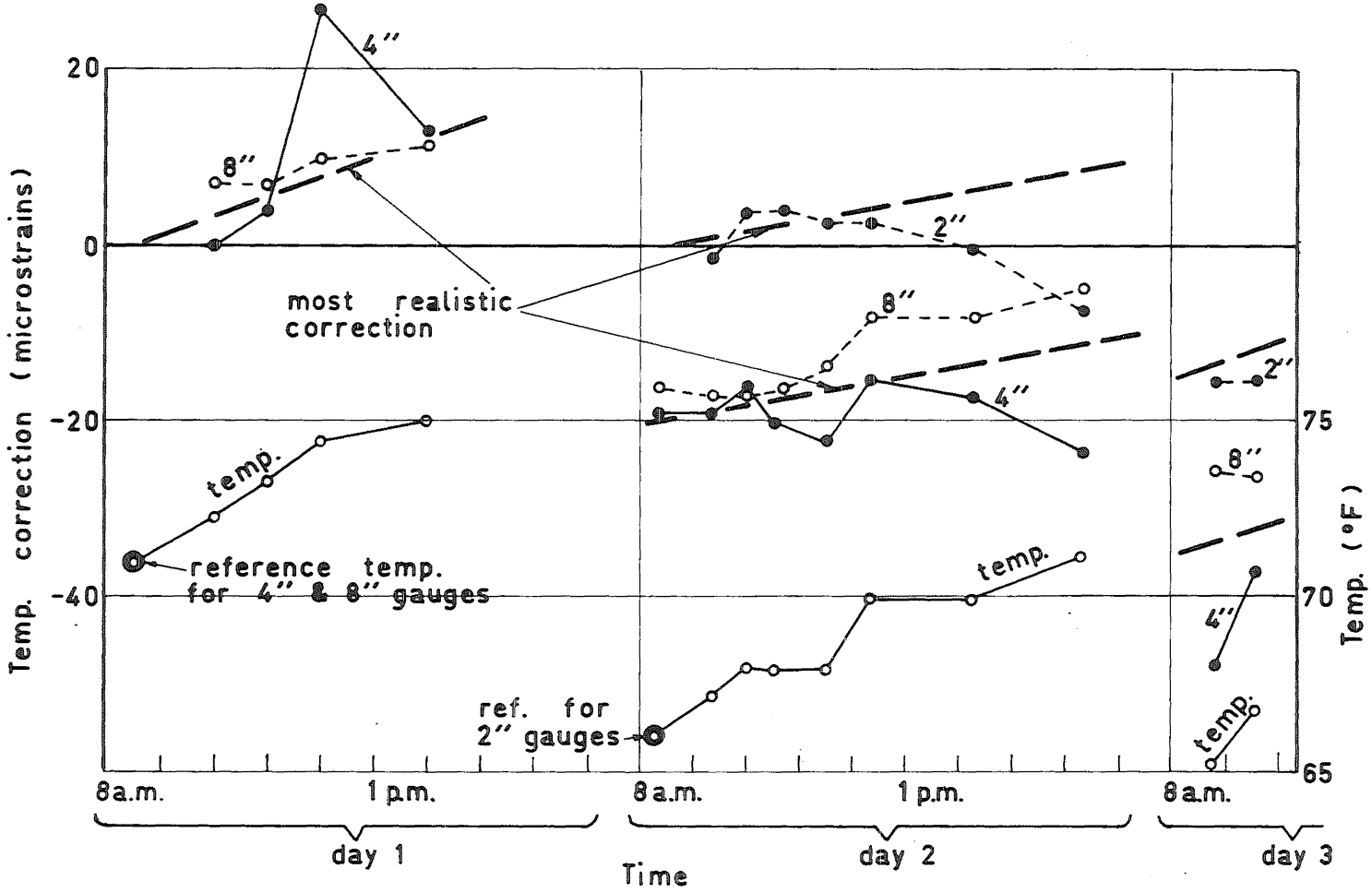

Fig. 3.7 Temperature Corrections for Demec Gauge Readings on Beam N1-S63

of the line of action of the load during a test. The dial gauge observations on beam N3-SO were not reliable. The readings on the gauges used on the other nine beams could be estimated to .0001 inch, one division on the dial being equal to .001 inch.

The positions of the dial gauges can be seen in fig. 3.6. As with the demec gauges all the dial gauges were duplicated on side 2 except for the gauge used to measure the separation of the top and bottom loading frames.

3.4.2.1 Beam Deflection Observations

The dial gauges used to find beam deflections were numbered 1 to 9 in a clockwise direction starting at the bottom left hand corner of fig. 3.6. The stand holding these nine pairs of dial gauges was bolted to the laboratory strong floor and was not in contact with any part of the loading frame.

The beam test length was assumed to be a cantilever fixed 1 inch below the lower reentry corner, i.e., at the section containing dial gauge 1 and the bottom row of demec points. All the deflection observations discussed in the following chapters are based on the deflection of this 40 inch cantilever.

Because there was some distortion of the bottom end block of the beam in the test frame dial gauges 1 to 9

did not measure the true cantilever deformations of the test length. The method of finding beam deflections from the nine pairs of readings was based on the assumption that the sections at the bottom and top of the 40 inch beam test length remained plane at all stages of loading.

Fig. 3.8 illustrates how the true cantilever deflection Δ, of a beam was found. The apparent deformation, as measured by the dial gauges, consists of a longitudinal and transverse rigid body translation and a rigid body rotation, as well as the true cantilever deflection. The following steps were taken to correct for the rigid body movements owing to deformation of the bottom end block of the beam.

(i) The transverse rigid body translation, Δ_t was corrected by subtracting the displacement Δ_t measured by dial gauge 1, from the readings of gauges 1 to 5.

(ii) To find the rigid body rotation Ψ_r, it was necessary to know the actual rotation of section AA' with respect to BB'. This was achieved by calculating the total elongation of the cantilever at various locations transversly across the beam. Summing demec gauge measurements on the concrete along the beam achieved this. From a linear regression analysis of the elongations, "plane" section AA'

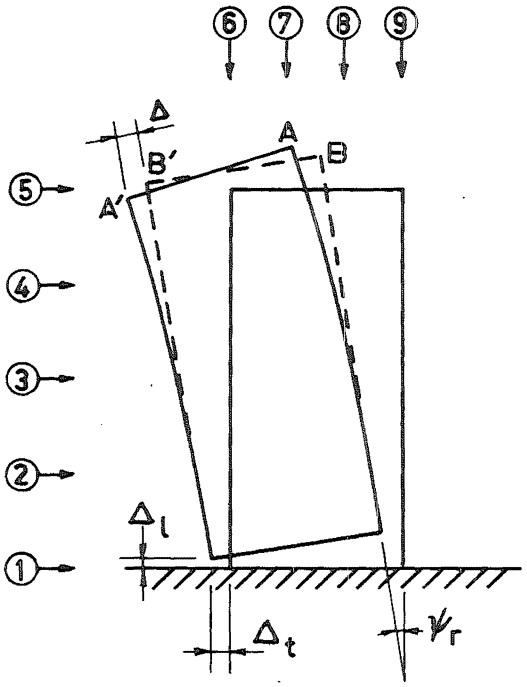

Fig. 3.8 Corrections to Dial Gauge Readings

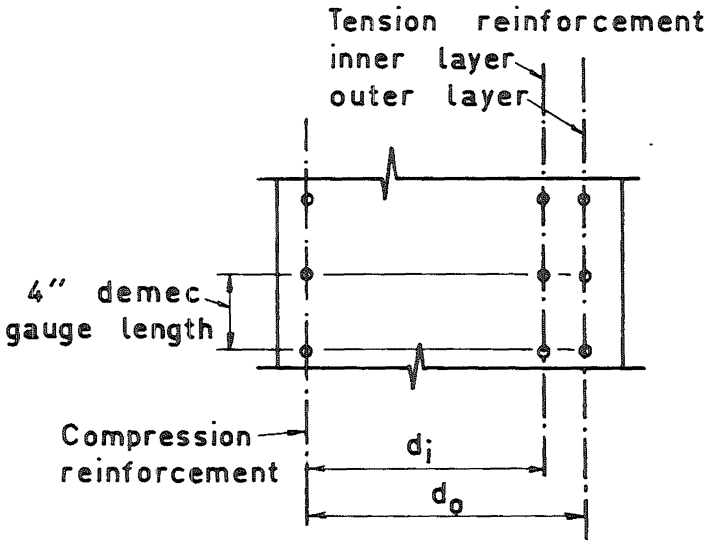

Fig. 3.9 Method of Calculating Curvatures

was defined in relation to section BB'. Section AA' was located by readings on dial gauges 6 to 9 as well. This "plane" section was also defined using a linear regression analysis on these dial gauge readings. The difference between the slopes of the "plane" sections calculated on the dial gauge readings and the total beam elongations represented the rigid body rotation ψ_r. This was used to correct readings of dial gauges 1 to 9 for the rigid body rotation.

(iii) Dial gauges 6 to 9 were corrected for the rigid body longitudinal translation Δ_1. It was found from the difference between the two "plane" section (defined in (ii) above) intercepts at the compression face of the beam, i.e., at dial gauge 6.

3.4.2.2 Location of the Line of Action of the Load

The line of action of the load was determined before the beam was tested. Small variations in this, which are listed in tables B.1 to B.10, were measured by the dial gauges on the right of the test section shown in fig. 3.6. The top and bottom gauges measured the movement of the top and bottom loading frames normal to the axis of the beam. The middle gauge measured the

relative movement of the two loading frames.

3.5 Method of Testing

The method of testing involved the following steps:

(i) Taking initial zero readings for all 8 and 4 inch demec gauges and dial gauges.

(ii) Loading the beam in at least two increments to the stage when flexural cracks were well developed. This was at approximately 30 to 40% of ultimate flexural capacity.

(iii) Unloading the beam to zero load and taking a complete set of readings.

(iv) Attaching the triangular sets of 2 inch demec gauge lengths across the cracks.

(v) Taking zero readings of the 2 inch gauges and also a set of readings on all the other demec and dial gauges. (From comparison of readings in steps (iii) and (v) it could be ascertained if the existing gauges had been inadvertantly tampered with when attaching the 2 inch gauge lengths).

(vi) Loading the beam in several increaments to failure.

3.5.1 Zero Readings

The demec gauge zero readings were all taken

at least twice. If the two readings were not within 10, 20 and 25 microstrains for the 8, 4 and 2 inch gauges respectively, then the gauge was read until this tolerance was obtained for at least two successive observations. The dial gauge zeros were also read twice.

3.5.2 Order of Operations at Each Load Increment

The following sequence of operations was observed at each load increment:

(i) The beam was loaded and the hydraulic line between the pump and jack was left open for a given time. The load and time were recorded.

(ii) The valve in the line was closed.

(iii) The beam was allowed to stand for several minutes for irreversible elastic deformations to occur, and cracks to develop.

(iv) The cracks were found using a x10 magnifier, and marked.

(v) If required the beam was photographed.

(vi) All demec gauge standard bars and temperature corrections were read.

(vii) The laboratory temperature, load on the beam and time were noted.

(viii) All dial gauges were read.

(ix) 4, 8 and 2 inch demec gauges were read in that order.

(x) All dial gauges were read again.

(xi) The load on the beam and time were recorded.

(xii) The standard bars were read.

(xiii) The beam was loaded to the next increment.

The load sequences for all the beams are presented in tables B.1 to B.10. As noted in the tables the loading sequence of four of the beams did not include the last part of step (i) nor step (ii).

3.6 The Results

3.6.1 Flexural Deflections

The flexural deflections of the test beams were calculated from curvatures, the definition of which will be discussed in chapter 4. Fig. 3.9 shows how curvatures were found from observations made on the beams. The demec gauge lengths used to calculate curvatures at each section of the test length were on both layers of tension reinforcement and on the compression reinforcement. If there was no compression steel the 4 inch gauge lengths on the concrete at $\frac{1}{4}$ inch from the compression face were used. The following strains were measured in the reinforcement (or compression zone concrete) at a section:

ε_{so} = strain in outer layer of tension steel

ε_{si} = strain in inner layer of tension steel

ε'_s = strain in compression steel (or concrete).

Two curvatures, one from each layer of tension steel, can then be found at a section

$$\varphi_o = \frac{\varepsilon_{so} - \varepsilon'_s}{d_o}$$

$$\varphi_i = \frac{\varepsilon_{si} - \varepsilon'_s}{d_i}$$

d_o and d_i are defined in fig. 3.9. The average value of the two curvatures was taken as the curvature φ, of the section, i.e.,

$$\varphi = \tfrac{1}{2}(\varphi_o + \varphi_i) \qquad (3.1)$$

From the known curvatures along the test length of the beam the flexural deflections can be calculated using a summation process. The rotation of an infinitesmal element of length s_e, is $\theta = s_e \varphi$. The deflection of one face of an element from the tangent at the other face is given by:

$$\delta = \frac{\theta s_e}{2}$$

The total deflection of n elements from the tangent at the face of the first one is

$$\Delta_n = \sum_{r=1}^{n} \delta_r + \sum_{r=2}^{n} \left(\sum_{i=r}^{n} s_{e_i} \right) \theta_{r-1} \qquad (3.2)$$

For the cantilever test length of the beams the curvatures of ten elements, each 4 inches in length is known. Hence the flexural deflections of the test beams are given by

$$\Delta = 8 \sum_{r=1}^{10} \varphi_r + 16 \sum_{r=2}^{10} \varphi_{r-1}(11-r) \qquad (3.3)$$

where φ_r is the average curvature of element r.

3.6.2 Presentation of Test Results

All the test results plotted in subsequent chapters, except for the displacements across cracks, are the average of observations on both sides of the test beams. Two examples of the advantage of averaging observations follow.

When reinforcement strains are measured localised effects of cracking cause variations in the strain distribution. Averaging strains from both sides of the beams enables smoother strain distributions to be plotted.

Slight differences in deflection characteristics of the beams were noted from observations on either side of the test beams. This was caused by twisting because of non-uniformity of beam properties. By plotting the average deflection the differences in the deflections owing to this effect were eliminated.

When plotting the tension reinforcement strain distributions the average of the strains in the four reinforcement bars was used. Fig. 3.10 shows a typical average strain distribution and the individual distributions of the four bars. The large variation of strains from the average in the region of gauge rows

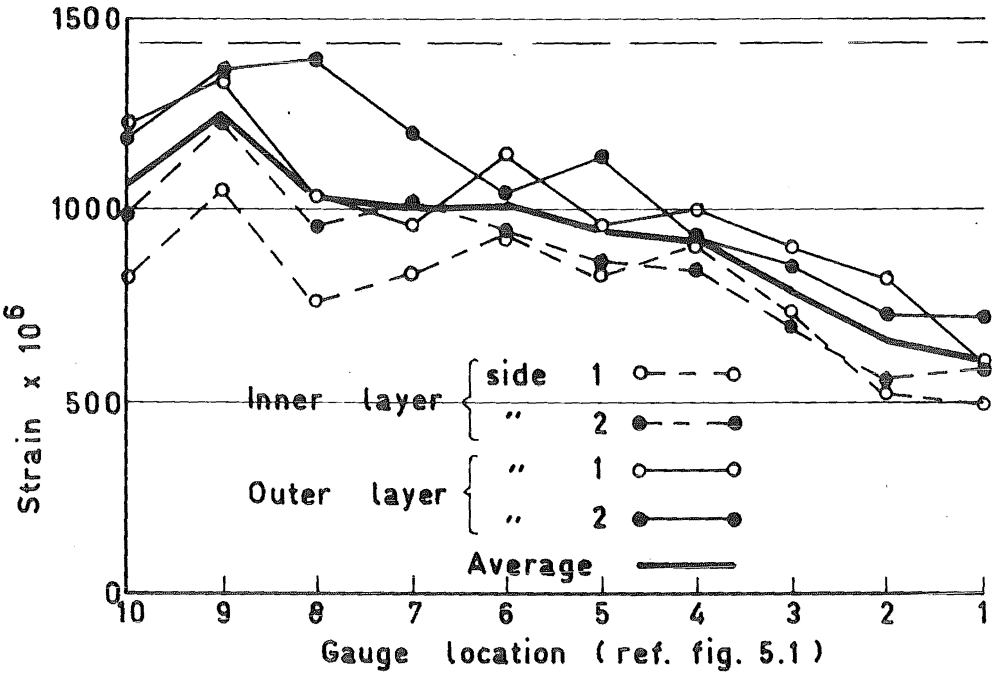

Fig. 3.10 Tension Reinforcement Strain Distribution in Beam N2-S32 at ·736 P_u^*

7 to 10 is caused by diagonal cracks intersecting the reinforcement at different gauge locations on either side of the beam.

In both the concrete and reinforcement strain distributions and various other plots presented in chapters 4 to 8, each distribution is identified by the proportion of the Whitney ultimate flexural capacity of the particular beam at which it was observed. These are given in tables B.1 to B.10. They are based on the load sustained by the beams after all the demec and dial gauges have been read, i.e., after short term creep of the beams and/or the loading system.

3.7 Time Effects of Loadings

Short term creep observations were made on the beams during testing. The load was recorded along with the time at three stages during each load increment; once when the maximum load was attained, again at the start of reading the gauges, and a third time after all these gauges were read. The load readings and times are given in tables B.1 to B.10.

The beams did not lose more than a few percent of yield load at any increment before yield of the tension reinforcement, but after this the loss was larger. Part of the loss of load after the valve in the hydraulic line was closed was a result of variations in the

hydraulic system. As the beam deformed after closure of the valve the volume of the jack reserviour increased and hence the pressure fell somewhat. However, the loading system was very nearly of the constant displacement type when the valve between the pump and jack was closed.

3.8 Shrinkage

Although the test beams were moist cured for seven days after casting they showed signs of considerable shrinkage. It was observed in all of the beams that cracks became visible at less than half of the theoretical cracking load based on the modulus of rupture of the concrete.

The stiffnesses of three of the test beams were measured at very low loads. Well before the theoretical cracking loads were reached the stiffnesses of these beams were found to be less than the theoretical stiffness based on an uncracked section. The premature formation of cracks is believed to be a result of tensile stresses set up in the concrete because of shrinkage.

In several of the beams with web reinforcement cracks were observed along the stirrups before any load had been applied. Some of these cracks developed across the full depth of the beams. Similar cracks appeared after the first load increment. These cracks along the stirrups formed predominantly on the top surface of the

beam (side 1) as cast. Normally they did not propagate or widen after the first or second load increment. It is believed that they did not effect the crack propagation characteristics of the beams at higher loads. The cracks along the stirrups were marked and they can be seen in the photographs of the beams shown in chapters 4 and 5. Their overall effect on beam behaviour is assumed to be negligible.

CHAPTER 4

BEAMS WITHOUT WEB REINFORCEMENT

4.1 Introduction

In this chapter the behaviour of three reinforced concrete beams tested to failure by the author will be discussed. These beams contained no web reinforcement in the test section, and all three were identically reinforced. They were loaded in such a way as to produce the combined action of shear, flexure and axial tension. The major variable in the three tests was the ratio of axial tension to shear force. The axial tension in each of the tests was nominally one, two and three times the applied shear. The beam designations are N1-S0, N2-S0 and N3-S0 respectively.

4.2 Scope of the Tests

The three tests were designed to find the effect of axial tension on the shear strength of reinforced concrete beams without web reinforcement. In order to obtain a shear failure in the beams the applied moment was as small as possible. To achieve this the loading assembly described in chapter 3 was as close to the tension face of the beam as allowed by the dimensions of the load cell and jack. This meant that the M/Vd

ratio was not constant for the three beams because of the necessary variation in the position of the points of zero moment. The inadequacy of the M/Vd ratio to explain some aspects of shear behaviour in these beams, will be discussed in section 4.7.3.

The concrete strength of the three beams was not intended to be varied. However, some variation was unavoidable, but this should not have affected the basic mechanisms of behaviour of the beams.

Strain measurements were made on the flexural reinforcement and the concrete. Crack widths, and displacements along the cracks were calculated from measurements made across selected cracks in each beam. Total deflections were found for beams N1-SO and N2-SO, and flexural deflections were found for the three beams. From this data, and from qualitative observations of crack patterns and failure modes, the influence of axial tension on the mechanism of shear failure of the beams is evaluated.

4.3 Definitions

4.3.1 Equivalent Curvature

The usual definition of curvature as applied to flexure, is the rotation per unit length of one section in a beam with respect to an adjacent section. Once a diagonal crack forms in a reinforced concrete beam,

plane sections do not remain even approximately plane. Hence this definition of curvature becomes meaningless in the region of diagonal cracking.

As described in chapter 3 curvatures have been calculated for the beams tested in this investigation. These will be called equivalent curvatures because they are influenced by diagonal cracking. All they represent is the rotation of imaginary plane sections. Fig. 4.1 is a sketch of deformations of sections at a diagonal crack. Let s_e be the distance between each section before application of load. Let l_c and l_t be the lengths of A'B' and AB respectively, after diagonal cracking, and let the original distance between them be d_1. The equivalent rotation between the two imaginary sections AA' and BB' is:

$$\frac{(l_t - s_e) - (l_c - s_e)}{d_1} \quad \text{radians}$$

The equivalent curvature φ_e of the element enclosed by the sections is then given by:

$$\varphi_e = \frac{l_t - l_c}{s_e d_1} \tag{4.1}$$

4.3.2 Section Rotation

Once yielding has developed in the tension reinforcement of a reinforced concrete beam, the section ductility can be defined as φ_u/φ_y where φ_u is the curvature of the section at ultimate load and φ_y is the

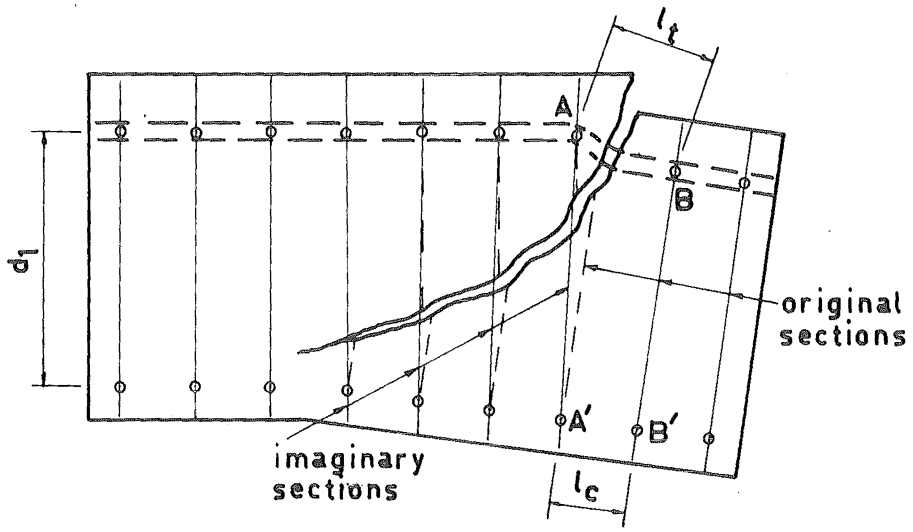

Fig. 4.1 Deformation of Sections at a Diagonal Crack

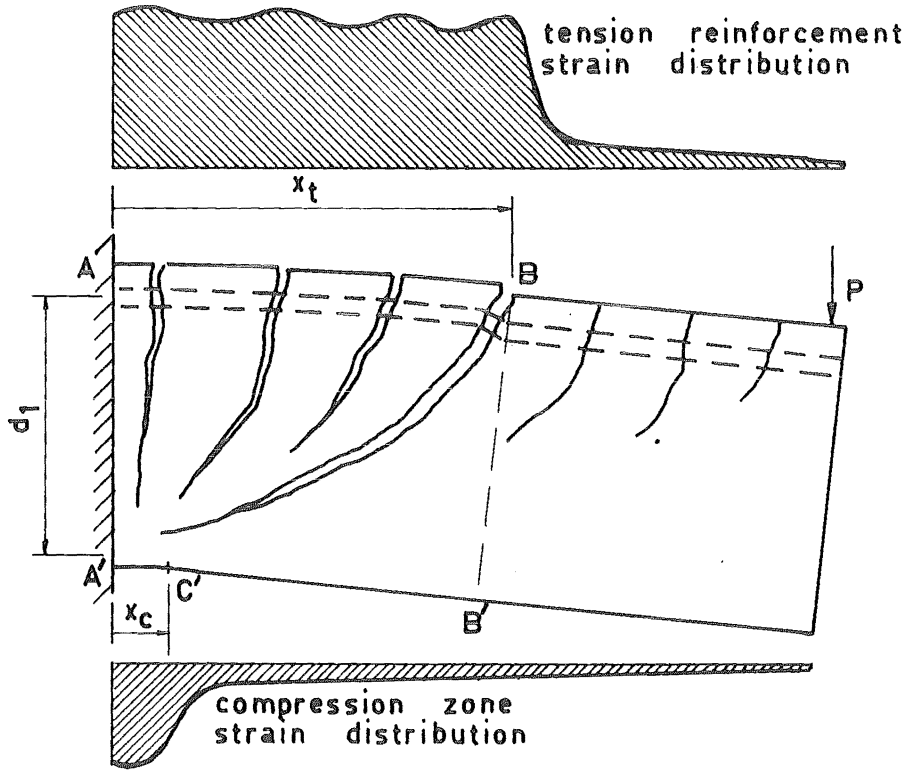

Fig. 4.2 Post-Elastic Deformations of a Cantilever Containing a Diagonal Crack

curvature at yield. If a diagonal crack has crossed the section, the curvature of the section has no meaning (see section 4.3.1). Therefore, to enable section ductility to be defined the rotation of a section of a beam crossed by a diagonal crack must be found.

Consider the cantilever shown in fig. 4.2. The elastic rotation θ_e of the section containing the diagonal crack is the rotation of section BB' with respect to section AA'.

$$\theta_e = s_e \sum_{i=1}^{x_t} \varphi_{e_i} \qquad (4.2)$$

where s_e is the distance between each section before load application. φ_e is defined in Eq. (4.1).

The strain distributions when plastic deformation has developed are as shown in the figure. Experimental evidence for the short region of plastic deformation in the compression zone is given in chapter 5. It is assumed that once the ultimate load on the cantilever is attained the triangular block of concrete BB' C' does not deform further. Using the notation of section 4.3.1. the plastic rotation between section AA' and BB' is

$$\theta_p = \frac{1}{d_1}\left(\sum_{i=1}^{x_t} (l_{t_i} - s_e) - \sum_{i=1}^{x_t} (l_{c_i} - s_e) \right) \qquad (4.3)$$

Eq. (4.3) ignores any strains between C' and B'. If these strains are included

$$\theta_p = \frac{1}{d_1}\left(\sum_{i=1}^{x_t} (l_{t_i} - l_{c_i})\right)$$

$$= s_e \sum_{i=1}^{x_t} \varphi_{e_i} \qquad (4.4)$$

Combining Eqs. (4.2) and (4.4) to give θ_p/θ_e gives

$$\frac{\theta_p}{\theta_e} = \frac{\left(\sum_{i=1}^{x_t} \varphi_{e_i}\right)_p}{\left(\sum_{i=1}^{x_t} \varphi_{e_i}\right)_e} \qquad (4.5)$$

If $\theta_e = \theta_y$ and $\theta_p = \theta_u$, where the subscripts y and u denote yield and ultimate load respectively, Eq. (4.5) gives the section ductility of a section containing an entire diagonal crack.

4.4 Beam N1-SO

Various aspects of the behaviour of beam N1-SO will now be discussed. The initial axial tension to shear force ratio, and the M/Vd ratio, were

N/V = 0.98	M/Vd = 2.88

The variation in the N/V ratio at each load increment is given in table B.1 of Appendix B. The

M/Vd ratio is based on the assumption that the point of zero moment in the beam is at the section where the line of action of the load crosses the geometric centre of the beam. Fig. 4.3 shows the line of action of the load and the 4 inch demec gauge row locations on beam N1-SO.

4.4.1 Behaviour of the Tension Reinforcement

The average strains from the four tension reinforcement bars are shown in fig. 4.4. Only the load increments from the second cycle of loading are shown in this figure. The results obtained at equal loading in the first and second load cycle were similar. This was the case for all the beams tested.

The dashed line in fig. 4.4 is the theoretical strain profile at .360 P^*_u, calculated on a cracked elastic section. The agreement is very good.

4.4.2 Concrete Strains

The maximum concrete compression observed during the test was 900 microstrains. This was measured one quarter of an inch from the compression face of the beam, at gauge row 10 (see fig. 4.3). The observation was made at 79.7% of the experimental failure load. The corresponding concrete stress was 66.1% of its ultimate strength.

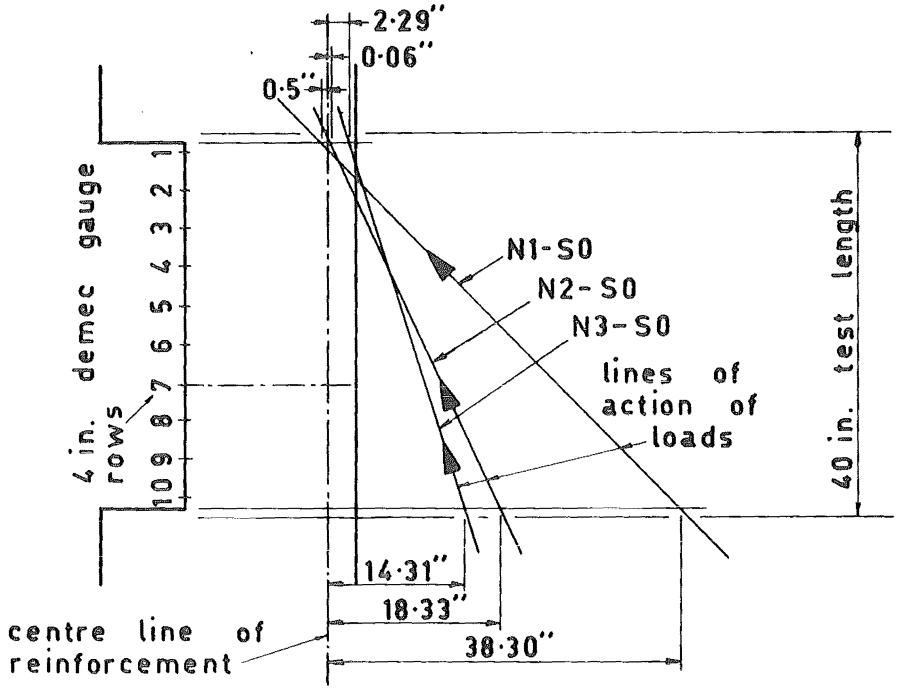

Fig. 4.3 Load Position and 4 inch Demec Gauge Row Position on the Beams Without Stirrups

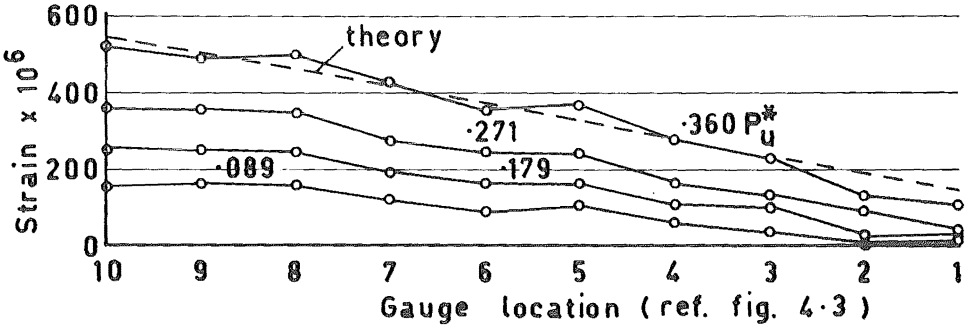

Fig. 4.4 Tension Reinforcement Strains in Beam N1-S0

4.4.3 Crack Development

A photograph of the failed test section of beam N1-SO is shown in fig. 4.5. All the observed cracks and the load increments at which they were formed have been marked. Load increments and corresponding loads are given in table B.1. The failure diagonal crack is seen to be an extension of a flexural crack.

Fig. 4.6 gives a schematic representation of the displacements across the cracks in side 1 of the beam. The failure crack is shown by the dashed line. Maximum crack widths observed were of the order of .002 inches with the widest crack being .0026 inches. The maximum displacement normal to the longitudinal axis of the beam was .00135 inches. These normal displacements will be referred to as displacements "along" a crack. In general the relative movement along the cracks in the beam is greater near the top of the crack than at the level of the reinforcement. This will be discussed further in section 4.7.1.

The crack spacing on both sides of the test section was uniform, the spacing being 4 inches at the height of the reinforcement. This uniformity is attributed to the discontinuities in the concrete where the gauge points on the reinforcement were located (see fig. 4.5).

The cracks in the beam developed slowly. There were several cracks at .088 P_u^* in the first load cycle. This

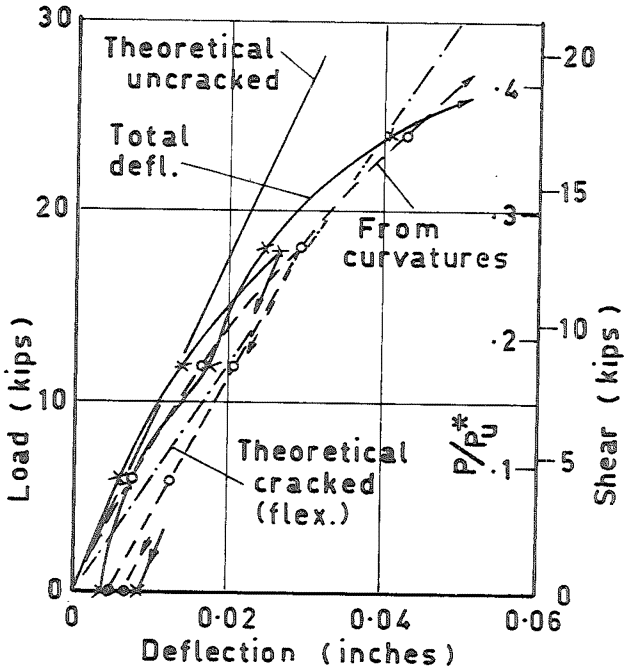

Fig. 4.7 Beam N1-S0 Load–Deflection Relationships

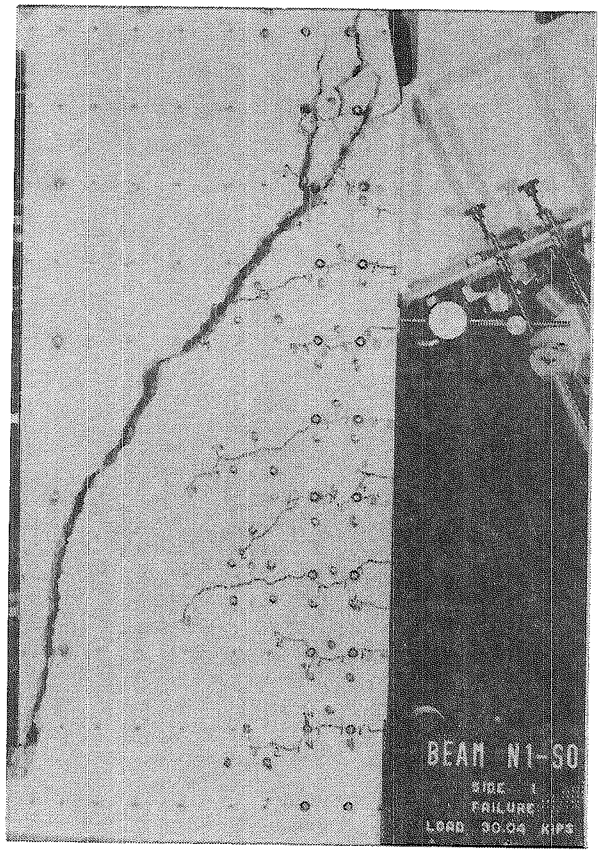

Fig. 4.5 Beam N1-S0 at Failure

(For Fig. 4.6 see p. 129)

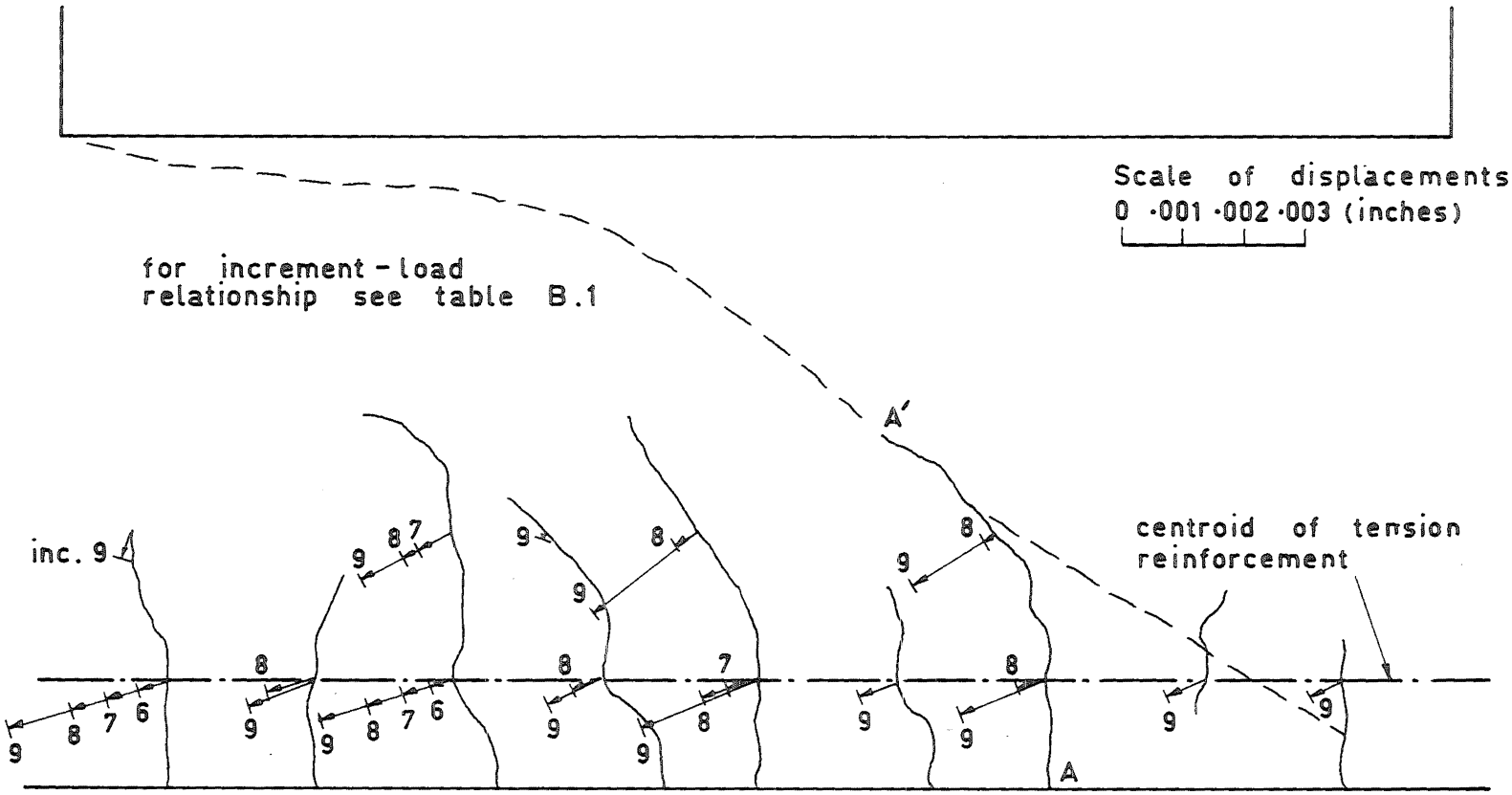

Fig. 4.6 Displacements Across Cracks in Side 1 of Beam N1-S0

was well below the theoretical cracking load based on the modulus of rupture of the concrete. Early cracking was observed in all the beams tested. The likely cause of it is shrinkage stresses set up during setting and curing of the concrete. The cracks, once formed, propagated slowly and inclined slightly towards the region of maximum moment. At no stage did the cracks give any indication of impending failure.

There was no evidence of dowel cracking or aggregate interlock cracking during the test. Both these types of cracking were defined by Fenwick [18]. In future they will be referred to as secondary tension cracks. In other tests these secondary cracks become visible only when flexural cracks were well developed. In this beam the cracks were not well enough developed for secondary cracking to occur. With relatively short cracks the displacements across them are not large enough to produce the dowel or aggregate interlock shears required to initiate secondary tension cracks.

4.4.4 Deformation Characteristics

The load deflection curves for beam N1-SO are shown in fig. 4.7. The theoretical deflection lines are based on the uncracked concrete section and on the flexural deformations of the flexurally cracked beam.

The transformed moment of inertia and the measured Young's modulus of the concrete were used in the calculation of the deflection of the uncracked beam. Shear deflections were also included. The deflection relationship shown by the dashed line is calculated from measured equivalent curvatures in the beam. Some of these are plotted in fig. 4.8. The full curves in fig. 4.7 give the load deflection relationship found from the dial gauge readings. The basis of the deflection measurements from dial gauges, and the method of calculating deflections from equivalent curvatures, were described in chapter 3.

The deflections calculated from equivalent curvatures should be less than the total observed deflection. The difference in the two is the shear displacement, which does not produce curvature. In fig. 4.7 this is seen not to be the case. The most probable explanation is the unsatisfactory dial gauge stand which was used during the tests of the beams without web reinforcement. This also accounts for the total deflection being smaller than the theoretical deflection, up to a load of 12 kips.

4.4.5 Failure

The failure of beam N1-SO occurred without warning. The load had been applied for several minutes when the diagonal crack started to form. It propagated very quickly and within a few seconds of the crack being

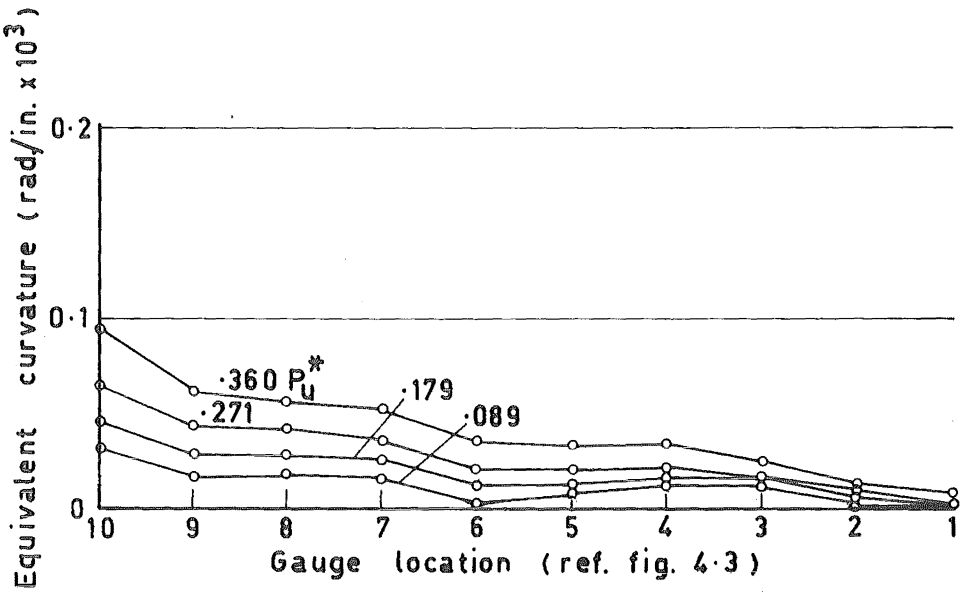

Fig. 4.8 Equivalent Curvatures in Beam N1-S0

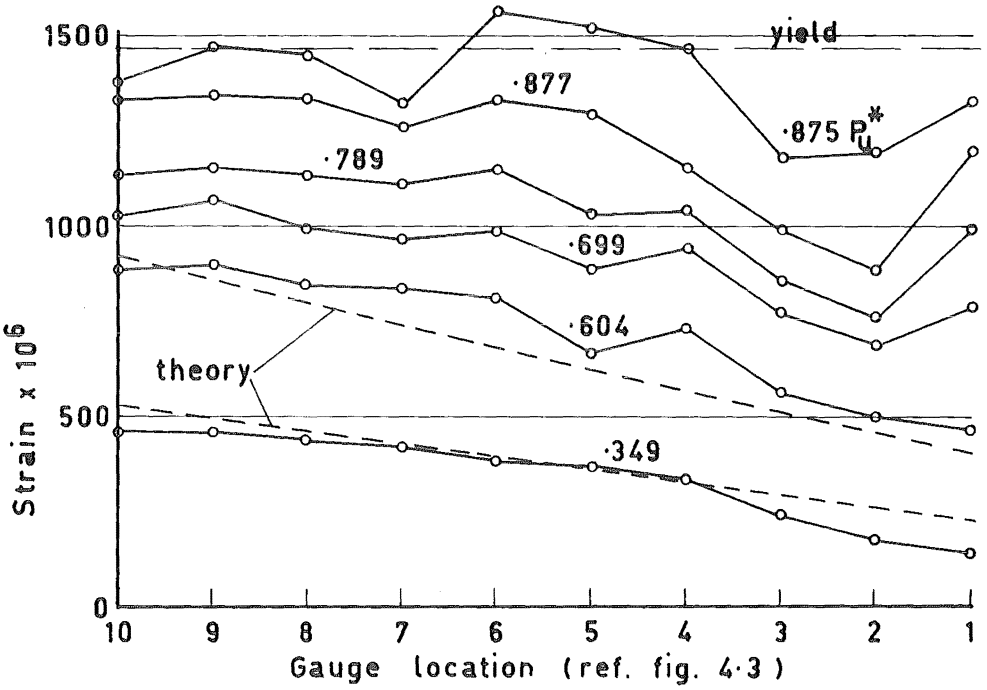

Fig. 4.9 Tension Reinforcement Strains in Beam N2-S0

first observed the beam had failed. At the time of failure the cracks at load increment 10 were being traced. The failure crack started as an extension of the crack AA' (see fig. 4.6). It propagated in both directions from A' as shown by the dashed line in the figure. The whole beam separated along the crack as can be seen in fig. 4.5.

4.5 Beam N2-SO

For beam N2-SO the initial ratio of axial tension to shear force and the M/Vd ratio were

$$N/V = 2.08 \qquad M/Vd = 3.36$$

The interpretation of the M/Vd ratio as applied to a beam subjected to axial load was reviewed in section 4.4. The position of the line of action of the load, and the 4 inch demec gauge rows, are shown in fig. 4.3.

4.5.1 Behaviour of the Tension Reinforcement

Selected longitudinal tension reinforcement strain profiles can be seen in fig. 4.9. The dashed lines are two theoretical strain profiles calculated on the assumption that the beam consists of cracked elastic sections. The loads used to calculate these strains correspond to .349 and .604 P^*_u. As is shown in the

figure, at .349 P_u^* the experimentally observed strains in the reinforcement are smaller than those determined from theory. This is due to some tension being carried by the concrete when the beam is in a lightly cracked state. However, at the higher load the measured strains are somewhat larger than the calculated ones. The high experimental reinforcement strains are a result of inclining of the cracks. An example of strains in the four separate reinforcing bars, and the two separate layers, have been shown in chapter 3. It is not intended to show these for every beam because the average strains from the four bars give an adequate representation.

Fig. 4.10 shows beam N2-SO at failure. The two major diagonal cracks cross the reinforcement at gauge rows 1 and 6. The upper crack formed at .699 P_u^*. In fig. 4.9 a sharp increase in the tension reinforcement strain at gauge row 1 can be seen after this load. Similarly the eventual failure crack first formed at .789 P_u^*. An increase in strains at gauge row 6 is also apparent in fig. 4.9. This becomes more pronounced as a crack developes.

The external moment at the top of a diagonal crack is resisted by the following forces; the tension reinforcement force where the diagonal crack crosses the tension steel, the compression force in the concrete and compression reinforcement above the crack, stirrup forces

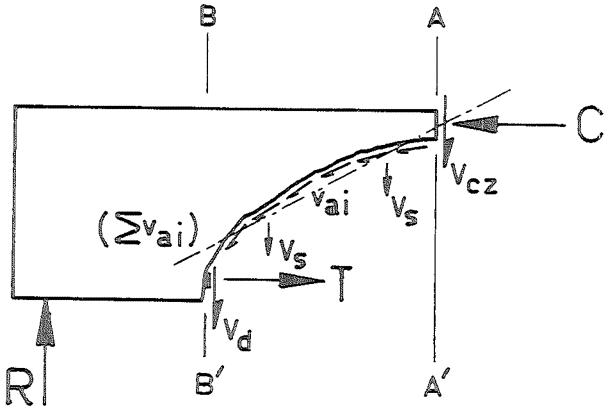

Fig. 4.11 Forces Across a Diagonal Crack

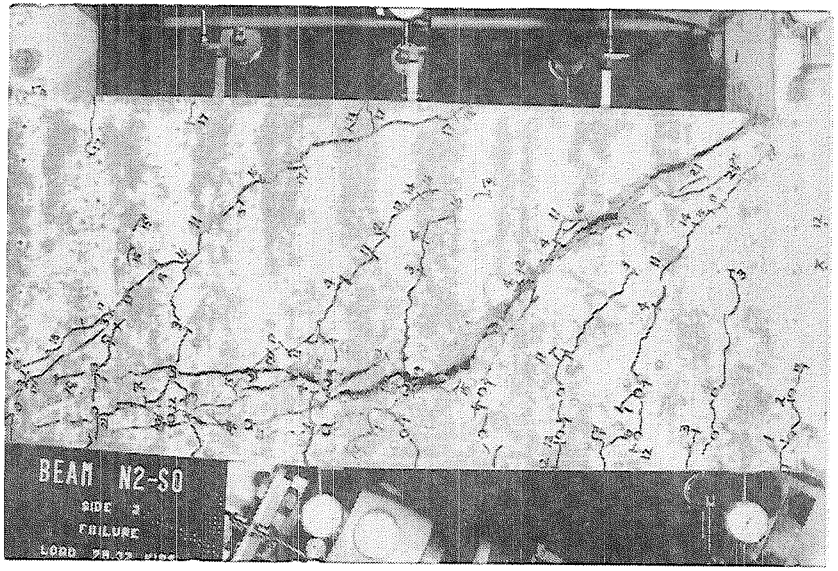

Fig. 4.10 Beam N2-S0 at Failure

if any, aggregate interlock along the crack, and dowel action of the tension reinforcement. These are shown in fig. 4.11. The resultant of the v_{ai} stresses along the crack pass close to the centroid of C at the top of the crack. Therefore their contribution to the resistance of the moment is likely to be small. Hence the only forces in beams without stirrups to resist the moment at section AA' are V_d and T. If the dowel shear is also small the tension reinforcement force at section BB' must resist the moment at section AA'. This accounts for the increased strains in the tension reinforcement where it is crossed by a diagonal crack. This is quantitatively evaluated in chapter 8.

4.5.2 Concrete Strains

At .875 P_u^* the concrete compression at gauge row 10 was 3400 microstrains. Even at this stage the concrete was showing no signs of crushing. The high strain was quite localised as only 1250 microstrains was measured at gauge row 9. The concrete compression zone was very shallow at this load. The failure diagonal crack had penetrated to within about $\frac{3}{4}$ inches of the compression face and below this the beam showed considerable flexural cracking. From traditional ultimate strength analysis of the beam the neutral axis depth would be 3.28 inches.

4.5.3 Crack Development

4.5.3.1 Flexural Cracking

Flexural cracking became visible at .087 P_u^* . Several cracks up to 5 inches long appeared although they were not expected to form until over twice this load. The early formation of these cracks can be attributed to shrinkage as was the case with beam N1-SO. Once the flexural cracks had formed they propagated progressively up the beam with increasing load. Again they formed 4 inches apart at the openings for gauge points.

At 50% of ultimate load the maximum crack widths were of the order of .0035 inches. At .604 P_u^* the maximum crack width was .0046 inches.

Displacements along and across cracks in side 2 of beam N2-SO are presented in fig. 4.12. The general crack pattern at .875 P_u^* is shown. Because of dowel cracking some of the measured displacements at higher loads became meaningless, so these have been omitted. It is worth noting that the displacements along the cracks are, in general, smaller near the tension face of the beam than near the centre. The exceptions to this are where secondary cracks have intercepted the 2 inch demec gauge positions.

4.5.3.2 Diagonal Cracking

After loading to .699 P_u^* the beam was

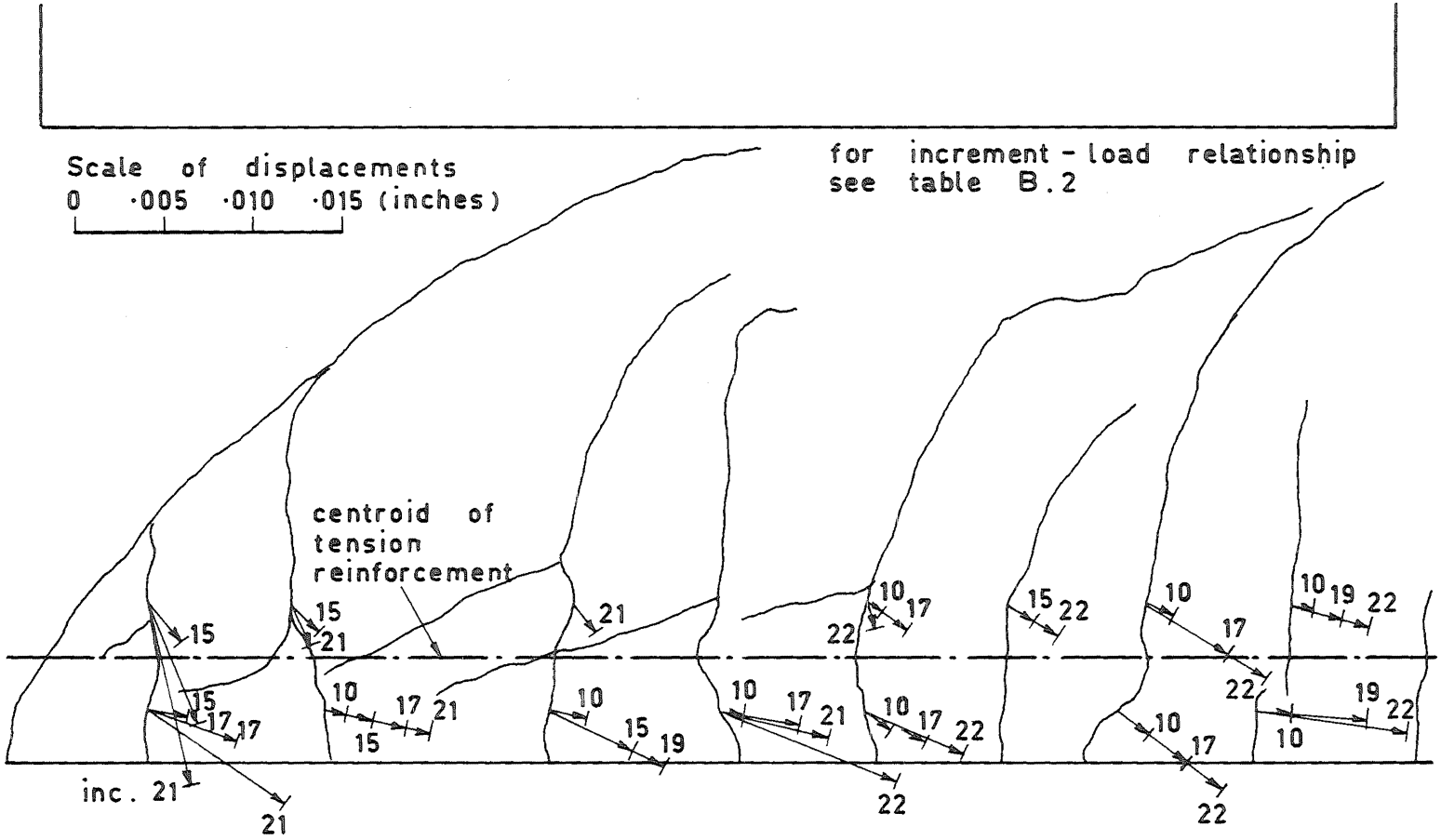

Fig. 4.12 Displacements Across Cracks in Side 2 of Beam N2-S0

left for some minutes before further observations were made. During this time the diagonal crack at the upper end of the beam formed. Fig. 4.13 shows the cracks in side 1 of beam N2-SO just before failure. The diagonal crack, clearly marked in this figure, was visible to the naked eye when it had just formed, and by .789 P_u^* it was approximately 1/16 inch wide at mid-depth of the beam. Cracks in the compression face of the beam can be seen above the diagonal crack. The cause of these will be discussed in section 4.5.5.

At .789 P_u^* a second diagonal crack formed closer to the section of maximum moment. This crack propagated some distance into the compression zone over the next few load increments, until it was right at the section of maximum moment (see fig. 4.13). It proved to be the failure crack.

4.5.4 Dowel Action

At .560 P_u^* the first cracks along the tension reinforcement were observed. These were not very prominent initially but they became more pronounced at .699 P_u^*. Dowel action and aggregate interlock are the cause of the nearly longitudinal splits in the beam. Fig. 4.13 shows well developed dowel cracks especially at the low moment end of the second diagonal crack. This diagonal crack proved to be the eventual failure crack.

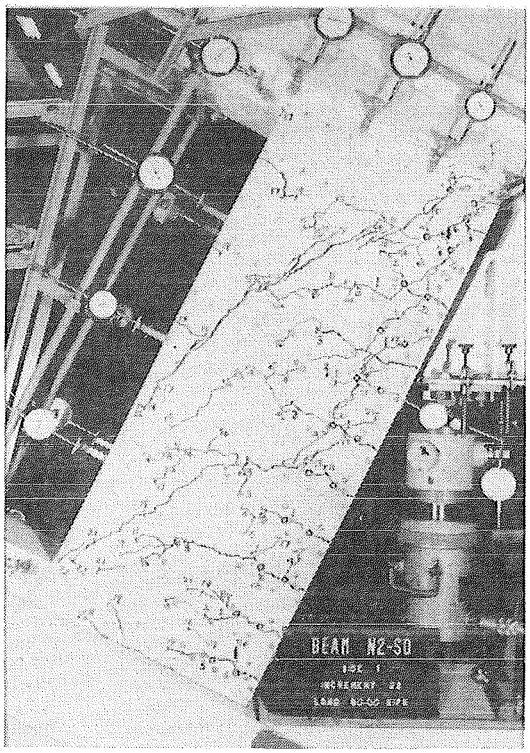

Fig. 4.13 Beam N2-S0

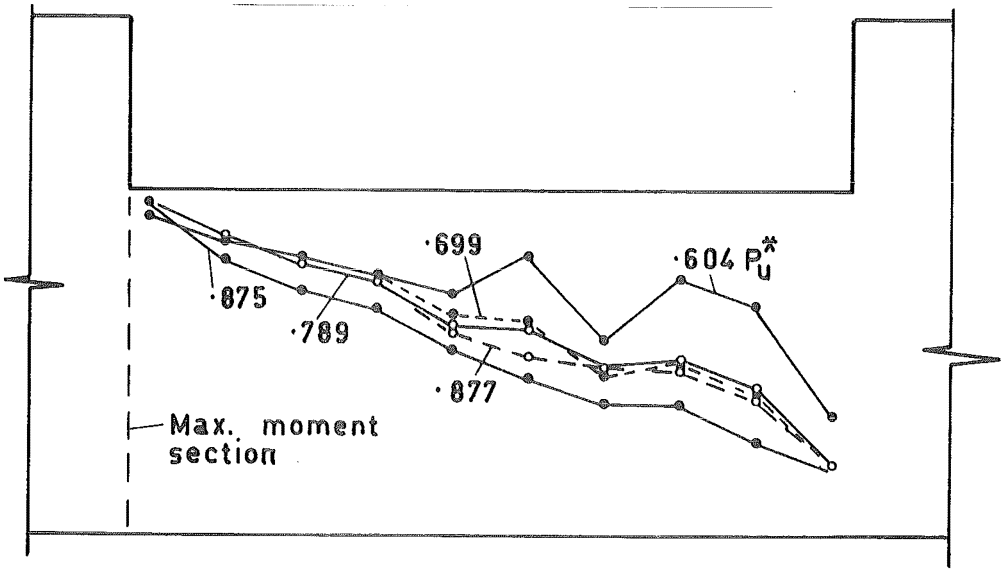

Fig. 4.14 Centre of Compression Force in Beam N2-S0

At failure it extended into the dowel cracks along the reinforcement (see fig. 4.10).

Displacements along the flexural cracks near ultimate load were of the order of .005 to .008 inches. So far dowel shear transferred by multiple layers of reinforcement has not been the subject of a detailed study to the knowledge of the author. However the contribution of the dowel shear transferred by the four reinforcement bars can be estimated from the findings of Baumann [12]. From Eqs. (2.10) and (2.11) it can be shown that the dowel cracking shear in this beam could be equal to the total shear on the beam at failure. This estimate of the dowel shear in the beam is obviously too great but it shows that the dowel shear resistance would have been a significant proportion of the total shear.

It can be seen in fig. 4.13 that the dowel cracks at the end of the eventual separation diagonal crack extend about three gauge lengths (12 inches) along the tension reinforcement. Gauge row 4 is the most critical section for bending of the dowel beam (see chapter 2). For simplicity assume the dowel beam is made up of the two layers of tension reinforcement only. At .877 P_u^* the tension in the inner layer was 970 microstrains at gauge row 4, and at .875 P_u^* (last load increment before

failure) the inner layer tension was just below yield at 1430 microstrains. Of the difference between the 970 and 1430 microstrains assume 400 is due to dowel beam bending and the remaining 60 to increased flexure of the whole beam. This is justified because the load intensities are almost equal, c.f. .877 P_u^* and .875 P_u^*. Therefore the force in the inner layer of reinforcement contributing to bending of the dowel beam is

$$\varepsilon_s E_s \frac{A_s}{2} = 400\times10^{-6} \times 30.3\times10^{6} \times 1.978 \text{ lb.}$$
$$= 24{,}000 \text{ lb.}$$

The distance between the two layers of reinforcement is $2\frac{1}{8}$ inches and the assumed lever arm is 12 inches. The dowel shear across the diagonal crack is therefore

$$V_d = 24{,}000 \times 2.125/12 \text{ lb.}$$
$$= 4220 \text{ lb.}$$

Because of the additional contribution to the flexural capacity of the dowel beam afforded by the concrete cover and the concrete between the two layers of reinforcement, the dowel shear resistance could well be doubled or even more enhanced. Thus dowel action alone could account for one quarter or more of the total shear resistance at the critical diagonal crack.

4.5.5 Arch Action

Cracks were observed in the compression face of beam N2-SO after diagonal cracking was initiated.

These opened up during subsequent loading. One of them, in gauge row 5 (see fig. 4.13), was .040 inches wide at .875 P_u^*. Some of the flexural cracks in the top half of the beam closed after the first diagonal crack had formed. Both of these pheonomena lead to the conclusion that the centre of the compression force in the beam had moved towards the tension face.

If concrete tension is ignored, the centre of the compression force can be found from consideration of the forces acting at a section of the beam. The compression force is the difference between the measured forces in the tension reinforcement and the external axial load. From the known moments at each section the line of action of this force can be determined. If the concrete is carrying significant tension, as it does at low load intensities, the analysis is erroneous as it is rather sensitive to the magnitude of the calculated compression force.

The lines of action of the compression force for various external loads on beam N2-SO are shown in fig. 4.14. At .604 P_u^* the line of action is at approximately constant depth in the beam. The variation in the actual location is influenced by the extend of cracking at the section. The marked increase of the depth of the compression force at the right hand end of the figure is attributed to the boundary conditions on the right of

this section. At .699 P_u^*, after diagonal cracking, the line of action is seen to drop very markedly in the right half of the figure. This inclination represents arch action. At .875 P_u^* the effect is even more apparent. Referring back to fig. 4.9 it can be seen that at and above .699 P_u^* the tension reinforcement strain profiles become flatter, i.e., the strains are more constant along the beam.

4.5.6 Deformation Characteristics

The load deflection relationships for beam N2-SO are presented in fig. 4.15. The theoretical lines show the deflection calculated for the uncracked beam, and the flexural deflection of the flexurally cracked beam. The total deflection of the beam is shown by the full line, and the deflections calculated from summing equivalent curvatures are shown by the dashed line. After .650 P_u^* the equivalent curvatures become meaningless because of cracking of the compression face of the beam. Large negative curvatures were observed at some sections at higher load intensities. The beam was loaded to .348 P_u^* and then unloaded. The deflections for the first cycle are seen as the left hand pair of curves. The second cycle relationship is the right hand set.

The first diagonal crack had formed before the deflection observations were made at .699 P_u^*. The exact shape of the flat part of the deflection curve

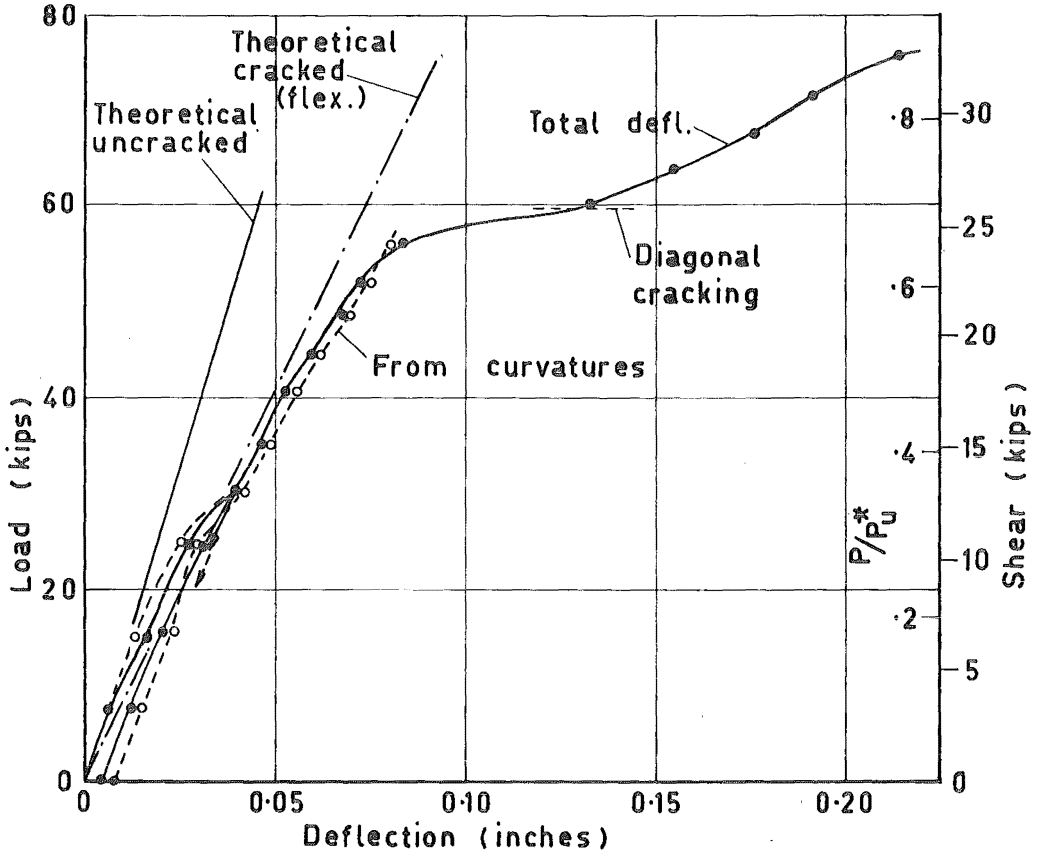

Fig. 4.15 Beam N2-S0 Load - Deflection Relationships

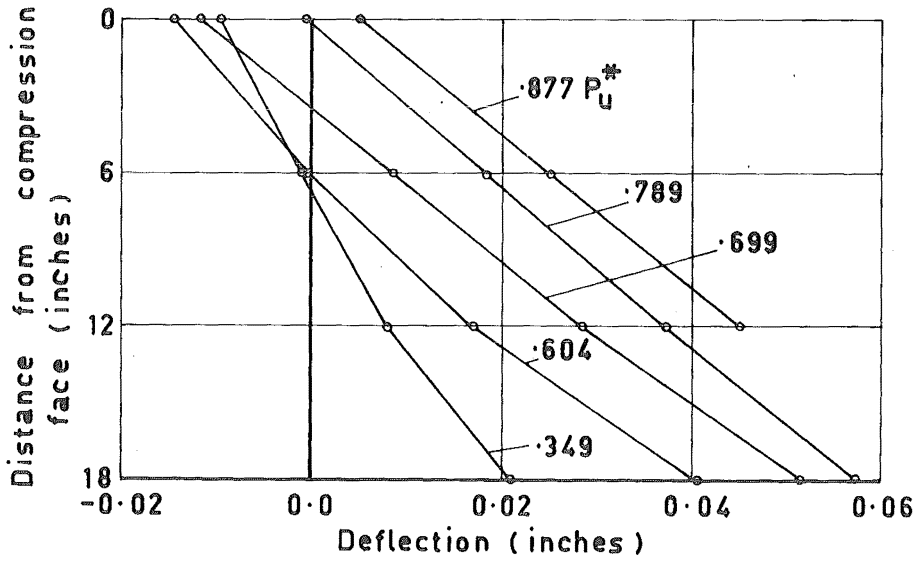

Fig. 4.16 Deformation of Top End Section of Beam N2-S0

just prior to this load intensity is doubtful. The discontinuity is caused by the large shear displacement at diagonal cracking. The sharp decrease in the stiffness of the beam after diagonal cracking is caused by the increasing shear displacement as a proportion of the total deflection.

At very low load the beam stiffness is approximately equal to the theoretical uncracked stiffness. Above about .1 P_u^* the observed stiffness is reduced by the formation of flexural cracks. At a load of half ultimate flexural capacity the deflection of the beam is almost twice as much as predicted from calculations based on the transformed concrete section.

The beam deflection calculated from summing equivalent curvatures follow the total measured deflection very closely. This indicates that until diagonal cracking the shear displacements were small. The unsatisfactory dial gauge stand is the cause of the flexural deflections being larger than the total deflections at some loads.

No reliable deflection observations were made at .875 P_u^*.

The displaced shape of the top section of the test length of the beam is shown in fig. 4.16. The profiles were measured by four dial gauges as described in chapter 3. Before diagonal cracking there is a destinct

kink in the profile at the tension face end. This kink is reduced once arch action is developed. The beam becomes longer as a whole (c.f. .604, .699 and .789 P_u^* profiles in the figure). The reading at the tension face at .877 P_u^* was not obtained.

Fig. 4.17 is a plot of the equivalent curvatures in beam N2-SO. The large negative equivalent curvature at gauge row 5 is a result of the wide crack in the compression face of the beam. Fig. 4.17 (a) shows equivalent curvatures up to .0002 radians/inch while part (b) shows those which occur outside this range at higher loads.

4.5.7 Failure

At .875 P_u^* wide dowel cracks were forming along the tension reinforcement for some time after this load had been applied. To avoid failure before the gauge readings were taken, the hydraulic line to the jack was closed 10 minutes after peak load had been reached. The load fell off because of plastic deformation once the line was closed. After all the gauge readings were taken the beam was further loaded. However, it failed at a load 700 lbs. below the peak attained at loading for increment 22. At no stage did all the four reinforcement bars reach yield stress together, although the bottom two bars first yielded

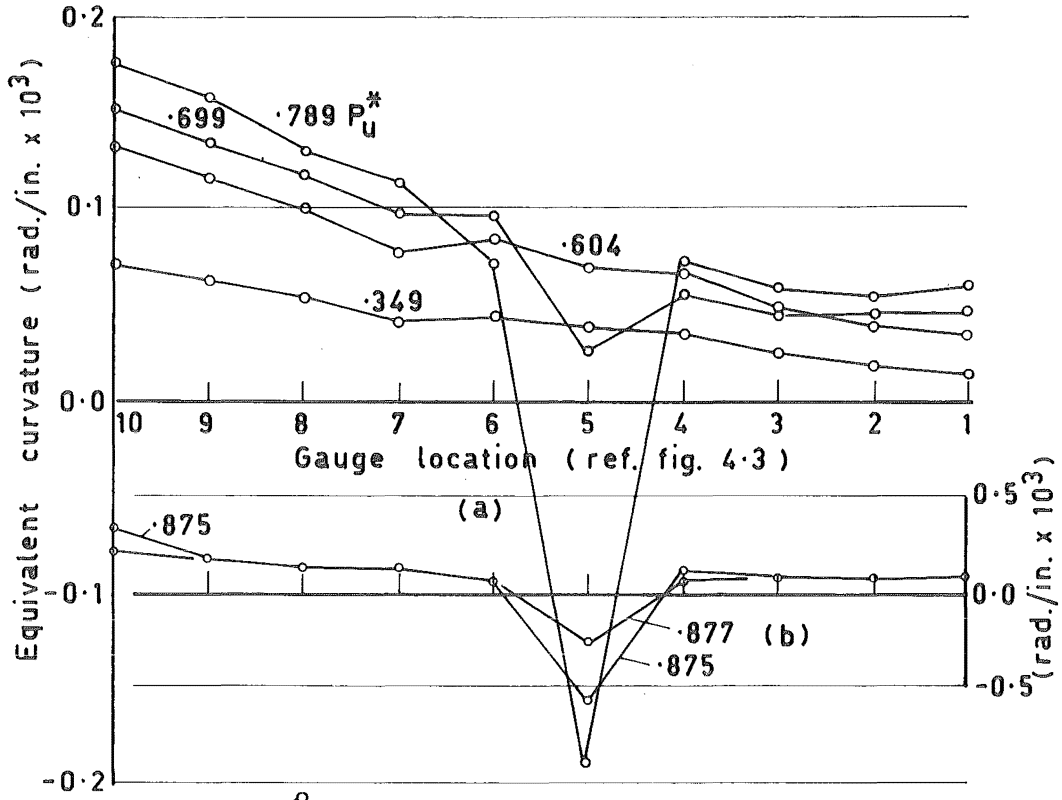

Fig. 4.17 Equivalent Curvatures in Beam N2-S0

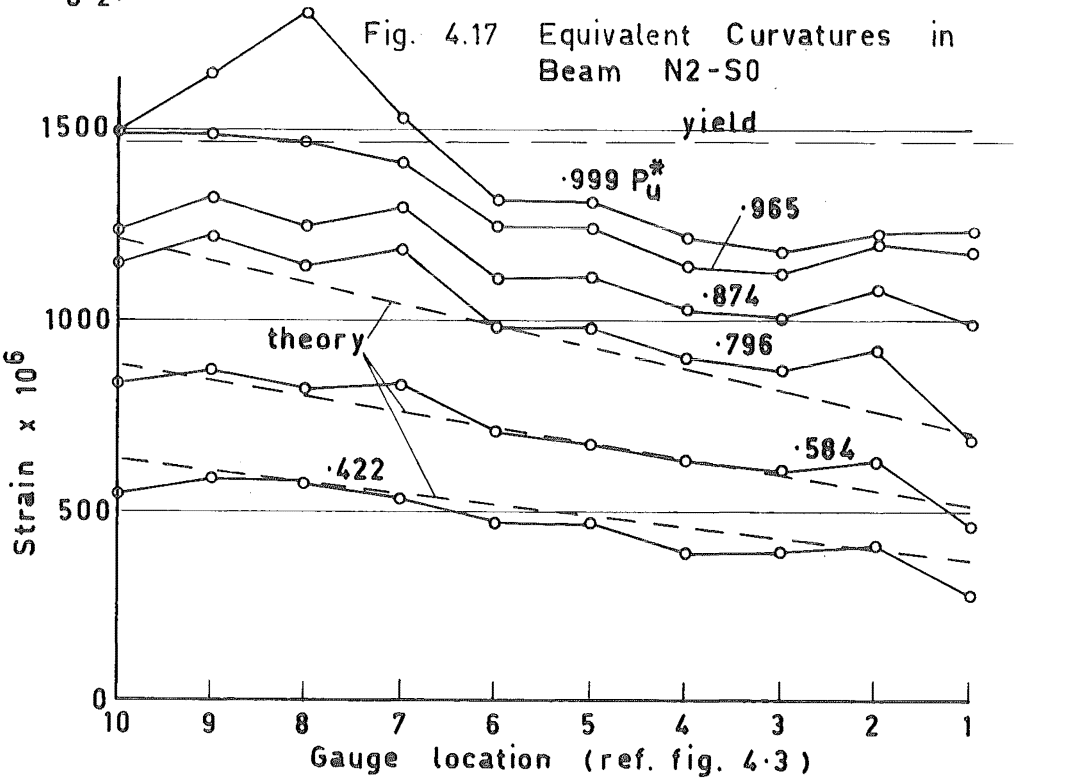

Fig. 4.18 Tension Reinforcement Strains in Beam N3-S0

at .831 P_u^*. The failure was quite sudden but not explosive. Ample warning of failure was afforded by the obvious splitting along the reinforcement. No crushing of the concrete was observed at the section of maximum moment even though the compression zone was very shallow because of penetration by the second diagonal crack. The failed beam is shown in fig. 4.10.

4.6 Beam N3-SO

The line of action of the load on beam N3-SO, and the positions of the 4 inch demec gauge rows, are shown in fig. 4.3. The initial axial load to shear force ratio and M/Vd ratio were

N/V = 3.16	M/Vd = 4.27

4.6.1 Behaviour of the Tension Reinforcement

Tension reinforcement strains at various load intensities have been drawn in fig. 4.18. The dashed lines are theoretical elastic strains calculated at .422, .584 and .796 P_u^*. At .422 P_u^* the beam was still only lightly cracked and consequently the calculated strains are slightly higher than those observed during the test. On the other hand at .796 P_u^* the experimental strains are larger than the theoretically

derived strains. At this stage of loading there was some inclination of flexural cracks. Even so the agreement between elastic theory and experiment is considered to be very good considering the applied load is over three quarters of ultimate.

A photograph of side 2 of the beam at .999 P_u^* can be seen in fig. 4.19. There was only one major diagonal crack at this stage. The crack crossed the longitudinal reinforcement at 4 inch gauge row 2. The strains shown in fig. 4.18 at this gauge location are seen to be higher than at the adjacent gauge rows.

4.6.2 Concrete Strains

The largest concrete compression measured at the last increment of loading was 2700 microstrains. It is estimated that at failure the strain in the extreme fibre at gauge row 10 would be .005 in/in. This estimation is from a lower bound extrapolation between the last two measured strains and corresponding loads, and the known failure load of the beam.

All along the test length $\frac{1}{4}$ inch from the compression face the concrete showed compression strains at all stages of loading. There was some reduction in these strains above the diagonal crack when it was formed.

(For Fig. 4.20 see p. 153)

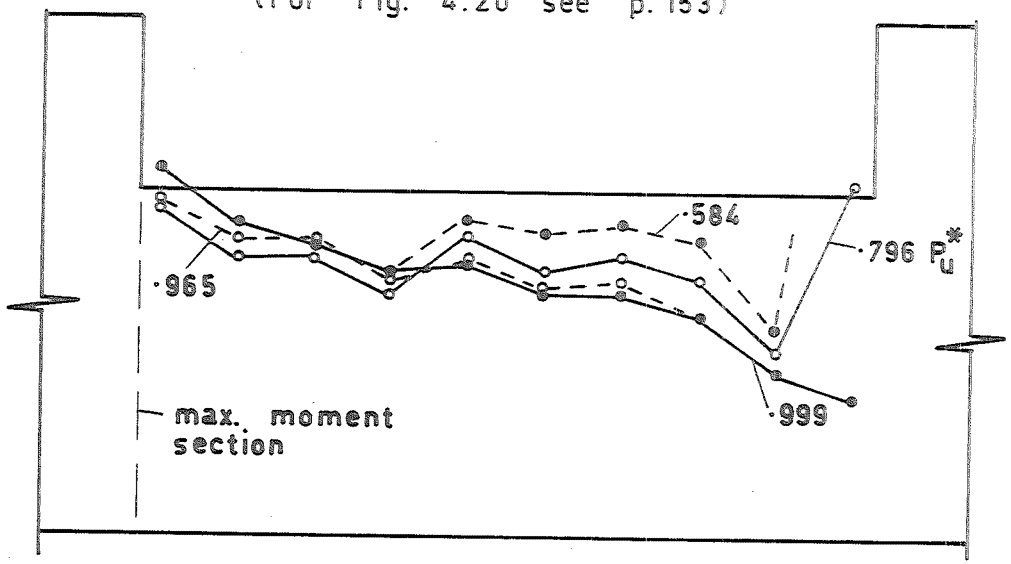

Fig. 4.21 Centre of Compression Force in Beam N3-S0

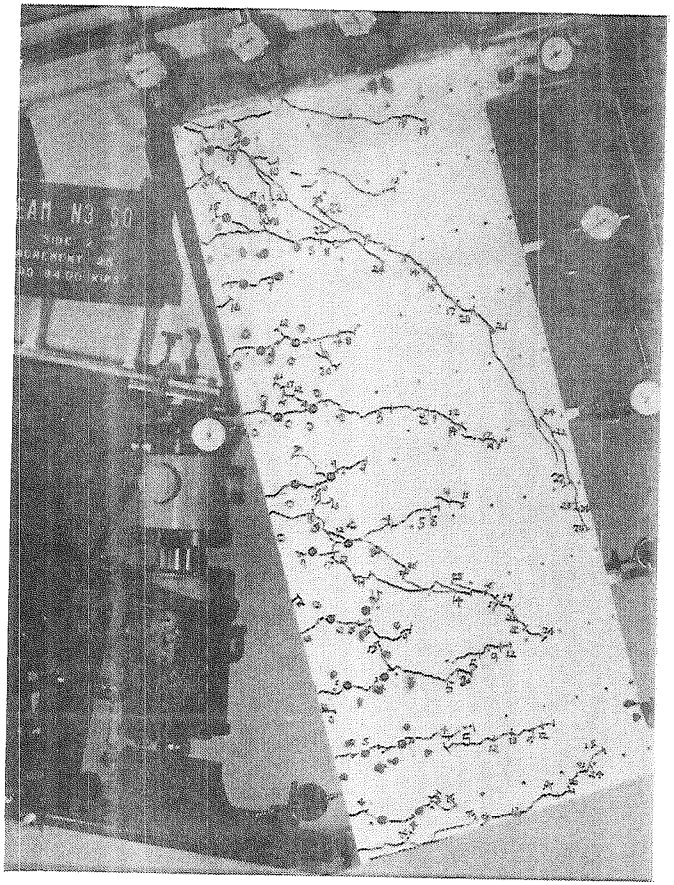

Fig. 4.19 Beam N3-S0

4.6.3 Crack Development

4.6.3.1 Flexural Cracking

The first cracks were observed in beam N3-SO at .161 P_u^*. These cracks propagated into the beam inclining only very slightly towards the load point up until .542 P_u^*. After .272 P_u^* in the first cycle of loading, the load on the beam was removed and the triangular sets of 2 inch demec gauges were fixed across the cracks. Fig. 4.20 shows the displacements measured across the cracks in side 2. As was the case with both the other beams discussed in this chapter the displacements along the cracks are greater towards the centre of the beam than nearer the tension face. From the observations on the crack movements no prediction could be made about which was to be the failure crack. The largest displacements were measured at the diagonal crack which formed at .874 P_u^*.

4.6.3.2 Diagonal Cracking

As can be seen in fig. 4.19, the top diagonal crack propagated gradually from .422 to .840 P_u^*. Two other cracks showed a definite tendency to incline towards the load point in this range of load intensities. At .874 P_u^* the major diagonal crack at that stage suddenly propagated to within an inch of the compression face

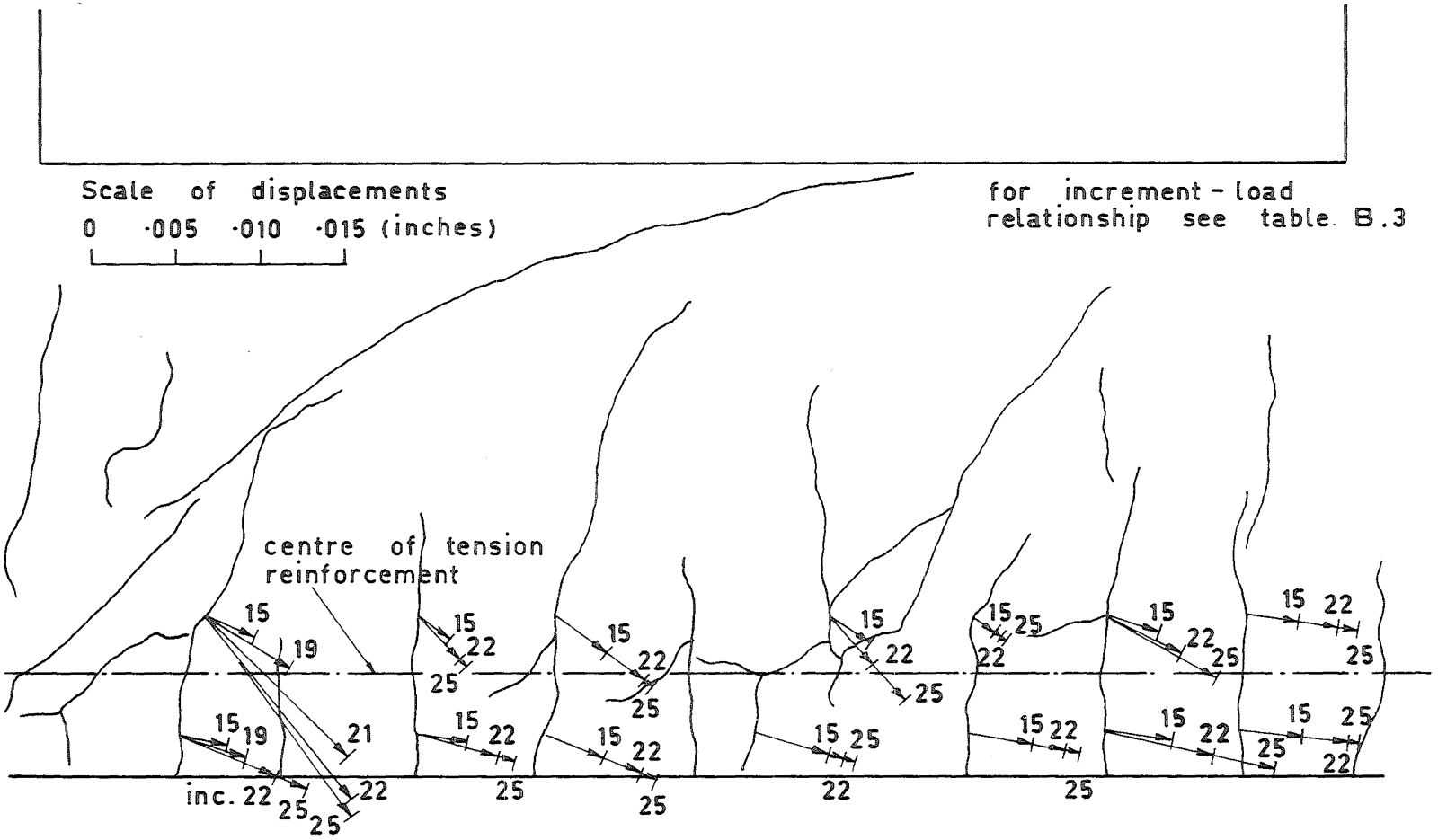

Fig. 4.20 Displacements Across Cracks in Side 2 of Beam N3-S0

of the beam. It then stabilised and increased in length only a small amount during subsequent loading. The concrete was in compression both above and below this crack from gauge row 4 to 7.

4.6.4 Dowel Action

Beam N3-SO did not show much tendency to form dowel cracks even at high loads. A few dowel cracks formed at .456 P_u^* but these did not propagate far at subsequent loading. Appreciable dowel cracking did occur at the failure crack even before it was well developed. Where dowel cracks did form displacements along the flexural cracks were of the order of .004 inches with a maximum of .012 inches at .999 P_u^* (see fig. 4.20). Where there was no dowel cracking maximum displacements along the cracks were .0015 inches. On the basis of the calculations for beam N2-SO in section 4.5.4, 25% or more of the total shear could have been transferred across the eventual failure crack by dowel action.

4.6.5 Arch Action

The position of the centroid of the compression force in the beam is shown in fig. 4.21. The downward shift after diagonal cracking is not so pronounced as with beam N2-SO, but there is a depression

in the right hand half of the diagram. The points where the centroid lies outside the beam are attributed to the concrete at these sections carrying some tension. This was not allowed for in the analysis.

Fig. 4.22 shows two typical sets of strain profiles of the concrete above the diagonal crack which formed at .874 P_u^*. In both cases the strain profile before diagonal cracking and consequent arching is approximately linear and of the expected triangular shape. After the crack has formed the extreme fibre compression strains are reduced and the profile becomes more rectangular. In the more typical case, shown, of gauge row 2, the fibre of zero stress moves away from the compression face of the beam.

4.6.6 Deformation Characteristics

The load deflection relationship for beam N3-SO was not successfully measured by dial gauges. The only deformation characteristics available are shown in fig. 4.23. The deflection of the beam was calculated from equivalent curvatures and compared with theoretical deflections of the uncracked and flexurally cracked beam. At loads up to .15 P_u^* the deflection based on the uncracked section is a good estimate of the deflection of the beam. Once cracking has developed, at about .15 P_u^*, the observed flexural deflections indicate

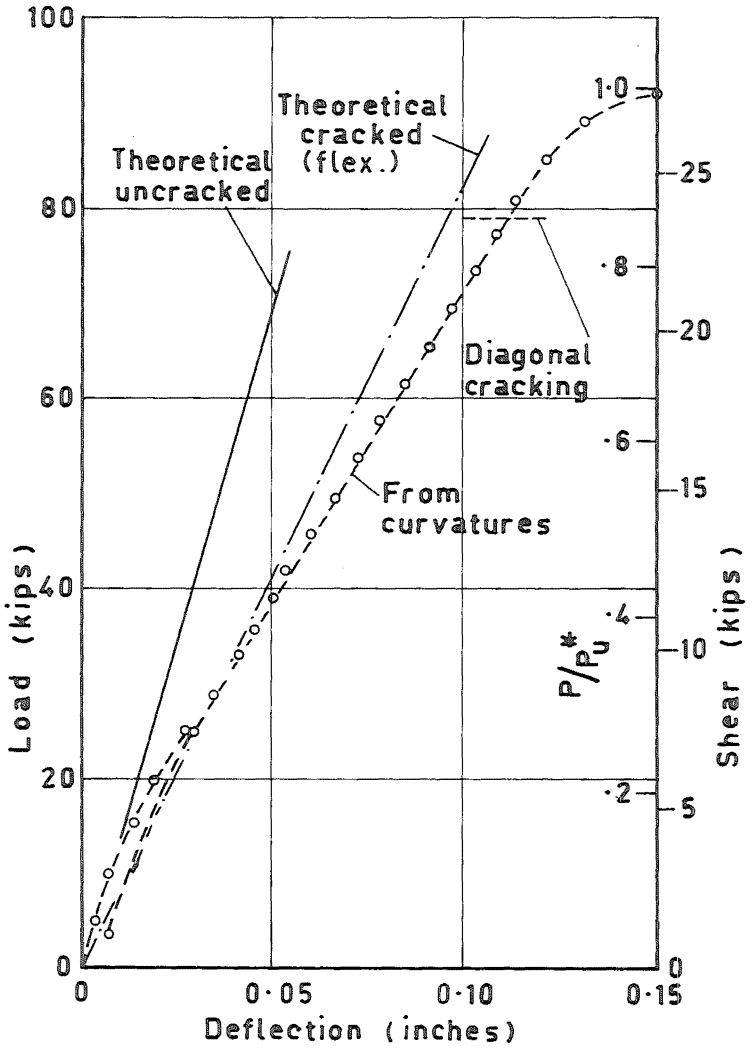

Fig. 4.23 Beam N3–S0 Load – Deflection Relationships

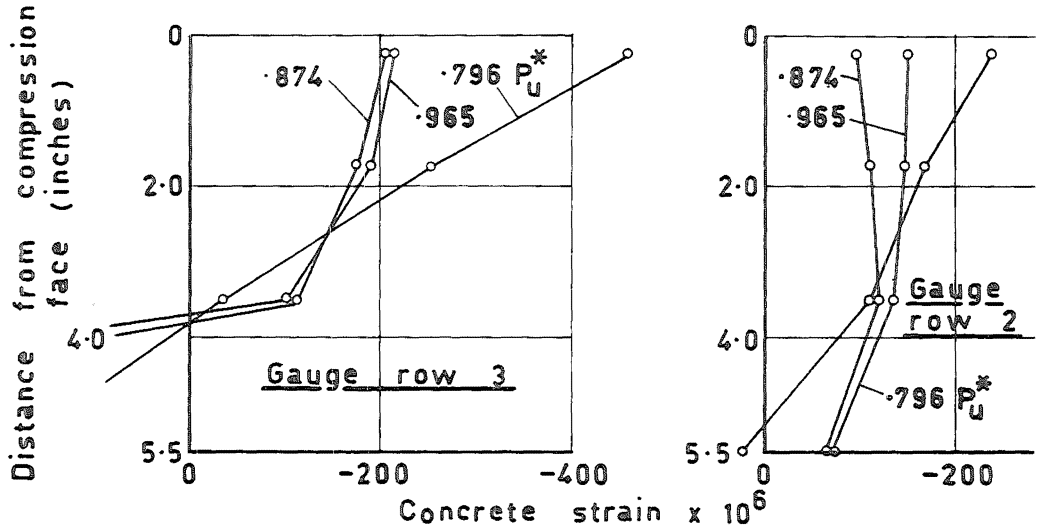

Fig. 4.22 Strain Profiles in the Concrete Above the Diagonal Crack in Beam N3–S0

constant stiffness up to .874 P_u^*. Beyond this the stiffness decreases because of the increased equivalent curvatures after diagonal cracking. In the working range of the beam the flexural stiffness is about half of that based on an uncracked section.

It is reasonable to assume that up to diagonal cracking the deflections calculated from equivalent curvatures are only slightly less than the total deflections. In fig. 4.15 it is shown that the shear deflections of beam N2-SO before the formation of a diagonal crack are small.

Equivalent curvatures at selected load intensities are drawn in fig. 4.24. Up to diagonal cracking the pattern is as would be expected. Once arch action is developed the equivalent curvatures do not increase much further in the region of the diagonal crack. This can be seen in the right hand portion of the figure. The reason for this is the decreasing compression strains in the extreme compression fibre of the concrete.

4.6.7 Failure

After making observations at .999 P_u^* the beam was loaded to failure. Before failure the tension reinforcement yielded for some distance along the beam from the section of maximum moment. Signs of

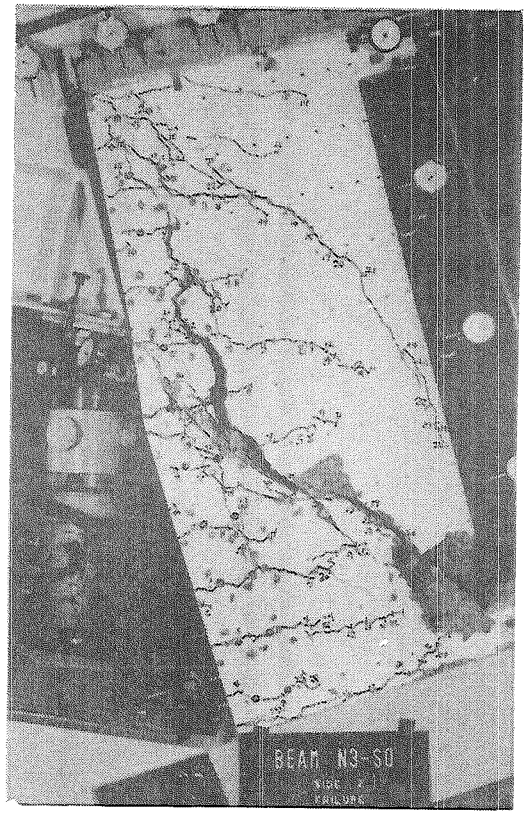

Fig. 4.25 Beam N3-S0 at Failure

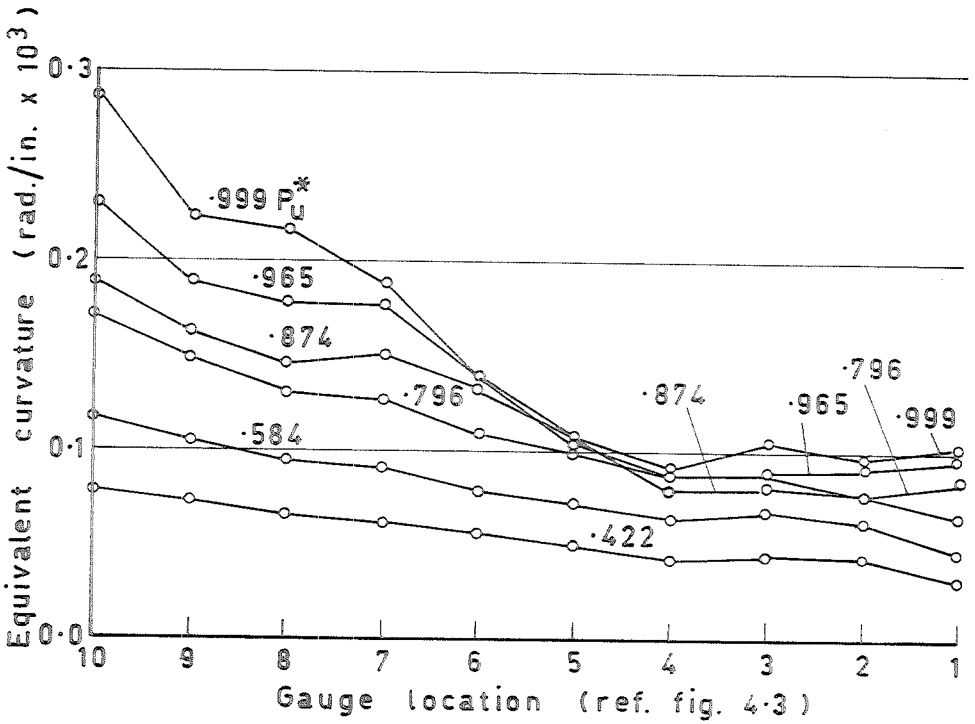

Fig. 4.24 Equivalent Curvatures in Beam N3-S0

crushing of the concrete at this section were observed. Failure was violent and occurred with little warning. Fig. 4.25. is a photograph of the beam after failure. The large area of crushed concrete in the right hand corner disintergrated suddenly and the diagonal crack formed at the same time. It is difficult to determine which was the primary cause of collapse as the beam was close to its flexural capacity. The dowel cracks at the end of the failure crack are seen to have propagated as a split along the reinforcement.

4.7 Comparison of Beams Without Web Reinforcement

Some points of similarity of behaviour of the three beams discussed in this chapter are presented. Detailed examination of the deflection characteristics of the beams are included in chapter 8 and failure comparisons are discussed in chapter 6.

4.7.1 Concrete Cantilevers

It has already been stated in this chapter that the displacements along cracks in the shear span of the beams are greater above than at the level of the longitudinal reinforcement. The forces that act on a concrete cantilever in the shear span have been identified by Fenwick [18]. They are shown in fig. 4.26 (a). In part (b) the resultant idealised bending moment produced

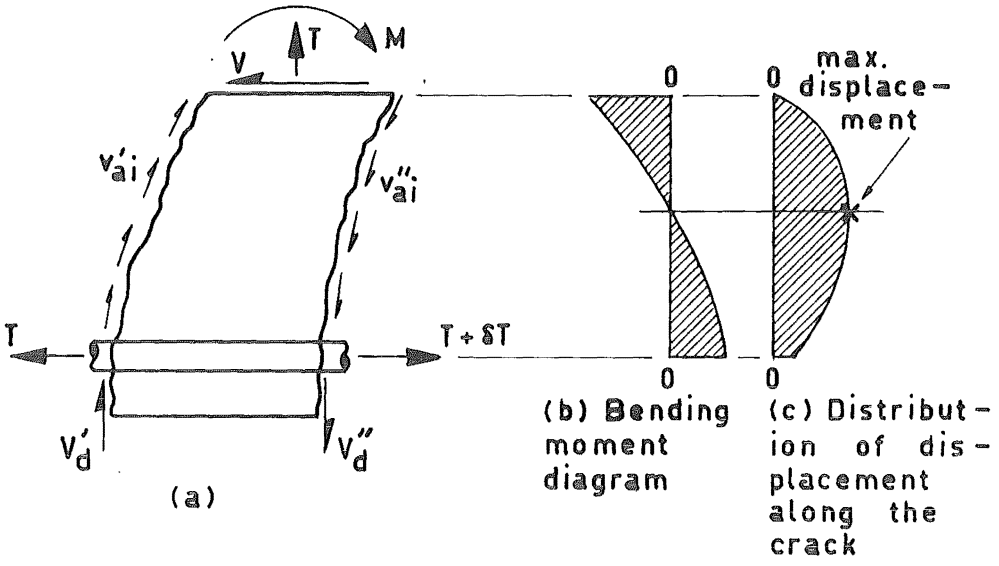

Fig. 4.26 Flexure of a Concrete Cantilever

P produces the actions N and R_i

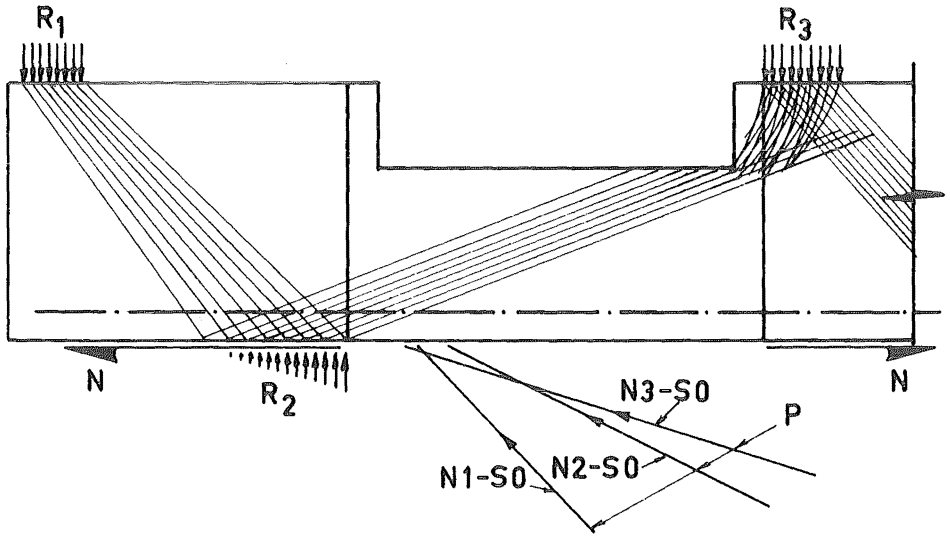

Fig. 4.27 Arch Action in the Test Beams

by these forces is shown, and (c) is the distribution of displacements along the crack between two such cantilevers. The point of contraflexure in the cantilever is somewhere above the reinforcement. At this point the displacement along the crack is a maximum. Below this the reverse curvature caused by the predominance of moment from the dowel shears reduces the displacement along the crack to a minimum at the level of the longitudinal reinforcement.

4.7.2 Crack Spacing and Crack Widths

The predominant crack spacing observed in the three beams was 4 inches. The reason for this particular spacing is discussed in section 4.4.3.

The maximum crack widths observed in any of the three beams at approximate working load was .0042 inches. The usual width was of the order of .002 - .0035 inches. Working load was taken as ultimate flexural capacity divided by between 1.75 and 1.95. In both beams N2-SO and N3-SO the maximum crack width occurred at the section of maximum moment. The crack widths measured in beam N1-SO were small compared to the other two beams because the beam failed at .452 P^*_u.

4.7.3 Arch Action

Arch action was observed in both beams N2-SO

and N3-SO. In beams with no applied axial load, appreciable arch action would not develop if the M/Vd ratio is greater than approximately 2.5 [27]. In laboratory tests of reinforced beams the springing required for arch action can be provided by the load or reaction plates. Taylor [47] and Ferguson [20] have shown that there is little reserve shear resistance in beams without web reinforcement loaded through secondary beams once diagonal cracks have developed. This is because there is no suitable springing for the arch when it forms.

Fig. 4.27 shows the arch action as it developed in the beams tested in this investigation. The bands of diagonal compression have been idealised somewhat but the pattern is clearly seen. The M/Vd ratio as defined in section 4.4 does not adequately describe the slope of the arch as it does in a simply supported beam. With all three N/V ratios it is clear that the arch in the test length is approximately the same slope although the M/Vd ratios range from 2.88 to 4.27. The arch in the test length of the beam, as it is drawn in the figure, corresponds to a shear span to depth ratio of approximately 2.7 in a simply supported beam. So far no adequate explanation has been found for the absence of appreciable arch action in beam N1-SO, while beams N2-SO and N3-SO displayed increase in shear strength because of arch action after diagonal cracking.

CHAPTER 5

BEAMS WITH WEB REINFORCEMENT

5.1 Introduction

The behaviour of seven beams tested to failure are examined in this chapter. All beams contained varying percentages of web reinforcement in the form of closed stirrups perpendicular to the longitudinal reinforcement. The designations of the beams, the actual range of axial tension to shear force ratios, and the M/Vd ratios are presented in table 5.1.

Table 5.1 Relationships Between Axial Tension, Applied Shear, and Moment for Beams With Web Reinforcement.

Beam	Range of N/V during Test		Initial M/Vd (1)
	Maximum	Minimum	
N1-S62	0.990	0.980	2.90
N1-S32	1.024	0.986	2.92
N1-S63	1.015	0.970	2.88
N2-S62	2.219	2.100	3.40
N2-S32	2.308	2.149	3.48
N2-S63	2.151	2.060	3.35
N3-S12,4	3.375	3.265	4.40

(1). For definition see section 4.4

5.2 Scope of the Tests

The beams were tested in several load increments to failure. They were loaded in two or three increments to a stage where flexural cracking was well developed. Then the beams were unloaded and sets of 2 inch demec gauge lengths were mounted across the flexural cracks. After the beams had been allowed to cool after application of the gas flame they were again loaded, this time to eventual failure.

Three beams, viz., N1-S32, N2-S32 and N3-S12,4, were loaded in small increments from the initial zero to the stage when cracking had developed. This was to obtain the load deflection relationships of the uncracked and lightly cracked beams. For most of these small load increments only deflection measurements were taken. The three beams also had deflection observations made on them to find their post-elastic deformation characteristics.

Load deflection relationships were found for all beams in the elastic range of loading. Concrete strains were measured in the compression zone of the beams and displacements across many cracks were observed. Strains were measured on both the tension and compression reinforcement as well as on the stirrups in the test sections of each beam. Crack patterns were marked and photographed.

5.2.1 Grouping of Beams

In this chapter the seven beams will be divided into three groups for the purposes of discussion. Each group will comprise the beams with the same nominal axial load to shear force ratio. The properties of the beams are given in table 3.1.

5.3 Beams N1-S62, N1-S32 and N1-S63

The location of the line of action of the load in each of the three beams, and the position of the 4 inch demec gauge rows are shown in fig. 5.1.

5.3.1 Behaviour of Longitudinal Reinforcement

5.3.1.1 Tension Reinforcement

Fig. 5.2 gives the average strains in the tension reinforcement at various load intensities for the three beams. The full lines are the strains from the experimental results, and the dashed lines are strains calculated from a conventional elastic analysis of a cracked section. The analysis is given in Appendix C. The loads used for the theoretical analysis correspond to actual loads at the various load intensities plotted.

Part (a) of the figure shows the strains in the tension steel of beam N1-S62. The high strain at

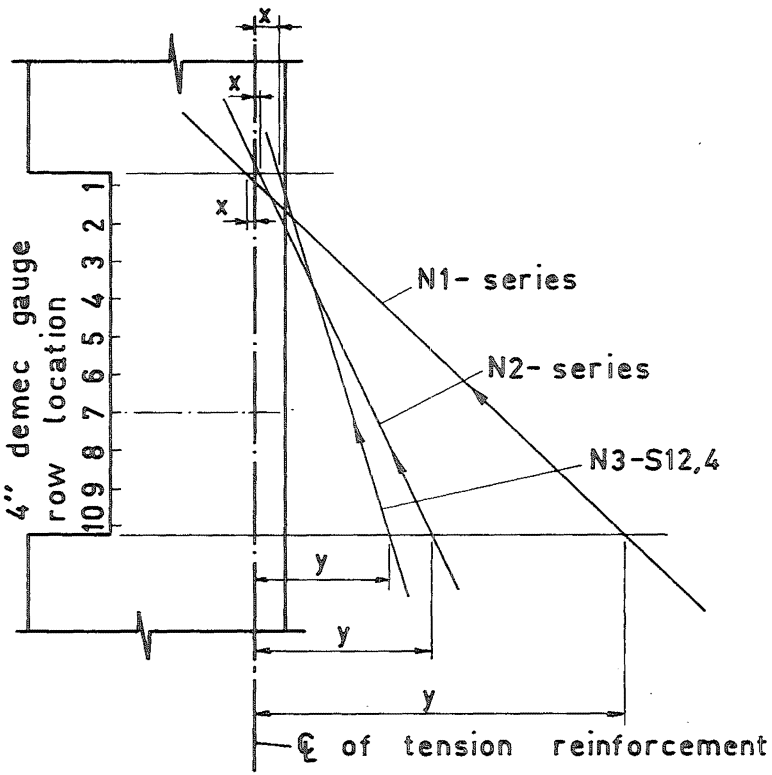

Beam	x (in.)	y (in.)
N1-S62	0.5	38.37
N1-S32	0.3	38.22
N1-S63	0.4	38.55
N2-S62	0.26	18.36
N2-S32	0.67	18.20
N2-S63	-0.02	18.42
N3-S12,4	2.48	14.03

Fig. 5.1 Load Position and 4 inch Demec Gauge Row Position on Beams With Stirrups

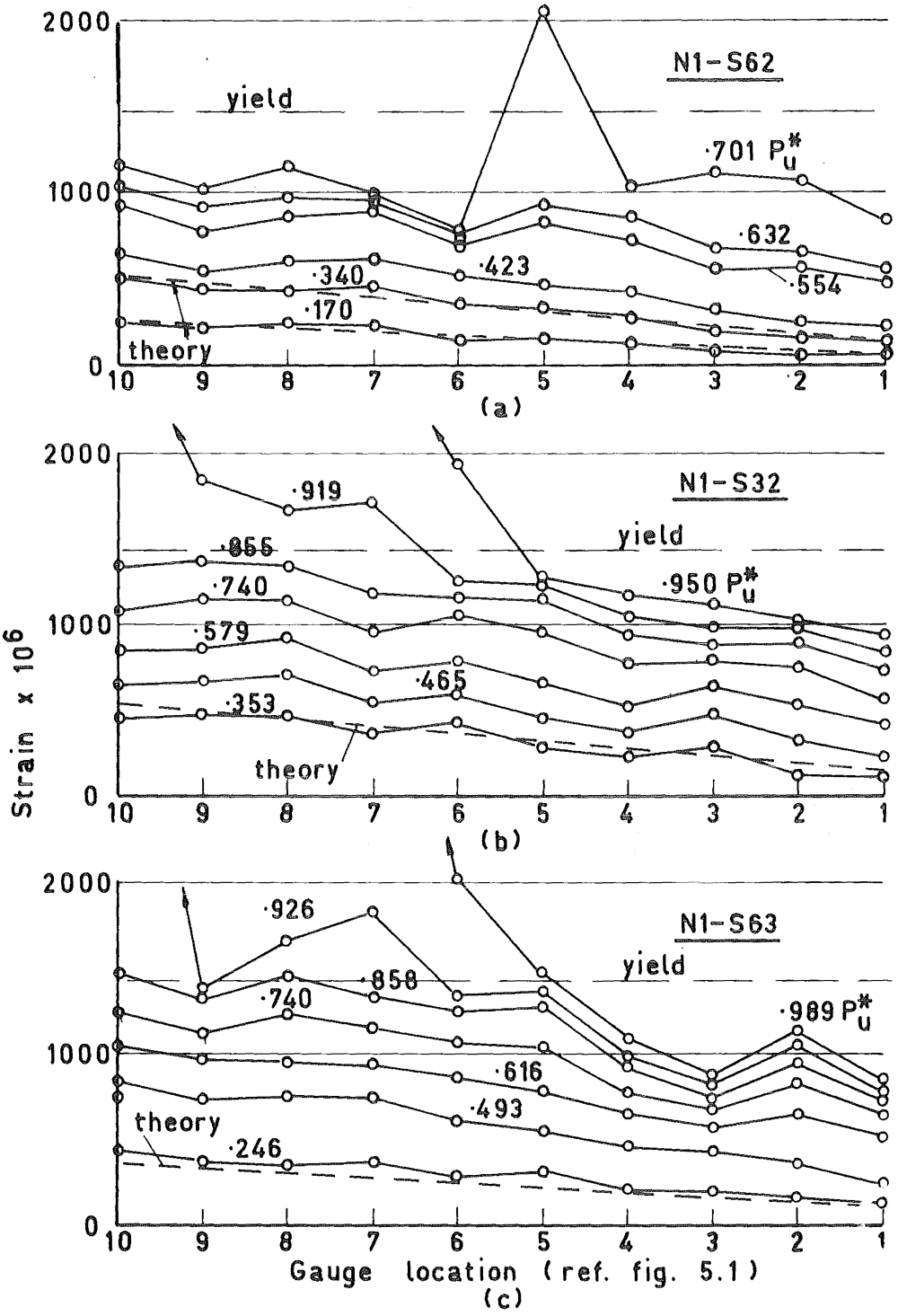

Fig. 5.2 Tension Reinforcement Strains in Beams N1-S62, N1-S32 and N1-S63

gauge row 5 should be noted. This is where the failure diagonal crack crossed the reinforcement. Fig. 5.3 is a photograph of side 1 of beam N1-S62 just prior to failure. The crack is clearly visible in the photograph.

Figs. 5.4 and 5.5 show side 1 of beams N1-S32 and N1-S63 respectively, just before failure. Although the diagonal cracks in these two beams are well developed there are no very pronounced kinks in the tension reinforcement strains where these cracks cross the tension steel (see figs. 5.2 (b) and (c)). The tension reinforcement strain distribution for all these beams after diagonal cracking will be discussed more fully in chapter 8.

At .170 and .340 P_u^* on beam N1-S62 the theoretical elastic strains are seen to show good agreement with the measured strains (see fig. 5.2). Diagonal cracking commenced before .423 P_u^* and hence the conventional theoretical analysis does not apply for higher load intensities. The agreement between theory and experiment at .353 P_u^* and .246 P_u^* on beams N1-S32 and N1-S63 respectively is also considered to be satisfactory. These beams showed diagonal cracking before the higher load intensities plotted in fig. 5.2.

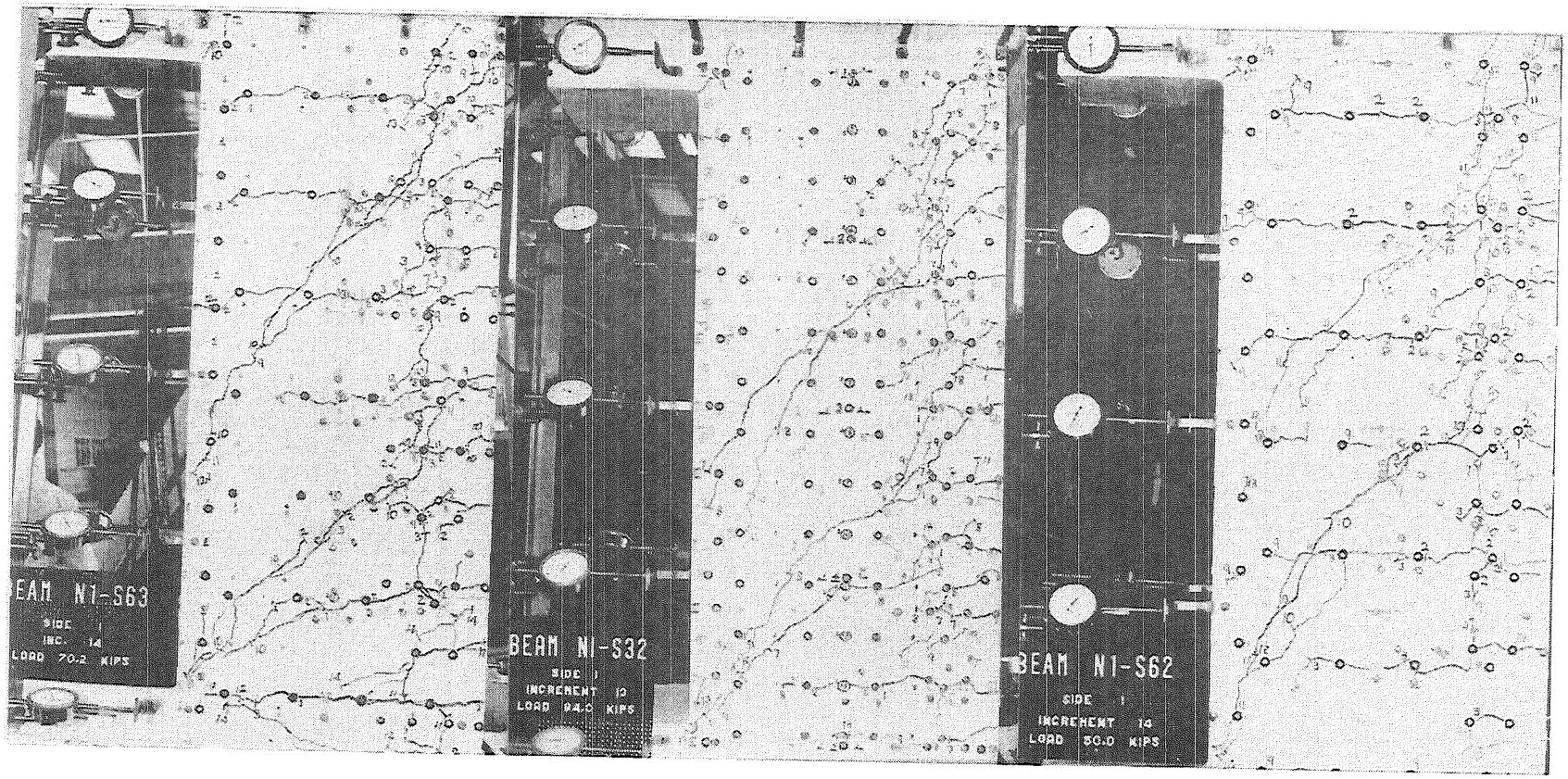

Fig. 5.5 Beam N1-S63

Fig. 5.4 Beam N1-S32

Fig. 5.3 Beam N1-S62

5.3.1.2 Compression Reinforcement

Compression reinforcement strain profiles for the three beams are shown in fig. 5.6. The compression steel is seen to be lowly stressed except at high loads at the section of maximum moment. Even then it yielded only over the last gauge length. In all cases the compression steel did not reach yield until the tension reinforcement at the particular section had yielded. No reliable measurement of the strain at gauge row 7 at .706 P_u^* on beam N1-S62 was obtained (see fig. 5.6 (a)). At all load intensities on all the beams, the compression strains at the centre of the test sections (gauge rows 3 to 6), were small.

Once diagonal cracking developed the compression reinforcement showed tension strains at the low moment end of the test section. This is consistent with the observed tension cracking in the compression face of the beams (see figs. 5.3, 5.4 and 5.5). More will be reported about this phenomenon in section 5.3.4.

The dashed lines drawn in fig. 5.6 are the theoretical compression reinforcement strains calculated on the basis of a conventional cracked elastic section. As was the case with the tension steel strains, the loads used in the analysis correspond with the experimental loads. The agreement between theory and experiment before the onset of

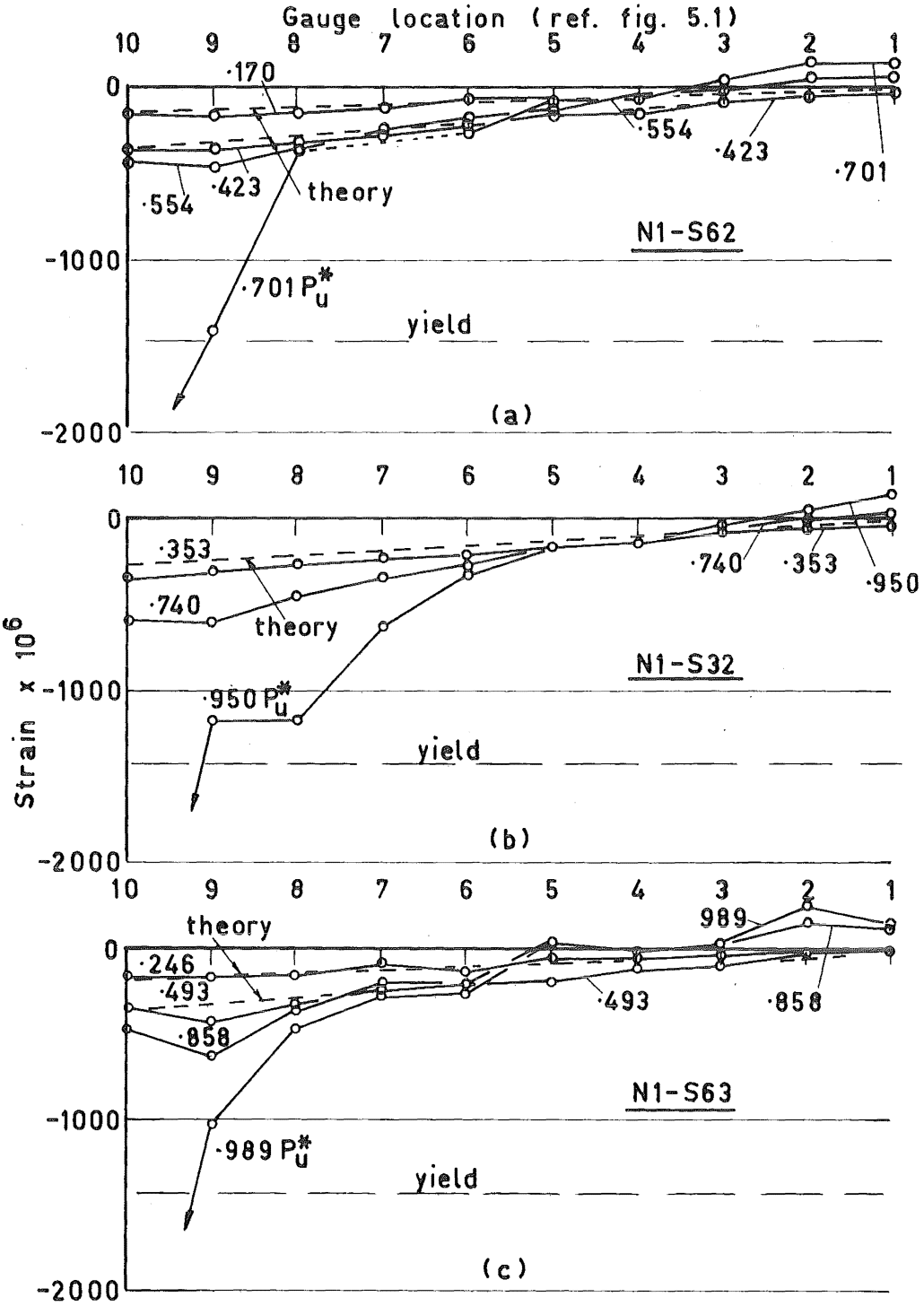

Fig. 5.6 Compression Reinforcement Strains in Beams N1-S62, N1-S32 and N1-S63

diagonal cracking is good. Even just after diagonal cracking in beams N1-S62 and N1-S63 the agreement is satisfactory (see .423 P_u^* fig. 5.6 (a), and .493 P_u^* fig. 5.6 (c)). The reason for this is that the compression steel strains are associated with the moment at the section, not the moment at a section closer to the point of maximum moment (see fig. 4.11).

5.3.1.3 Equivalent Curvatures

Equivalent curvatures for these beams were found from the strains measured in the longitudinal reinforcement. They are shown in figs. 5.7, 5.8 and 5.9. In figs. 5.8 (a) and 5.9 (a) the equivalent curvatures prior to plastic deformation of the beams are presented. Part (b) of both figures show post-elastic behaviour to a reduced scale. The three figures indicate that, in general, the equivalent curvatures along the beams are uniform. The large increase at gauge row 5 of beam N1-S62, at .701 P_u^* in fig. 5.7, corresponds with the high tension reinforcement strain where the critical diagonal crack crosses the reinforcement (see fig. 5.2 (a)).

5.3.2 Concrete Strains

The maximum concrete compression measured in beam N1-S62 was 2400 microstrains at .706 P_u^*. This strain was high considering that the tension reinforce-

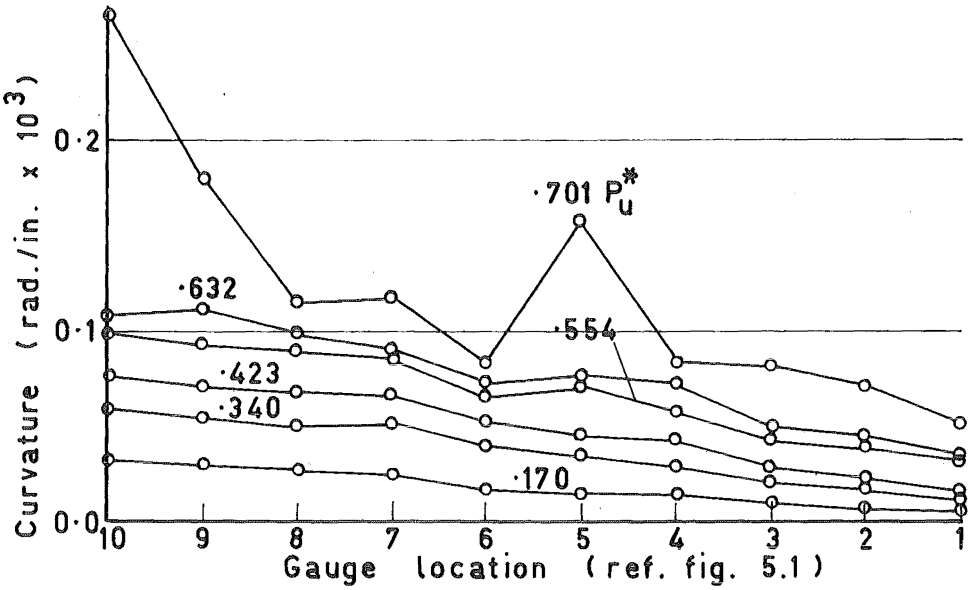

Fig. 5.7 Equivalent Curvature in Beam N1-S62

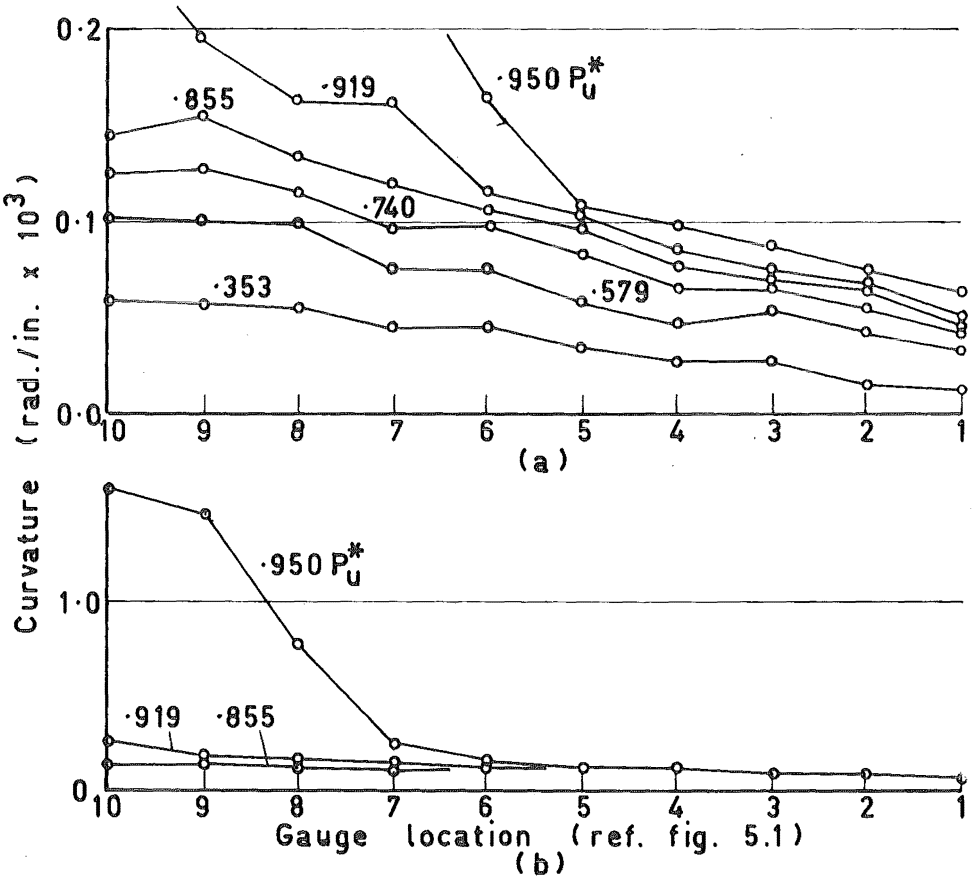

Fig. 5.8 Equivalent Curvature in Beam N1-S32

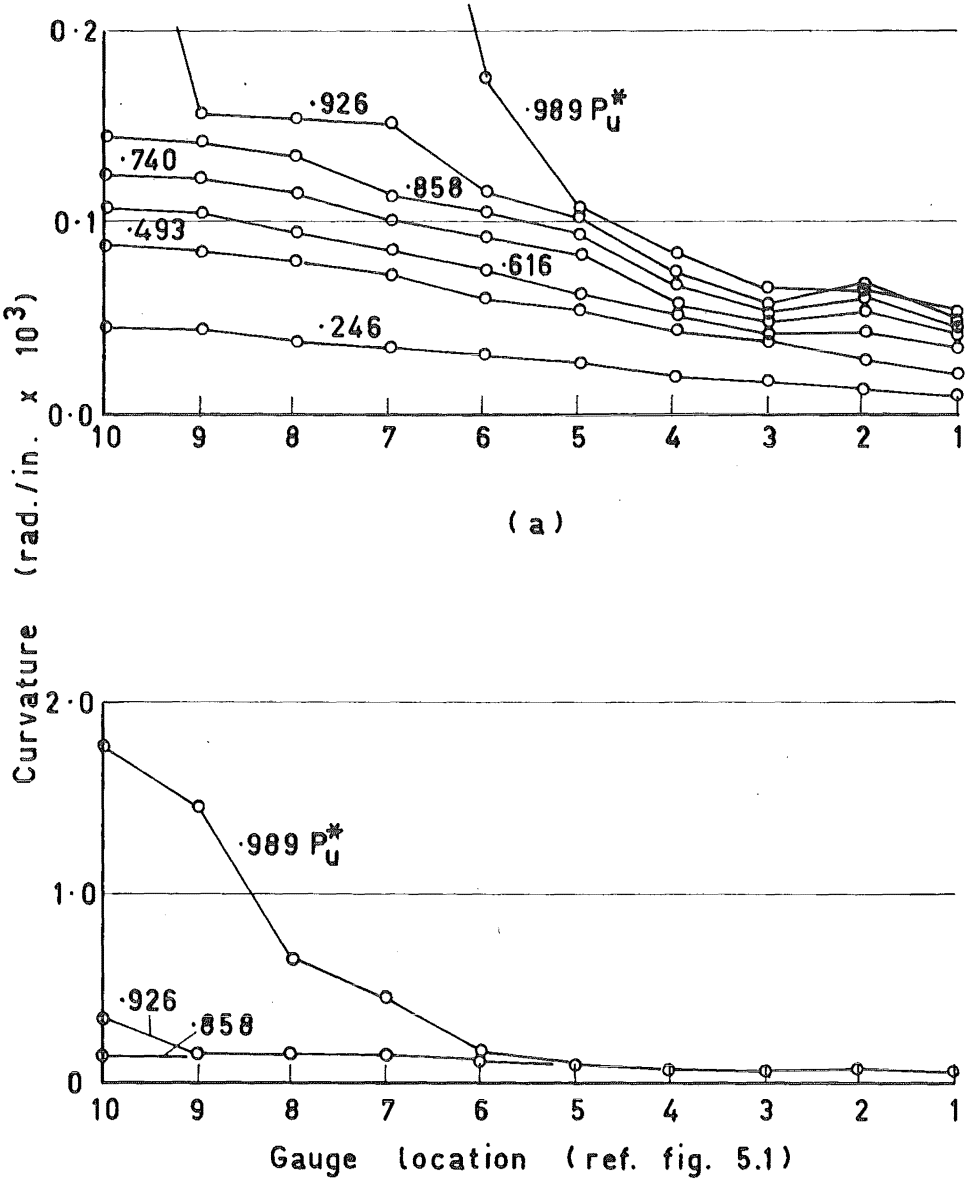

Fig. 5.9 Equivalent Curvature in Beam N1-S63

ment at the section had not yielded. The effective compression zone was small because of the penetration of the diagonal crack (see fig. 5.3). Again from fig. 4.11 it can be seen that only the concrete above the diagonal crack is effective in resisting the moment at the section AA'.

Maximum concrete compression observed in beam N1-S32was 3600 microstrains at .919 P_u^*. 2600 microstrains were measured in beam N1-S63 at .926 P_u^*. Unfortunately the maximum unconfined compressive strains could not be obtained from the tests.

5.3.3 Cracking

The cracking can conveniently be divided into four types, three of which are; flexural, diagonal, and dowel and aggregate interlock cracking. A fourth type is cracking of the compression zone owing to arch action. This will be described briefly in section 5.3.4.

5.3.3.1 Flexural Cracking

Fig. 5.10 is a diagramatic representation of the displacements along and across some cracks in side 2 of beam N1-S32. The displacements shown are typical of those measured in the other two beams being discussed. As was found in the beams without web

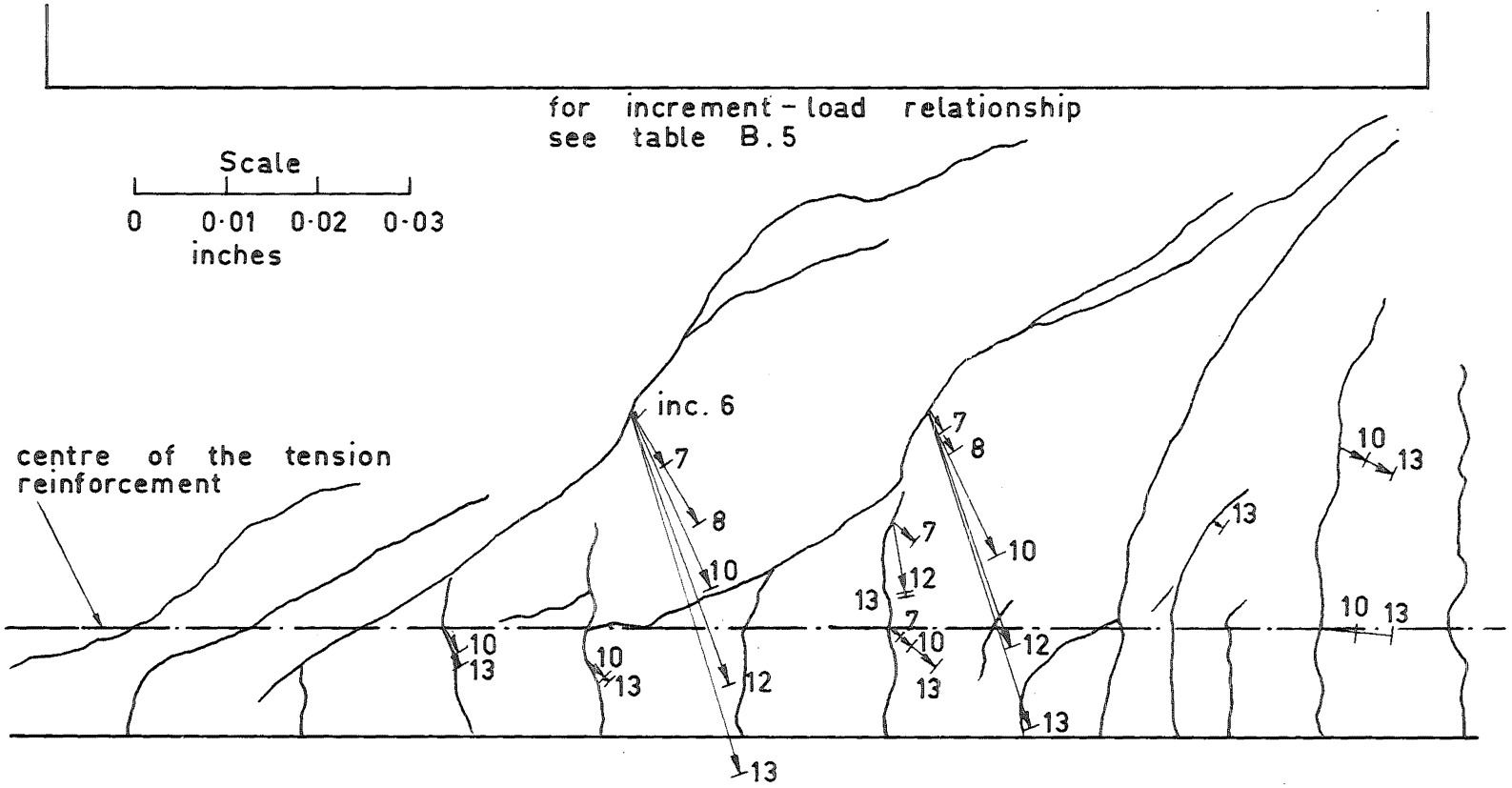

Fig. 5.10 Displacements Across Cracks in Side 2 of Beam N1-S32

reinforcement the displacement along the cracks is smaller at the level of the reinforcement than nearer the centre of the beam. All the secondary cracks have not been shown in this figure for clarity.

From figs. 5.3, 5.4 and 5.5 it can be seen that there was only light flexural cracking in the top of the test sections. No real distinction can be made between flexural and diagonal cracking especially in the region of low moment. When the cracks formed in this region they were inclined and none penetrated far normal to the axis of the beams. As was discussed in chapter 3 shrinkage cracks formed along the stirrups but these were considered to have negligible effect on flexural and diagonal cracking.

5.3.3.2 Diagonal Cracking

In each of the three beams two diagonal cracks formed almost at the same load intensity. In all cases the cracks propagated relatively slowly compared with the corresponding beam without web reinforcement. Figs. 5.3, 5.4 and 5.5 show the load increments at which the cracks formed, and to where they propagated. The crack at the low moment end of the test section stabilised once the second diagonal crack was well developed. This crack then propagated progressively towards the section of maximum moment

until it had penetrated deep into the compression zone. The crack patterns for the three beams are all similar. A third diagonal crack, much steeper than the other two, formed also. It was an extension of a well developed flexural crack near the maximum moment section. The most critical of the three diagonal cracks in each beam was the middle one, which had a slope of approximately 45^{o} to the longitudinal axis of the beam. It was along this crack that separation occurred in two of the beams.

5.3.3.3 Dowel and Aggregate Interlock Cracking

There was very little dowel or aggregate interlock cracking in any of the beams between the section of maximum moment and the nearest diagonal crack. Dowel cracking was well developed on the low moment side of these diagonal cracks. They did not form until the diagonal cracks had formed. Most of them propagated along the tension reinforcement to the adjacent flexural crack but a few stabilised short of the next crack as can be seen in fig. 5.5.

5.3.4 Arch Action

Once the first diagonal crack had developed some cracks appeared in the compression face of the three beams (see figs. 5.3, 5.4 and 5.5). Where there

were none of these cracks the concrete in the compression zone above the diagonal crack showed smaller compressive strains. Fig. 5.11 shows selected strain profiles in the concrete above the diagonal crack nearest the section of zero moment. These profiles are obtained from measurements at load increments just before and just after formation of the diagonal crack. All the profiles drawn show a decrease in compression of the extreme compression fibre and an increase in compression of the concrete further down the beams after diagonal cracking. This indicates that the centre of the compression force in the section has moved towards the tension reinforcement when diagonal cracking has developed. The position of the centre of the compression force for the three beams has been plotted in fig. 5.12. The method of determining this has been described in section 4.5.5. It follows a smoother profile at high loads than low loads (see fig. 5.12 (b) and (c)). This is due to the evening out of tension reinforcement stresses along the beam by diagonal cracking of the beam and yielding of the reinforcement (see fig. 4.2)

5.3.5 Deformation Characteristics

For the purposes of the deformation chatacteristics the beams are considered to be fully

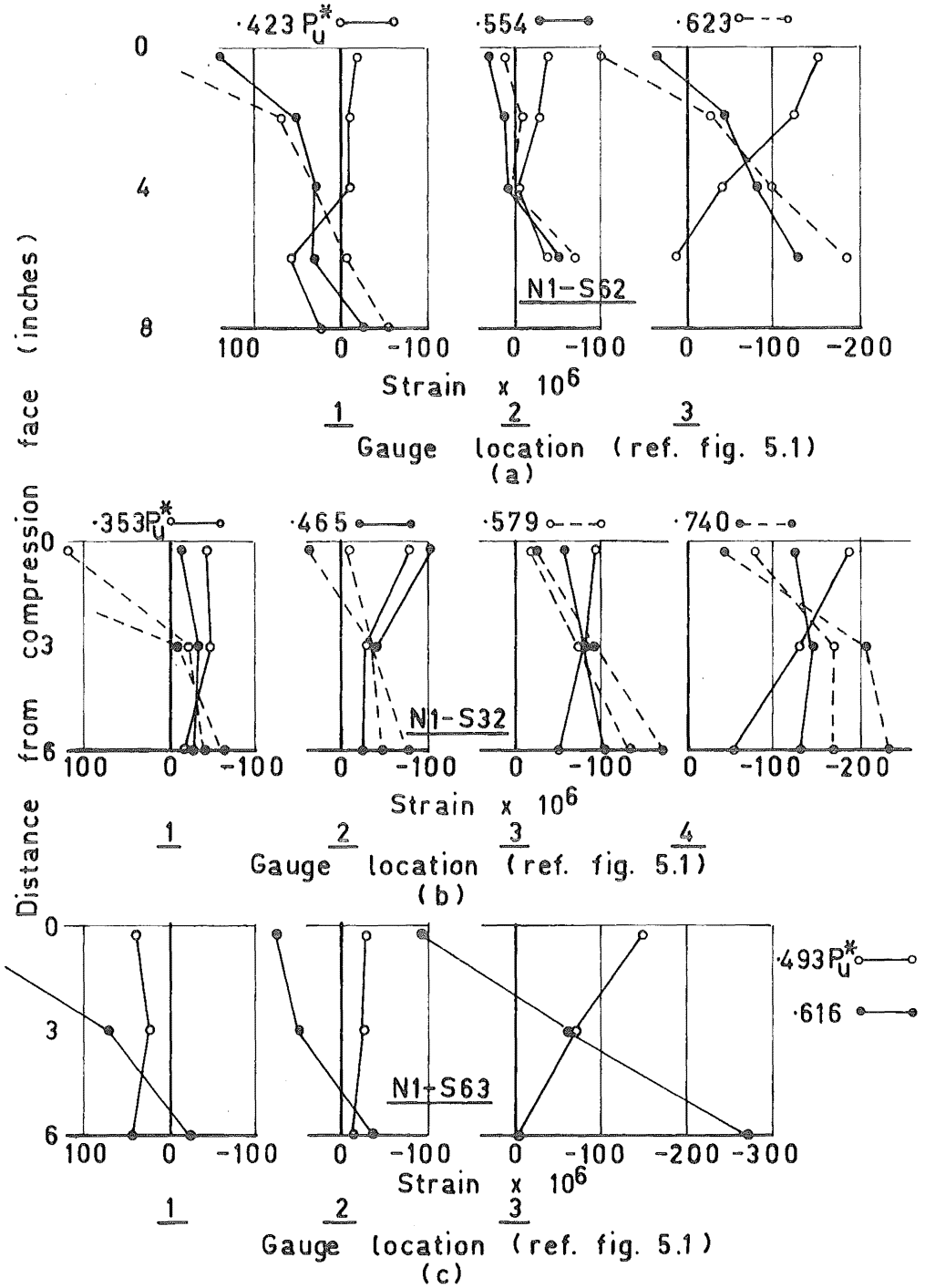

Fig. 5.11 Concrete Strain Profiles above the Top Diagonal Crack in Beams N1-S62, N1-S32 and N1-S63

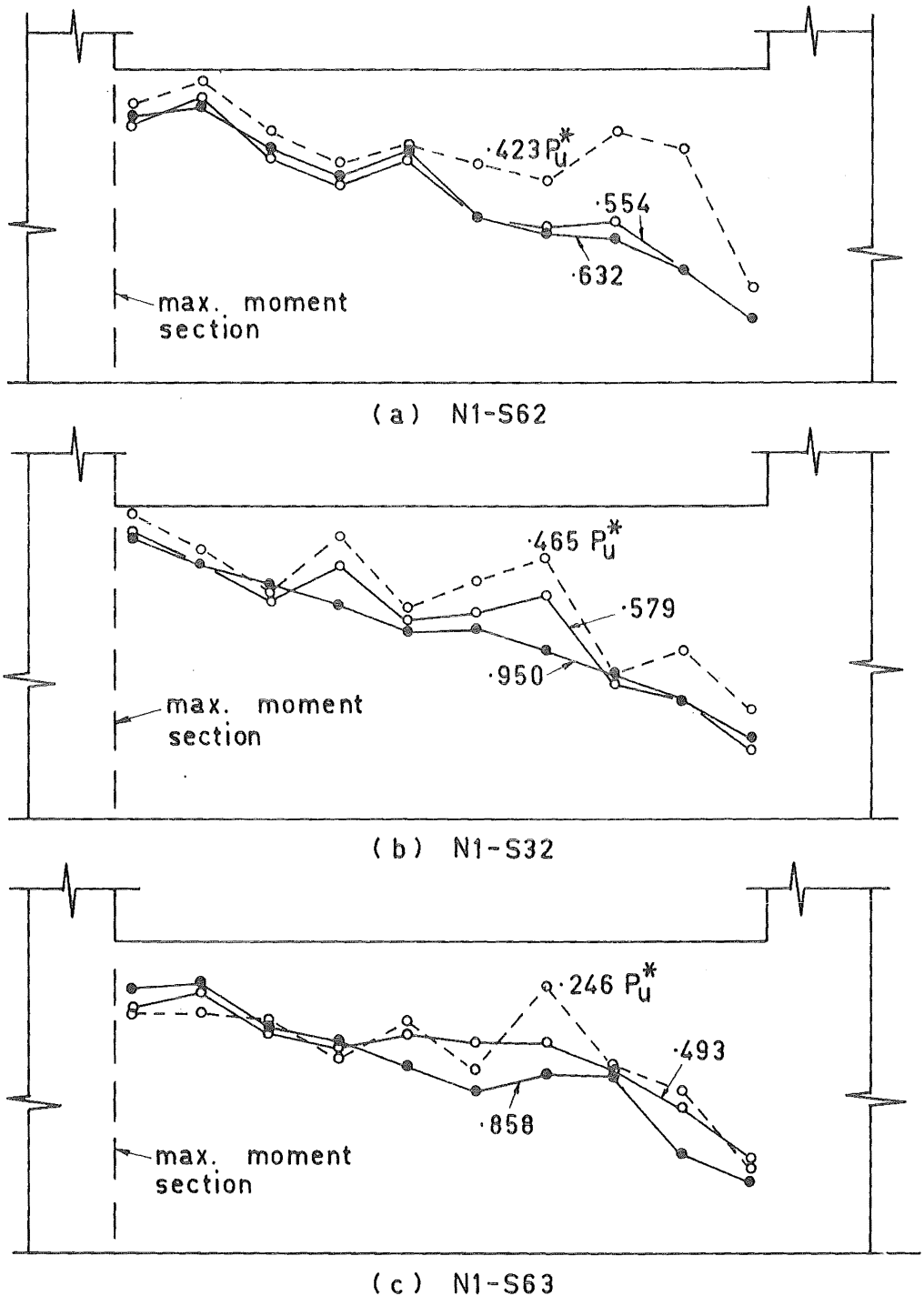

Fig. 5.12 Centre of Compression Force in Beams N1-S62, N1-S32 and N1-S63

fixed as shown in fig. 5.13.

5.3.5.1 Transverse Expansion

When a diagonal crack forms in a beam it becomes deeper by virtue of the crack opening in a direction normal to the beam's axis. This will be termed transverse expansion. Because of this effect the measured deflection of the tension and the compression faces will be different. Figs. 5.14 (a), (b) and (c) show the transverse expansion of the three beams. Both expansions measured over 89% of the overall beam depth and 76% of the stirrups are presented in the figures. The transverse expansion measured on the stirrups corresponds to 67% of the overall beam depth.

The diagonal crack first became apparent in beam N1-S62 at .423 P_u^*, in beam N1-S32 at .465 P_u^*, and in beam N1-S63 at .493 P_u^*. This is evident from the first significant transverse expansion measured on the beams as shown in fig. 5.14. After first cracking the diagonal cracks open up uniformly. The jump shown between .740 and .858 P_u^* on beam N1-S63 was a result of sudden formation of dowel cracks (see fig. 5.5).

The transverse expansion from stirrup strains are seen to be always smaller than the expansion measured on the concrete across the entire beam. The distribution of total stirrup elongation is approximately parabolic

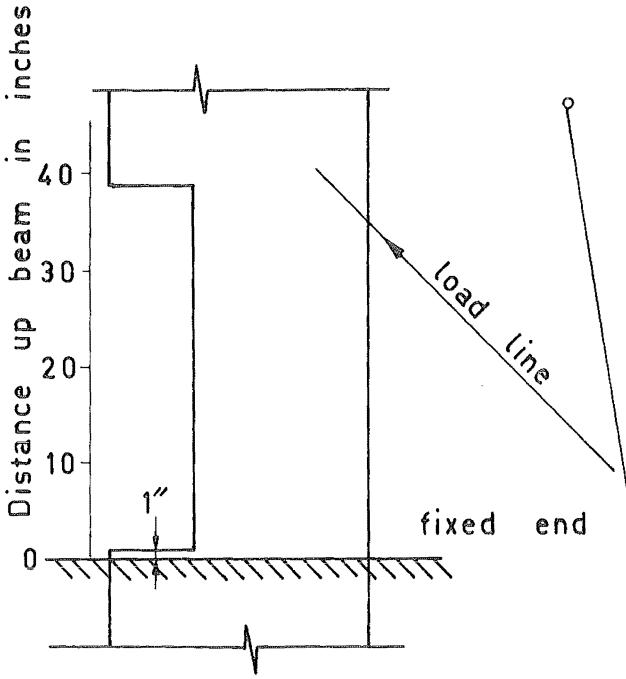

Fig. 5.13 Position of Beam Fixing

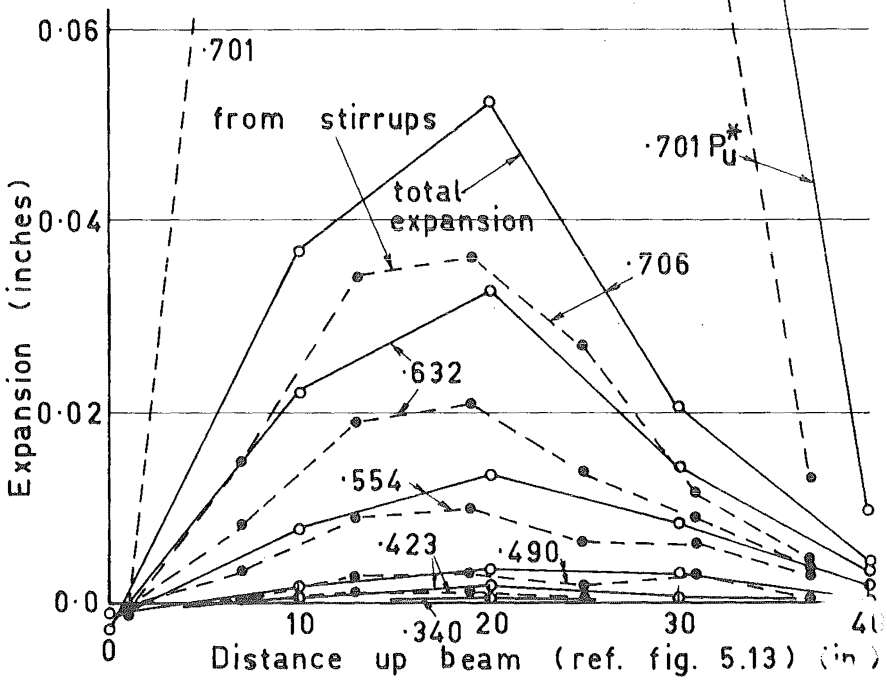

Fig. 5.14(a) Transverse Expansion of Beam N1-S62

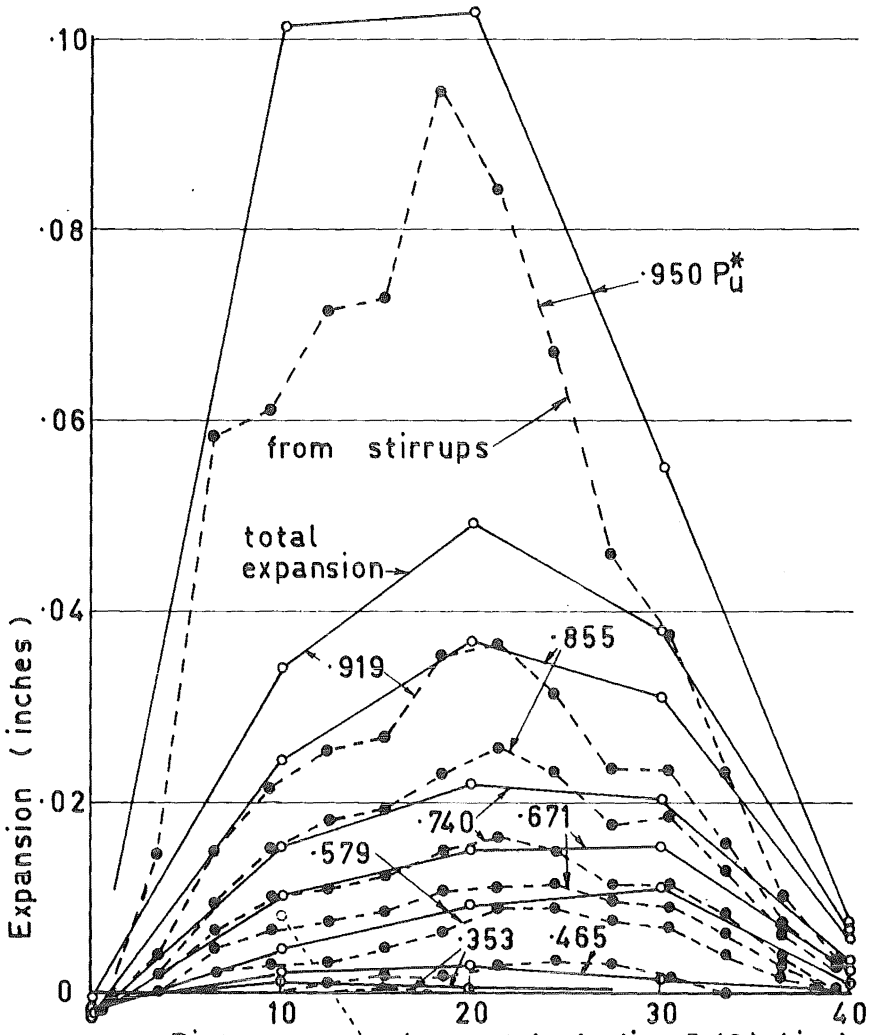

Fig. 5.14(b)&(c) Transverse Expansion of Beams N1-S32 and N1-S63

for stirrups over the extent of a diagonal crack. To see this compare fig. 5.14 with the corresponding photographs of the crack patterns of the three beams, viz., fig. 5.3, 5.4 and 5.5

The deflected shape of beam N1-S63 has been drawn in fig. 5.15. The deflection of the compression face is shown by the full lines and that of the tension face by the dashed lines. A noticable reverse curvature can be seen in the compression face at and after .616 P_u^*. This is caused by arch action and the consequent cracking of the compression face at the upper end of the beam. The tension face shows a more normal deflected shape of single curvature. This type of deflected shape is typical of the three beams being discussed. The slope of the beam at the built in end is due to shear deformations.

5.3.5.2 Deformation of the End Section

The deformation of the sections at the upper end of the test length of the beams are plotted at selected load intensities in fig. 5.16. Unfortunately the only section observed once yield was well developed in the tension reinforcement, was on beam N1-S32. As can be seen in the figure, the section at .950 P_u^* was not plane but the deviation from a plane section was no more than at lower load intensities.

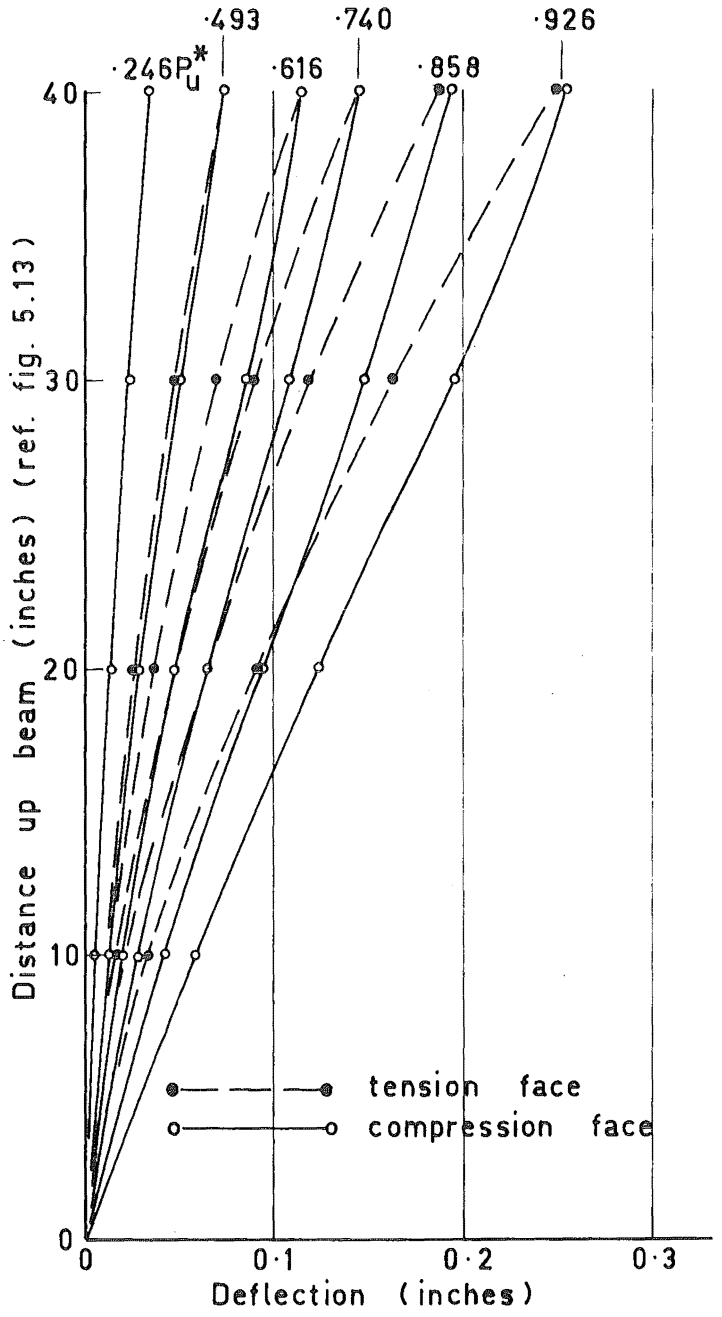

Fig. 5.15 Deflected Shape of Beam N1–S63

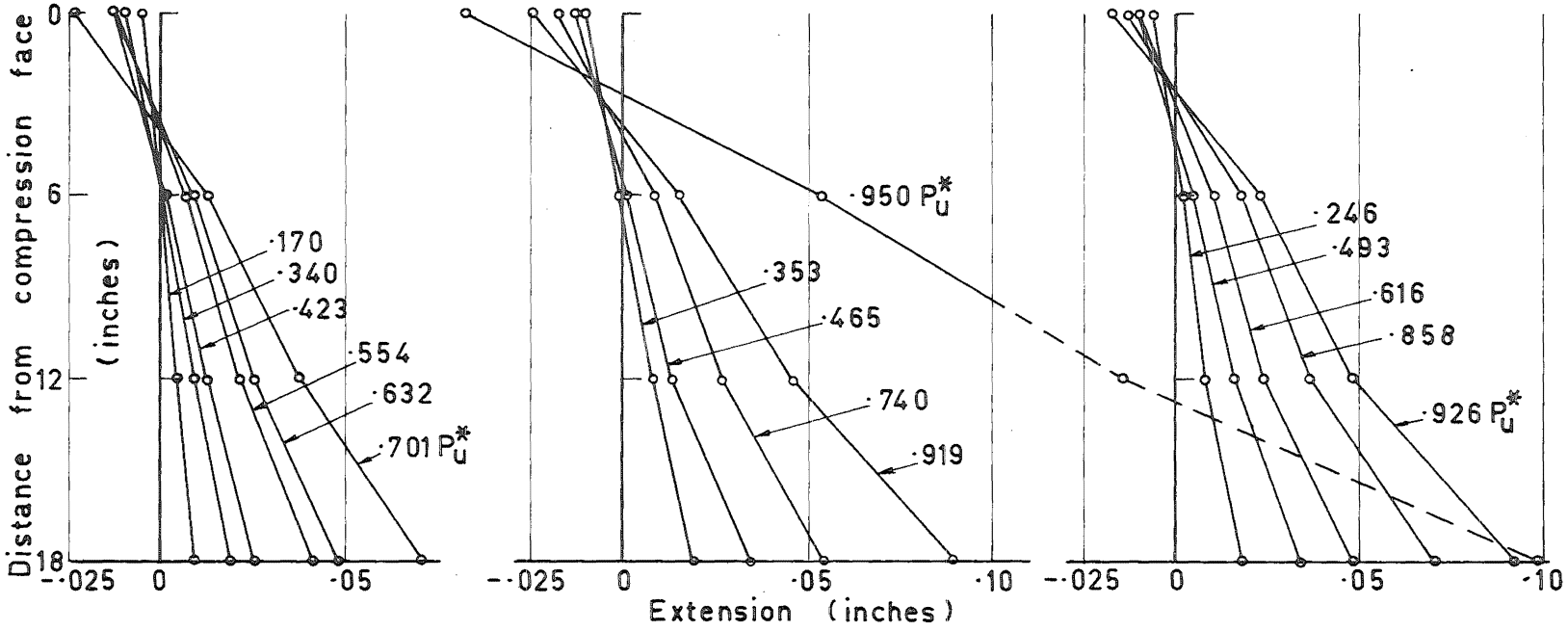

Fig. 5.16 Deformation of Top End Section of Beams N1-S62, N1-S32 and N1-S63

The shape of the section in all three beams was the same, being described approximately as a very flat "S". Fig. 5.17 shows the deformation of a section in a cracked reinforced beam subjected to shear. The bending moment diagram of the concrete cantilever is sketched and so is the deflected shape this produces. Superimposing it on the plane deflected shape of the section gives the deformed shape of section AA'. It is seen that this flat "S" corresponds with those measured.

5.3.5.3 Load Deflection Characteristics

The total beam deflections were measured by dial gauges and corrected for movement of the whole loading frame as described in chapter 3. Flexural deflections were calculated by summing the equivalent curvatures at each section of the beams. The method of finding deflections in this way was also described in chapter 3. Figs. 5.18, 5.19 and 5.20 show the load deflection relationships for beams N1-S62, N1-S32 and N1-S63 respectively. Also included in these figures are the theoretical deflections of the uncracked and flexurally cracked beams. These will be discussed more fully in chapter 8.

Part (a) of fig. 5.18 is the deflection of beam N1-S62 in the elastic range. This beam, which failed in shear, was subjected to small plastic deformations

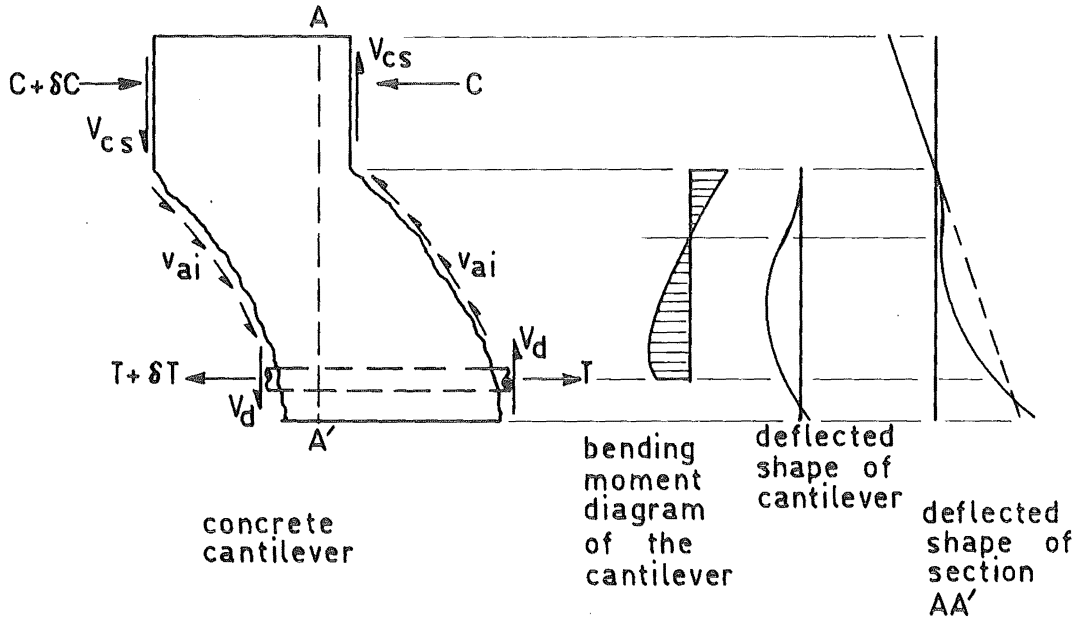

Fig. 5.17 Deformation of a Section in the Shear Span of a Beam

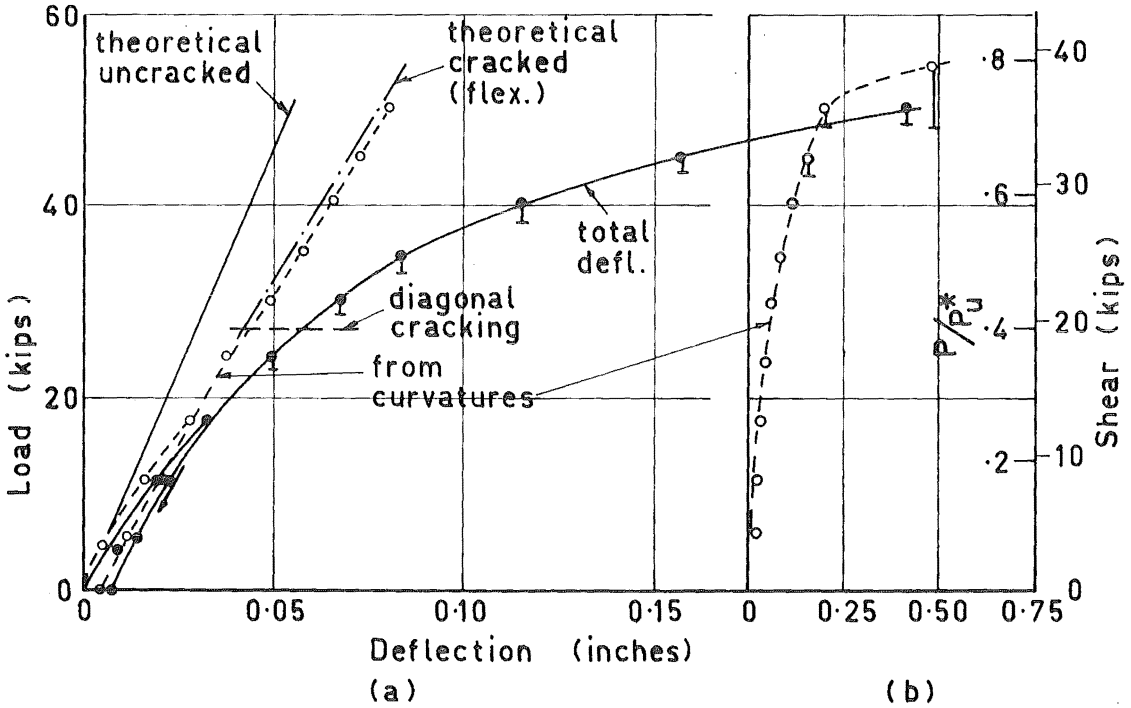

Fig. 5.18 Beam N1-S62 Load - Deflection Relationship

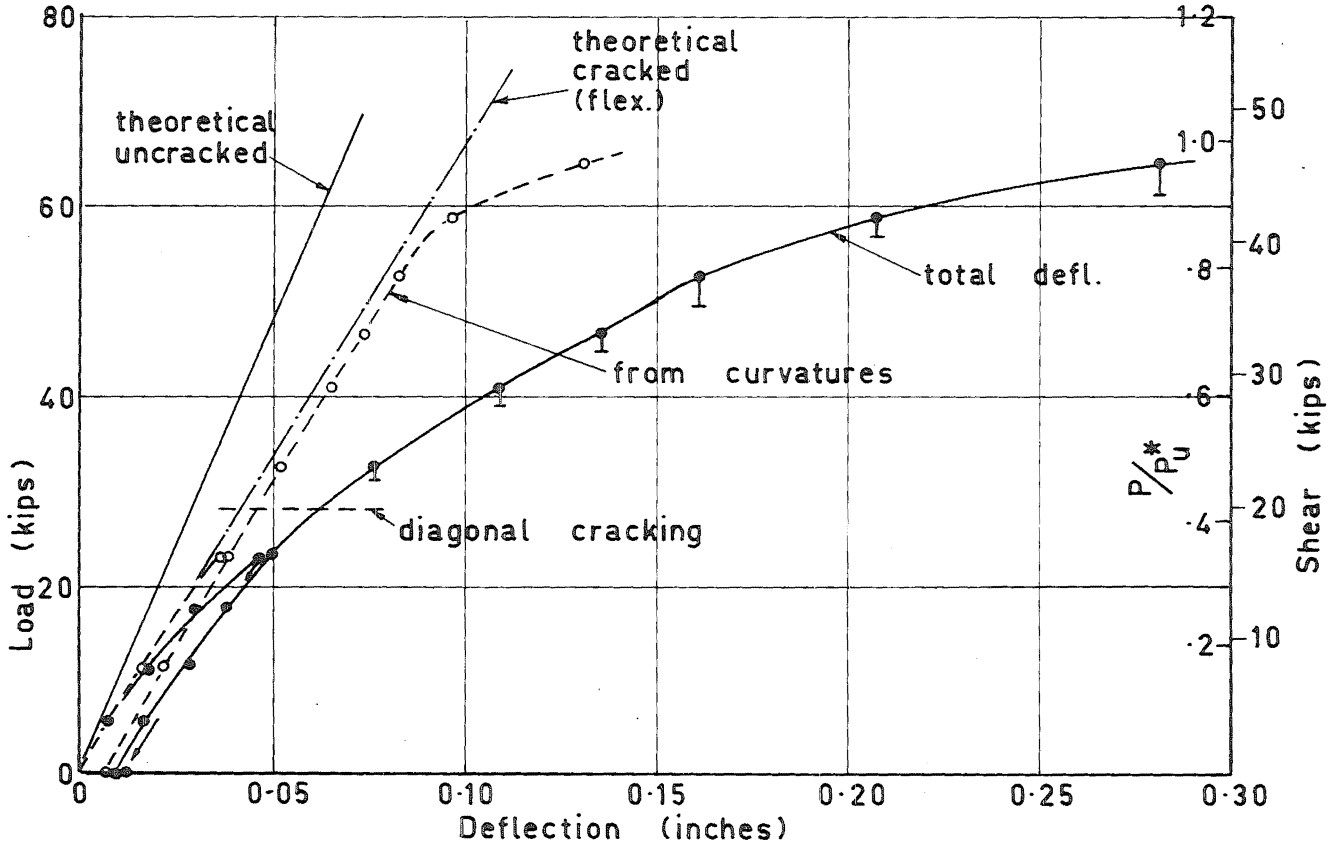

Fig. 5.19(a) Beam N1-S32 Load - Deflection Relationship

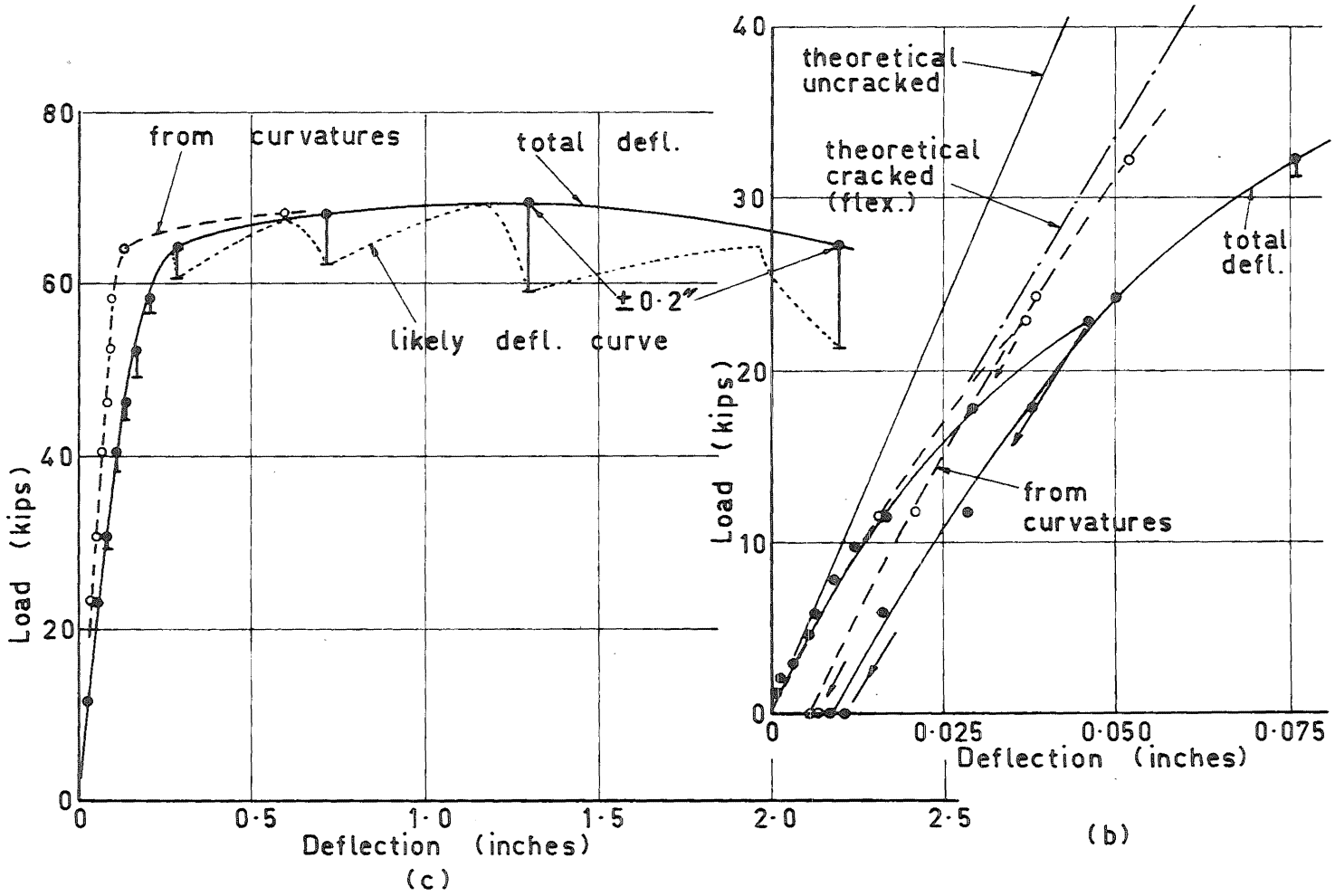

Fig. 5.19 (b)&(c) Beam N1-S32 Load – Deflection Relationship

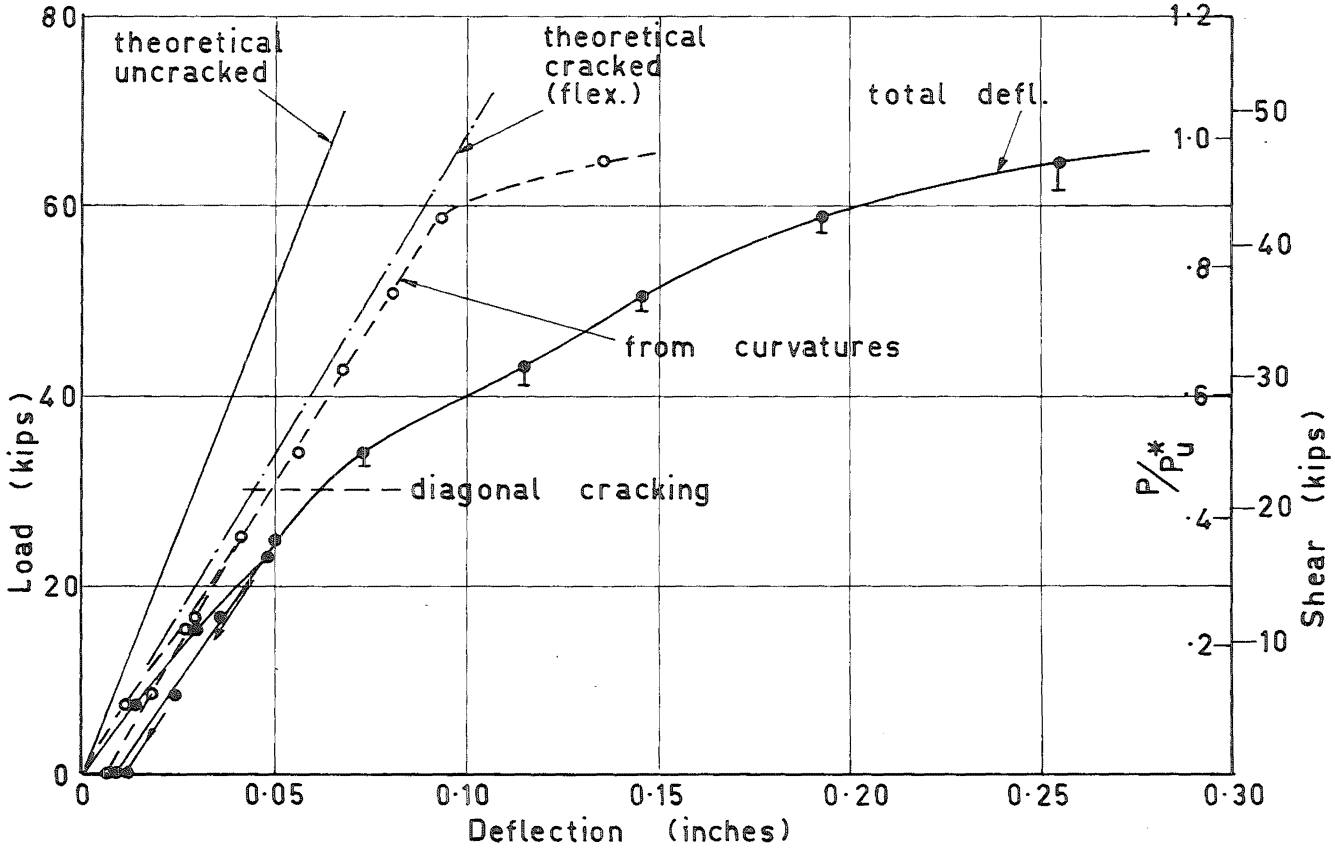

Fig. 5.20 Beam N1-S63 Load-Deflection Relationship

before failure. These may be seen in part (b). At higher loads there was considerable creep in all the beams with web reinforcement. The deflections have been plotted to the load attained at the particular increment. A dotted curve showing the approximate path of the load deflection relationship taking short term creep into account is also shown. The fall off in load was measured (see tables in appendix B) at each load increment.

The difference between the total deflection and the deflection calculated from equivalent curvatures is the shear displacement in the beams. Once diagonal cracking has been initiated the shear displacement is seen to become an appreciable proportion of the total. At .632 P_u^* on beam N1-S62, over half of the total deflection was due to shear deformations. The kink at .059 P_u^* in the first load cycle (see fig. 5.18 (a)), is probably an incorrect dial gauge reading.

Part (a) of fig. 5.19 shows the deflection of beam N1-S32 in the predominantly elastic range. Part (b) is the initial loading section of (a) enlarged to show details of the curves. As can be seen in the figure several small load increments were used to find the stiffness of the beam prior to cracking. As was the case with beam N1-S62, once diagonal cracking had developed at .465 P_u^*, the shear displacement became a very

significant proportion of the total deflection. The load deflection curve extending into the plastic range is shown in fig. 5.19 (c). The beam is seen to be very ductile, having a member deflection ductility factor of at least 8. This is calculated from the deflection on the falling branch of the curve at a load corresponding to the yield load, divided by the deflection at the yield load. As the curve shows s smooth transition from elastic to plastic, the yield deflection, and load, are found from extrapolation of the adjacent straight portions of the relationship.

The shape of the load deflection relationship of beam N1-S63 shown in fig. 5.20 is similar to that of beam N1-S32. Slight diagonal cracking had commenced by .493 P_u^* and above this the shear deformations became increasingly significant. No post-elastic deflections were measured on this beam.

5.3.6 Failures

At this stage it is appropriate to discuss qualitatively the failure of the three beams. Beam N1-S62 failed in shear by separation across the critical diagonal crack as seen in fig. 5.21. Details of the separation of the compression zone are shown in fig. 5.22. The three stirrups that crossed the separation crack all yielded. At failure the crack

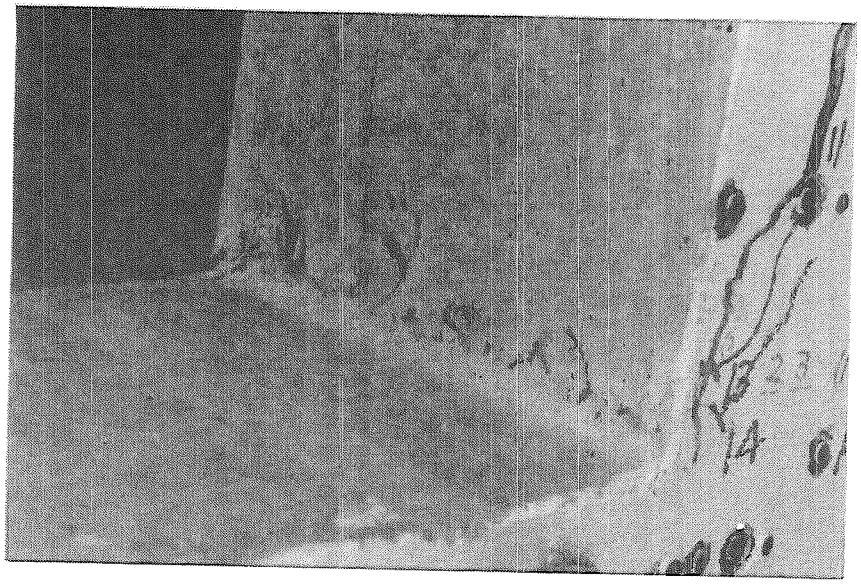

Fig. 5.22 Critical Compression Zone of Beam N1-S62 at Failure

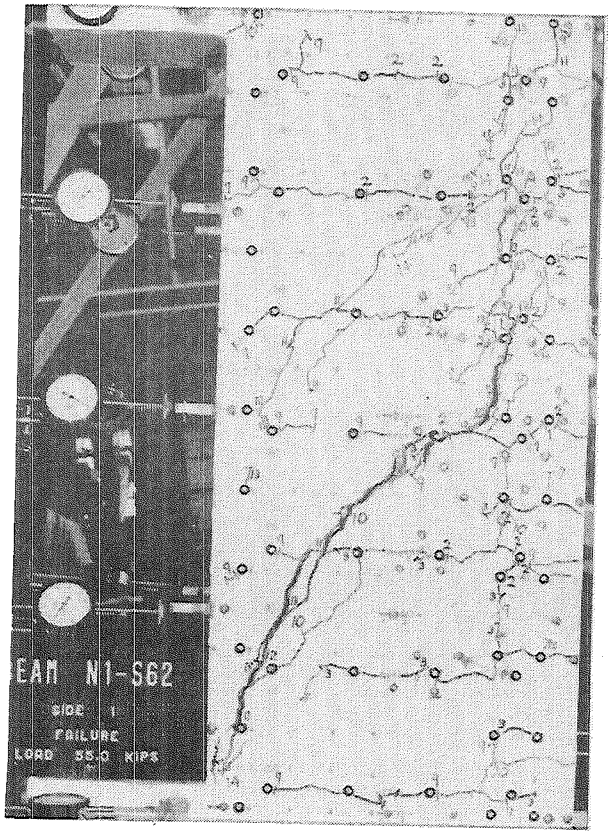

Fig. 5.21 Beam N1-S62 at Failure

propagated right to the compression face of the beam and the split along the tension reinforcement opened by as can be seen in fig. 5.21. At load increment 15 the load on the beam was held at 54.90 kips (.80 P_u^*) for one minute, but when the valve to the hydraulic jack was closed it dropped back to 48.46 kips after 14 minutes.

Beam N1-S32 failed in a shear-flexure type mode. This is characterised by separation along a diagonal crack as well as considerable post-elastic deformation of the beam and crushing of the compression zone concrete. Fig. 5.23 shows side 1 of beam N1-S32 at failure. The stirrups yielded across the diagonal cracks which opened near failure. The concrete began to crush at 1.02 P_u^*. When the crushed concrete was removed after failure it was found that the stirrup at this section was bowed outwards considerably. Fig. 5.24 shows a close up view of this stirrup where the bow is clearly visible. It is believed that the lateral force exerted by the confined concrete caused the stirrup to bend in this manner. The compression reinforcement did not buckle although it showed strains considerably in excess of yield.

A photograph of side 1 of beam N1-S63 after failure is shown in fig. 5.25. The failure is seen to be of the shear-flexure type with very distinct separation along a diagonal crack. Details of the

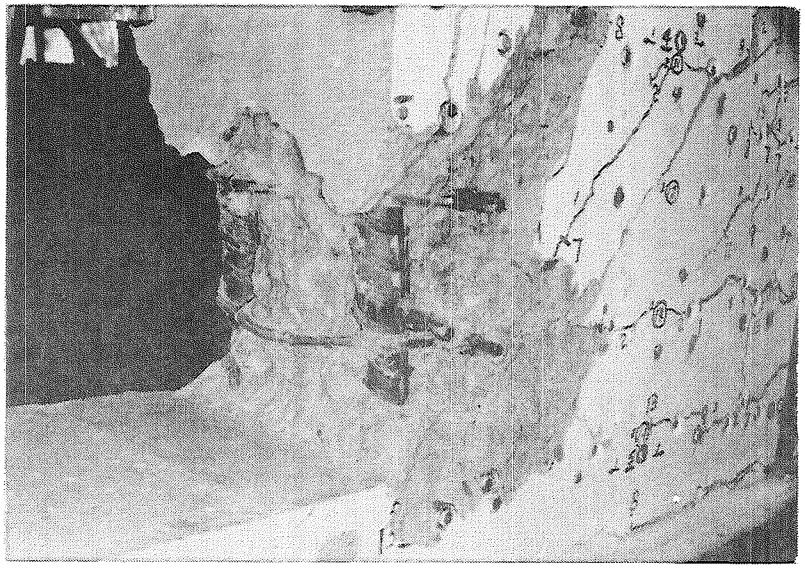

Fig. 5.24 Critical Compression Zone of Beam N1-S32 at Failure

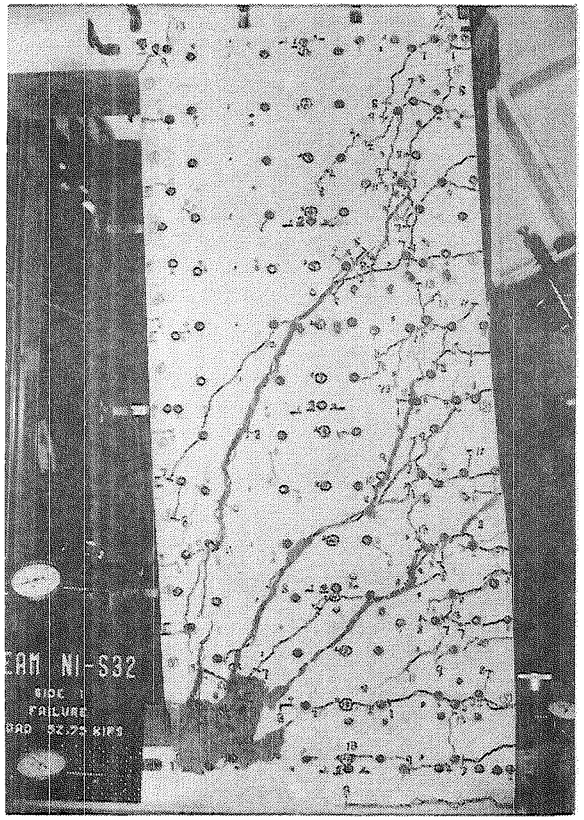

Fig. 5.23 Beam N1-S32 at Failure

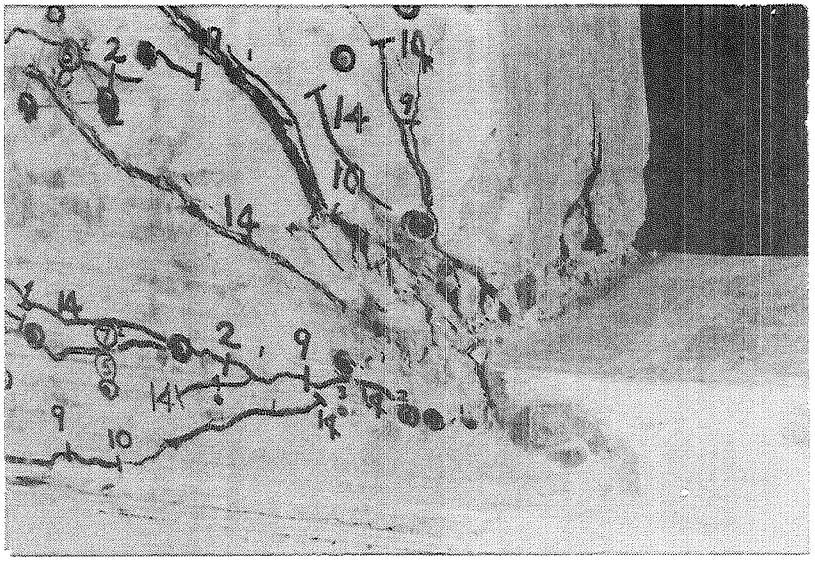

Fig. 5.26 Critical Compression Zone of Beam N1-S63 at Failure

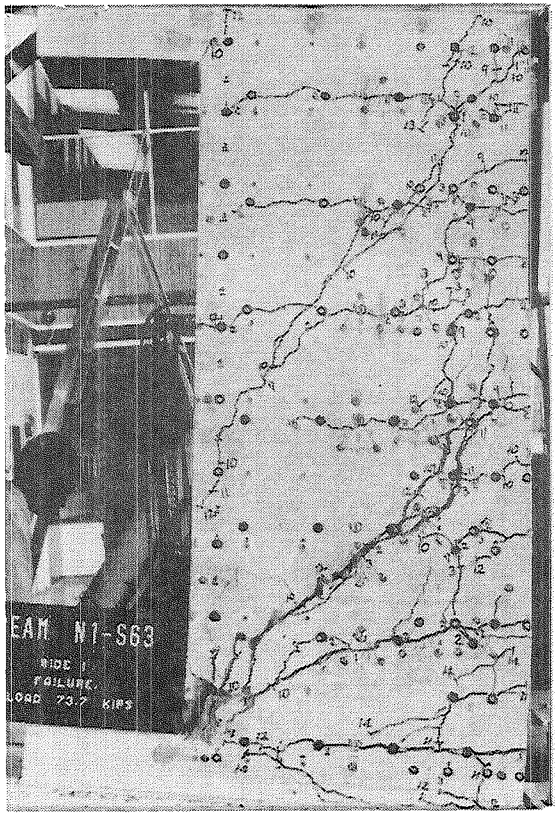

Fig. 5.25 Beam N1-S63 at Failure

crushed compression area of the beam can be seen in fig. 5.26. There are definite signs of crushing and spalling along with penetration of the diagonal crack right to the compression face of the beam. All except one of the stirrups that crossed the critical diagonal crack had yielded at .989 P^*_u. Concrete was spalling from the compression zone at 1.08 P^*_u. No signs of compression reinforcement buckling were observed.

5.4 Beams N2-S62, N2-S32 and N2-S63

The position of the 4 inch demec gauge rows, and the position of the line of action of the load on the three beams are shown in fig. 5.1.

5.4.1 Behaviour of the Longitudinal Reinforcement

5.4.1.1 Tension Reinforcement

The average strains in the tension reinforcement of the three beams are presented in fig. 5.27. Only selected load intensities have been plotted. These have been chosen at critical stages in the loading of the beams. The dashed lines show the theoretical strains based on a conventional cracked elastic analysis reviewed in appendix C. The load used in this analysis corresponds with the load intensity for

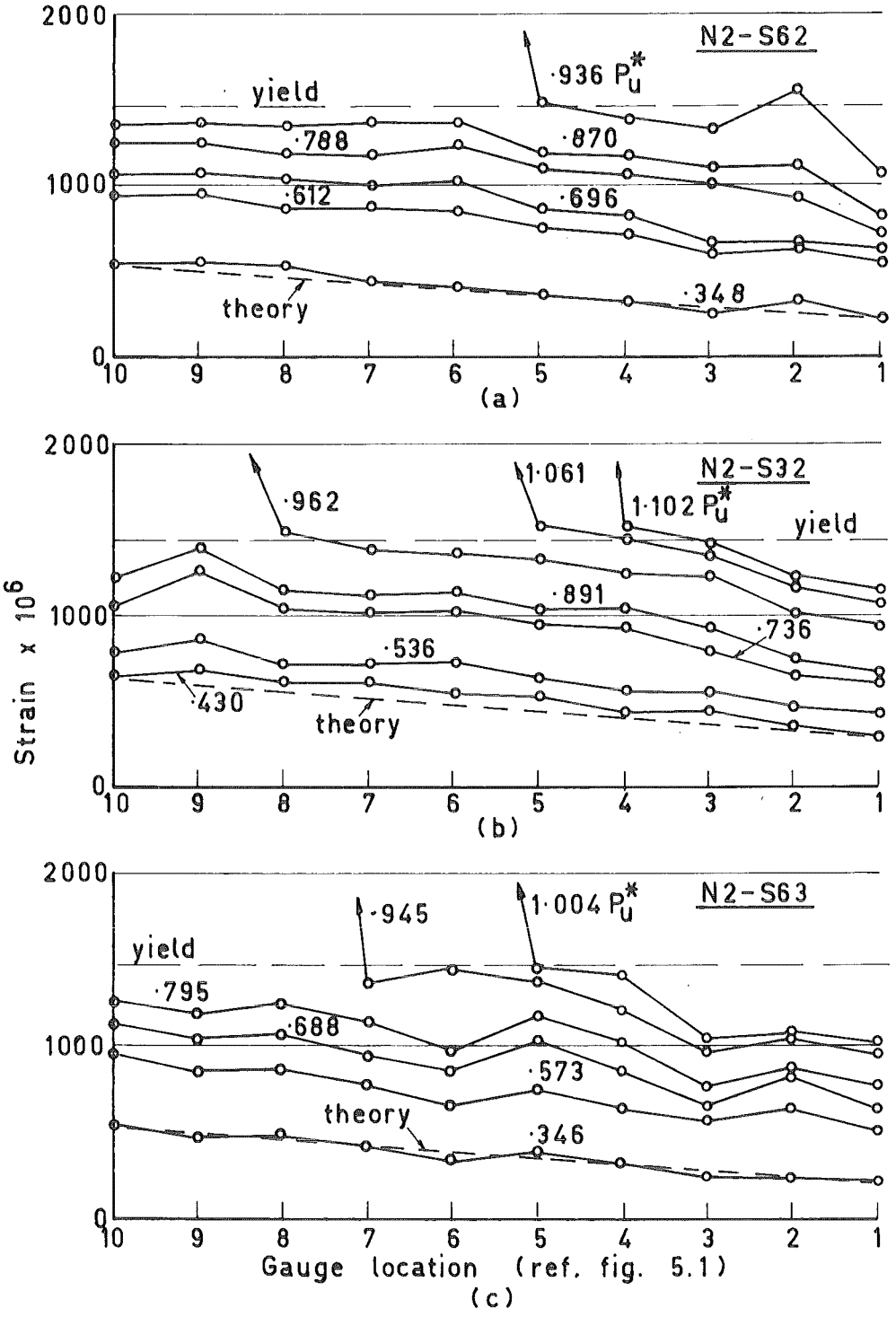

Fig. 5.27 Tension Reinforcement Strains in Beams N2-S62, N2-S32 and N2-S63

the lowest observed strain profiles plotted. These theoretical and measured strain profiles agree well for beams N2-S62 and N2-S63. Beam N2-S32 profiles do now show such good agreement. It is thought that slight diagonal cracking is the reason for this.

Figs. 5.28, 5.29 and 5.30 are photographs of side 1 of beams N2-S62, N2-S32 and N2-S63 respectively. As has already been discussed in section 5.3.1.1, kinks occur in the tension reinforcement strain profiles where the diagonal cracks cross the reinforcement. Fig. 5.27 (a) shows an interesting very distinct flattening of the strain profile at .870 P_u^* and to a lesser extent at .696 and .788 P_u^*. The theory presented in chapter 8 adequately explains this.

5.4.1.2 Compression Reinforcement

Strains in the compression reinforcement of the three beams at various load increments are shown in fig. 5.31. Theoretical strains calculated on a conventional cracked elastic section are shown by the dashed lines. Good agreement between observed and theoretical strains have been obtained at .348 P_u^* on beam N2-S62, and at .430 P_u^* on beam N2-S32. The theoretical strains are low at .346 P_u^* on beam N2-S63.

As can be seen from the figure, once diagonal cracks have formed the compression reinforcement goes

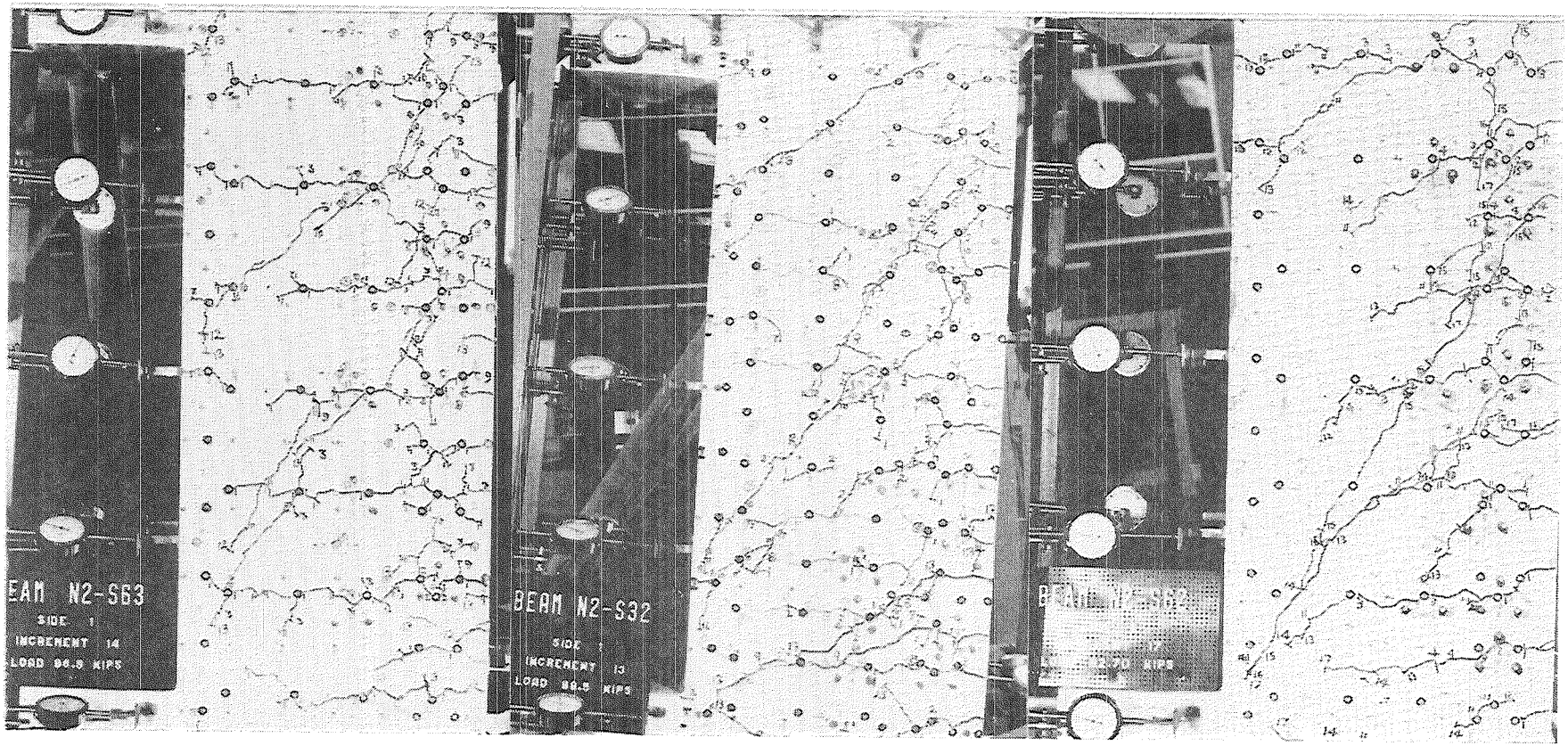

Fig. 5.30 Beam N2-S63

Fig. 5.29 Beam N2-S32

Fig. 5.28 Beam N2-S62

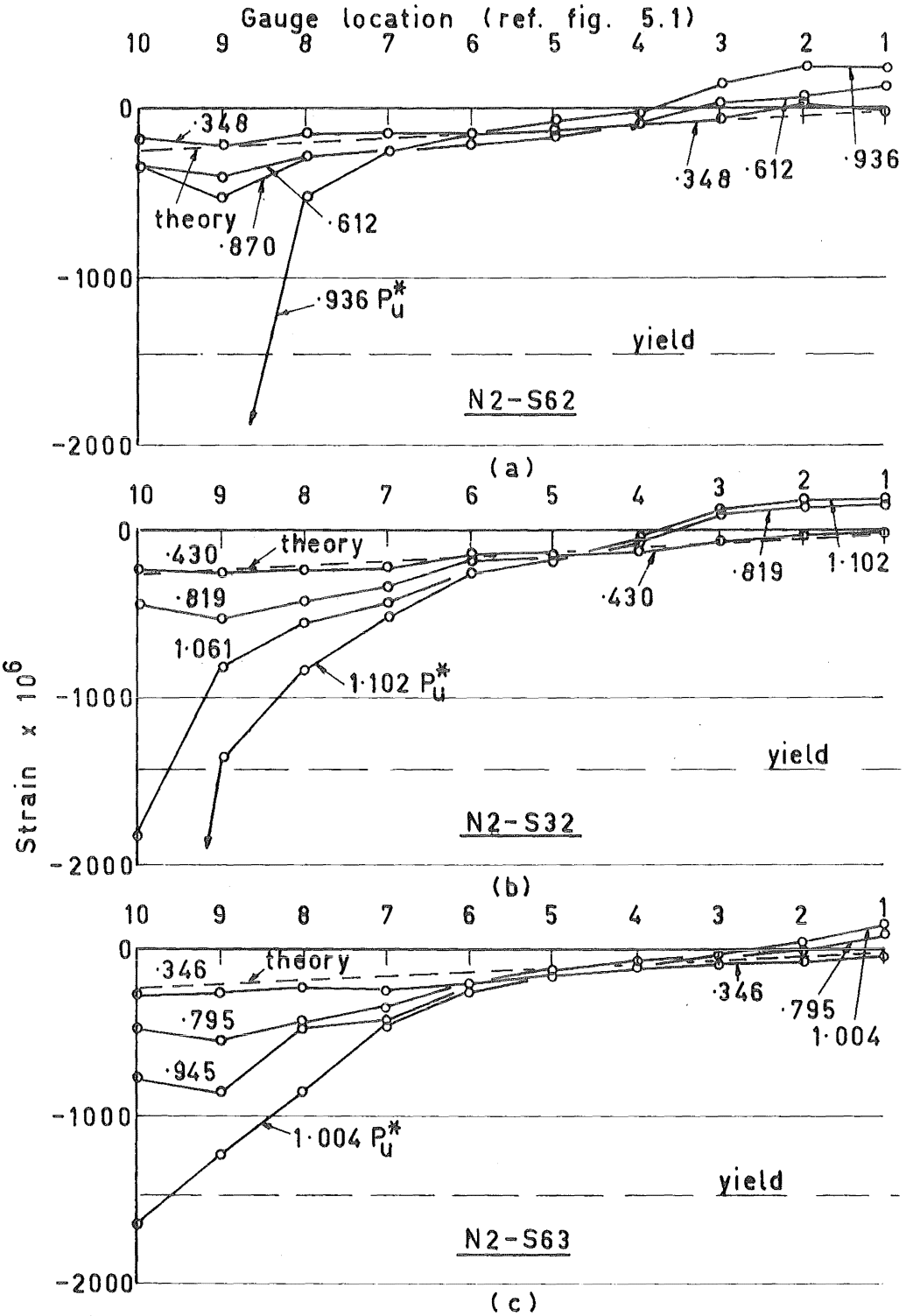

Fig. 5.31 Compression Reinforcement Strains in Beams N2-S62, N2-S32 and N2-S63

into tension at the low moment end of the beam. This has been discussed in section 5.3.1.2. The compression steel yielded only when all the tension steel had yielded at the particular section. Until that point the strains in the compression reinforcement were low.

5.4.1.3 Equivalent Curvatures

Figs. 5.32, 5.33 and 5.34 show the equivalent curvatures calculated from the reinforcement strains in beams N2-S62, N2-S32 and N2-S63 respectively. Part (a) of each figure shows the equivalent curvatures prior to yield of the tension reinforcement and part (b) shows those in the post-elastic range. They are much the same as those from the N1 - series beams. The longer length of plastic deformation in the N2 - series beams is to be expected because the moment gradient along the beam is not so high as in the N1 - series. When the load increased above that causing yield at the maximum moment section, the yield would spread along the reinforcement more rapidly.

5.4.2 Cracking

The crack propagation characteristics of the three beams were similar to those of beams in the N1 - series discussed in section 5.3.3. Thus only new features will be presented here.

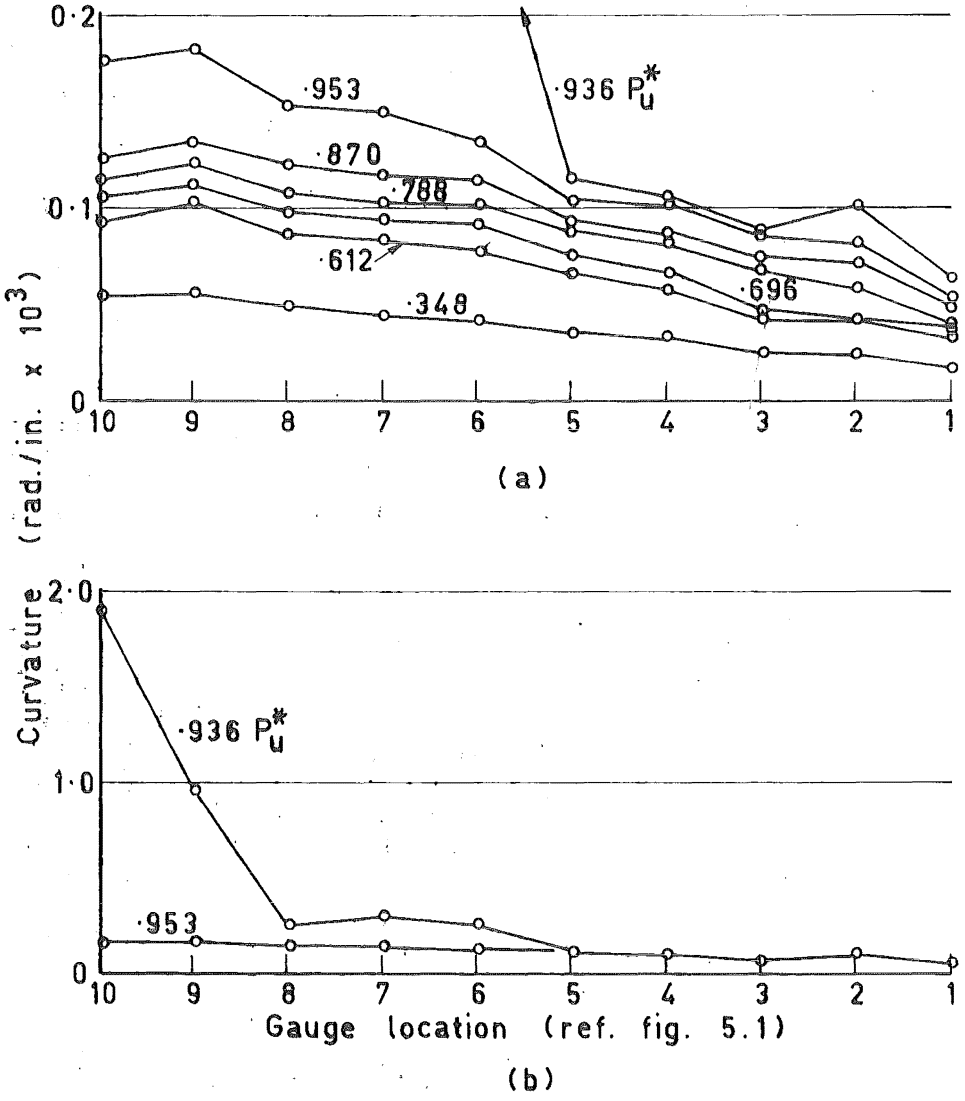

Fig. 5.32 Equivalent Curvatures in Beam N2-S62

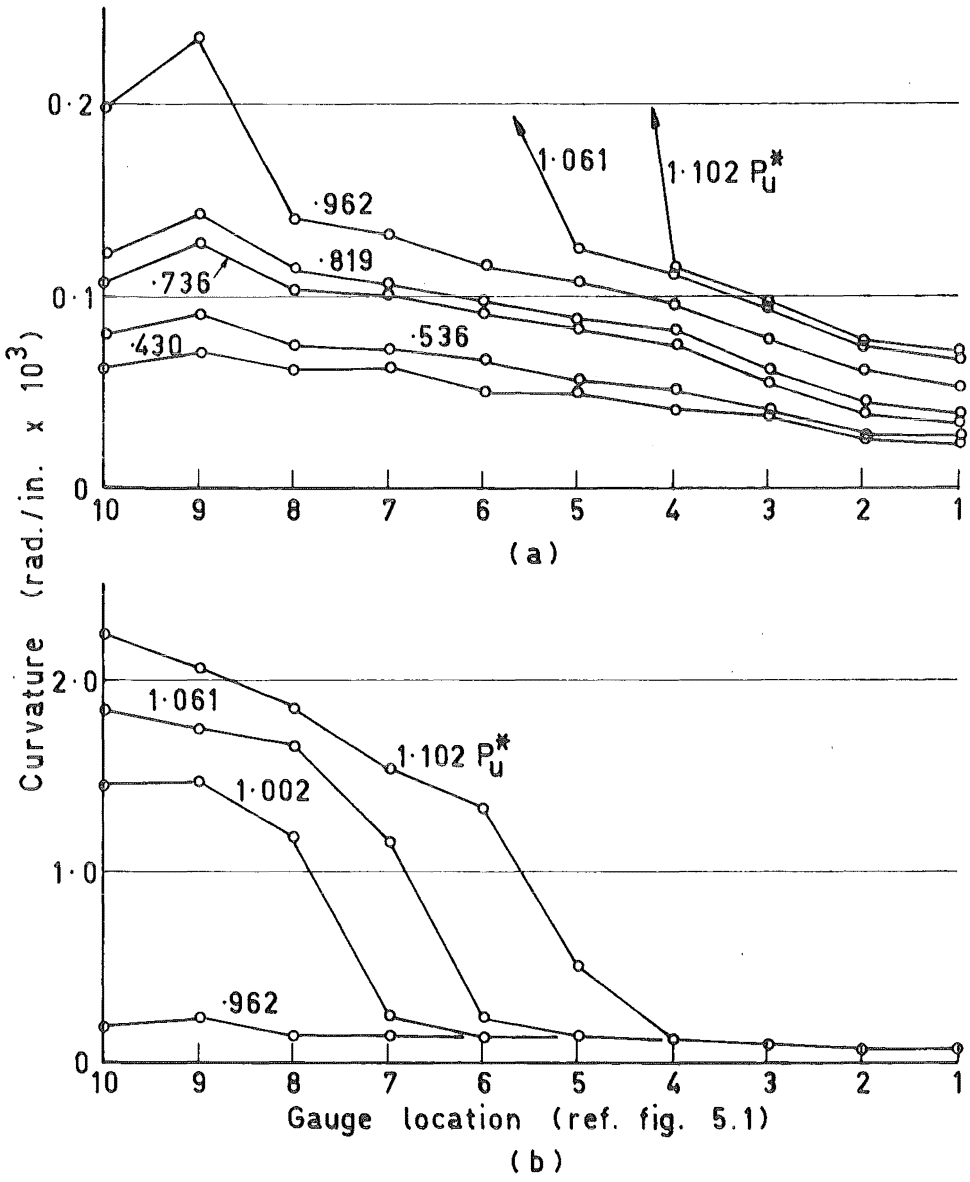

Fig. 5.33 Equivalent Curvatures in Beam N2-S32

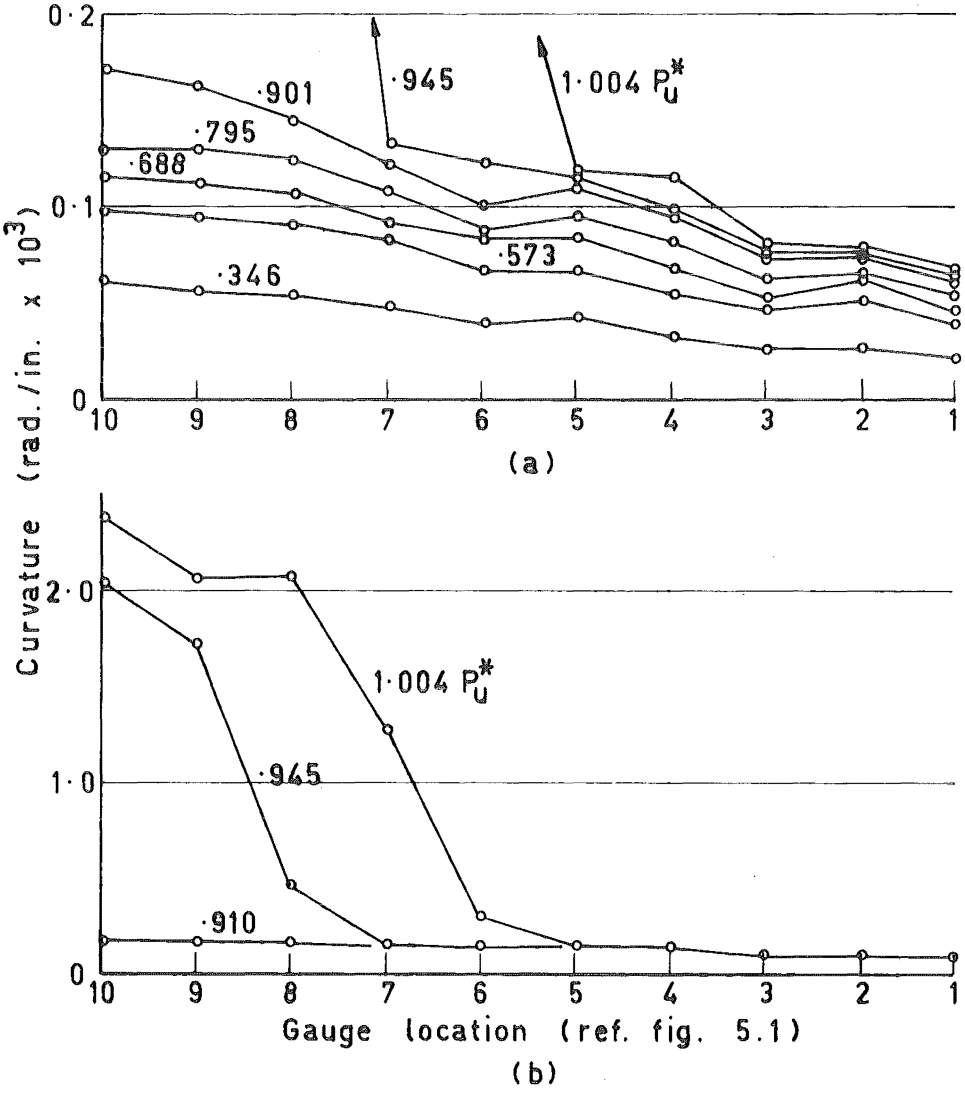

Fig. 5.34 Equivalent Curvatures in Beam N2-S63

5.4.2.1 Flexural Cracking

Beam N2-S32 showed considerable cracking prior to loading. These cracks can be seen in fig. 5.29, as lightly drawn with the marking "0" at either end. Beam N2-S63 showed a tendency to crack along the stirrups at low load intensities. They are not considered to be flexural cracks.

As with previous beams the spacing of the flexural cracks is affected by discontinuities in the concrete. Cracks formed sooner than expected from consideration of the measured modulus of rupture of the concrete. This is attributed to shrinkage.

Displacements along and across some cracks in side 2 of beam N2-S63 are shown in fig. 5.35. The displacements across the diagonal cracks near ultimate load were large. The largest displacements observed were towards middepth of the beam. Unfortunately the pattern of relative deformations of the concrete cantilevers is not very consistent for these beams as all showed considerable secondary cracking caused by dowel and aggregate interlock action.

5.4.2.2 Diagonal Cracking

Diagonal cracks formed in these three beams in much the same way as those previously discussed. In beam N2-S62 the first diagonal crack was

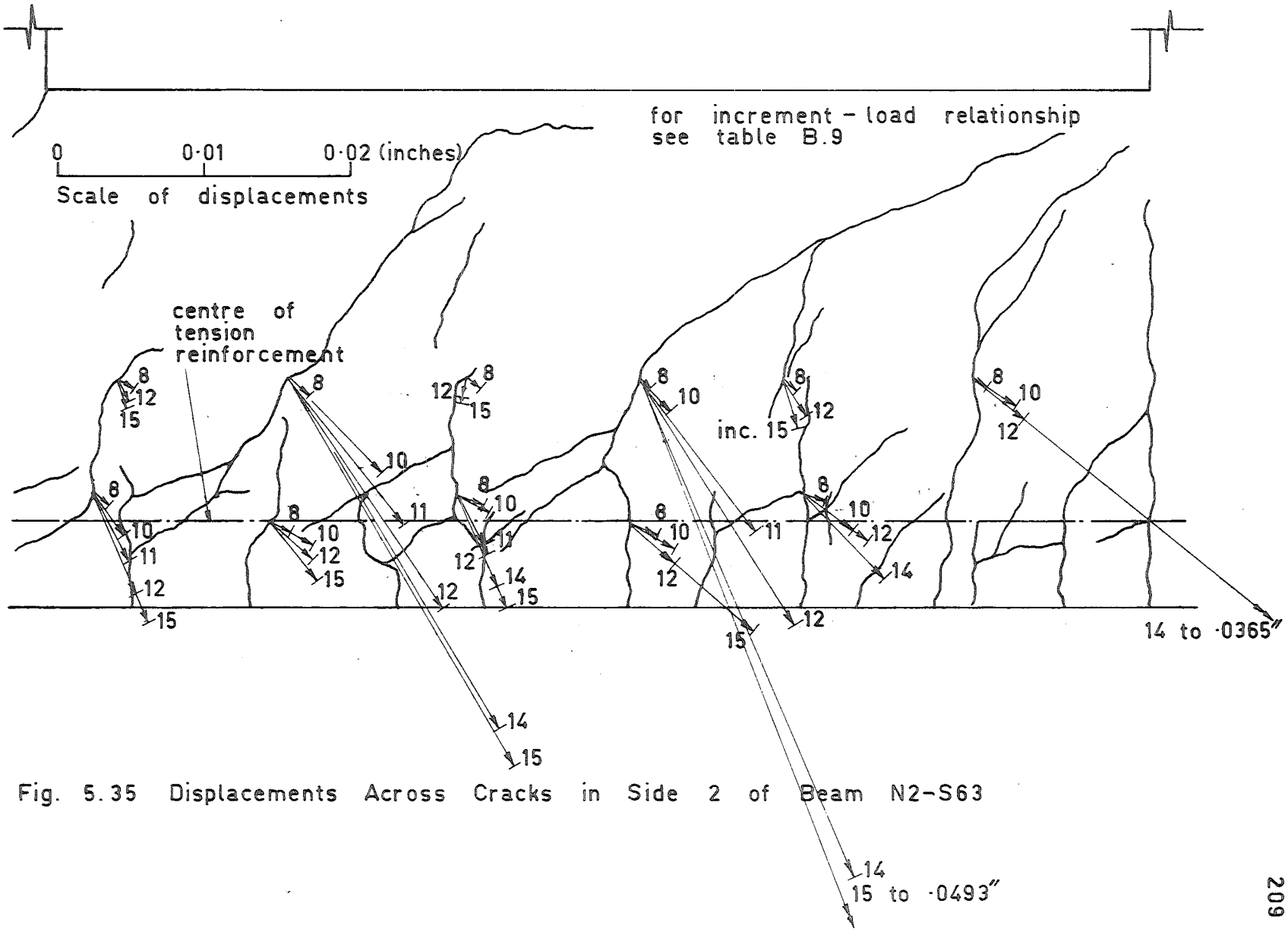

Fig. 5.35 Displacements Across Cracks in Side 2 of Beam N2-S63

detected at .525 P_u^*. There was some tendency for cracks to become inclined from .438 P_u^*. The crack along which eventual separation of the beam occurred formed at .788 P_u^* (see fig. 5.28). Both beams N2-S32 and N2-S63 also showed significant stirrup strains the load increment before diagonal cracking was observed. The load intensities at which these first formed were .536 P_u^* and .573 P_u^* respectively.

The diagonal cracks did not show any particular way of forming. Some of them were extensions of flexural cracks which had become inclined and then had suddenly propagated as diagonal tension cracks. Others propagate in both directions at quite a flat angle from the head of a flexural crack. The diagonal crack that formed at .788 P_u^* in beam N2-S62 is an example of this (see fig. 5.28). Both types of behaviour were observed in beams previously discussed.

Once the diagonal crack had formed it usually propagated slowly towards the section of maximum moment. The crack nearest the point of zero moment (see figs. 5.28, 5.29 and 5.30) stabilised once arch action was well developed in the beams. Cracks closer to the critical section continued to propagate right to eventual failure.

5.4.2.3 Dowel Cracking

Very little dowel cracking was observed in any of the beams before diagonal cracking. As with beams of the N1 - series there were few dowel cracks between the critical diagonal crack and the section of maximum moment. The displacements along the cracks were too small for these to form. On the other hand the beams showed considerable cracking along the tension reinforcement as extensions of the diagonal cracks. This can be seen in beam N2-S62 in fig. 5.28. There are so many cracks in beam N2-S32 (see fig. 5.29) that it is difficult to tell which are surface shrinkage cracks and which are dowel cracks. Beam N2-S63 exhibits some well developed dowel cracking like beam N2-S62 (see fig. 5.30).

5.4.3 Arch Action

The behaviour of the compression faces of the three beams were similar to those of the N1 - series beams after the onset of diagonal cracking. It can be seen from fig. 5.31 that the compression reinforcement towards the low moment end of the test length showed significant tensile strains once diagonal cracking had developed.

Fig. 5.36 shows the position of the centre of the compression force in the three beams at various load

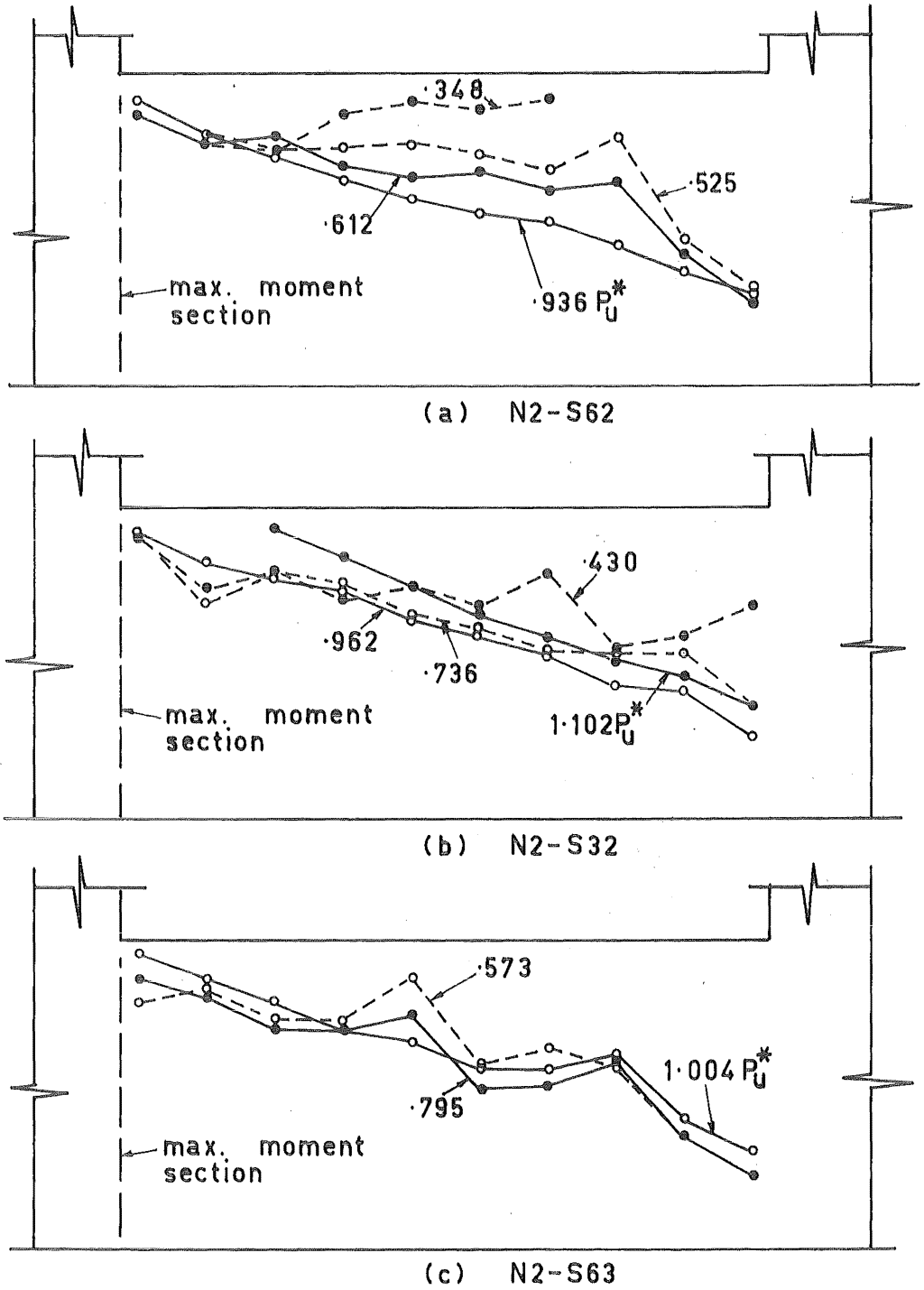

Fig. 5.36 Centre of Compression Force in Beams N2-S62, N2-S32 and N2-S63

intensities. Unfortunately beam N2-S63 had not cracked sufficiently before .573 P_u^* for the analysis to be valid. Thus no centre of compression force was computed before diagonal cracking was initiated. The kink just on the maximum moment side of midspan of the beam is caused by low tension reinforcement stresses at 4 inch demec row 6. The results at .348 P_u^* of beam N2-S62 were also useless at the low moment end of the test length. Thus the discontinuity at this load intensity in fig. 5.36 (a). The traces of the compression force centre in fig. 5.36 are all similar to those shown in fig. 5.12 for the N1 - series beams. Arch action is quite pronounced in these beams of the N2 - series.

5.4.4 Deformation Characteristics

The beams are considered fully built in as shown in fig. 5.13.

5.4.4.1 Transverse Expansion

Transverse expansion of the three beams is shown in fig. 5.37. Both the expansion measured over 89% of the total beam depth and 76% of the stirrups are included, except for beam N2-S62 where no readings were made over 89% of the depth. All demec gauge readings on the concrete of beam N2-S32 were discontinued

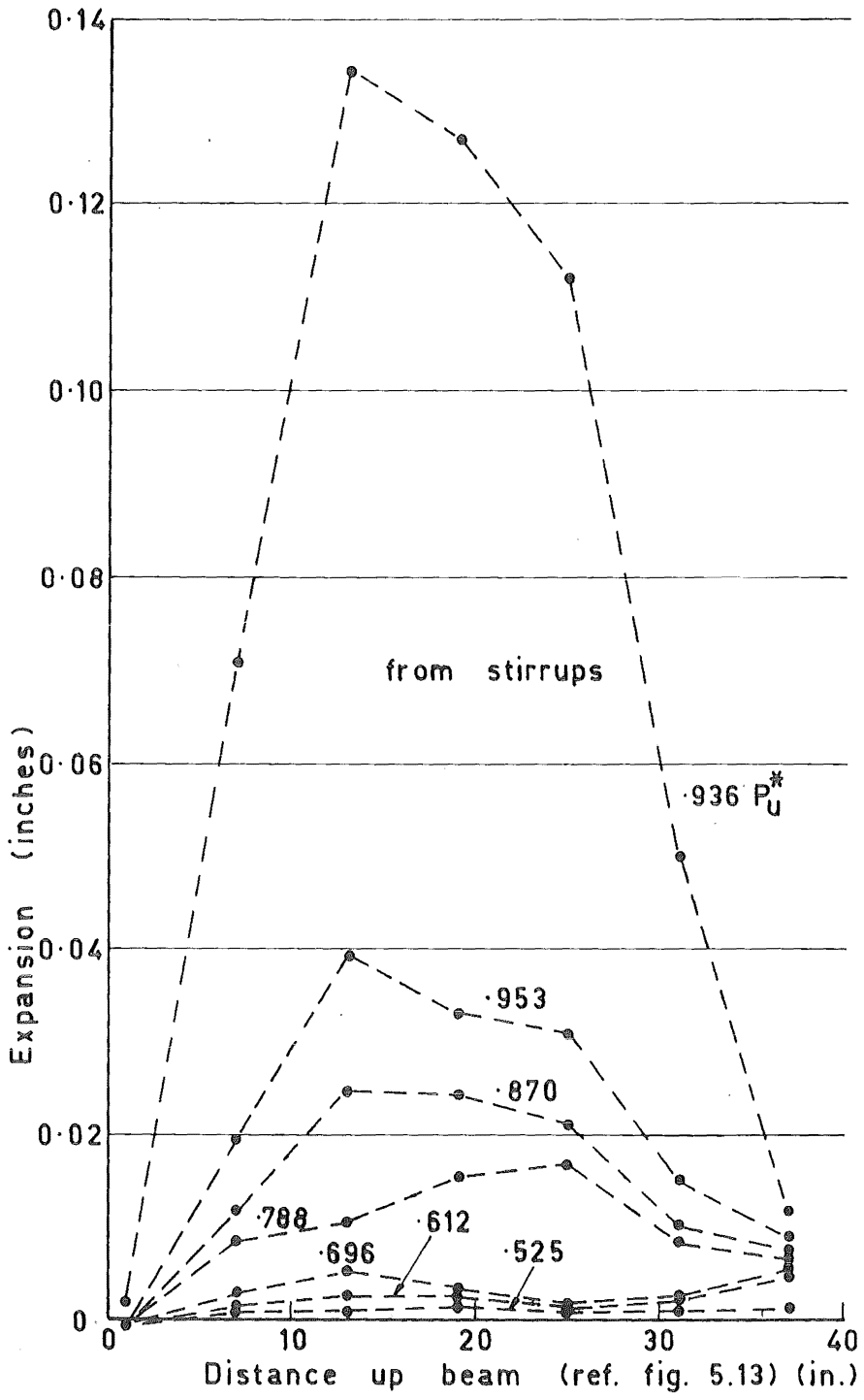

Fig. 5.37(a) Transverse Expansion of Beam N2-S62

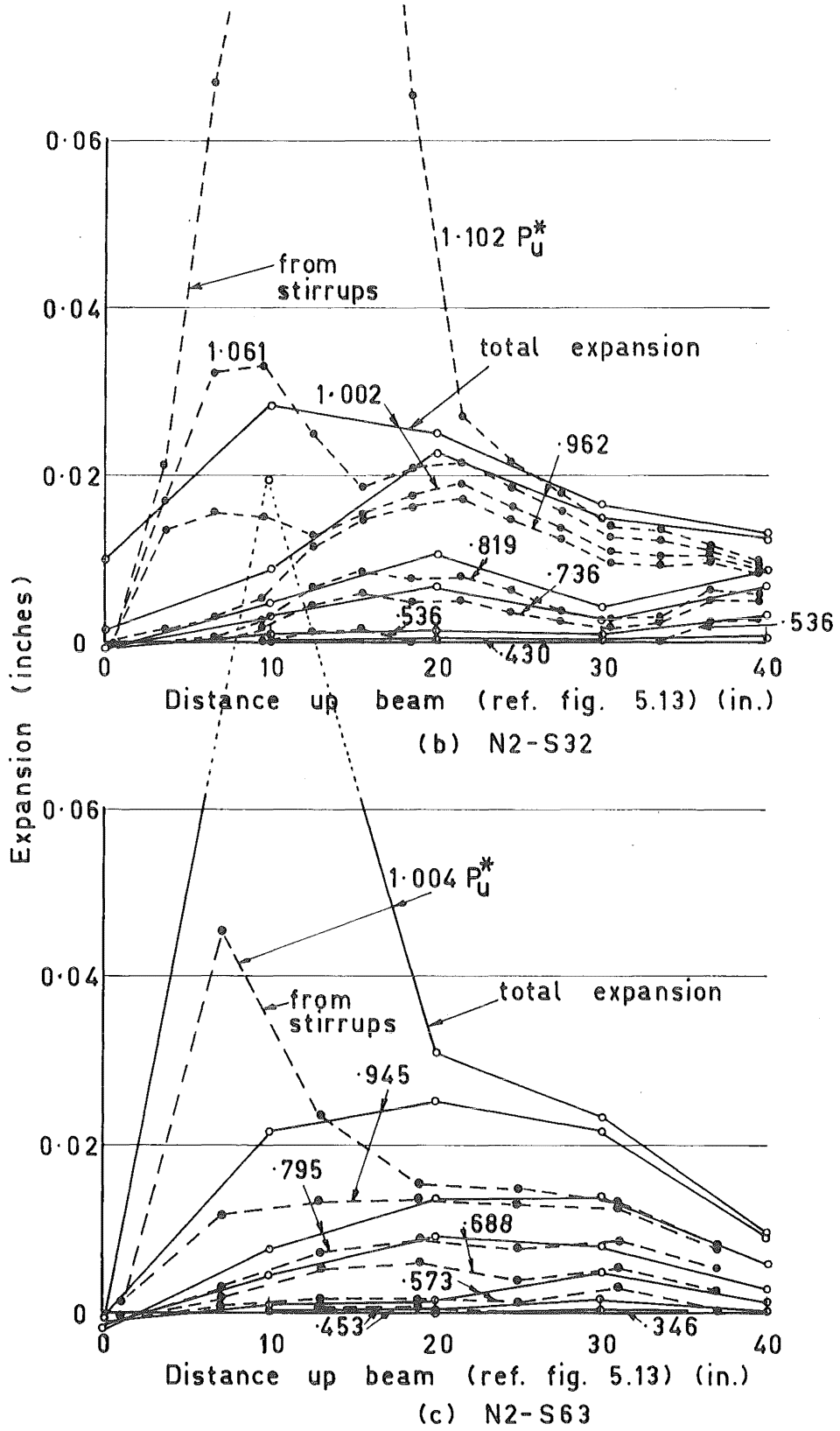

Fig. 5.37(b)&(c) Transverse Expansion of Beams N2-S32 and N2-S63

after 1.002 P_u^* and hence the transverse expansion for this beam was not obtained for large post-elastic deformations. In all cases the transverse expansion measured across the concrete of the beam is greater than that from summing stirrup strains. Once the stirrups had yielded the expansion increased very rapidly (see fig. 5.37 (a) and (b)). Again the parabolic distribution of strains in the stirrups crossing a particular diagonal crack is apparent. This is especially true of beam N2-S32 where the stirrups are close together.

From fig. 5.37 (a) it can be seen that transverse strains in beams N2-S62 were significant at .525 P_u^*. The diagonal cracks in this beam first formed at this load intensity. The positions at which these cracks formed are shown to be around 15 and 35 inches from the fixed end of the beam. This can be verified by referring to fig. 5.28. By similar interpretation of figs. 5.37 (b) and (c) it can be seen that diagonal cracking was initiated at .536 and .573 P_u^* in beams N2-S32 and N2-S63 respectively.

5.4.4.2 Deformation of End Sections

The deformations of the section at the low moment end of the test lengths of the beams are drawn in fig. 5.38. As with the beams of the N1-series, the general shape is not plane but rather a

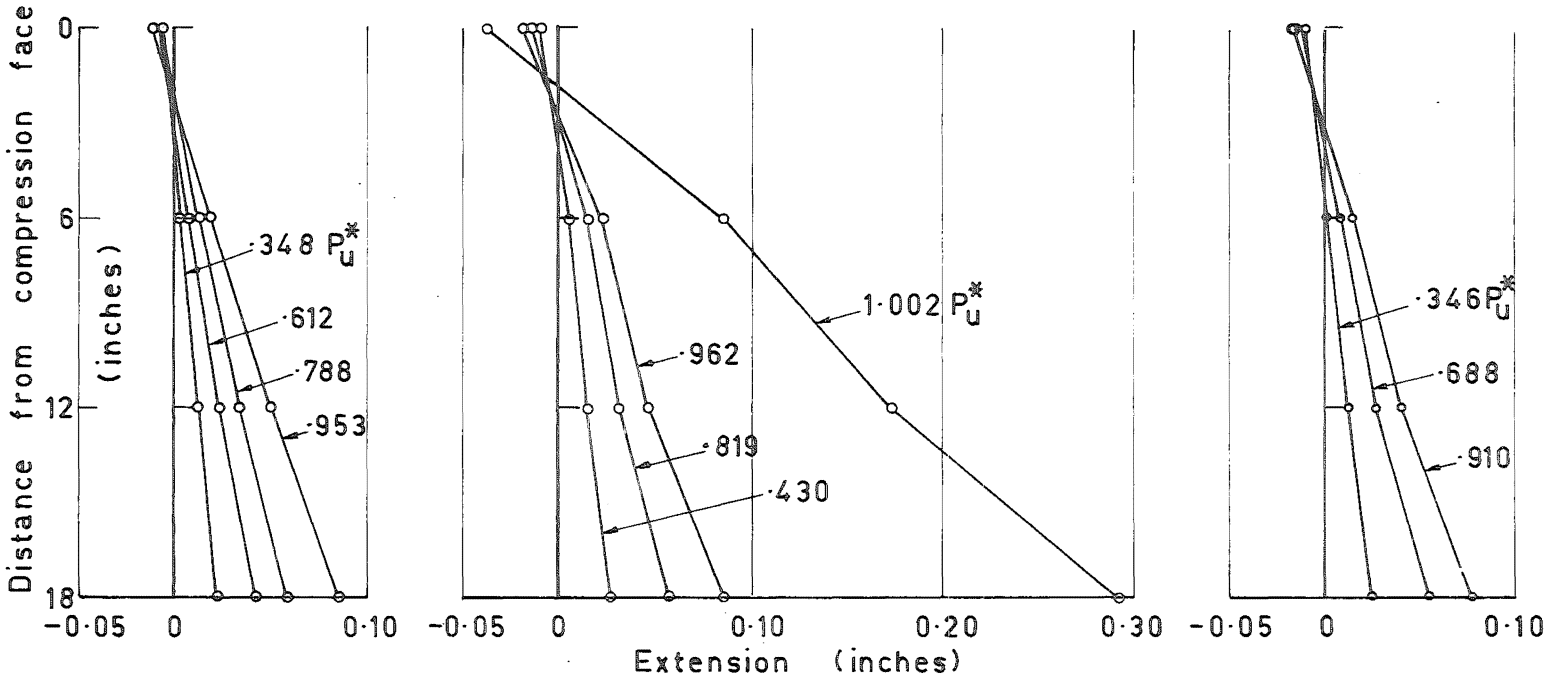

(a) N2-S62 (b) N2-S32 (c) N2-S63

Fig. 5.38 Deformation of Top End Section of Beams N2-S62, N2-S32 and N2-S63

very flat "S". This was discussed in section 5.3.5.2. 1.002 P_u^* was after large plastic deformations had occurred. As far as beam behaviour is concerned the deformation of the end section is of little importance.

5.4.4.3 Load Deflection Characteristics

Figs. 5.39, 5.40 and 5.41 show the theoretical and observed load deflection relationships for beams N2-S62, N2-S32 and N2-S63 respectively. The deflection characteristics for the three beams are similar. The flexural deflections calculated from equivalent curvatures agree very well with each other. The flexural stiffnesses are seen to be almost constant right up to yield of the tension reinforcement (see figs. 5.39, 5.40 (a) and 5.41 (a). Once diagonal cracking started the shear deformation in the beams increased rapidly until it made up about half the total deflection at yield of the tension reinforcement.

Fig. 5.40 (c) shows the ductility characteristics of beam N2-S32. The dotted line is the approximate path of the actual load deflection relationship. The fall off in load at each increment is known but the curve between each known deflection was not accurately determined. Beam N2-S32 had a ductility with respect to member deflection of at least $16\frac{1}{2}$. The test was

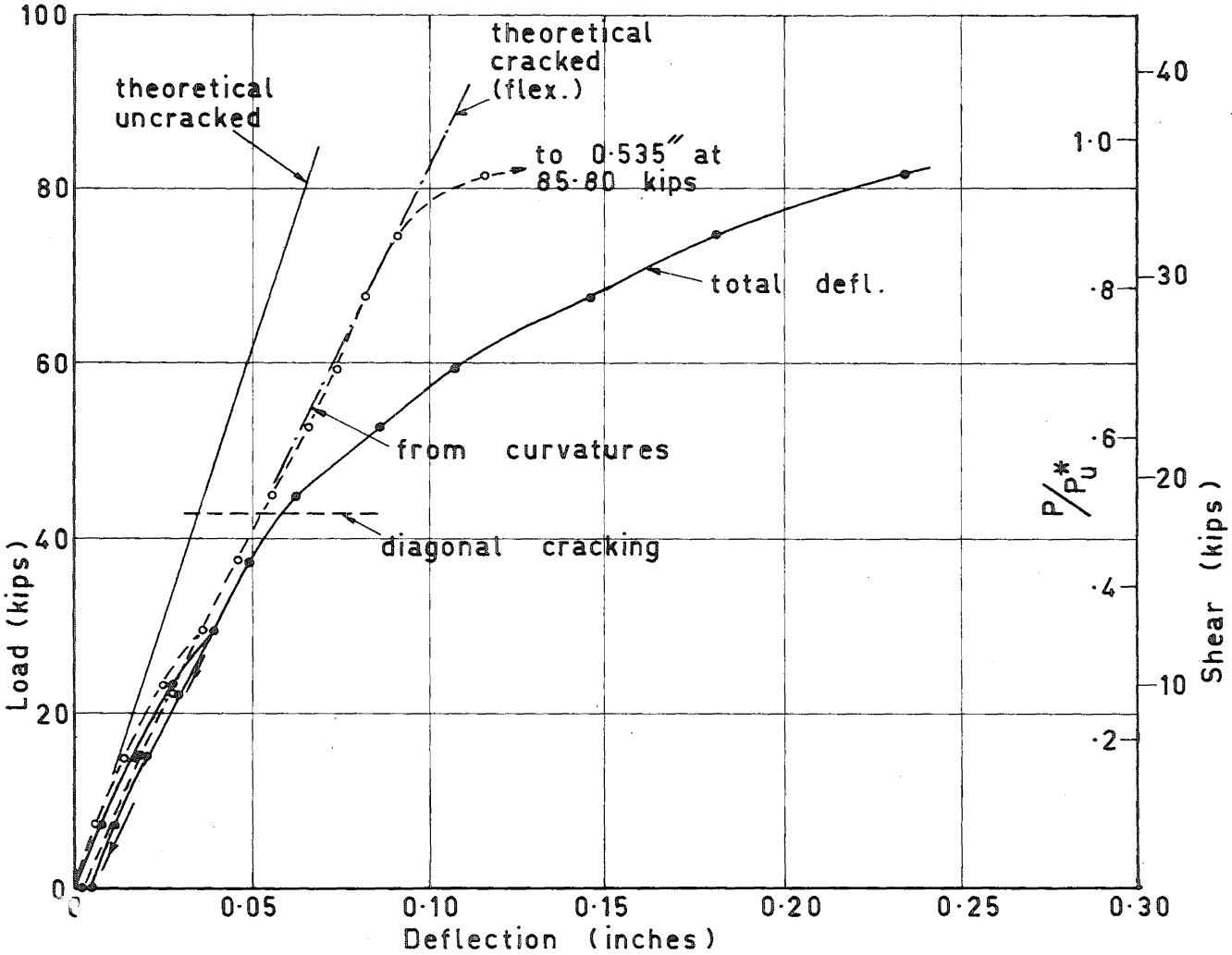

Fig. 5.39 Beam N2-S62 Load – Deflection Relationships

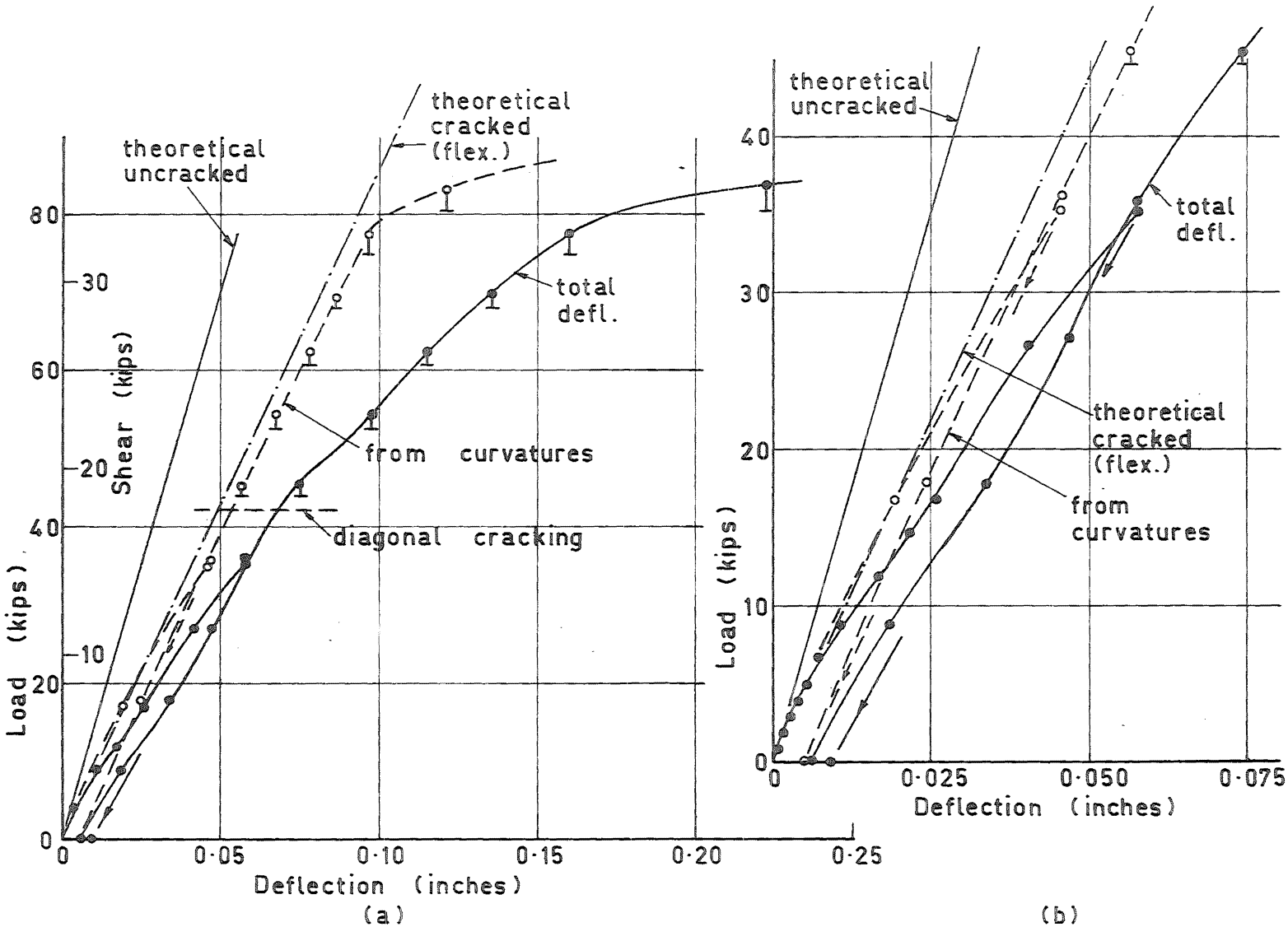

Fig. 5.40(a)&(b) Beam N2-S32 Load – Deflection Relationships

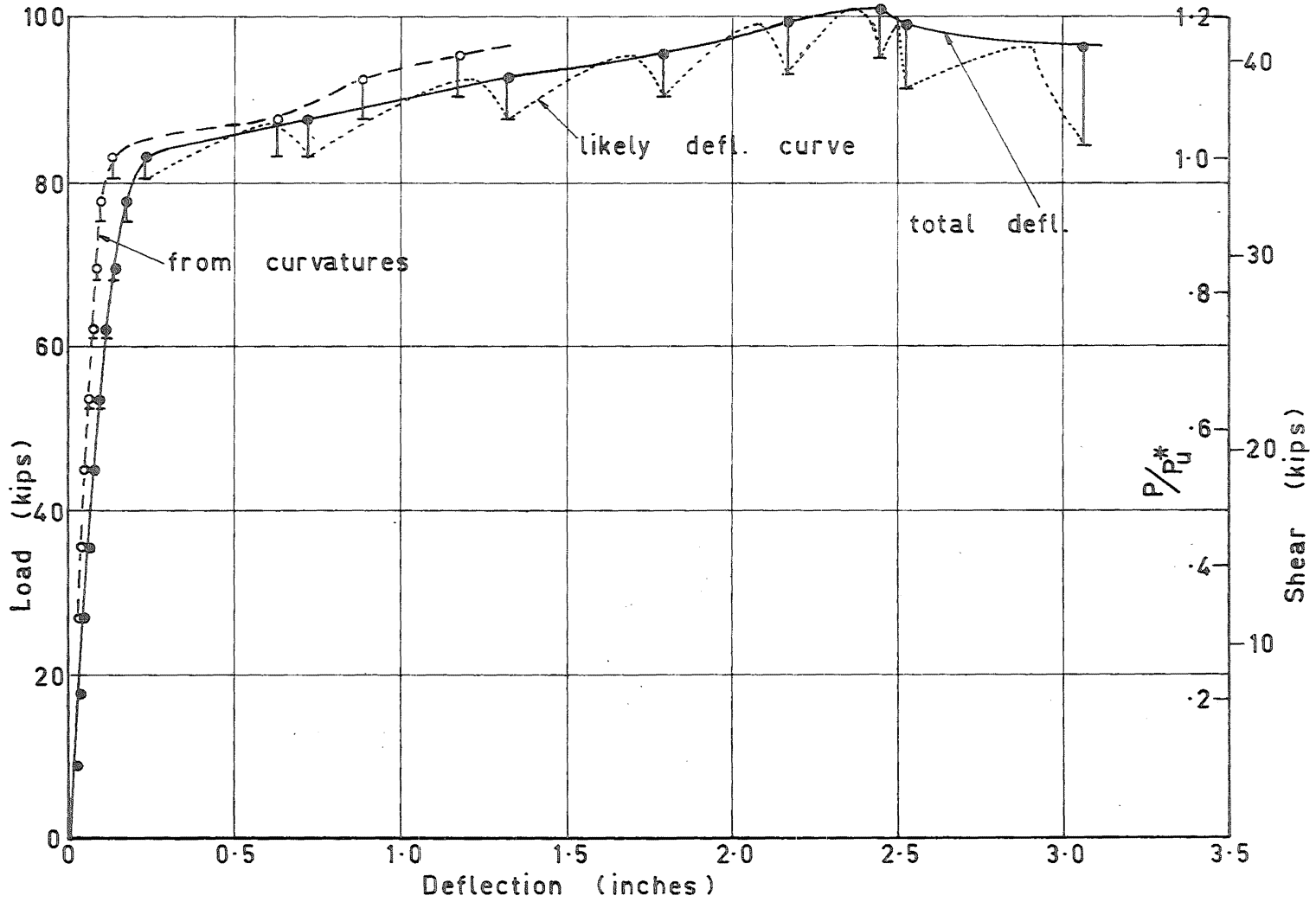

Fig. 5.40(c) Beam N2-S32 Load – Deflection Relationships

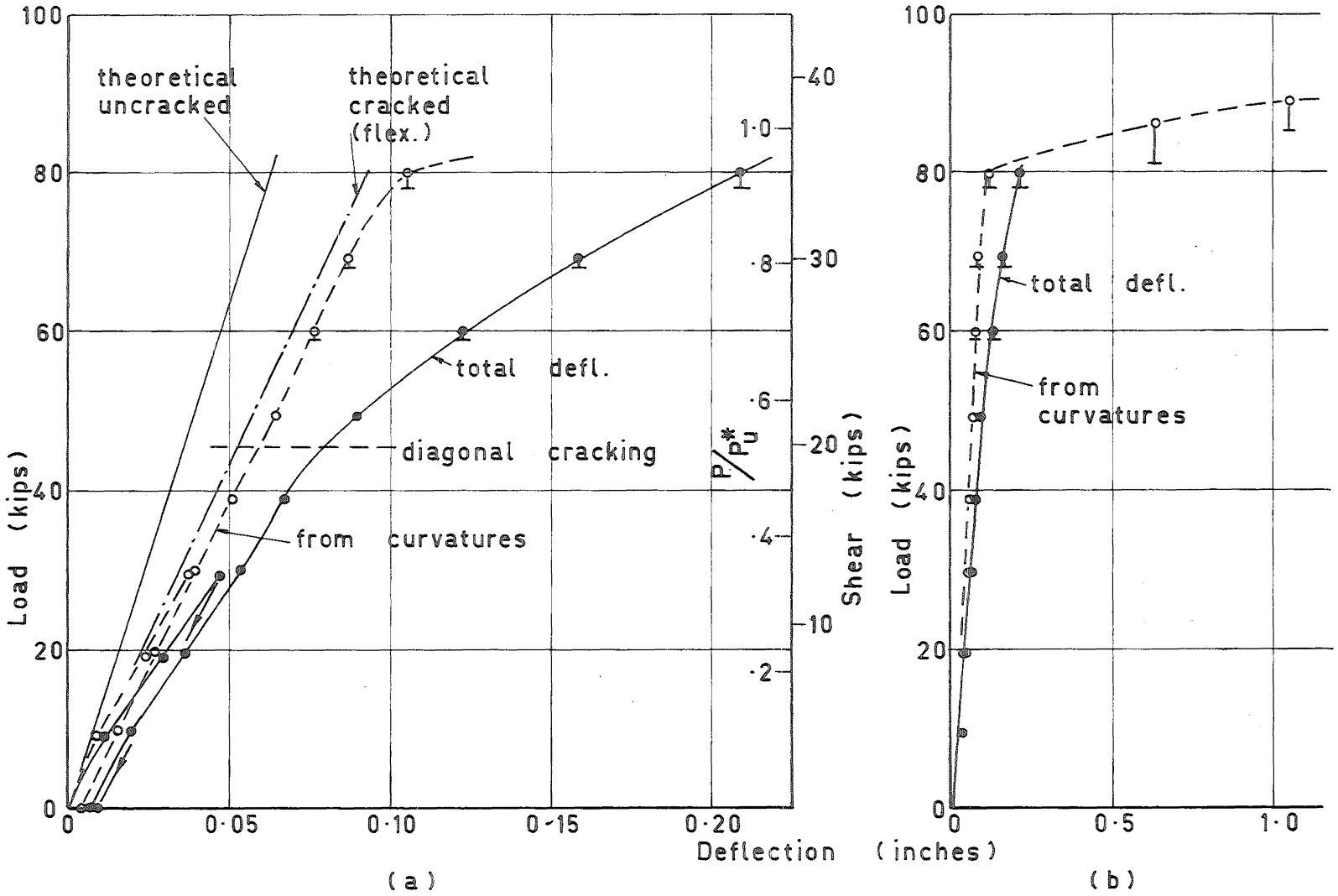

Fig. 5.41 Beam N2-S63 Load – Deflection Relationships

discontinued at a deflection of 3 inches and at this stage the load on the beam was still greater than the yield load. Fig. 5.41 (b) shows the post-elastic flexural deflections observed in beam N2-S63. The overall deflections in the plastic range could not be obtained from the test.

5.4.5 Failures

Side 1 of beam N2-S62 after failure is shown in fig. 5.42. The highest compression observed in the concrete of the beam was 4200 microstrains $1\frac{3}{4}$ inches from the compression face at gauge row 9 at .936 P_u^*. No measurements on the concrete were taken at gauge row 10 at this load intensity as the concrete had begun to spall away. After the observations were made for the increment the load was increased to 1.030 P_u^* at which stage it fell of suddenly. Failure was quite slow with gradual widening of the diagonal crack. It was a typical shear failure with yielding of all the stirrups across the diagonal crack at .87 P_u^*, and separation along this crack. Details of the critical compression zone area of the beam at failure are shown in fig. 5.43.

Fig. 5.44 is a photograph of side 1 of beam N2-S32 are failure. The concrete at the critical section had begun to show signs of crushing at 1.002 P_u^*. The tension reinforcement had yielded completely at .962 P_u^*

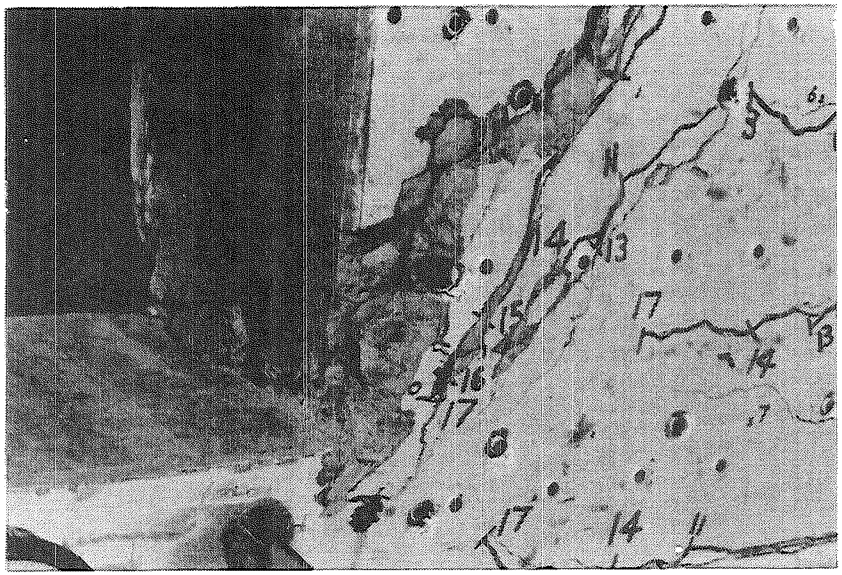

Fig. 5.43 Critical Compression Zone of Beam N2-S62 at Failure

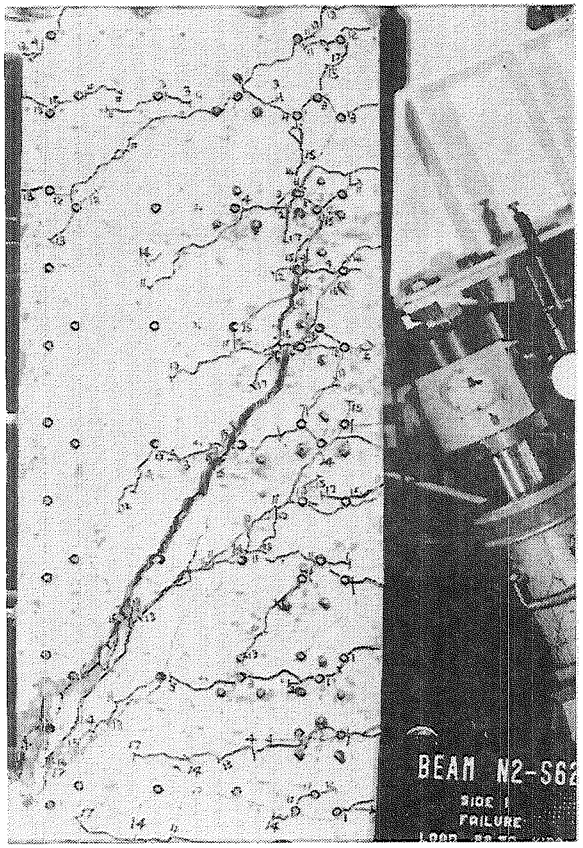

Fig. 5.42 Beam N2-S62 at Failure

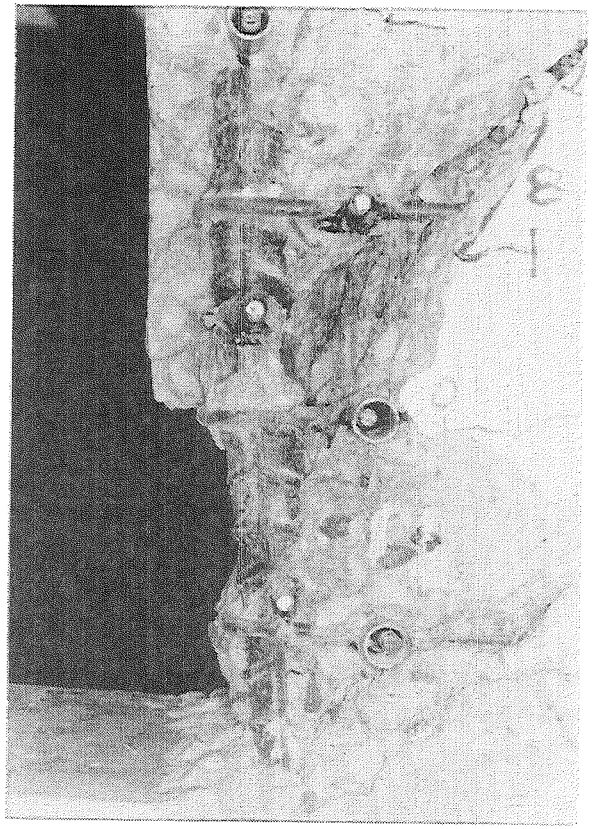

Fig. 5.45 Critical Compression Zone of Beam N2-S32 at Failure

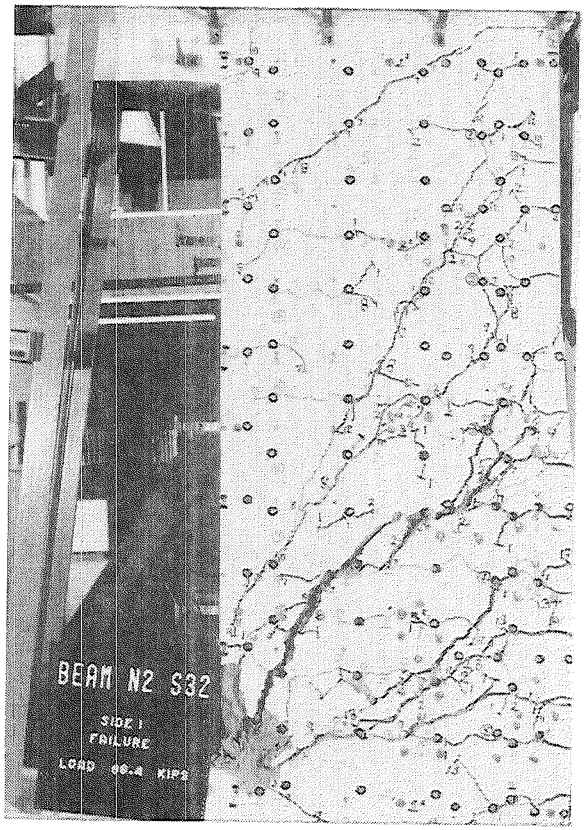

Fig. 5.44 Beam N2-S32 at Failure

and the stirrups crossing the failure diagonal crack had all yielded at 1.102 P^*_u. The beam continued to carry increasing load, eventually reaching a maximum of 1.230 P^*_u. The large rotation at gauge row 10 can be seen in fig. 5.44. The side of the name plate at the base of the beam was parallel to the compression face before loading. After the beam had failed the crushed concrete was removed. This can be seen in fig. 5.45. It is apparent that the compression reinforcement did not buckle. The critical diagonal crack did not intersect stirrup 13 (the bottom stirrup uncovered in the photograph). The failure was of the flexural-shear type. It is believed that the added shear resistance after yield of the stirrups across the failure diagonal crack was afforded by dowel action. More will be said about this in chapter 7.

Beam N2-S63 failed in a flexural-shear mode although the diagonal cracks opened up little at failure. Side 1 of the beam after failure is shown in fig. 5.46. It was somewhat twisted at this stage. The diagonal cracks in side 2 had opened up to a greater extent and showed destinct signs of separation. Hence the failure was influenced by shear. The maximum load attained was 1.097 P^*_u. The tension reinforcement had all yielded by .945 P^*_u and the concrete had begun to

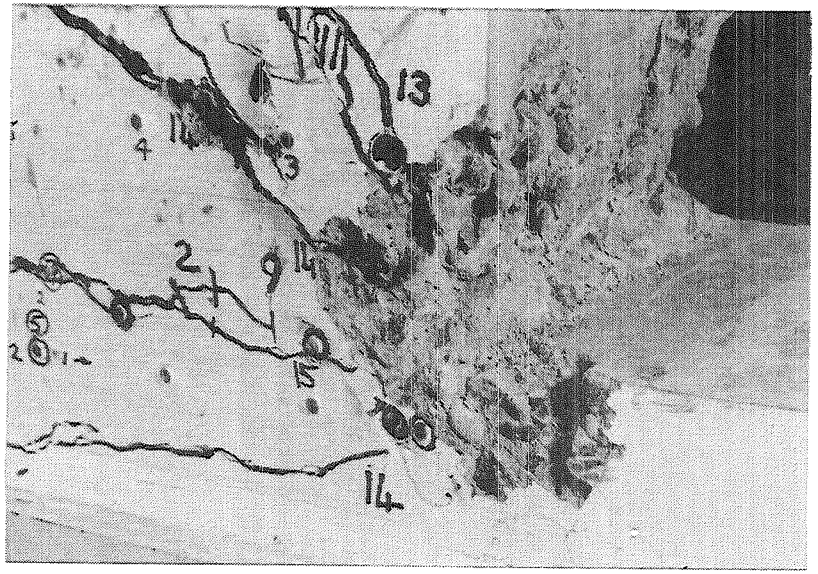

Fig. 5.47 Critical Compression Zone of Beam N2-S63 at Failure

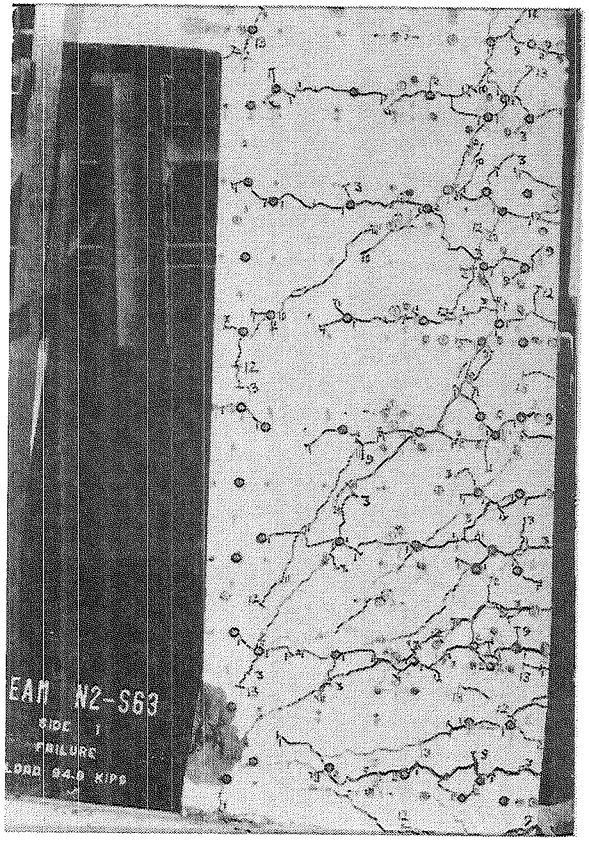

Fig. 5.46 Beam N2-S63 at Failure

crush at this load intensity. There was no buckling or kinking in the compression reinforcement although it had also yielded. Fig. 5.47 shows details of the crushed compression area in this beam. The photo is taken from side 2 and shows some separation along a diagonal crack.

5.5 Beam N3-S12,4

In this beam the stirrup spacing was 12 inches. The beam was designed with this wide stirrup spacing so that if a potential separation crack formed at a steep angle it would cross only one or even no stirrups. Thus ideal conditions for a premature shear failure would be created although an adequate volume of web reinforcement was provided.

The location of the line of action of the load, and of the 4 inch demec gauge rows, are shown in fig. 5.1.

5.5.1 Behaviour of Longitudinal Reinforcement

5.5.1.1 Tension Reinforcement

Tension reinforcement strain profiles at selected load intensities are shown in fig. 5.48. The dashed lines are the strains predicted

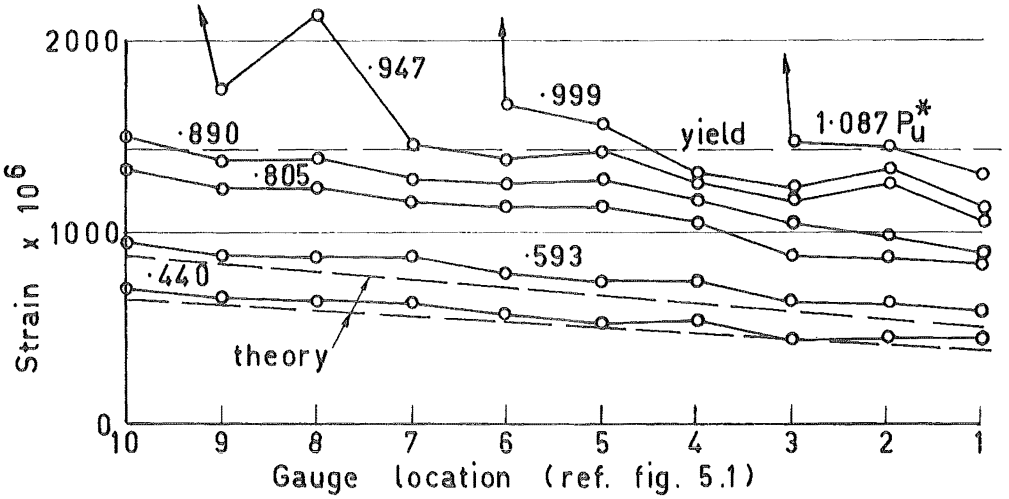

Fig. 5.48 Tension Reinforcement Strains in Beam N3-S12,4

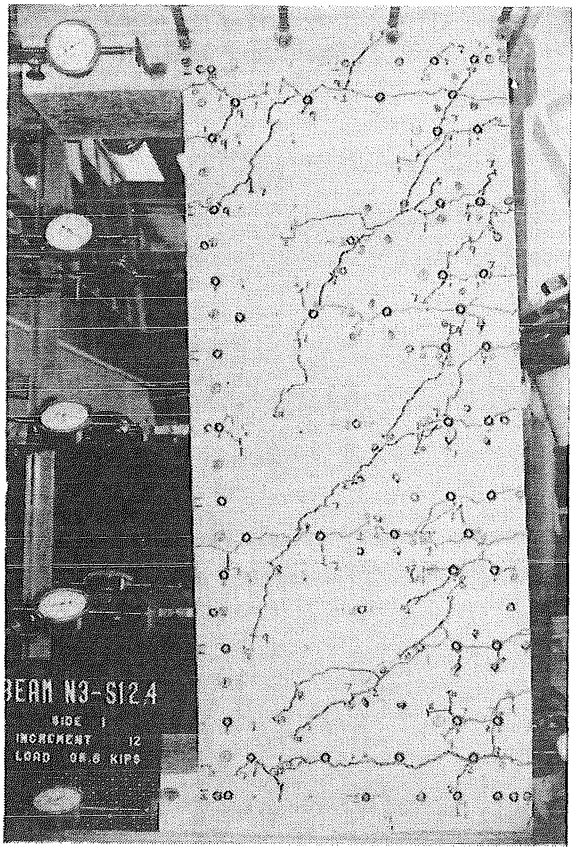

Fig. 5.49 Beam N3-S12,4

at .440 P_u^* and .593 P_u^* by the conventional elastic theory presented in appendix C.

A photograph of side 1 of beam N3-S12,4 is shown in fig. 5.49. The kinks in the strain profiles in fig. 5.48 are seen to correspond with the gauge rows where the diagonal cracks cross the tension reinforcement.

5.5.1.2 Compression Reinforcement

The compression reinforcement strain profiles are presented in fig. 5.50. The agreement with the theoretically derived strain at .440 P_u^* is good. As can be seen from the figure, the compression steel did not yield until 1.087 P_u^*. At this stage the tension steel had reached yield along three quarters of the test length (see fig. 5.48). At no stage did the compression reinforcement go into tension at the low moment end of the beam. However, once diagonal cracking was well developed, the compression strains were reduced in this region.

5.5.1.3 Equivalent Curvatures

Fig. 5.51 is a plot of the equivalent curvatures calculated from longitudinal reinforcement strains in the beam. Part (a) shows them before yield of the tension reinforcement and part (b) is drawn to

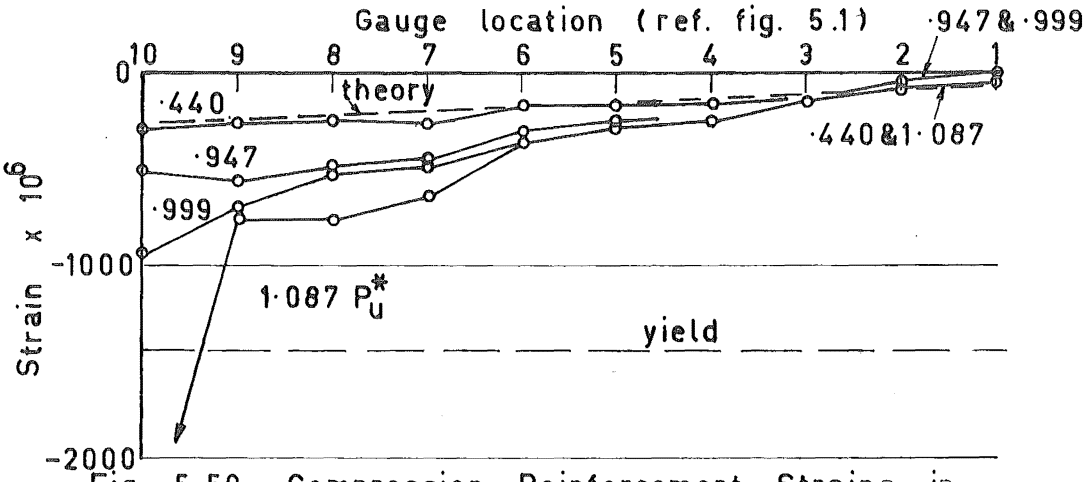

Fig. 5.50 Compression Reinforcement Strains in Beam N3-S12,4

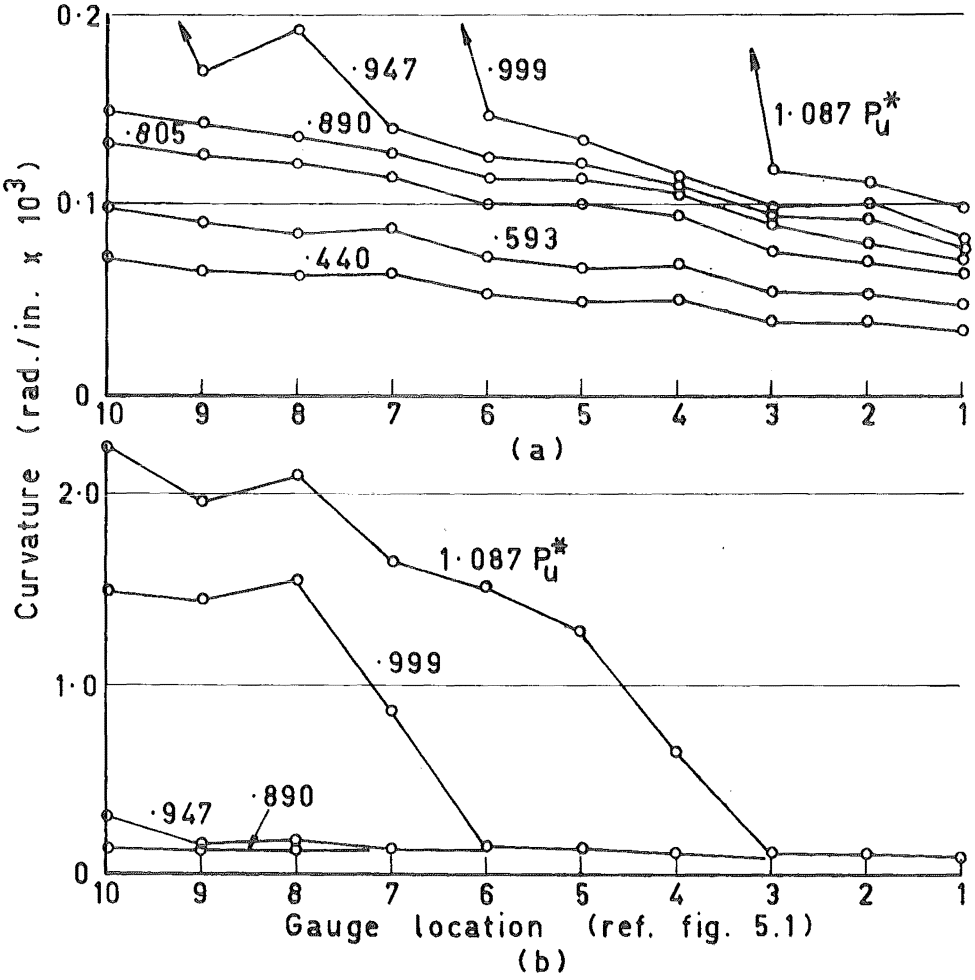

Fig. 5.51 Equivalent Curvatures in Beam N3-S12,4

a reduced scale to show the post-elastic equivalent curvatures. A small amount of yield was observed in the tension reinforcement at .947 P_u^* as can be seen in part (b) of the figure.

5.5.2 Concrete Strains

At .947 P_u^* concrete compression $\frac{1}{4}$ inch from the compression face of the beam was 2200 microstrains at the critical section. This concrete had begun to crush at the next increment although the compression reinforcement had reached only 65% of yield strain. Very small tensile strains were only observed in the compression zone concrete above the diagonal cracks at gauge row 1 at .947 and .999 P_u^*.

5.5.3 Cracking

The crack propagation and crack patterns were similar in this beam to the other beams already discussed in this chapter. Some random cracking was observed before the beam was loaded but it was not considered to affect the behaviour of the beam during testing.

5.5.3.1 Flexural Cracking

Several flexural cracks formed at .216 P_u^* in the first cycle of loading. Fig. 5.52 is a dia-

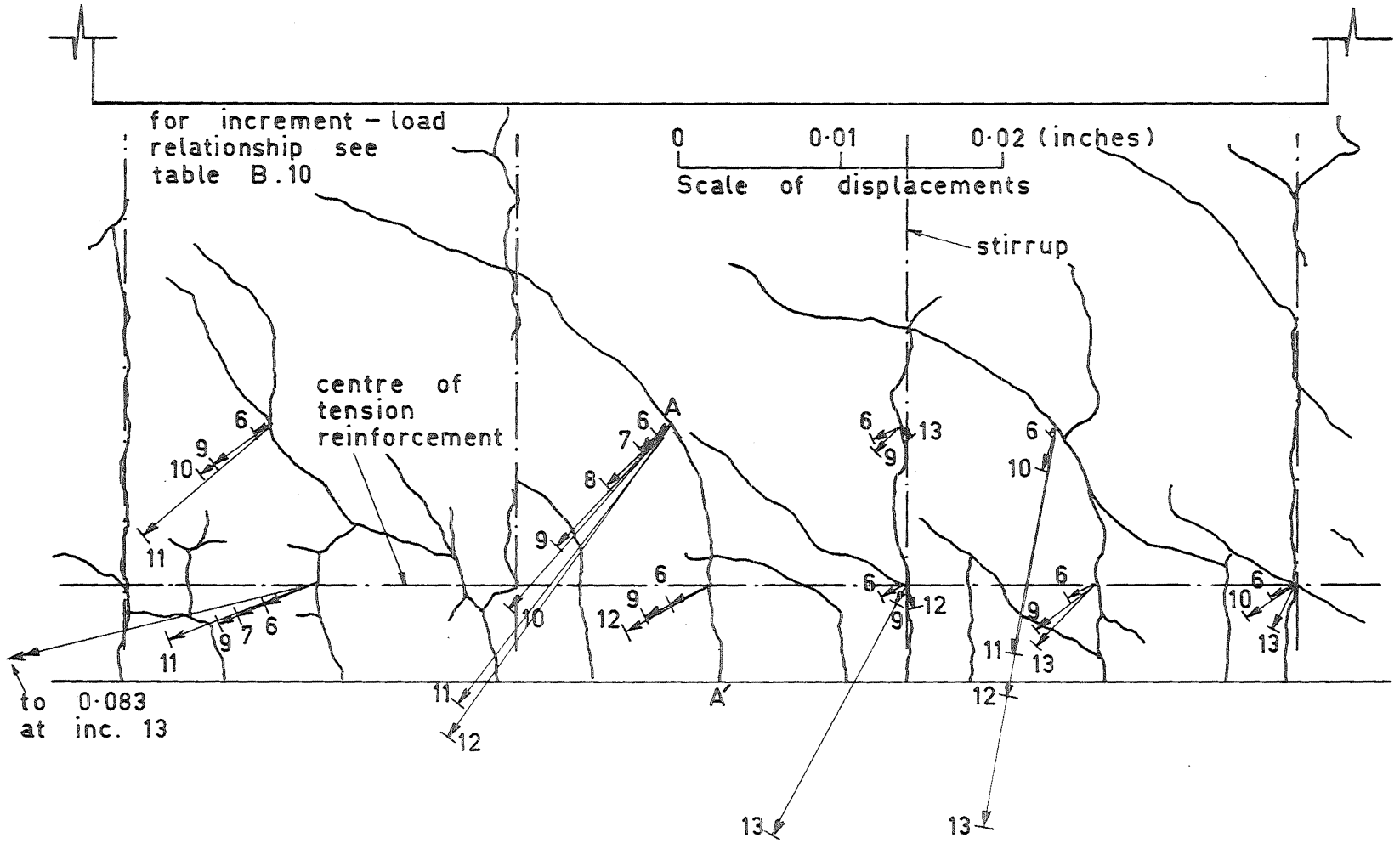

Fig. 5.52 Displacements Across Cracks in Side 1 of Beam N3-S12,4

grammatic representation of the diaplacements across some of the cracks in side 1 of the beam. The general trend is the same as was observed in the beams previously discussed.

It is interesting to note the two lots of displacements measured across the crack marked AA'. The very large displacement both along and across the crack at A compared to those nearer the tension face of the beam should be noted. The difference is markedly influenced by the dowel crack between the two gauge positions. A similar but less pronounced effect has been noted in other beams tested. An explanation was given in section 4.7.1.

5.5.3.2 Diagonal Cracking

The first diagonal cracks had formed by .700 P_u^*. Once of them was at the low moment end of the test section while the other crossed the tension reinforcement about half way along (see fig. 5.49). The later diagonal crack propagated steadily up to .947 P_u^*. It was still narrow at this stage. At 1.087 P_u^* it propagated further and opened up along its whole length.

5.5.3.3 Dowel Cracking

Substantial dowel cracking was observed on the low moment side of each of the three main diagonal

cracks. The dowel cracks formed at approximately the same time as the diagonal cracks and propagated back as far as the next flexural crack, or even through it to the one beyond. Even near failure these dowel cracks did not open up appreciably. A typical width at 1.087 P_u^* was0.035 inches.

5.5.4 Arch Action

Arch action did not develop to the same extent in this beam as in the beams already discussed in this chapter. As mentioned in section 5.5.2 very little tension was observed in the compression face of the beam. Neither did the compression reinforcement go into tension at the low moment end of the test section after diagonal cracking had developed (see fig. 5.50). There was a tendency for the centre of the compression force at this end to move down the section after diagonal cracks had formed. Fig. 5.53 shows the position of the centre of the compression force in the beam at various load intensities. At 1.087 P_u^* the compression force is shown outside the beam. This is because the tension reinforcement was strain hardening. No allowance was made for this in the analysis.

5.5.5 Deformation Characteristics

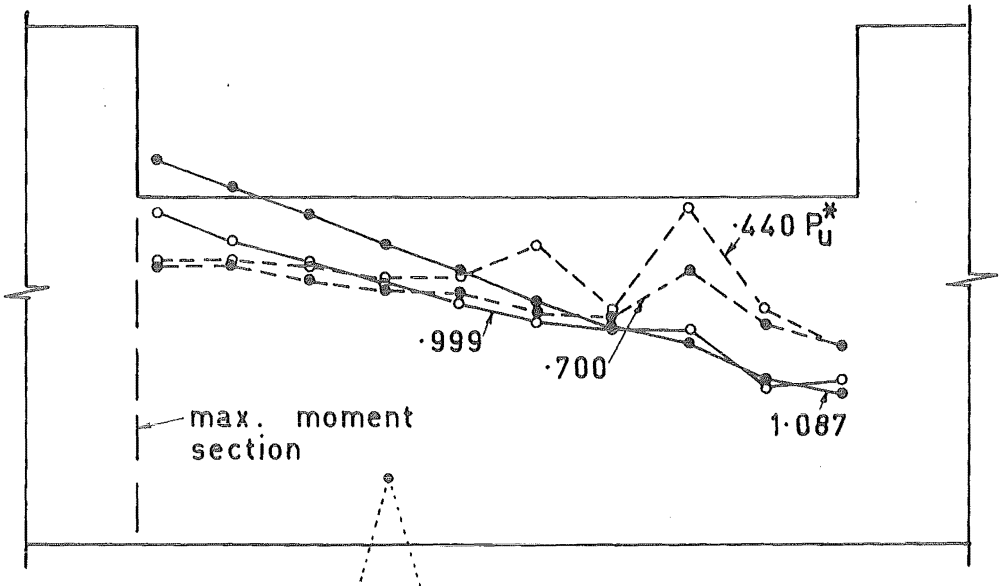

Fig. 5.53 Centre of Compression Force in Beam N3-S12,4

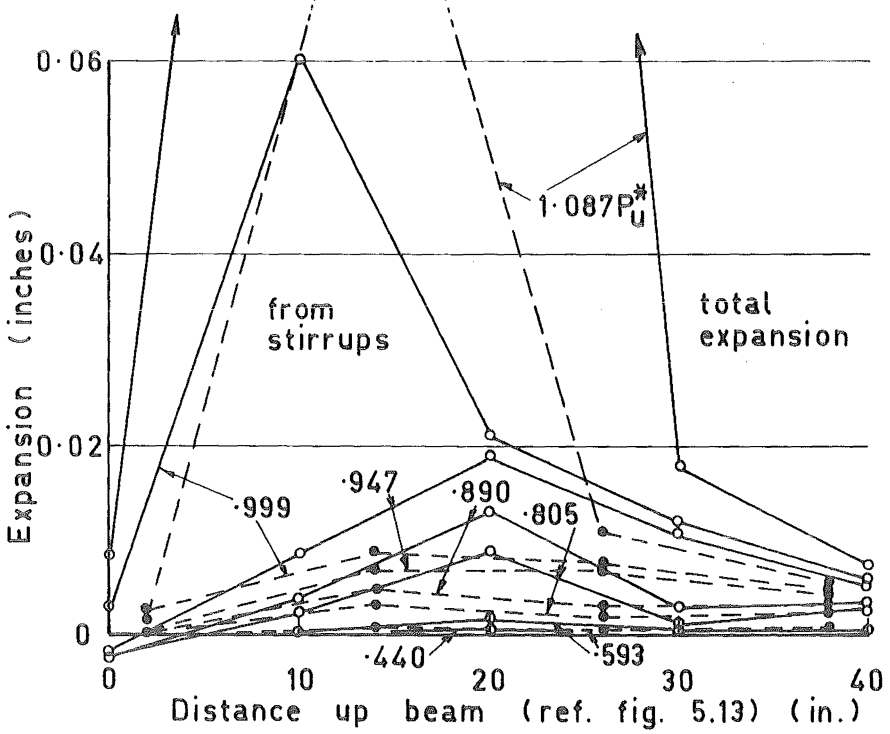

Fig. 5.54 Transverse Expansion of Beam N3-S12,4

5.5.5.1 Transverse Expansion

The transverse expansion of the beam is shown in fig. 5.54. Diagonal cracking started at .700 P_u^*, and this can be verified by the appreciable expansion at this load stage. The sharp rise of the measurements over the total beam depth at .999 P_u^* is not present in the expansion from stirrup strains. This is because the diagonal crack that caused the increase did not cross any of the gauge lengths on the stirrups. The very sudden increase in the transverse expansion from stirrup strains at 1.087 P_u^* was a result of yielding of a stirrup.

5.5.5.2 Deformation of the End Section

The deformation of the section at the low moment end of the test length is shown in fig. 5.55. The shape of the section is seen to be similar to those illustrated in figs. 5.16 and 5.38. No post-elastic deformations were observed on this section.

5.5.5.3 Load Deflection Characteristics

Deflection measurements were made both at very small load increments at initial loading, and in the post-elastic range of loading. The load deflection relationships are drawn in fig. 5.56. Part (a) shows the relationships up to yielding of the tension reinforcement. Both flexural and total

(For fig. 5.56 see pages 239 and 240)

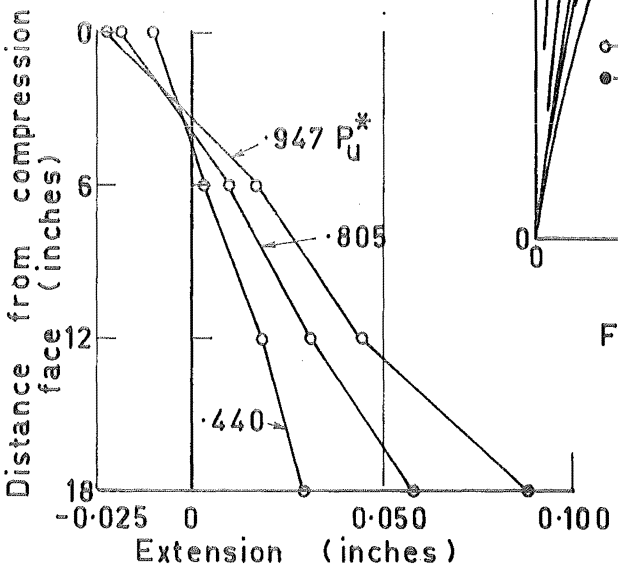

Fig. 5.55 Deformation of Top End Section of Beam N3-S12,4

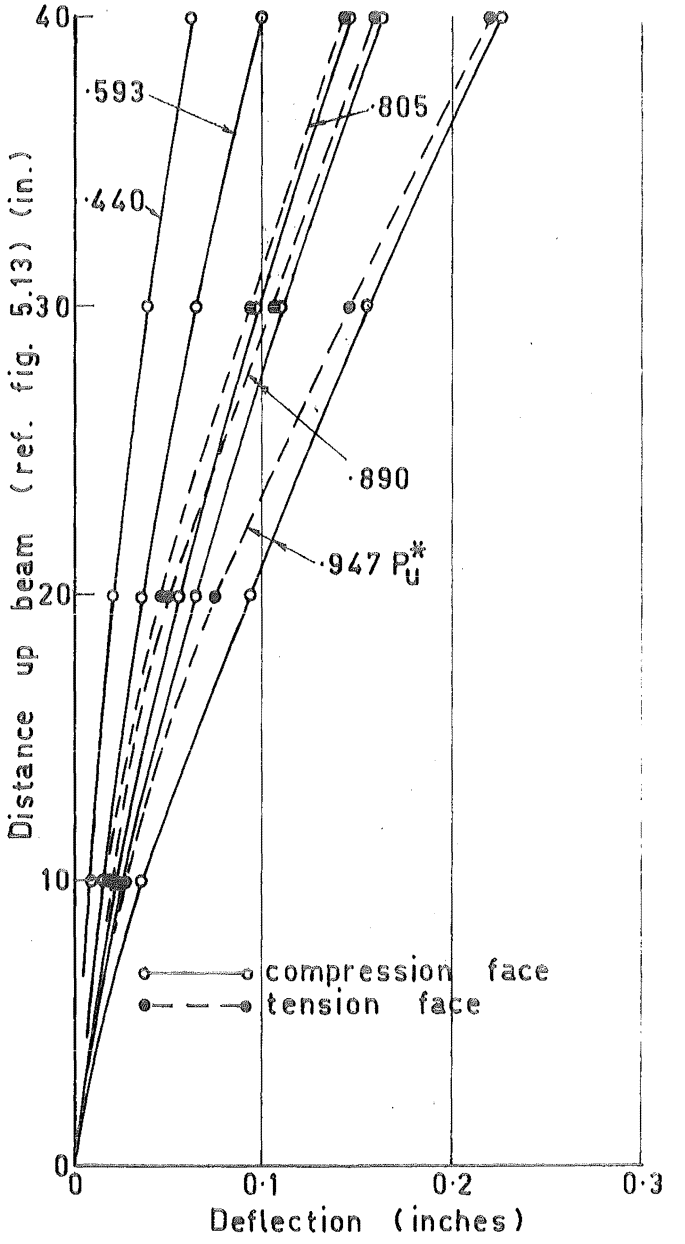

Fig. 5.57 Deflected Shape of Beam N3-S12,4

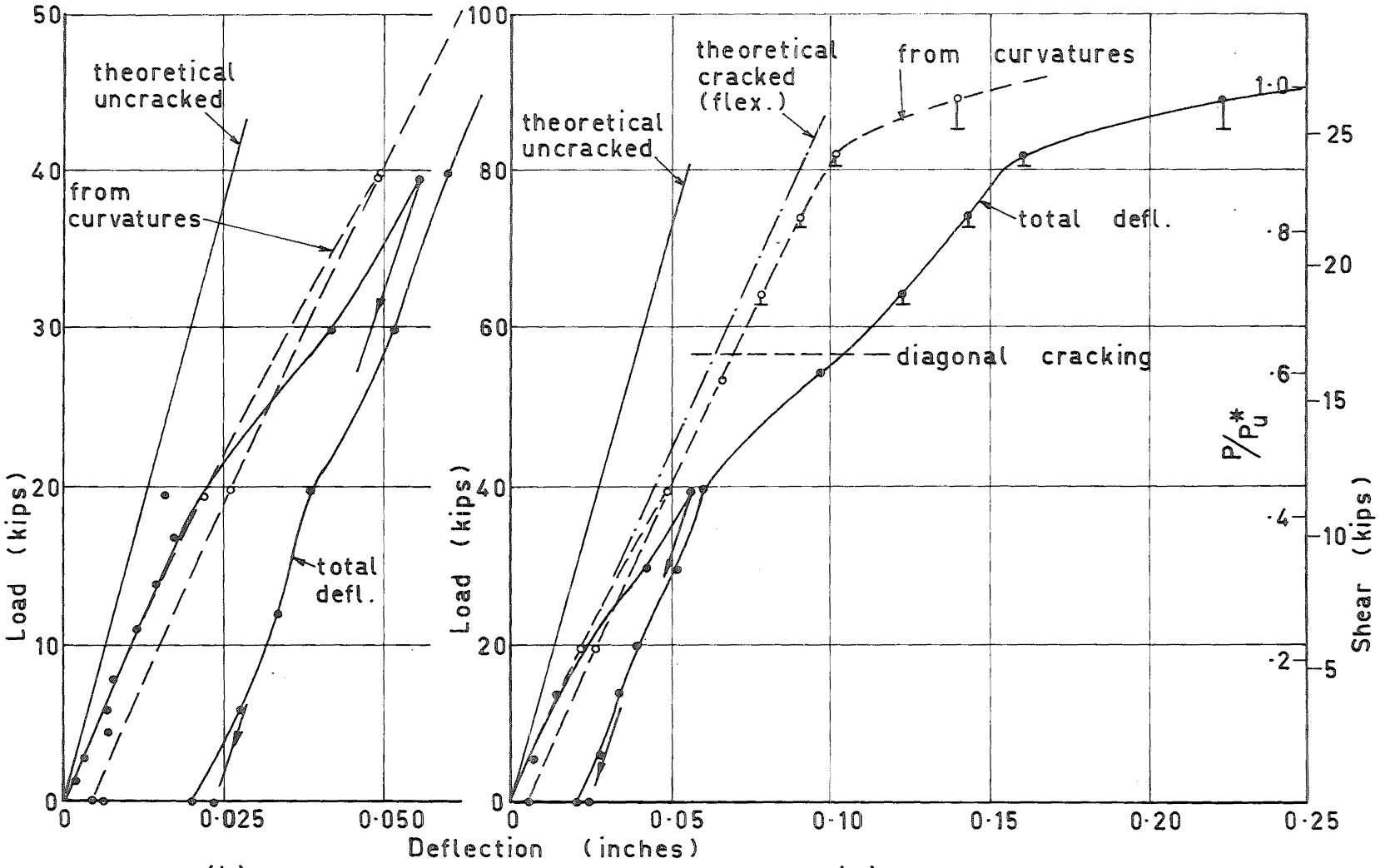

Fig. 5.56(a)&(b) Beam N3-S12,4 Load - Deflection Relationships

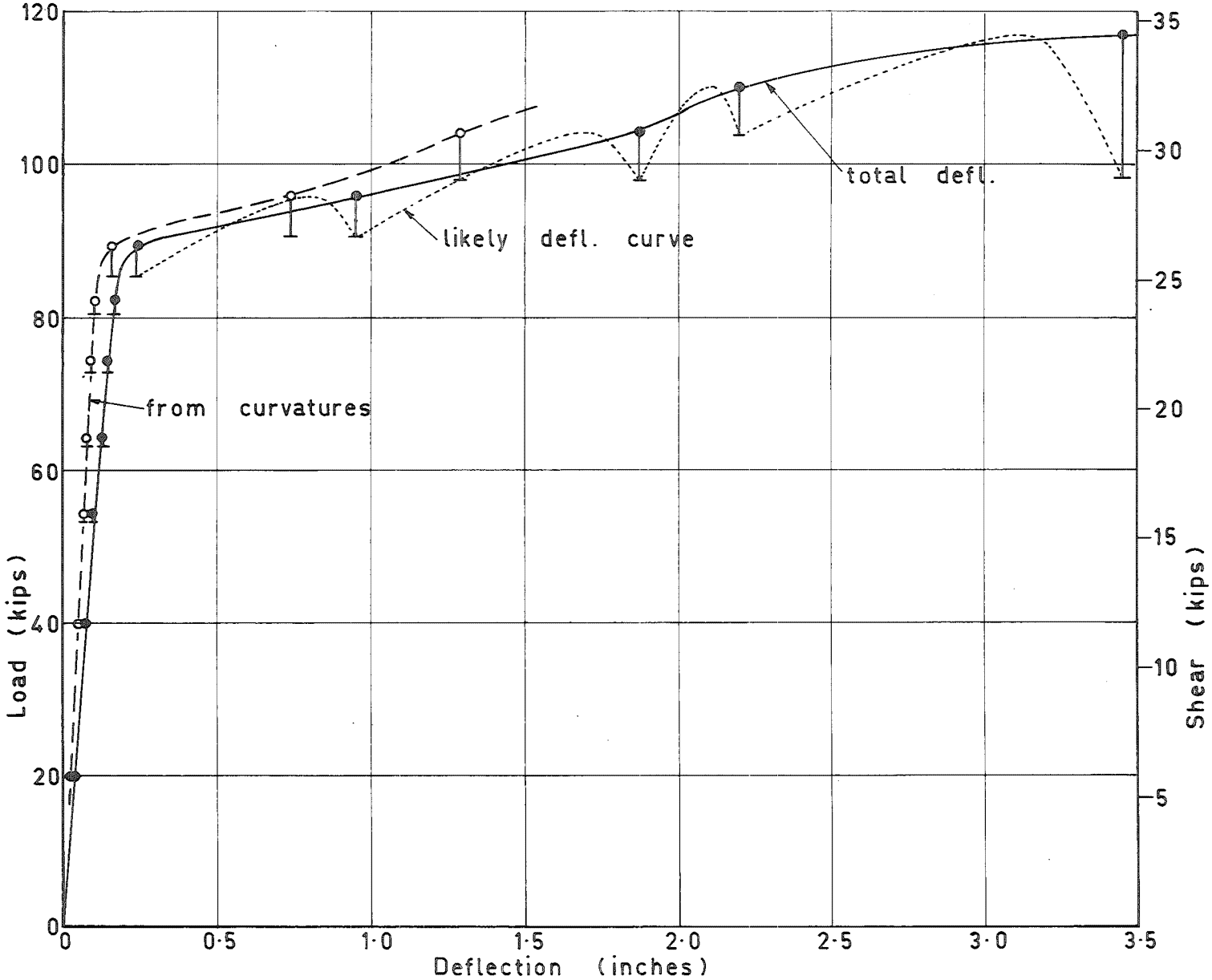

Fig. 5.56(c) Beam N3-S12,4 Load - Deflection Relationships

deflections are included. In both (a) and (b) theoretical deflection relationships are also included. Part (b) gives details of the observed deflections at initial loading.

The post elastic deformation on the beam is shown in fig. 5.56 (c). Even though the stirrup spacing in this beam was very large, the beam proved to be very ductile as can be seen in the figure. Even at a deflection of $3\frac{1}{2}$ inches no appreciable reduction in the load carrying capacity was observed. The beam had a ductility of at least $19\frac{1}{2}$ with respect to member deflection. These load deflection curves show no trends which have not been discussed previously.

Fig. 5.57 shows the deflected shape of the beam up to .947 P_u^*. Both the deflected shapes of the tension and compression faces are included where there is an appreciable difference because of transverse expansion.

5.5.6 Failure

A photograph of side 1 of beam N3-S12,4 at failure is shown in fig. 5.58. The failure was of the flexural type with the diagonal cracks having little apparent influence. The concrete began crushing at the maximum moment section at .999 P_u^*, and the compression reinforcement yielded at 1.087 P_u^*. As can be seen in fig. 5.56 (c) the load still continued to

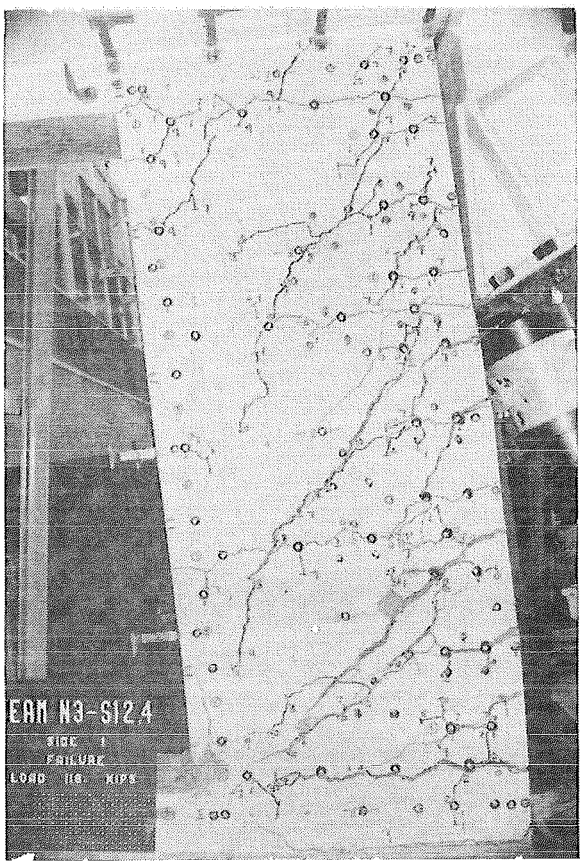

Fig. 5.58 Beam N3-S12,4 at Failure

increase substantially after this. At failure the beam was twisted but inspite of this the load attained was 1.302 P_u^* due to strain hardening of the tension reinforcement. At a deflection of $3\frac{1}{2}$ inches the beam could not sustain the applied load even for a few seconds. At constant displacement the load dropped by .19 P_u^* in five minutes. There was no sign of buckling of the compression reinforcement although it was only confined 1 inch above the reentry corner at the critical section and then 12 inches further up the test length.

5.6 Summary

5.6.1 Longitudinal Reinforcement

Prior to diagonal cracking the conventional analysis of a cracked section (see appendix C) yields both tension and compression reinforcement strains which agree well with those observed in the tests.

After diagonal cracking an analysis to find tension reinforcement strains must take account of internal load redistribution resulting from diagonal cracking. This analysis is developed in chapter 8.

Yield in the tension reinforcement spread along the tension steel, from the maximum moment section, a distance of 2d in beam N3-S12,4. The length of yielded

tension reinforcement decreased with decreasing axial tension to shear force ratio.

The compression reinforcement only yielded after yield of the tension steel was well developed. Its region of yield was confined to the 4 inch demec gauge length at the maximum moment section. Along the rest of the compression reinforcement the strains were low at all stages of loading.

5.6.2 Cracking

5.6.2.1 Crack Widths

The maximum crack width observed at working load (taken as $P_u^*/1.75$) in any of the beams was .009 inches, with average widths of the order of .005 inches. These crack widths are within the limits of the ACI Building Code [5].

5.6.2.2 Dowel Cracking

Dowel cracking, and also aggregate interlock cracking, was not initiated until diagonal cracks had formed. Dowel cracking did not develop to any appreciable extent on the high moment side of the major diagonal crack, except when the beams were close to failure.

5.6.2.3 Diagonal Cracking

The slope of the diagonal cracks that

formed in the test beams were little different from those that would occur in beams not subjected to axial tension. The crack patterns were all similar although the axial load to shear force ratio varied from 1 to $3\frac{1}{4}$. Where a beam failed by separation across a diagonal crack, the critical crack was inclined to the longitudinal axis of the beam at an angle of less than 45^{o}.

5.6.3 Deformation Characteristics

5.6.3.1 Transverse Expansion

Significant transverse expansion was observed only after formation of a diagonal crack. This expansion affects the deflected shape of the beam as was shown in figs. 5.15 and 5.57. The expansion calculated from summing stirrup strains was always smaller than that measured on the concrete of the beam. There are three reasons for this.

(i) The inability to measure the strain over the whole stirrup.

(ii) Slip of stirrup anchorages. This is discussed in chapter 8.

(iii) In some beams both diagonal and dowel cracks did not always intersect a stirrup, but rather propagated above or below them.

5.6.3.2 Section Deformation

The method described in chapter 3 for calculating the deflection of the test length of the beam depends, for its validity, on the planess of the two sections at either end of the test length. From the sections plotted in figs. 5.16, 5.38 and 5.55 it can be seen that the section at the low moment end did not remain plane. The idealised section on which the method is based uses a line of best fit through the known deflection measurements. It is believed that the method is adequate considering the uniform shape of all the sections plotted and their relatively small departures from planess.

5.6.3.3 Load Deflection Relationships

The beams showed similar load deflection relationships. Within each group of constant axial load to shear force ratio the flexural deflections right up to yield were equal, with the flexural stiffness being almost constant.

After diagonal cracking considerable shear deflections were observed. The shear deflection did not increase linearly with load but rather it increased rapidly immediately after diagonal cracking and then, at higher load intensities, somewhat less rapidly. This is attributed to the initial slip in

stirrup anchorages when the stirrups were initially stressed. The contribution of stirrup extension to shear deflection is discussed in chapter 8.

The member ductilities of the three beams on which this characteristic was observed, were large. It is believed that provided separation failure is avoided, the deflection ductility of the beams is enhanced by diagonal cracking because of the longer length of tension reinforcement which yields.

5.6.4 Arch Action

Arch action developed after diagonal cracking in all the beams with web reinforcement. It was less pronounced in beam N3-S12,4 than in the beams with lower axial tension to shear force ratio. There was little difference in the arch action observed in the beams of the N1 - and N2 - series beams. Some cracking of the compression faces of the beams was observed above the diagonal cracks and the compression reinforcement showed small tensile strains at the low moment end of the test section.

5.6.5 Effect of Stirrups on Beam Behaviour

One of the two major variables in this series of tests was the amount and spacing of web reinforcement. The effects of variations in each on the

beam behaviour are listed below.

5.6.5.1 Percentage of Web Reinforcement

Increasing stirrup percentage while keeping spacing constant results in the following:-

(i) Shear deflection after diagonal cracking decreases.

(ii) Shear strength after diagonal cracking increases.

(iii) Rate of diagonal crack propagation is decreased.

(iv) Decreases diagonal crack width hence transverse expansion.

(v) Does not influence crack patterns.

5.6.5.2 Spacing

Decreasing stirrup spacing keeping percentage constant results in the following:

(i) Shear deflection after diagonal cracking is not altered.

(ii) Shear strength after diagonal cracking is not altered.

(iii) Decreases rate of diagonal crack propagation.

(iv) Increases resistance to buckling of the compression reinforcement.

(v) Increases confinement of the concrete.

(vi) Except where the stirrup spacing is very wide it has little effect on diagonal crack width, hence transverse expansion.

(vii) Does not influence the crack pattern.

Some of the effects listed above were only of marginal significance over the range of the tests.

CHAPTER 6

LOAD CAPACITY OF THE TEST BEAMS

6.1 Introduction

In this chapter the diagonal cracking loads, loads at yield of the tension reinforcement, and failure loads of all the beams tested will be discussed and compared with present theory. A theory will be developed to account for failure loads in excess of those calculated with the use of the conventional Whitney [49] stress block. Axial stresses and nominal shear stresses of the beams at various important load intensities will be presented and compared with current ACI Building Code [5] recommendations. A summary of the loads on the test beams is presented in table 6.1.

6.2 Diagonal Cracking Load

6.2.1 Definition

The diagonal cracking load of reinforced concrete beams can be defined in various ways. Bresler and MacGregor [15] define it as the practical ultimate load for beams without web reinforcement. Others including Moore [38] define the diagonal cracking load for beams with web reinforcement as the load at which there

Table 6.1 A Comparison of the Loads on all Beams

1	2	3	4	5	6	7	8	9	10	11	12	13	14	15	16	17
Beam	V_{dc}	v_{dc}	v_c	$\frac{v_{dc}}{v_c}$	N_y	N_y^*	$\frac{N_y}{N_y^*}$	v_y	N_u	v_u	n_u	N_u^*	$\frac{N_u}{N_u^*}$	N_u^{**}	$\frac{N_u}{N_u^{**}}$	$\frac{N_u^{**}}{N_u^*}$
	Kips	psi	psi	-	Kips	Kips	-	psi	Kips	psi	psi	Kips	-	Kips		
N1-S0	21.04	174	155	1.12	-	44.1	-	-	19.01	174	132	44.66	0.43	-	-	
N2-S0	25.05	207	166	1.25	-	73.0	-	-	69.25	278	481	75.60	0.92	-	-	
N3-S0	22.44 to 23.35	187 to 194	148	1.26	90.0	83.7	1.07	234	93.50	243	651	85.85	1.09	-	-	
N1-S62	16.76 to 21.28	140 to 178	148	0.95	-	44.7	-	-	36.47	323	254	46.15	0.79	46.22	-	1.00
N1-S32	16.87 to 22.60	140 to 188	143	0.98	43.1	43.5	0.99	376	47.55	401	330	44.85	1.06	47.19	1.01	1.05
N1-S63	17.86 to 23.95	149 to 200	157	0.95	43.4	43.3	1.00	381	50.33	428	350	44.74	1.12	48.52	1.04	1.08
N2-S62	15.69 to 18.85	131 to 157	153	0.86	71.7	73.2	0.98	290	77.67	297	539	75.34	1.03	80.12	0.97	1.06
N2-S32	14.94 to 18.75	124 to 156	150	0.83	73.6	72.0	1.02	289	90.83	330	632	73.44	1.24	90.08	1.01	1.23
N2-S63	17.12 to 21.45	142 to 178	140	1.01	75.8	73.7	1.03	300	82.46	321	573	75.07	1.10	86.47	0.95	1.15
N3-S12,4	15.56 to 18.53	130 to 154	143	0.91	83.7	82.9	1.01	216	110.89	276	773	84.65	1.31	112.03	0.99	1.32

2. Shear at diagonal cracking.

3. $v_{dc} = \frac{V_{dc}}{bd}$

4. $v_c = 1.9\sqrt{f'_c} + \frac{2500\ pVd}{M - N\left(\frac{4t - d}{8}\right)}$ (A.C.I. Eq. 17.2)

5. Minimum value shown in col. 3.

6. Axial Tension at onset of yield.

7. Yield axial tension from elastic theory.

9. Nominal shear stress at yield.

10. Ultimate axial tension N_u.

11. $v_u = \frac{V_u}{bd}$

12. $n_u = \frac{N_u}{bt}$

13. Ultimate axial tension from Whitney Theory.

15. Ultimate axial tension from modified Whitney theory. (see section 6.4.1.)

is significant increase in stirrup strains. This definition of diagonal cracking load is preferred in this project. It was found from observations of the cracks in the beams that the increase in stirrup strains corresponded with appreciable inclining of flexural cracks. Average stirrup tension of up to 150 micor-strains was not considered significant in the terms of this definition. For the beams without web reinforcement the diagonal cracking load was taken as the load at which a diagonal crack propagated into the flexural compression zone. There was no difficulty in determining this load for two of the beams as the cracks propagated suddenly to within 1 inch of the compression face (see figs. 4.5 and 4.13). In beam N3-SO the diagonal crack was taken to form at .874 P_u^* (see fig. 4.19), although several flexural cracks inclined towards the load point at lower load intensities.

6.2.2 Diagonal Cracking Loads of the Test Beams

The diagonal cracking shear force and nominal shear stress in the beams tested in this project are presented in columns 2 and 3 of table 6.1. The exact diagonal cracking load could not be determined from the experiments because of the size of the load increments. Where the crack was initiated between two load increments,

the loads at both increments are given. These values include the effect of dead load on the beams. Column 4 of the table gives the nominal shear stress at diagonal cracking as implied by the ACI Code Eq. (17.2). The equation without the capacity reduction factor is reproduced here for convenience.

$$v_c = 1.9\sqrt{f'_c} + \frac{2500pVd}{M-N\frac{(4t-d)}{8}} \qquad (6.1)$$

(N is negative for axial tension in Eq. (6.1). The moment M, can be replaced for eccentric axial tension by (see section 4.4)

$$-N(e' + d - \frac{t}{2})$$

where e' = the eccentricity of the axial tension from the centroid of the tension reinforcement.

Therefore

$$v_c = 1.9\sqrt{f'_c} + \left(\frac{V}{N}\right)\frac{2500pd}{(e'+\frac{7}{8}d)} \qquad (6.2)$$

(N in Eq. (6.2) is positive for axial tension). Eq. (6.1) was developed by ACI - ASCE Committee 326 [2] from consideration of the principal stress at the head of a crack. Column 5 of table 6.1 gives the ratio v_{dc}/v_c.

In the case of the three beams without web reinforcement the ratio v_{dc}/v_c is greater than unity, and it increases with increasing axial tension to shear force ratio.

From the fact that Eq. (6.1) gives conservative results for the three beams, it can be concluded that it predicts the diagonal cracking load of beams with N/V ratio lower than 3.5 with reasonable reliability. No tests have been conducted to enable predictions to be made when N/V is greater than 3.5. The other ACI Code limitation on the shear permitted to be carried by the concrete implies an even more conservative diagonal cracking shear.

$$v_c \not> 3.5\sqrt{f'_c(1 + 0.002N/A_g)} \qquad (6.3)$$

(N in Eq. (6.3) is negative for axial tension). It can be seen that no shear is permitted to be carried by the concrete if the axial stress exceeds 500 psi. At ultimate flexural capacity all the beams of the N2 - and N3 - series had an axial tension stress in excess of this.

The prediction of the diagonal cracking load of the beams with web reinforcement by Eq. (6.1) is seen to be better than for those without web reinforcement. The minimum nominal shear stress at which diagonal cracking could have occurred in the tests is lower than v_c in six of the beams. In all these, however, v_c lies within the load range in which the crack formed. In the other beam v_c is only 1% lower than the minimum observed diagonal cracking load of the beam.

The diagonal cracking loads in beams N2-SO and N3-SO are higher than in their counterpart beams with web reinforcement. This is attributed to some transverse tension in the latter beams caused by shrinkage of the concrete along the stirrups.

6.3 Load at Yield of the Tension Reinforcement

Park [41] has stated that, for under-reinforced beams the yield load can be found from the elastic analysis of a cracked section. Column 6 of table 6.1 presents the observed axial tension on the beams at full yield of the tension reinforcement. The axial yield load predicted by the theoretical elastic analysis is given in column 7. The analysis is outlined in appendix C. Column 8 of the table shows the ratio of experimental to theoretical yield load, while column 9 gives the nominal shear stress at observed yield of the tension reinforcement.

Except for beam N3-SO the agreement between theory and experiment is excellent. The beams N1-SO, N2-SO, and N1-S62 did not show full yield of the tension reinforcement before failure. The high observed yield load for beam N3-SO is believed to be caused by abnormally high yield strength of the tension reinforcement at the critical section.

6.4 Ultimate Flexural Capacities of the Beams

The ultimate flexural capacities of the beams were calculated using Whitneys [49] equivalent stress block. The ultimate concrete strain was assumed to be .003in/in. The analysis of a section subjected to axial tension at ultimate flexural capacity is summarised in appendix C. No account of strain hardening of the tension reinforcement was allowed for. A modified version taking strain hardening into consideration is presented in section 6.4.1.

Column 10 of table 6.1 gives the measured ultimate axial tension on the beams. An allowance for the beam dead load and top portion of the loading frame is included. Column 11 presents the nominal shear stress at ultimate load and column 12 gives the axial tension stress calculated on the gross sectional area of the beams. The ultimate axial tension predicted by the conventional Whitney ultimate theory is given in column 13, and the ratio of experimental to theoretical is presented in column 14.

Except for the three beams that did not attain their yield loads the beams all showed ultimate strengths in excess of N_u^*. Beam N2-S62 showed an almost pure shear failure (see fig. 5.42). However it attained its ultimate flexural capacity. The high observed ultimate strength of beam N3-SO is also believed

to be caused by abnormally high yield of the tension reinforcement.

6.4.1 Modified Ultimate Flexural Capacity of Beams With Compression Reinforcement

Two modifications of the conventional flexural theory are required to explain the increase in the flexural capacity of the test beams. These are:

(i) strain hardening in the tension reinforcement, and

(ii) confinement of the compression concrete.

It is assumed that the concrete cover above the stirrups crushes successively as each fibre attains its ultimate strain. It is further assumed that once the concrete has spalled from above the compression reinforcement, the remaining concrete maintains a constant strength of $.85f'_c$. No concrete crushes below the level of the top surface of the compression reinforcement.

Kent[29] has shown that the stress strain relationship in the strain hardening range of the reinforcement* commonly used in this laboratory can be described by the following function:

* The reinforcement is manufactured by "Pacific Steel Ltd", Auckland, New Zealand.

$$f_s = f_y\left[\frac{w_h(\varepsilon_s - \varepsilon_{sh}) + 2}{60(\varepsilon_s - \varepsilon_{sh}) + 2} + \frac{(\varepsilon_s - \varepsilon_{sh})}{(\varepsilon_{su} - \varepsilon_{sh})}\left(\frac{f_u}{f_y} - w_a\right)\right] \tag{6.4}$$

where f_s = steel stress

f_y = yield stress

f_u = ultimate stress

ε_s = steel strain

ε_{sh} = strain at onset of strain hardening

ε_{su} = ultimate strain.

For the particular steel used

$$\varepsilon_{su} = \varepsilon_{sh} + 0.14 \tag{6.5}$$

w_h and w_a are factors given by

$$w_h = 91.9\frac{f_u}{f_y} - 32.0 \tag{6.6}$$

$$w_a = 0.0137w_h + 0.1922 \tag{6.7}$$

Both w_h and w_a depend on $(\varepsilon_{su} - \varepsilon_{sh})$ but for the purposes of this analysis this has been taken as 0.14 as given by Eq. (6.5).

Fig. 6.1 shows the strain and idealised stress profiles at ultimate load of a doubly reinforced concrete beam subjected to an eccentric tension force. The notation used in the analysis of this beam is as follows:

ε_{cu} = ultimate unconfined concrete strain

ε_c = strain at the compression face of the beam

f_s = stress in tension reinforcement

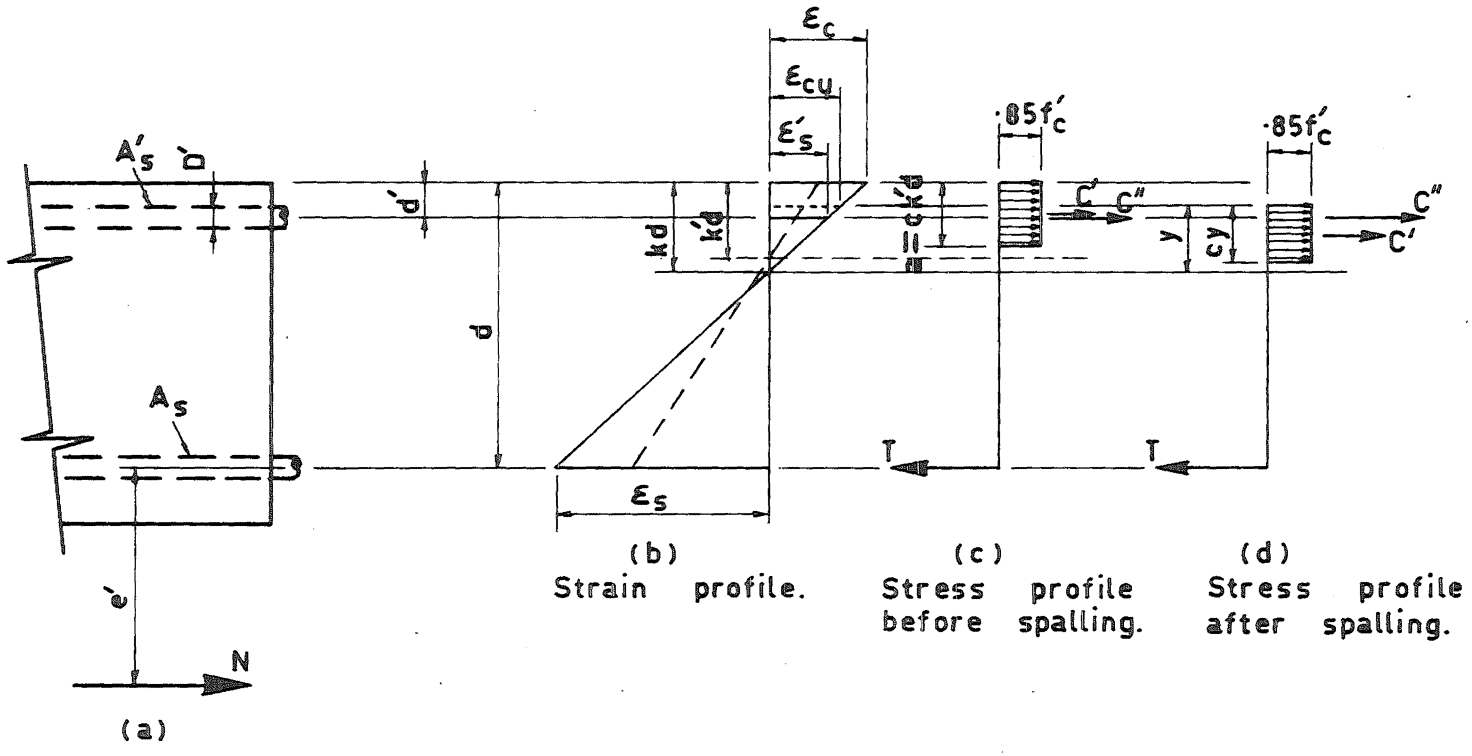

Fig. 6.1 Modified Whitney[49] Analysis of the Ultimate Flexural Capacity of the Test Beams

E_s = Young's modulus of the tension reinforcement

f'_s = stress in compression reinforcement

f'_y = yield stress of compression reinforcement

E'_s = Young's modulus of the compression reinforcement

c = ratio of the depth of the equivalent rectangular stress block to the depth of the compression zone concrete.

For equilibrium resolving forces in figs. 6.1 (a) and (d)

$$N + C' + C'' = T \qquad (6.8)$$

Taking moments about the tension reinforcement

$$Ne' = C''(d - d') + C'\left(d - (kd - y) + \frac{cy}{2}\right) \qquad (6.9)$$

From fig. 6.1 (b)

$$k = \frac{\varepsilon_c}{\varepsilon_s + \varepsilon_c} \qquad (6.10)$$

$$\varepsilon'_s = \varepsilon_c\left(\frac{kd - d'}{kd}\right) \qquad (6.11)$$

Four stages of concrete behaviour in the compression zone must be considered.

Stage 1: - Concrete has not commenced spalling, and compression reinforcement is completely above the neutral axis, i.e.,

$$\varepsilon_c \leqslant \varepsilon_{cu}$$

and $$kd \geqslant d' + \frac{D'}{2}$$

Referring to fig. 6.1 (b) and (c)

$$y = k'd \tag{6.12}$$

$$C' = .85f'_c bck'd \tag{6.13}$$

$$C'' = A'_s(f'_s - .85f'_c) \tag{6.14}$$

where $$f'_s = \varepsilon'_s E'_s \tag{6.15}$$

when $$\varepsilon'_s < f'_y/E'_s$$

or $$f'_s = f'_y \tag{6.16}$$

when $$\varepsilon'_s \geq f'_y/E'_s$$

Stage 2 : - Concrete has not commenced spalling and the neutral axis is above the bottom face of the compression reinforcement, i.e.,

$$\varepsilon_c \leq \varepsilon_{cu}$$

and $$kd < d' + \frac{D'}{2}$$

y is given by Eq. (6.12) and C' by Eq. (6.13)

$$C'' = A'_s f'_s \tag{6.17}$$

f'_s is given by Eqs. (6.15) or (6.16)

Stage 3 : - Concrete has commenced spalling and compression reinforcement is completely above the neutral axis, i.e.,

$$\varepsilon_c > \varepsilon_{cu}$$

and $$kd \geq d' + \frac{D'}{2}$$

Referring to fig. 6.1 (b) and (d)

$$y = \frac{\varepsilon_{cu}}{\varepsilon_c} kd \qquad (6.18)$$

or $$y = kd - d' + \frac{D'}{2} \qquad (6.19)$$

The larger value of y from Eqs. (6.18) and (6.19) is taken.

Now $$C' = .85 f'_c bcy \qquad (6.20)$$

and C" is given by Eq. (6.14).

Stage 4 : - Concrete has commenced spalling and the neutral axis is above the bottom face of the compression reinforcement, i.e.,

$$\varepsilon_c > \varepsilon_{cu}$$

and $$kd < d' + \frac{D'}{2}$$

Fig. 6.1 (d) shows y which is given by Eqs. (6.18) or (6.19). C' and C" are found from Eq. (6.20) and Eq. (6.17) respectively.

This analysis is only applicable for an underreinforced section so the tension reinforcement has already yielded.

When $$\varepsilon_y < \varepsilon_s \leqslant \varepsilon_{sh}$$

$$f_s = f_y$$

when $$\varepsilon_s > \varepsilon_{sh}$$

then f_s is given by Eq. (6.4)

$$T = f_s A_s \qquad (6.21)$$

The trial and error method of finding the modified ultimate flexural capacity of the section is as follows:

Step 1 - Choose ε_s

Step 2 - Estimate ε_c

Step 3 - Find k or k' and ε'_s from Eqs. (6.10) and (6.11) respectively.

Step 4 - Find y from Eqs. (6.12), (6.18) or (6.19).

Step 5 - Find T, C' and C" from the appropriate Eq. of (6.13), (6.14), (6.17), (6.20) and (6.21)

Step 6 - Find N from both Eqs. (6.8) and (6.9)

Step 7 - The two values of N are compared and if they are equal the value of N is the eccentric axial tension for the particular ε_s chosen in Step 1. If N from Eq. (6.8) is smaller than that obtained from Eq. (6.9), ε_c is decreased and the computations are started at Step 3. If N from Eq. (6.8) is larger than from Eq. (6.9), ε_c is increased and the computations proceed again from Step 3.

Step 8 - A new value of ε_s is chosen and the calculation commenced from Step 1.

The largest value of N obtained before complete yield of the compression reinforcement is considered to be the ultimate axial tension N_u^{**}, the section will sustain. The values of this are given in column 15 of table 6.1, and column 16 gives the ratio N_u/N_u^{**}. The ultimate unconfined concrete strain used to calculate N_u^{**} was taken as .004in/in. The ratio N_u^{**}/N_u^{*} is given in column 17.

As can be seen from the ratio N_u/N_u^{**} in table 6.1, the modified theoretical ultimate flexural capacity gives good agreement with the observed failure loads of the beams that failed in the post-elastic range. The two beams, N2-S32 and N3-S12,4, that showed the largest increase of strength after yield of the tension reinforcement, give excellent agreement with the modified theory. From consideration of the ratio N_u^{**}/N_u^{*} it is apparent that the higher the ratio of N/M, the greater the effect strain hardening of the tension reinforcement has on the ultimate flexural capacity of a beam.

6.4.2 Effect of Diagonal Cracking on Ultimate Flexural Capacity

The short length of compression zone between the head of a diagonal crack and the section of maximum moment is associated with tension reinforcement strains along the longer length of beam between

the point where the major diagonal crack crosses the tension steel and the section of maximum moment (see fig. 4.2). If it is assumed that the right hand portion of the cantilever rotates about the head of the diagonal crack then it can be shown that, for compatibility of strains, the compression zone is shallower than would be calculated from conventional flexural theory. However, at ultimate load the difference in the depth of the compression zone is small relative to the effective beam depth and thus the internal lever arm is only slightly longer in beams with diagonal cracks than in beams without. By halving the depth of the compression zone in the modified ultimate load analysis of beam N3-S12,4 the internal lever arm is increased less than 5%. A reduction to this increase is afforded by the constant lever arm to the compression reinforcement, which, at ultimate load, resists approximately 80% of the compression force in the beam. Thus it is apparent that the internal lever arm is only marginally affected by diagonal cracking in the test beams. Because the ultimate flexural capacity is directly proportional to the internal lever arm it can be concluded that shear and diagonal cracking does not significantly effect the modified ultimate load analysis.

6.4.3 Flexural Reinforcement Strains from the Modified Theory

Fig. 6.2 shows longitudinal reinforcement strains at the critical flexural section plotted against the applied post-elastic axial tension on beams N2-S32 and N3-S12,4. The modified theoretical tension and compression reinforcement strains are plotted to different scales. Also the observed tension steel strains at the critical flexural section are included. These two beams were chosen as representative examples, as the enhancement of their ultimate strengths as a result of strain hardening of the tension reinforcement was the greatest of any of the beams tested. The full line in the figure is the modified theoretical tension steel strain, and the dash-dotted line is the theoretical compression steel strain. Both are calculated on the assumption that the confined compression zone concrete maintains a constant strength of $.85f'_c$ up to a strain in excess of 1%. The dashed lines drawn at the onset of strain hardening show the likely actual tension reinforcement strain relationship taking into account the effect of two layers of tension reinforcement. The theoretical analysis did not consider this. The various critical points marked on the theoretical curves are given in the key to the figure. The compression reinforcement is assumed to yield when its centroid reaches

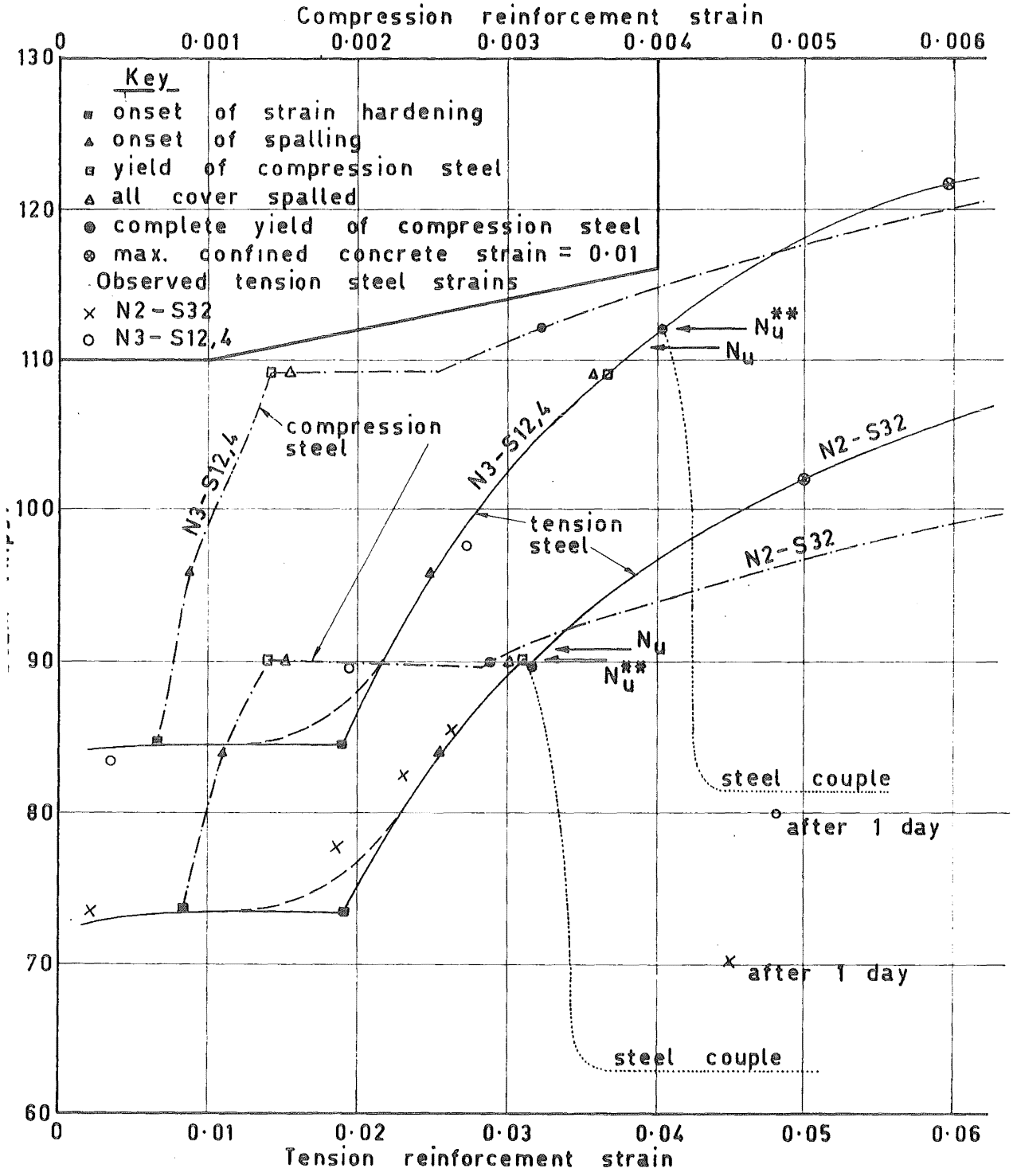

Fig. 6.2 Applied Axial Tension – Tension Reinforcement Strain Relationships for Beams N2-S32 and N3-S12,4

yield strain. Complete yield, on the other hand, occurs when the whole cross section of the bars have yielded. The highest load attained up to complete yield of the compression steel is considered to be the failure load N_u^{**}. If the confined concrete is no longer effective after N_u^{**} is obtained, the steel couple may resist the applied load. This is shown by the dotted line in the figure. The two points marked "after 1 day" give the load sustained by the two beams one day after the tests were completed. Also marked on the theoretical curves are the observed failure loads.

6.4.4 Buckling of the Compression Reinforcement

It was noted in the various sections describing beam failures in chapter 5, that there was little or no buckling of the compression reinforcement once it had yielded. Beam N3-S12,4 was a good example of this. The compression steel was restrained by a stirrup 1 inch above the critical section and no more restraint was present over the next 12 inches of compression reinforcement. It is obvious that any tendency to buckle was in the plane of the beam towards the tension reinforcement where adequate resistance to buckling was afforded by the concrete. This would be the most likely direction because of the curvature induced in the bars by bending of the beam in this

plane. However, it is surprising that the reinforcement did not buckle outwards normal to the plane of the beam. It is believed that the relatively small area of crushed concrete is responsible for this. Sufficient concrete remained intact in the compression zone, except right at the section of maximum moment, to prevent this type of buckling.

6.5 Shear - Flexural Failures

In chapter 5 several of the beams were described as failing in a shear-flexural type mode. It was noted that the critical area of the compression zone of these beams was cracked along planes radiating from the reentry corner (see figs. 5.26 and 5.45). These planes are normal to the directions of the principal tensile stresses in the critical zone.

When a beam contains diagonal cracks, which have propagated towards the critical flexural compression zone, the planes previously mentioned are sources of potential cracking in the compression zone as a result of incompatibility of deformations on either side of the diagonal crack. If the stirrups across the diagonal cracks are still below yield, the cracks do not penetrate far into the compression zone. Once the stirrups have all yielded across a diagonal crack, the crack widens and propagates further into the com-

pression zone. Eventually the flexural compression is not sufficient to prevent the crack propagating to the compression face of the beam (see figs. 5.25 and 5.26). Displacement occurs along the crack and thus the beam separates. If the beam is in the post-elastic range when this happens, this type of failure is regarded as the shear-flexural type.

CHAPTER 7

SHEAR BEHAVIOUR OF BEAMS

7.1 Introduction

The resistance to applied shear of reinforced concrete beams subjected to axial tension has received little attention from previous investigators. The recommendations for the shear resisted by the concrete in both the ACI Code [5] and the National Building Code [40] are based on a series of only 11 beam tests conducted by Elstner and Hognestad in 1956 [17]. More recently Mattock [35] has reported tests on 14 beams without web reinforcement subjected to axial tension and then loaded to failure in shear.

The load applied to the test beams in this project produced a sensibly constant axial tension to shear force ratio. Comparisons of diagonal cracking loads are made with those predicted by present code recommendations and other investigators. The shear carried by web reinforcement is studied. Dowel action is considered and it is shown to be an effective means of additional shear resistance after yield of the stirrups across a diagonal crack.

7.2 Shear Behaviour of the Test Beams

7.2.1 Before Diagonal Cracking

Before diagonal cracking in the beams with web reinforcement observed stirrup tension was below 150 microstrains. The shear carried by each $\frac{1}{4}$ inch stirrup was therefore less than 450 lb., hence being considered negligible. Therefore until a diagonal crack formed in the web of the test beams all the applied shear was resisted by three mechanisms; the concrete above flexural cracks, dowel action and aggregate interlock action. It has been shown in chapters 4 and 5 that displacements along flexural cracks were small prior to the formation of a diagonal crack, thus the contribution of the latter two mechanisms was small. Consequently before diagonal cracking the concrete above flexural cracks carried almost all the applied shear.

7.2.2 Diagonal Cracking Shear

There have been several equations proposed to predict the diagonal cracking shear of beams subjected to axial compression but only four specifically take axial tension into account. Table 7.1 summarises the diagonal cracking load of the test beams as predicted by equations proposed by several investigators [8, 10, 14, 16, 35], as well as the ACI

Table 7.1 Comparison of Diagonal Cracking Shears.

	Nominal shear stress at diagonal cracking:- v_{dc} in psi.								
Beam	Experimental	ACI 318-63[5]	National Building Code[40] and ACI Code Amendments[37]	Mattock[35]	Mattock[35]	Blume et al[14]	Diaz de Cossio and Siess[16]	Baldwin and Viest[8]	Baron and Siess[10]
	(1)	(2)	(3)	(4)	(5)	(6)	(7)	(8)	(9)
N1-S0	174	148	52	240	165	68	191	241	243
N2-S0	207	0	0	246	175	39	194	237	240
N3-S0	187-194	0	0	232	168	13	162	204	238
N1-S62	140-178	136	47	233	161	65	184	232	238
N1-S32	140-188	136	48	245	160	62	178	227	229
N1-S63	149-200	151	53	259	166	73	193	244	241
N2-S62	131-157	0	0	245	169	37	180	223	234
N2-S32	124-156	0	0	248	165	36	175	218	225
N2-S63	142-178	0	0	235	161	26	166	209	221
N3-S12,4	130-154	0	0	220	163	20	154	195	230

(1) For explanation see chapter 6.

(2) $$v_c = 1.9\sqrt{f'_c} + \frac{2500pVd}{M - N\left(\frac{4t-d}{8}\right)} \qquad (7.1)$$

with the limitation $$v_c \not> 3.5\sqrt{f'_c(1 + .002N/A_g)} \qquad (7.1A)$$

(3) $$v_c = 2.0\sqrt{f'_c}(1 + .002N/A_g) \qquad (7.2)$$

(4) $$v_{dc} = v_{flex} + (1.25 + 5.0np)\sqrt{f'_c} \qquad (7.3)$$

(5) $$v_{dc} = (1.25 + 5.0np)\sqrt{f'_c}$$ (If flexural cracking shear is zero) (7.4)

(6) $$v_c = \left(1 + \frac{N}{8A_{tr}\sqrt{f'_c}}\right)1.9\sqrt{f'_c} \qquad (7.5)$$

(7) $$v_{dc} = \left[2.14\sqrt{f'_c} + 4600p\left(\frac{Vd}{M}\right)_x\right]\left[1 + .04\left(\frac{N}{V}\right)_x\right] \qquad (7.6)$$

(8) $$v_{dc} = \left[1.425 + \frac{38}{\frac{\left(\frac{M}{V}\right)_c}{npd} + 10}\right]\sqrt{f'_c} \qquad (7.7)$$

where $$\left(\frac{M}{V}\right)_c = a_c - \frac{N}{V}\left(\frac{t}{2} - \frac{d}{8}\right)$$

and a_c is given by:- $a_c = 0$ for $d \geqslant a$

$a_c = a - d$ for $a \geqslant d \geqslant \frac{a}{2}$

$a_c = \frac{a}{2}$ for $\frac{a}{2} \geqslant d$

(9) $$v_{dc} = \left[\frac{120p + 4.3}{23 + \frac{2a}{d}}\right]\left[\frac{f'_c}{1 + \frac{.85f'_c}{1000}}\right] + \frac{N}{\frac{7}{8}bd}\left[.270 - 3.4p - .034\frac{a}{d}\right] \qquad (7.8)$$

N.B. In all the equations N is negative for tension. It is taken as N_u^* rather than the axial tension at diagonal cracking in Eqs. (7.1A), (7.3), (7.5) and (7.8).

Code [5], the proposed amendment [37], and the National Building Code [40]. The equations are included at the bottom of the table. It should be noted that Eqs. (7.6), (7.7) and (7.8) were derived from tests on beams subjected to axial compression. The authors did not claim that these equations apply to beams with axial tension. They have been included merely to provide additional material for comparison with the test results.

The proposed amendment to the ACI Code provision for the shear carried by the concrete in beams subjected to axial tension [37], is more conservative than the relevant clause in the 1963 Code. This new recommendation has been in the Canadian Code since 1965.

The values given by Eq. (7.3) include the shear at theoretical flexural cracking of the beams plus the increment of shear between flexural and diagonal cracking given by Eq. (7.4). The test beams all showed cracking at very low load intensities as a result of shrinkage stresses. Therefore the shear stress increment given by Eq. (7.4) has been included in table 7.1.

From the table it can be seen that the ACI and Canadian Code equations, and that proposed by Blume et al are conservative for all the beams tested. It has been shown in chapter 6 that Eq. (7.1) gives good

correlation with experiment. The more stringent limitation imposed by Eq. (7.1A), especially for beams with large axial tension, makes the ACI Code recommendation conservative.

If it is assumed that the test beams cracked at very low loads then the agreement between the observed diagonal cracking loads and those predicted by Mattock is only slightly on the unsafe side. If the theoretical flexural cracking load is taken into account Eq. (7.3) is unconservative.

The diagonal cracking shears calculated from Eqs. (7.6), (7.7) and (7.8) are all on the unsafe side. It can thus be concluded that these equations developed for beams subjected to axial compression are not applicable to beams with axial tension.

7.2.3 After Diagonal Cracking

7.2.3.1 Beams Without Web Reinforcement

When diagonal cracks form in a beam without web reinforcement there is considerable displacement along these cracks. Consequently dowel action and aggregate interlock action become significant mechanisms in resisting the applied shear. Once secondary tension cracks (for definition see section 4.4.3 and Fenwick [18]) form in the concrete cantilevers

these two mechanisms cannot sustain significant increase in shear [12, 44].

It was found from beams N2-SO and N3-SO that significant dowel and aggregate interlock cracks formed immediately at diagonal cracking. In figs. 4.14 and 4.21 arch action was also shown to develop on formation of the first diagonal crack. Fenwick and Paulay [19] have shown that perfect beam action and full arch action are not compatible so in these two beams almost all the applied shear after diagonal cracking must have been resisted by dowel action as discussed in section 4.5.4, and arch action. The diagonal cracks were too wide for any appreciable aggregate interlock to develop.

7.2.3.2 Beams With Web Reinforcement

Where web reinforcement is present it reduces the rate of propagation of both the diagonal tension cracks and the secondary tension cracks. If increased shear resistance in the beams is afforded by aggregate interlock and dowel action when secondary tension cracks form, the stirrups crossing these cracks will be stressed. Thus the additional shear resistance is primarily supplied by the web reinforcement.

Parts (a) of figs. 7.1 to 7.7 are sketches of the beams with web reinforcement showing the position of the load lines, the stirrups and the major diagonal cracks. Part (b) of each figure shows the shear force carried by the stirrups and other mechanisms across a section formed by the diagonal crack and the concrete above the head of it. It can be seen from these that once diagonal cracks form, i.e., the stirrups show significant strains, the concrete plus dowel and aggregate interlock action carry decreasing shear until yield of the stirrups, and then they carry increasing shear again. After yield of the stirrups all the additional shear must be taken by the intact concrete at the head of the diagonal crack and dowel action where the crack crosses the tension reinforcement. The crack would be too wide for appreciable aggregate interlock to develop.

The reason for the decreasing shear carried by the concrete plus dowel and aggregate interlock action is the following. As the load increases on the beam the cracks get wider and thus aggregate interlock is reduced[18]. Dowel action may increase somewhat but the shear carried by the concrete at the head of the crack is unlikely to increase after diagonal cracking. The overall effect is that up to yield of the stirrups the shear carried by the three mechanisms is reduced somewhat.

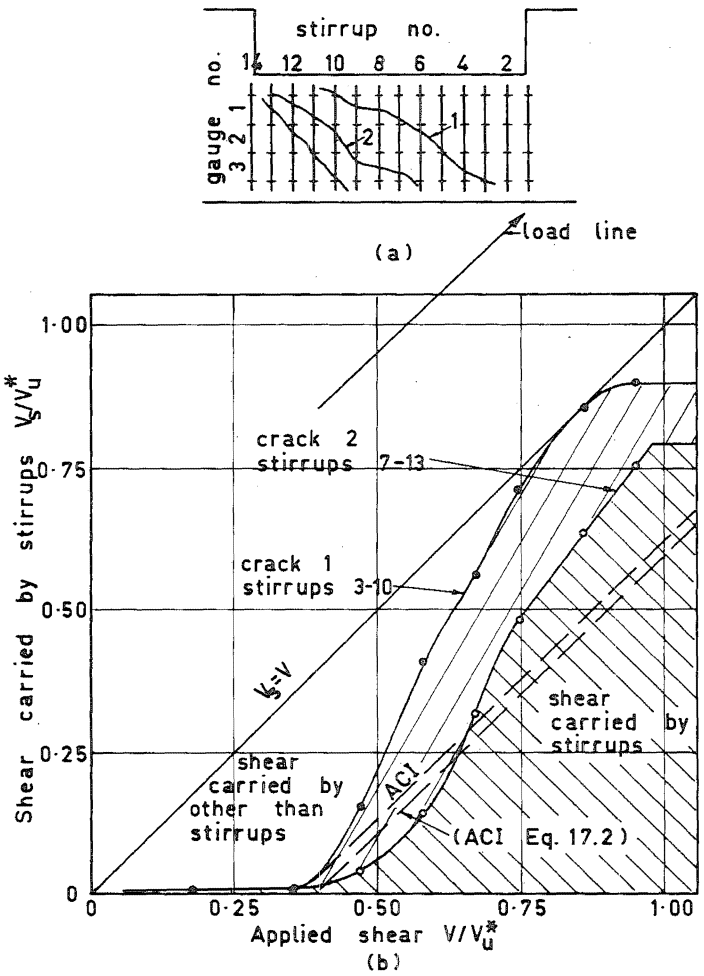

Fig. 7.2 Shear Resistance of Beam N1-S32

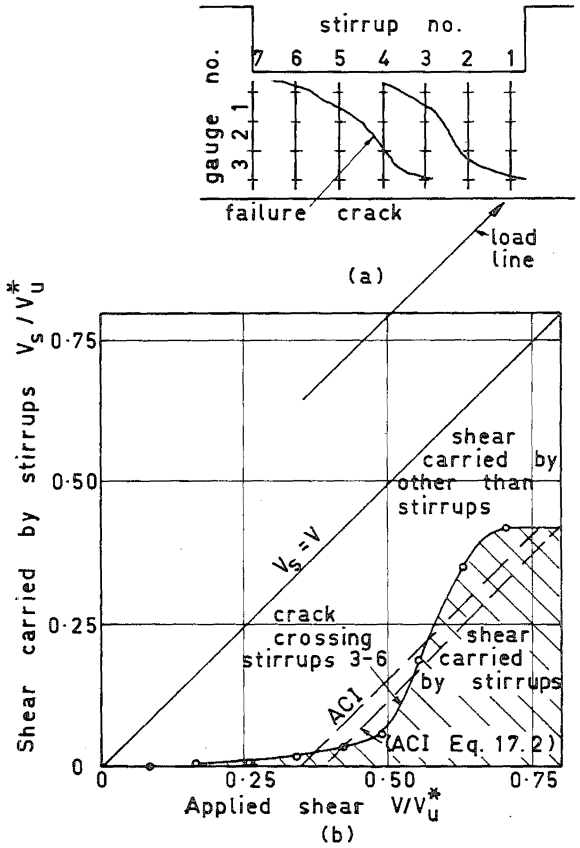

Fig. 7.1 Shear Resistance of Beam N1-S62

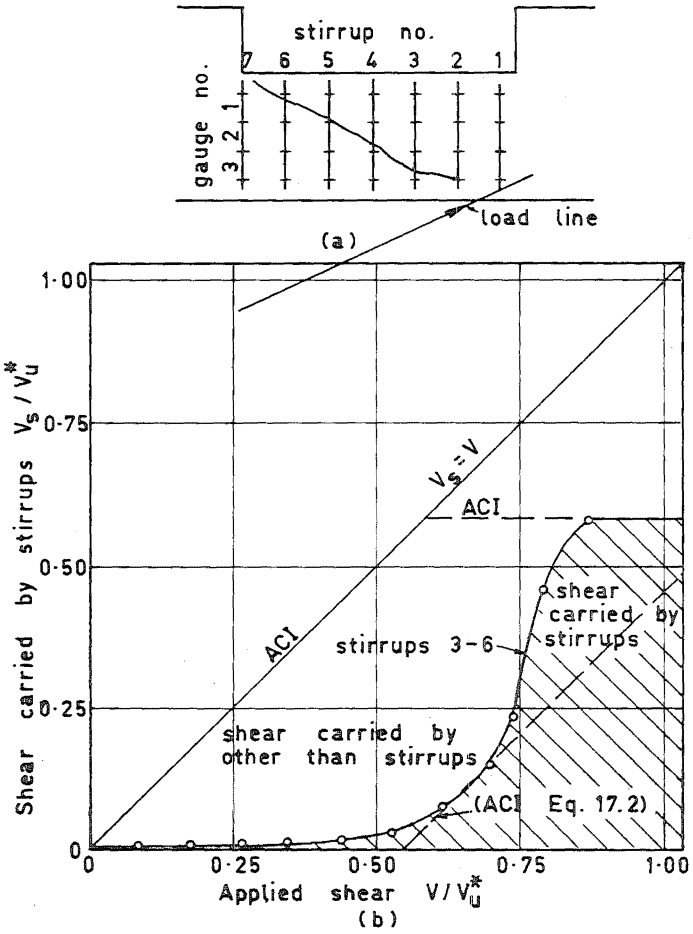

Fig. 7.4 Shear Resistance of Beam N2-S62

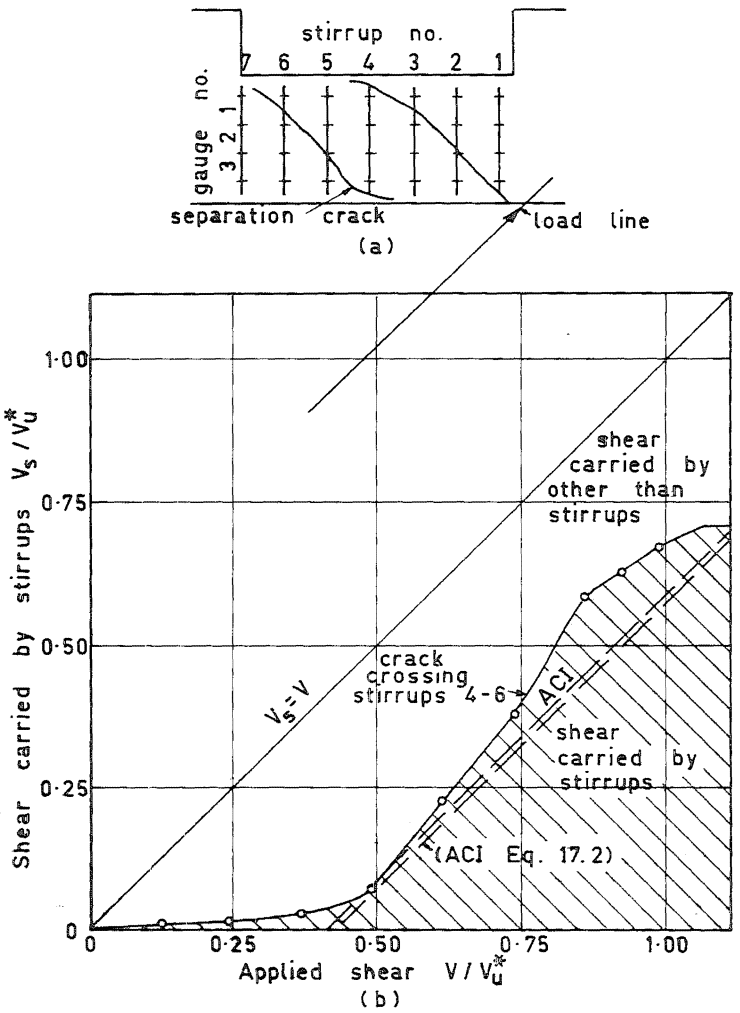

Fig. 7.3 Shear Resistance of Beam N1-S63

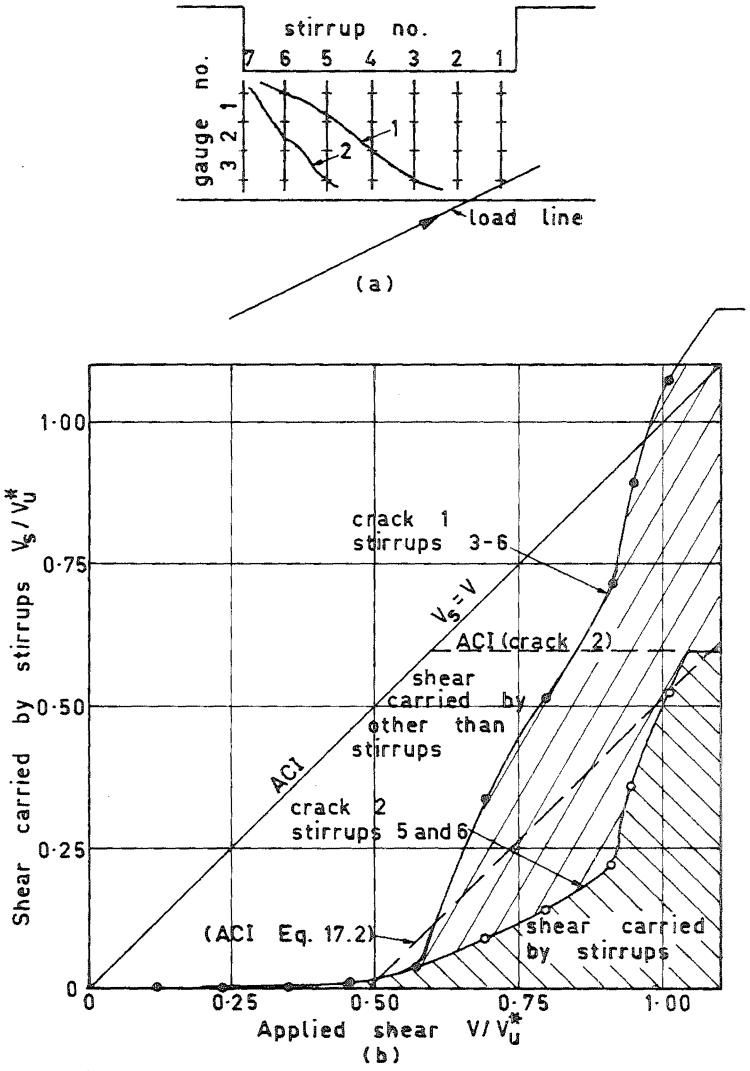

Fig. 7.6 Shear Resistance of Beam N2-S63

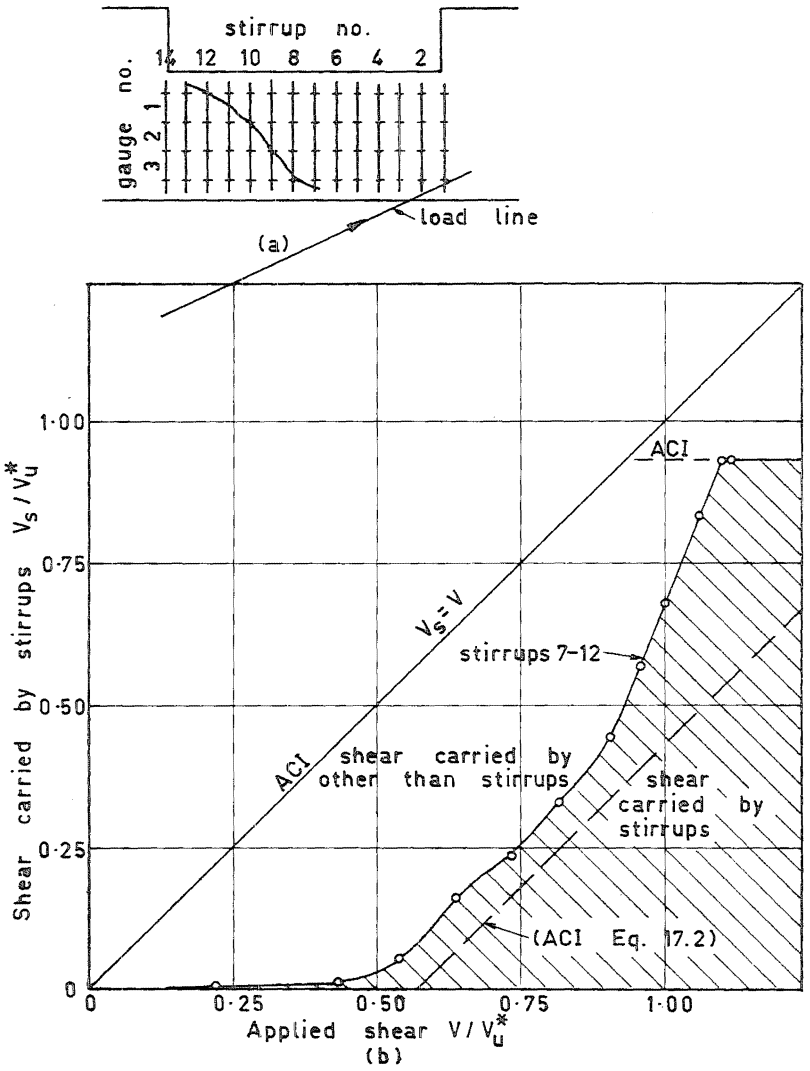

Fig. 7.5 Shear Resistance of Beam N2-S32

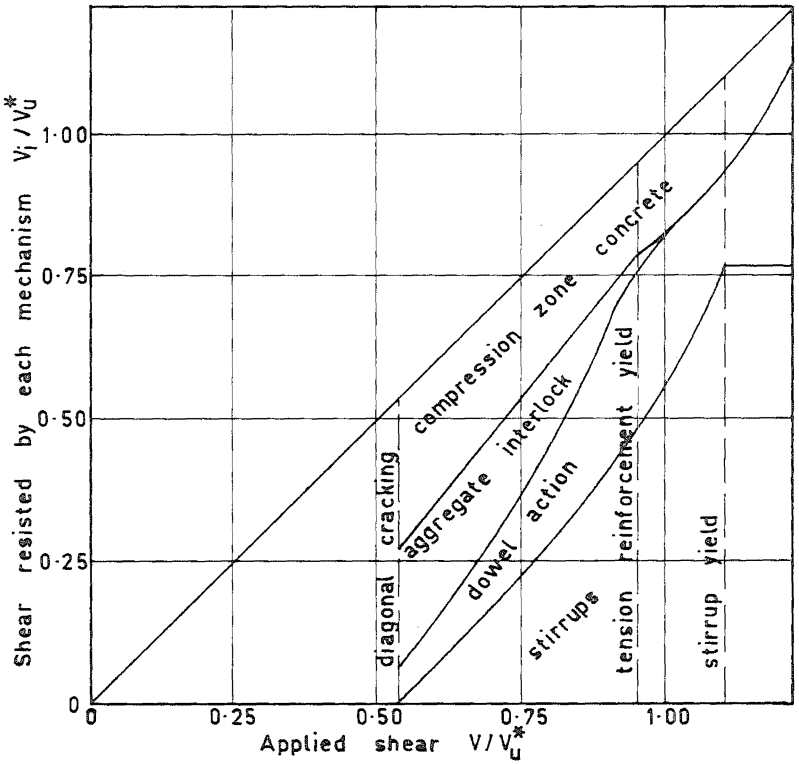

Fig. 7.8 Idealized Shear Resistance of the Test Beam

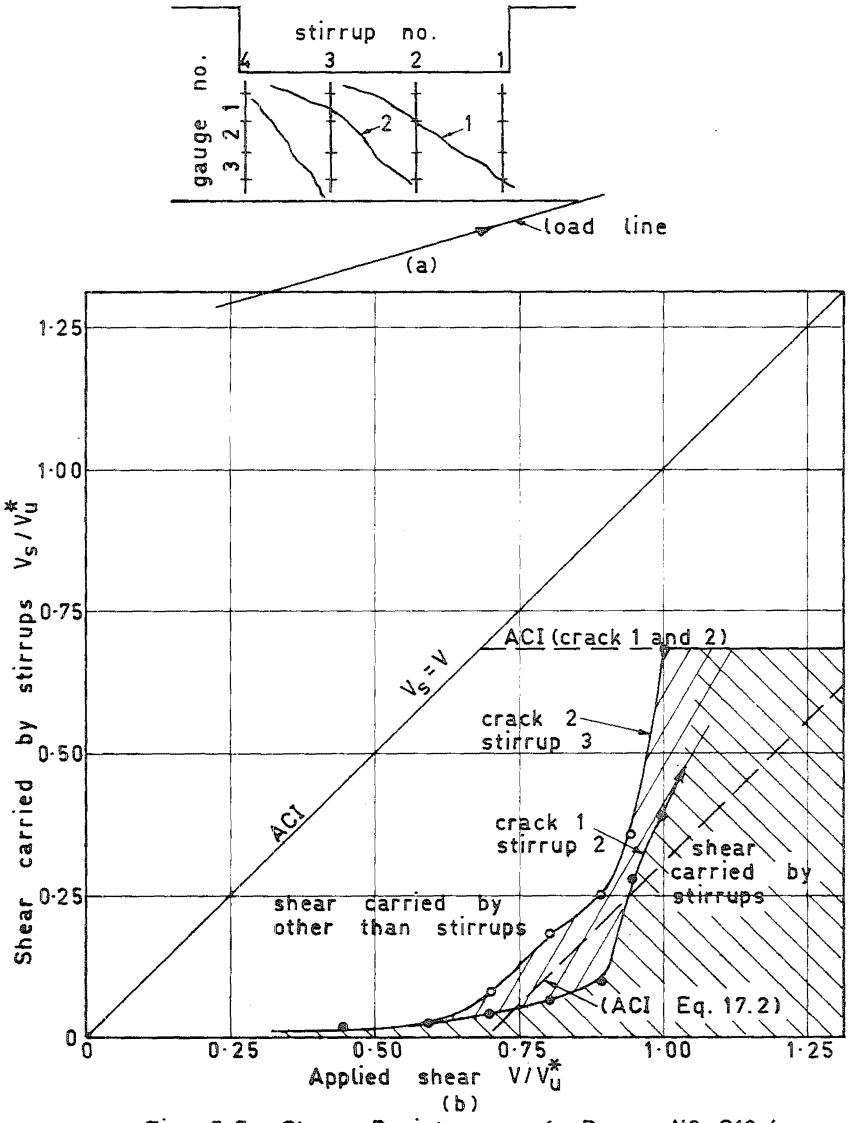

Fig. 7.7 Shear Resistance of Beam N3-S12,4

It should be noted that in fig. 7.6 (b) it appears that the shear carried across crack 1 is greater than the applied shear near ultimate load. This indicates that separation across this crack is impossible because the crack does not form a continuous potential separation surface.

7.2.4 Dowel Action

It has been shown in section 4.5.4 that the contribution of dowel action to the shear resistance of a beam without web reinforcement could be as high as 8 kips or more. Fenwick [18] has postulated that up to 20% of the total applied shear resisted by beam action in beams without stirrups can be attributed to dowel action. This figure was derived from tests on beams with only one layer of tension reinforcement. Dowel action is considerably enhanced where multiple layers of reinforcement are used [12]. The limit to the extent of dowel action is the resistance to splitting of the beam at the level of the tension steel.

Where web reinforcement is present the resistance to splitting depends on the stirrup size and spacing. It has been shown in chapter 2 that dowel action is then limited by the flexural strength of the dowel beam and by the strength of stirrups on the low moment side of the diagonal crack. In parts (b) of figs. 7.1 to 7.7

dowel action has been included with the shear taken by the concrete, except where the diagonal crack is obviously extending as a split along the tension steel (see fig. 7.3 (a) stirrup no. 4). In a situation such as this the stirrup force across the dowel crack at the end of the diagonal crack is included in the sum of the stirrup forces across the diagonal crack although it is producing dowel shear resistance. Unfortunately the decision whether a particular stirrup force is included in the shear carried by stirrups across a diagonal crack is somewhat arbitrary.

Also in chapter 2 tests were described which indicate that dowel action could still exist once the tension reinforcement had yielded. The phenomenon is referred to as the kink effect. The increased shear resistance after yield of the stirrups across a potential separation crack is provided by this effect. All the beams with web reinforcement showed increased shear strength after yield of the stirrups. In figs. 7.1 to 7.7 parts (b) this is seen as the portion of shear carried by the concrete etc., at the upper right hand corner of the diagrams. At this stage of loading all the beams except beams N1-S62 and N2-S62 showed complete yield of the tension reinforcement. The order of displacements observed along the critical cracks in the

test beams was 0.05 inches after yield of the stirrups.

Once the tension steel had yielded in beams N2-S32, N2-S63 and N3-S12,4, the shear carried by the concrete and dowel action decreased markedly until the stirrups crossing the major diagonal crack had yielded. This is attributed to the loss of aggregate interlock because of the widening of the flexural and diagonal cracks once yield of the tension reinforcement had set in. Only after yield of the stirrups did dowel action increase to carry the additional increment of shear. The reason for this is that the shear carried by the kink effect is proportional to the displacement across the diagonal crack at the level of the tension steel. This displacement increases substantially only after the crack is allowed to open because of yield of the stirrups crossing it. In the other beams the decrease in shear carried by the concrete and dowel action was not no prominent because the stirrups had yielded or were near yield when the tension reinforcement yielded, thus allowing the kink effect to become immediately effective.

7.2.5 Arch Action

It was shown in chapters 4 and 5 that arch action developed in the beams after diagonal cracking. Appreciable arch action can only be present after beam action has broken down, i.e., after loss of aggregate

interlock. It is therefore likely that only a small amount of arch action occurred in the beams with stirrups before yield of the tension reinforcement because aggregate interlock action was preserved up to this stage. Arch action and dowel action are not incompatible because dowel action may be associated with direct shear transfer across a potential separation crack.

In the discussion in this chapter arch action is included with the shear resisted by the concrete above the head of a diagonal crack.

7.2.6 Quantitative Evaluation of the Shear Resisted by Mechanisms Other Than Stirrup Resistance, in Beams With Web Reinforcement

After diagonal cracking has been initiated it has already been noted that the total shear resisted by the concrete plus dowel and aggregate interlock action is reduced to a minimum at a load a little less than that at yield of the stirrups. If the stirrups do not yield until after yield of the tension reinforcement there can be no appreciable aggregate interlock because the cracks are too wide.

Therefore at diagonal cracking the shear resisted by aggregate interlock may be assumed to be the difference of the total shear at diagonal cracking, and the shear carried by the concrete and dowel action at

yield of the web reinforcement. The shear resisted by dowel action at diagonal cracking is estimated from the observed displacements along the diagonal crack. The dowel shear is then calculated from the corresponding dowel shear dowel displacement relationships shown in chapter 2 and is adjusted for the number of bars involved. The proportion of shear not carried by aggregate interlock or dowel action is carried by the concrete in the compression zone of the beam above the head of the diagonal crack.

To find the proportion of shear resisted by the various mechanisms at yield of the tension reinforcement similar calculations were made. No significant shear was assumed to be transferred across the diagonal crack by aggregate interlock. The dowel shear is estimated in the same way as at the diagonal cracking load. The shear resisted by the stirrups is known and the remaining shear is carried by the intact concrete.

At ultimate load of the beams the stirrups shear resistance is known. It is reasonable to assume that as the diagonal cracks propagate further in to the compression zone of the beams the shear carried by the intact concrete above the head of the crack decreases somewhat. The rest of the shear not resisted by the compression zone concrete or stirrups is carried by

kinking of the tension reinforcement.

Very little shear is transferred by dowel action of the compression reinforcement because there is no displacement across the bars until separation of the beam takes place along a diagonal crack. At this stage the beam fails. No dowel action of the compression reinforcement is taken into consideration when calculating the shear resistance of the test beams.

Fig. 7.8 is a schematic diagram showing the approximate shear resisted by the four mechanisms across the section formed by the critical diagonal crack and the concrete at the head of the crack. The results from beams N1-S63, N2-S32 and N3-S12,4 have been averaged to produce this figure. These three beams were chosen as they were the only ones where all the information was readily available. The critical points on the diagram are as follows:

(i) Diagonal cracking at $.54V_u^*$.

(ii) Yield of the tension reinforcement. The aggregate interlock is lost so this shear is taken by truss action and arch action.

(iii) Yield of the stirrups. All the additional shear is carried by dowel action and the concrete above the head of the crack.

(iv) Ultimate flexural capacity. The shear is carried by increased dowel action owing to the kink effect. This makes up for the additional shear which the stirrups are unable to sustain. The shear carried by the concrete is likely to be small.

The proportion of the total shear resisted by each of the four mechanisms contributing to the total shear resistance at the critical load stages are summarised in table 7.2. The values in the table were obtained as discussed in this section above.

It should be noted that the examination presented in this section is rather approximate and that fig. 7.8 is based on likely behaviour between the critical points listed above. It should not be taken as quantitatively correct.

7.2.6.1 The Kink Effect

No attempt has been made to quantitatively calculate the kink effect in the test beams except by the difference of the total applied shear and the shear attributed to the stirrups and uncracked concrete near failure of the beams. From observations of the photographs of the beams near failure the kinked length of the tension reinforcement cannot be determined accurately enough to obtain reliable dowel shears.

Table 7.2 Shear Across the Major Diagonal Crack Resisted by Various Mechanisms in Beams N1-S63, N2-S32, and N3-S12,4

	At Diagonal Cracking				At Yield of the Tension Reinforcement				At Yield of the Web Reinforcement				At Ultimate Flexural Capacity			
	Uncracked Concrete	Dowel Action	Aggregate Interlock	Stirrups	Uncracked Concrete	Dowel Action	Aggregate Interlock	Stirrups	Uncracked Concrete	Dowel Action	Aggregate Interlock	Stirrups	Uncracked Concrete	Dowel Action	Aggregate Interlock	Stirrups
N1-S63																
%	57	13	30		4	32		64				66	4	32		64
Shear (kips)	11.8	2.7	6.2		1.8	14.1		28.2				31.4	2.0	15.8		31.4
N2-S32																
%	36	6	58		34	22		44				81	10	15		75
Shear (kips)	5.9	1.0	9.6		10.8	7.0		13.9				29.5	3.9	5.9		29.5
N3-S12,4																
%	53	14	33		6	59		35				62	5	43		52
Shear (kips)	8.4	2.2	5.2		1.5	14.8		8.8				17.1	1.6	14.1		17.1
Average																
%	49	11	40	0	15	38	0	47	12	19	0	69	7	30	0	63

Referring to table 7.2 it can be seen that dowel shears of up to 16 kips must be produced by the kink effect at failure of the beams. For a kinked length of 2 inches this would be provided at a displacement along the failure diagonal crack of 0.05 inches. Displacements of this order were observed in the beams.

7.2.7 Behaviour of Web Reinforcement

7.2.7.1 Effect of Diagonal Compression at the Section of Maximum Moment

In all seven beams the stirrup nearest the critical flexural section was observed to be in compression over a portion of its length at all load intensities. This was caused by diagonal compression in this section of the beams. As can be seen in fig. 3.4 the transverse reaction on the bottom end block of the beam is provided by the stirrup bolted to the bottom loading frame. The bearing of this stirrup produces high transverse compression in the end block adjacent to the critical flexural section of the test length. In turn this produces transverse compression at the critical flexural section. This is confirmed by the observed transverse compression shown in figs. 5.14, 5.37 and 5.54.

7.2.7.2 Interpretation of the ACI Code [5]

The ACI Code implies in section 1702 that at yield of the stirrups the concrete sustains shear equal to the applied shear at diagonal cracking. However it does not claim that between diagonal cracking and yield of the stirrups the stirrup strains vary linearly. For the purposes of comparison in this thesis it is convenient to make this assumption.

7.2.7.3 Stirrup Behaviour

Stirrup strain applied shear relationships for the stirrups in beams N1-S62 and N2-S63 are shown in figs. 7.9 and 7.10 respectively. These are typical examples of the relationships for all the beams tested. The observations on the gauge length on each stirrup crossed by the critical separation diagonal cracks have been drawn as heavier lines than the other observations. The assumed ACI Code recommendations are shown as the broken lines in the figures. For the N2 - series beams and beam N3-S12,4 no shear is allowed to be carried by the concrete according to the ACI Code. Also shown in fig. 7.10 are the calculated stirrup strains based on a diagonal cracking load predicted by Eq. (6.2), i.e., ACI Code Equation (17.2).

It can be seen from the two figures that once diagonal cracking is initiated the stirrup strains

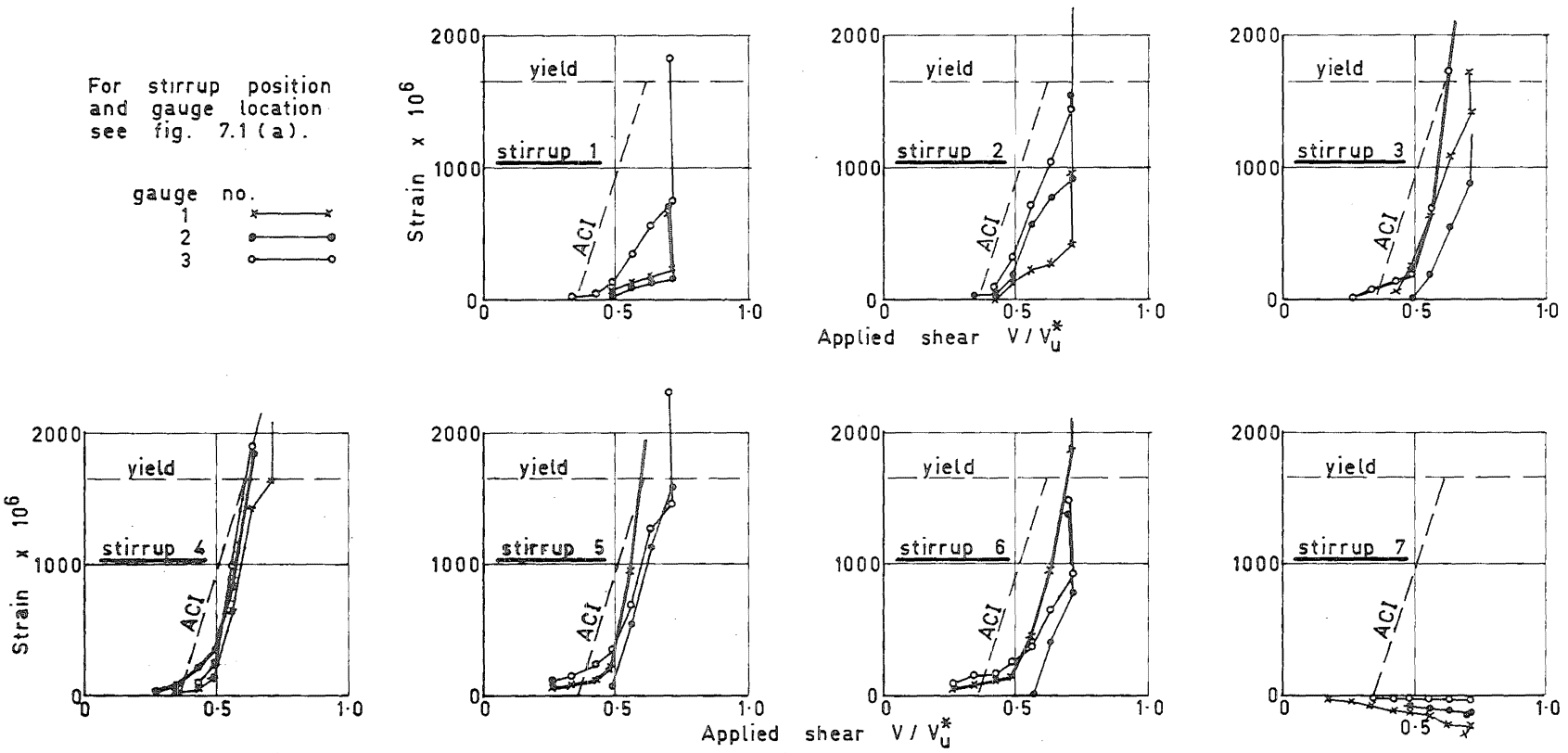

Fig. 7.9 Stirrup Strain – Shear Relationship for Beam N1-S62

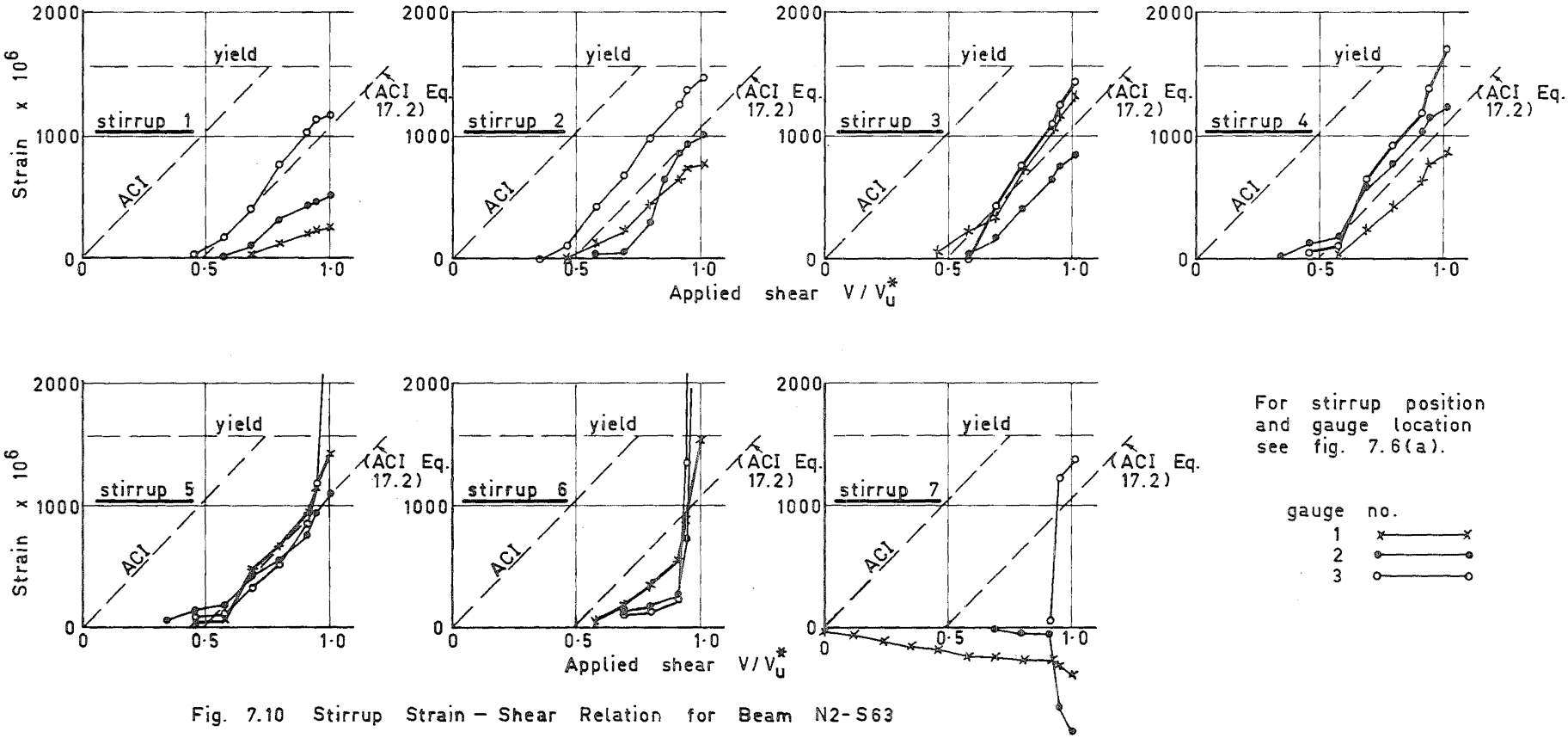

Fig. 7.10 Stirrup Strain – Shear Relation for Beam N2-S63

increase at approximately the same rate as the broken lines representing the assumed stirrup strains. As pointed out previously the strains increase more rapidly when the flexural yield of the tension reinforcement is reached (see fig. 7.10). This is due to increased dowel and truss action because of the loss of aggregate interlock when the cracks open. The most rapid increase is in gauge length no. 3 which indicates that part of the cause is dowel action.

The load strain characteristics of the stirrups crossed by the major diagonal crack in some of the test beams are shown in figs. 7.11 to 7.15. Only the strain in the critical gauge length in each stirrup is considered. As in figs. 7.9 and 7.10 the load strain relationship from the assumed ACI recommendations are shown by the broken lines. In all cases the stirrups that cross the critical crack below middepth of the beam are stressed before those nearer the section of maximum moment. This is because the rate of propagation of the diagonal crack is reduced by the presence of stirrups and thus the crack does not cross the stirrups near the critical flexural section for some time after diagonal cracking. This is most noticable in beams N1-S32 and N2-S32 thus indicating the advantage of closely spaced stirrups in reducing the rate of propagation of diagonal cracks.

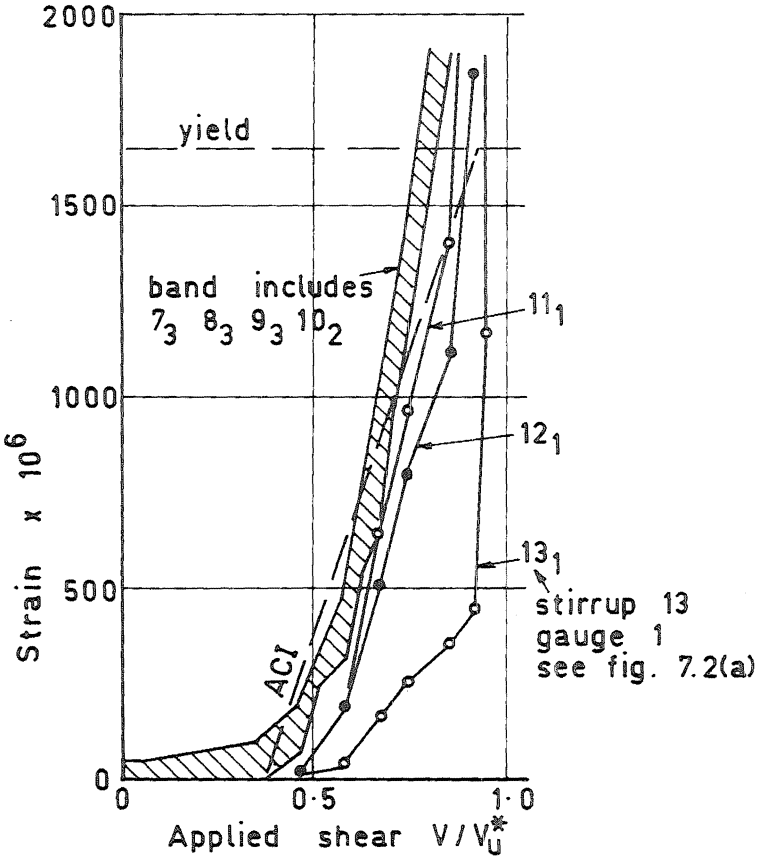

Fig. 7.11 Beam N1-S32 Stirrup Strain - Shear Relationship

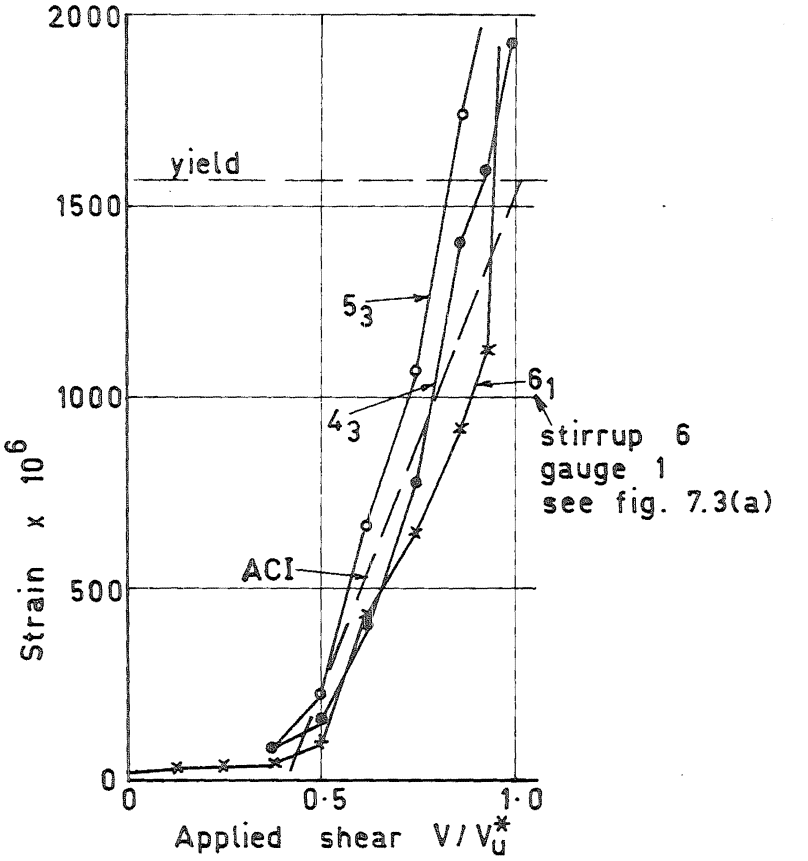

Fig. 7.12 Beam N1-S63 Stirrup Strain - Shear Relationship

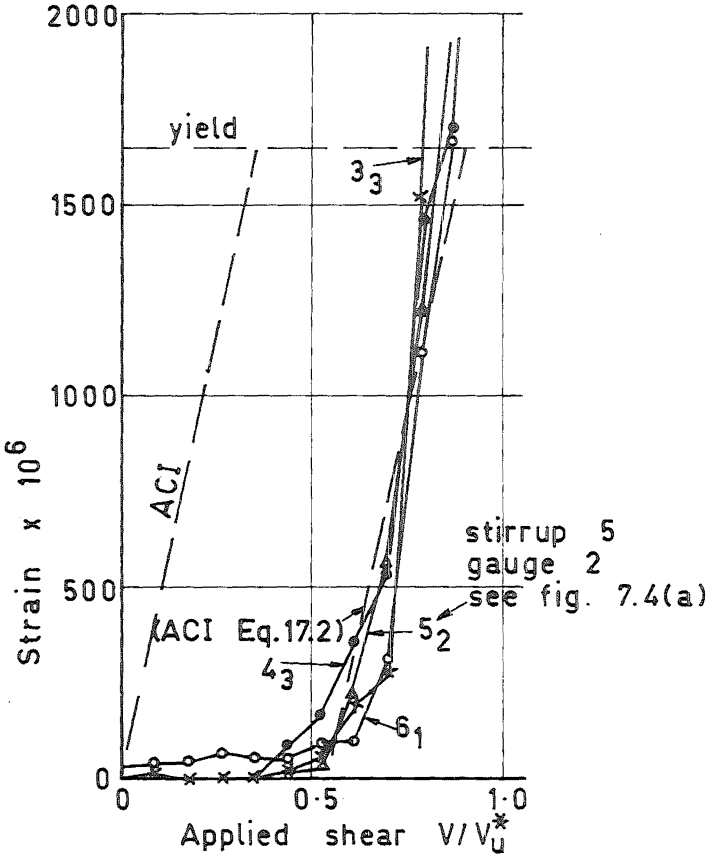

Fig. 7.13 Beam N2-S62 Stirrup Strain – Shear Relationship

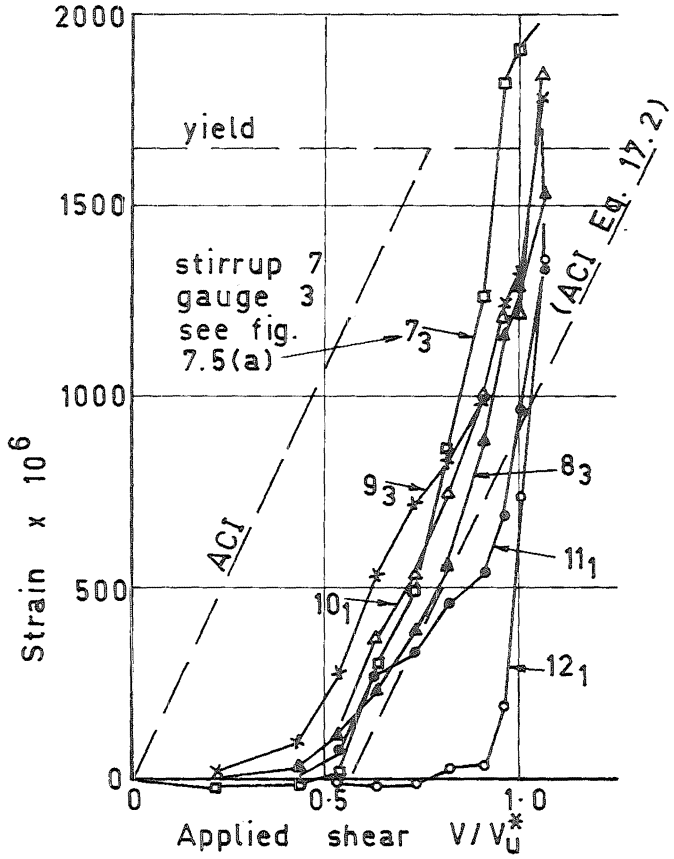

Fig. 7.14 Beam N2-S32 Stirrup Strain – Shear Relationship

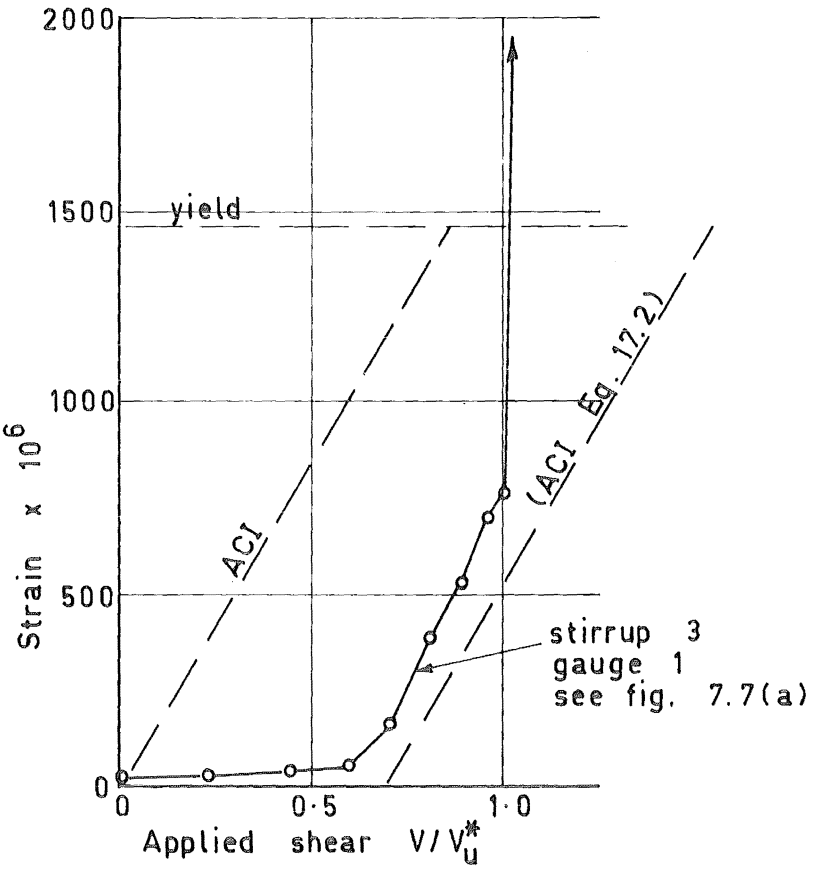

Fig. 7.15 Beam N3-S12,4 Stirrup Strain – Shear Relationship

The total shear carried by the stirrups crossing a diagonal crack was shown in figs. 7.1 to 7.7 parts (b). The relationship assumed from the ACI Code (see section 7.2.7.2 above) was shown by a broken line. It should be noted that the assumed relationships are based on the actual cracks in the test beams and not a 45^{o} crack. Consequently the calculated yield load on the stirrups across the separation cracks is equal to the observed maximum shear force carried by the stirrups in a test beam.

As was discussed in section 7.2.3.2 dowel and aggregate interlock action can be attributed to stirrup resistance after secondary tension cracking has developed. Figs. 7.2 (b) and 7.6 (b) illustrate this, in particular with reference to dowel action. In figs. 7.2 (b) it can be seen that crack 1 passes across stirrups 3 and 4 at the level of the tension reinforcement. The action of these two stirrups is to increase the dowel shear capable of being resisted by the tension steel rather than to transfer direct tension across the diagonal crack. Similar reasoning applies to stirrup 3 in fig. 7.6 (b).

7.3 Shear Strength of the Test Beams as Compared to ACI Recommendations

The philosopy of ultimate design of reinforced

concrete beams is based on the desirability of a ductile flexural failure rather than a brittle shear failure. Therefore, to avoid a shear failure, there must be sufficient shear resistance including web reinforcement to resist the applied shear at ultimate flexural capacity. The ACI Code recommends that a certain shear can be resisted by the concrete and the remainder must be resisted by web reinforcement. The potential failure diagonal crack in design is assumed to form at 45^{o} to the longitudinal axis of the member.

Table 7.3 gives the recommended shear that can be carried by the test beams according to the ACI Code. It can be seen from column 5 that beam N1-S63 was the only beam which was adequately reinforced against a shear failure. However, as has already been noted, all the beams with web reinforcement except N1-S62 attained their ultimate flexural capacity based on the Whitney stress block. It should be noted that the ACI recommendations given in column 3 are based on a crack inclined at 45^{o}, although the critical diagonal cracks which formed in the test beams were inclined at a less steep angle to the longitudinal axis.

Column 6 of table 7.3 gives the ratio of the observed shear at failure of the test beams to the ultimate shear, as recommended by the ACI Code, presented in column 4. The ACI recommendations are

Table 7.3 ACI Code Shear Recommendations for the Test Beams

Beam		Allowable shear force in accordance with ACI recommendations				
	V_u^* kips	V_c kips	V_s kips	$V_u = V_c + V_s$ kips	V_u/V_u^*	$V_{u\,test}/V_{u\,ACI}$
	1	2	3	4	5	6
N1-S0	45.25	17.8	0	17.8	0.39	1.18
N2-S0	36.80	0	0	0	0	-
N3-S0	26.90	0	0	0	0	-
N1-S62	46.75	16.3	12.3	28.6	0.61	1.35
N1-S32	43.75	16.3	24.7	41.0	0.94	1.18
N1-S63	44.10	18.1	26.2	44.3	1.00	1.16
N2-S62	33.95	0	12.4	12.4	0.37	2.88
N2-S32	31.65	0	24.8	24.8	0.78	1.60
N2-S63	34.90	0	26.2	26.2	0.75	1.47
N3-S124	25.10	0	21.7	21.7	0.86	1.53

1. Shear at Whitney ultimate flexural capacity.
2. Shear carried by concrete as recommended by ACI 318-63.
3. Shear arrived by stirrups based on a 45° crack as recommended by ACI 318-63.
4. Ultimate allowable shear as recommended by ACI 318-63.

conservative for all the beams.

7.4 Propagation of Diagonal Cracks in Reinforced Concrete Beams Subjected to Axial Tension

The stresses at the head of a crack in a reinforced concrete beam are likely to be responsible for the propagation of that crack. In beams both with or without applied axial tension these stresses are similar. MacGregor and Hanson [37] have shown that for equal applied bending moment the cracks in beams subjected to axial tension penetrate deaper into the section than in beams with no axial tension. Because the stresses for equal angle of crack propagation are therefore closer to the compression face in beams with axial tension it is reasonable to expect diagonal cracks to be more steeply inclined in beams with axial tension than in beams without.

It can be seen from the photographs in chapters 4 and 5 that the crack patterns in the beams tested in this project are little different from those of beams tested with no axial tension [32]. This is not surprising since the difference in height of the flexural cracks in both of the MacGregor and Hanson beams with and without axial tension were of the order of 5% of the beam depth.

The cracks at the low moment end of the test beams were much flatter than 45^{o} to the longitudinal axis. It was shown in figs. 4.14, 4.21, 5.12, 5.36, and 5.53 that the centre of compression force in the beams in this region was further down the beam section than would be expected from normal flexural behaviour. Thus the stress condition at the heads of the cracks would lead to a flat crack as was observed in the tests.

At a point of contraflexure in a beam there is no flexural compression across the whole beam section and consequently if the tension applied to the beam is sufficient to crack the concrete the diagonal cracks can become very steep. The tests carried out by Elstner and Hognestad [17] show this. More investivation of this area of the problem is required.

7.5 Conclusions

The shear that is carried by the concrete is conservatively estimated by both the ACI Code [5] and the National Building Code [40]. If the test beams are assumed to be cracked (shrinkage cracks) at zero load, Mattock [35] predicts the diagonal cracking shear on the beams successfully. Within the range of the experiments the amount of axial tension applied to the test beams does not substantially effect the diagonal cracking load or crack inclination.

In beams with web reinforcement, once diagonal cracks have formed, the shear resisted by the concrete plus dowel and aggregate interlock action decreases. The additional applied shear across the potential failure section formed by the diagonal crack and the intact concrete at the head of the crack is carried by the stirrups. At yield of the tension reinforcement aggregate interlock is lost and the shear carried by this mechanism is redistributed. After yield of both the tension steel and the stirrups all additional shear resistance is provided by dowel action and the intact concrete at the head of the crack. The dowel action is limited by the capacity of the stirrups on the low moment side of where the diagonal crack intersects the tension reinforcement.

The stirrup spacing in the beams is important. The possibility of a diagonal crack crossing fewer stirrups than required to provide adequate shear resistance, although the crack is at a flatter angle than 45^{o}, increases with increasing stirrup spacing. An example of this is provided by beam N3-S12,4. Although the beam did not fail in shear only one stirrup crossed the critical diagonal crack where, in fact, one and one quarter stirrups were required for the designed shear protection. The crack was inclined

at an angle of less than 45°. Closely spaced stirrups decrease the rate of propagation of diagonal cracks.

CHAPTER 8

A THEORETICAL STUDY OF STIFFNESS AND A COMPARISON WITH EXPERIMENTS

8.1 Introduction

Two theoretical models will now be developed. One is used to predict the tension reinforcement strain distribution along the test beams taking account of diagonal cracking and the forces acting across these cracks. The other is an extension of this to enable the total deflections of the beams to be calculated including the shear deflections resulting from diagonal cracking and consequent truss action. Observed and theoretical tension reinforcement strain distributions and beam deflections will be compared.

8.2 Tension Reinforcement Strain Distributions

The conventional elastic analysis of a cracked beam subjected to moment and axial tension is summarised in appendix C. The analysis is not applicable after diagonal cracking, except at the critical flexural region, because it does not consider the redistribution of forces in the portion of a beam containing diagonal cracks. The critical flexural region of a beam is not

crossed by diagonal cracks and hence the analysis is applicable at this particular section. It was considered necessary to develop a model which could be used to predict the tension reinforcement strains in the test beams once diagonal cracking has commenced.

8.2.1 The Model

After study of the crack patterns in nine of the ten beams tested, the general crack pattern shown in fig. 8.1 (a) is preposed. Beam N1-SO was excluded from consideration as it failed at its diagonal cracking load. The cracks that cross the tension reinforcement over the length l_1 radiate from the compression corner of the critical section AA'. Those that cross the tension steel over the length l_2 are all assumed to be parallel to the crack labelled B.

8.2.2 Forces Across the Diagonal Cracks

A typical section across a beam with all the known forces acting on it is sketched in fig. 8.1 (b). For the purposes of this analysis the beam is considered to be built in at section AA' rather than 1 inch below this section (see fig. 5.13). The internal forces at the section are:

(i) the compression force C, in the concrete and compression reinforcement

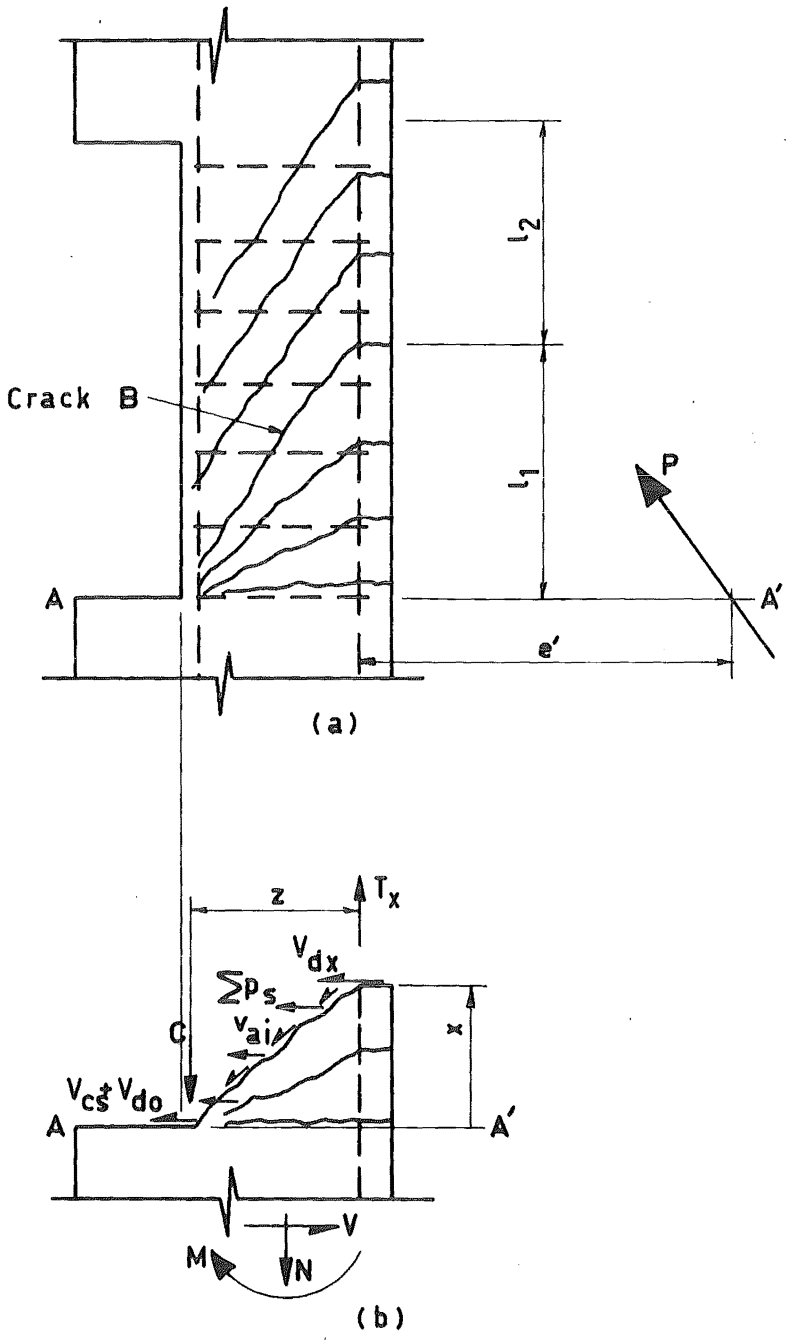

Fig. 8.1 Model Cracked Beam

(ii) shear transferred by the compression zone concrete V_{cs}, and compression reinforcement dowel action V_{do},

(iii) the tension reinforcement force T_x, at a distance x from section AA',

(iv) the dowel shear V_{dx}, of the tension reinforcement

(v) aggregate interlock forces v_{ai} across the diagonal crack,

(vi) stirrup force per unit length p_s, along the axis of the beam, and

(vii) dowel forces across the stirrups. These have been ignored as it is believed that they are negligible.

The line of action of the aggregate interlock forces is assumed to pass through the centre of the compression force at section AA'. For a crack that is approximately straight this is a close approximation to the actual conditions in the test beams.

The dowel shear of the tension reinforcement is assumed to vary linearly from zero a section AA' to a maximum V_d, at a distance l_1 along the tension steel, and from there on to remain constant. This is based on observed displacements across the cracks in the test beams (see fig. 4.12). The maximum is taken as a

given percentage η_d, of the total applied shear V.

$$V_{dx} = \frac{x}{l_1}\eta_d V \qquad (8.1)$$

where $V_{dx} \leqslant \eta_d V$.

The total shear taken by the stirrups across a potential separation section as shown in fig. 8.1 (b) is V_s, which is a proportion η_s of the total applied shear. V_s is assumed to be zero at the diagonal cracking shear V_{dc}, and to equal the additional applied shear after diagonal cracking.

$$V_s = V - V_{dc} \qquad (8.2)$$

This relationship is based on the stirrup shear applied shear relationships for the beams (see figs. 7.1 to 7.7). V_s is calculated across the last crack in span l_1 (see crack labelled B in fig. 8.1 (a)). Fig. 8.2 shows a schematic diagram of the shear carried by the various mechanisms across this crack at an applied shear V.

Discreet stirrup forces across the diagonal cracks are replaced by a continuous constant stirrup force per unit length p_s, given by:

$$p_s = \frac{V_s}{l_1} \qquad (8.3)$$

where $p_s \leqslant \frac{A_v f_y}{s}$ (8.4)

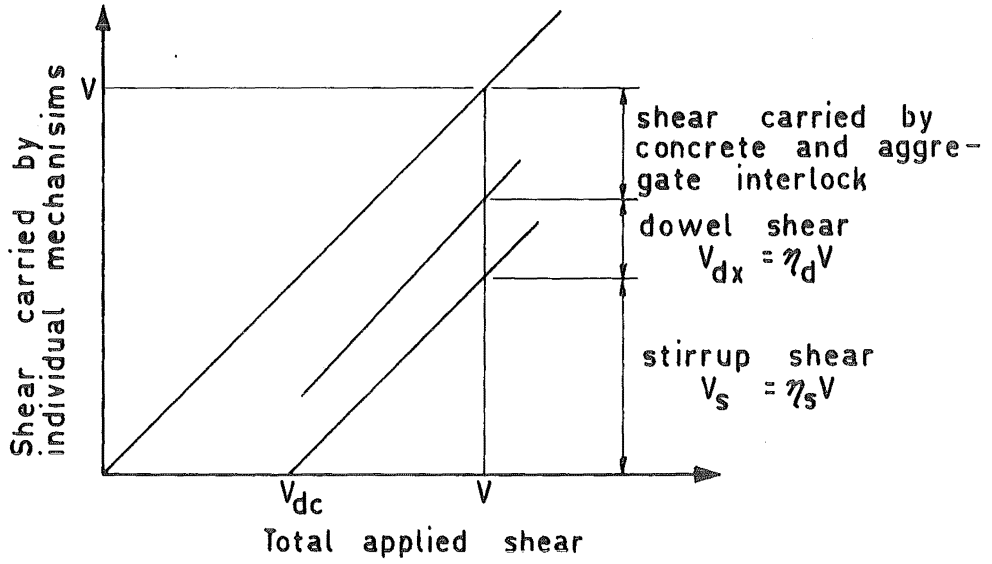

Fig. 8.2 Shear Carried by Individual Mechanisims Across the Critical Separation Diagonal Crack

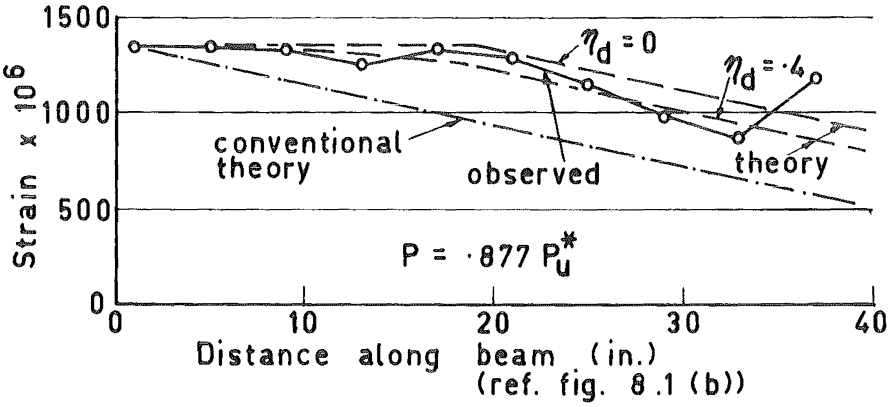

Fig. 8.3 Tension Reinforcement Strains in Beam N2-S0

The entire length of the stirrups are assumed to be uniformly stressed.

8.2.3 The Analysis

Referring to fig. 8.1 (b) and taking moments about the centre of the compression force at section AA':

$$N(e' + z) = T_x z + V_{dx} x + p_s x \frac{x}{2}$$

From Eqs. (8.1) (8.2) and (8.3) the tension force along the reinforcement is given by

$$T_x = N\left(\frac{e'}{z} + 1\right) - \left(\frac{x^2}{z l_1} V(\eta_d + \tfrac{1}{2}) - \frac{V_{dc}}{2}\right) \qquad (8.5)$$

From Eqs. (8.2), (8.3) and (8.4)

$$V \leqslant \frac{A_v f_y l_1}{s} + V_{dc} \qquad (8.6)$$

Eq. (8.5) is valid provided the applied shear does not produce yield stresses in the stirrups. If V is greater than the maximum value given by Eq. (8.6), V in Eq. (8.5) is replaced by the maximum value given by Eq. (8.6). The reason for this is that the last term in Eq. (8.5) represents the flexural resistance at a section provided by the stirrups and dowel action. Once the stirrups have yielded they can provide no additional contribution to the flexural resistance of the member.

With the aid of fig. 8.1 (a) the analysis may be extended. The forces across the diagonal crack marked

B are assumed to be the same as across all the other cracks parallel to it. Hence the moment about the centre of the compression force at a section formed by any one of these parallel cracks is resisted by the tension reinforcement where the crack crosses the reinforcement, and a constant moment produced by the stirrup forces and dowel shear. Therefore the tension steel strain distribution has the same slope as the applied bending moment diagram but is displaced along the beam because of the effect of diagonal cracking. The strain past the point where the crack marked B crosses the tension steel reduces at the same rate as the bending moment diagram.

8.2.4 Comparison With Test Results

For each of the beams tested the length l_1 (see fig. 8.1 (a)) was determined from observations of photographs of the beams at high load intensities. T_x derived from Eq. (8.5) is compared with measured values from selected beams in figs. 8.3 and 8.4. Steel strains have been plotted rather than forces. The derived strain distribution for two values of η_d are presented to indicate the variation caused by different proportions of total shear resisted by dowel action. The strain distributions over the lengths l_2 of the beams are also shown in the figures. The dashed lines are the tension

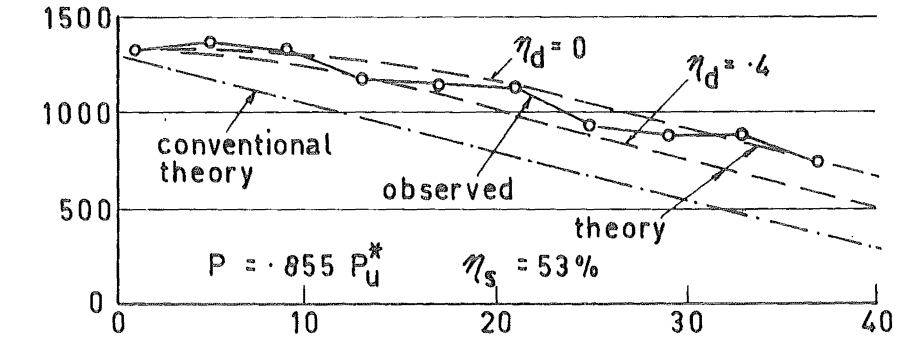

(a) Beam N1-S32

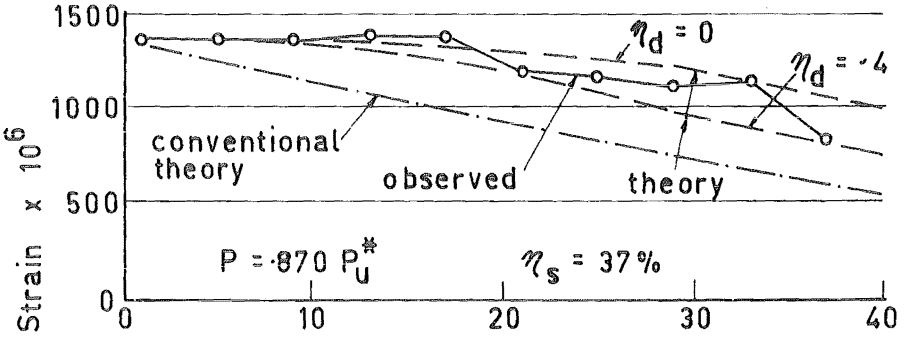

(b) Beam N2-S62

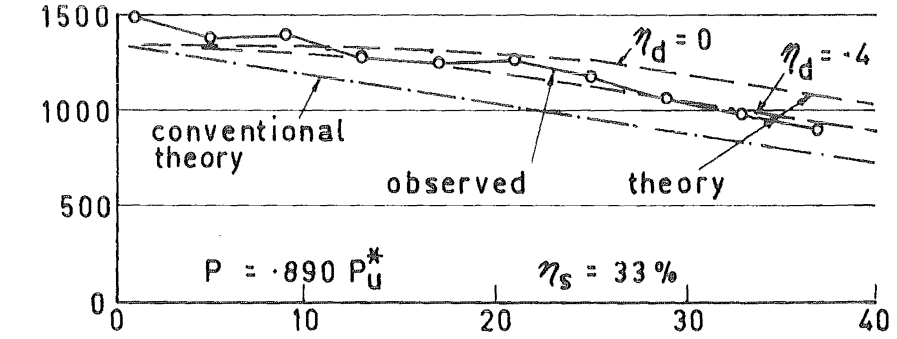

(c) Beam N3-S12,4

Fig. 8.4 Tension Reinforcement Strains in Selected Beams With Stirrups

reinforcement strains calculated on a conventional cracked elastic section.

The agreement between the strains calculated using the model presented in fig. 8.1 (a), and the observed values is good. The influence of dowel shear is seen to be relatively small when it is appreciated that the two theoretical distributions plotted in figs. 8.3 and 8.4 are for 0 and 40% of the total shear being resisted by dowel action.

8.3 Flexural Deflections of Beams

The tension reinforcement strains derived from analysis of the model beam shown in fig. 8.1 can be used to find flexural deflections of the test beams. Equivalent curvatures, as defined in chapter 4, can be found provided that either the compression reinforcement strains or the depths of the equivalent neutral axis is known. These equivalent curvatures may then be used to calculate the flexural deflections.

8.3.1 Equivalent Neutral Axis

In reinforced concrete beams the neutral axis or line of zero flexural stress is difficult to find because it varies in height depending on the presence of cracks. Once diagonal cracks have formed truss and arch action develop and consequently the

term neutral axis becomes meaningless. To find the flexural deflections of the test beams from the theoretically derived tension reinforcement strains use can be made of the equivalent neutral axis. This is found from analysis of the conventional cracked elastic section (see appendix C.)

8.3.2 Predicting Flexural Deflections

The equivalent curvature for each unit length of a beam is found from the relationship

$$\varphi_e = \frac{\varepsilon_s}{(1 - k)d} \qquad (8.7)$$

These were summed along the 40 inch test length of the beam, as described in chapter 3, to give the theoretical flexural deflection

$$\Delta_{flex} = \tfrac{1}{2} \sum_{r=1}^{40} \varphi_{e_r} + \sum_{r=2}^{40} (41 - r)\varphi_{e_{r-1}} \qquad (8.8)$$

8.4 Shear Deflection of Beams With Web Reinforcement

Once diagonal cracks have formed in a reinforced concrete beam with web reinforcement the stirrups form a truss mechanism to resist some of the applied shear. This truss mechanism consists of diagonal compression members formed by the concrete between adjacent diagonal cracks, and tension members consisting of the web reinforcement. The top and bottom chords of the truss are

the compression zone of the beam and the tension reinforcement respectively.

By calculating the deformations of the web members of the analogous truss the shear deflection of the diagonally cracked beams may be estimated. If there is arch action or any other mechanism of shear resistance in the beam it is only necessary to know the shear resisted by any one of these mechanisms to be able to find the total shear deflection of the beam. This follows from compatibility of all the mechanisms of shear resistance. The deflections calculated from each mechanism must be equal.

As the shear carried by the stirrups in the test beams is known the theoretical shear deflections are to be found from the analogous truss.

8.4.1 The Analogous Truss

The analogous truss is shown in fig. 8.5 (a). It has been derived from the model crack pattern shown in fig. 8.1 (a). In the idealised truss there are several (three) paths by which the shear applied at C can be transferred to A. No matter which way the shear is divided between the various paths the deflections at C calculated from each path must be equal.

Therefore the method of calculating the truss deflection is a trial and error type of solution.

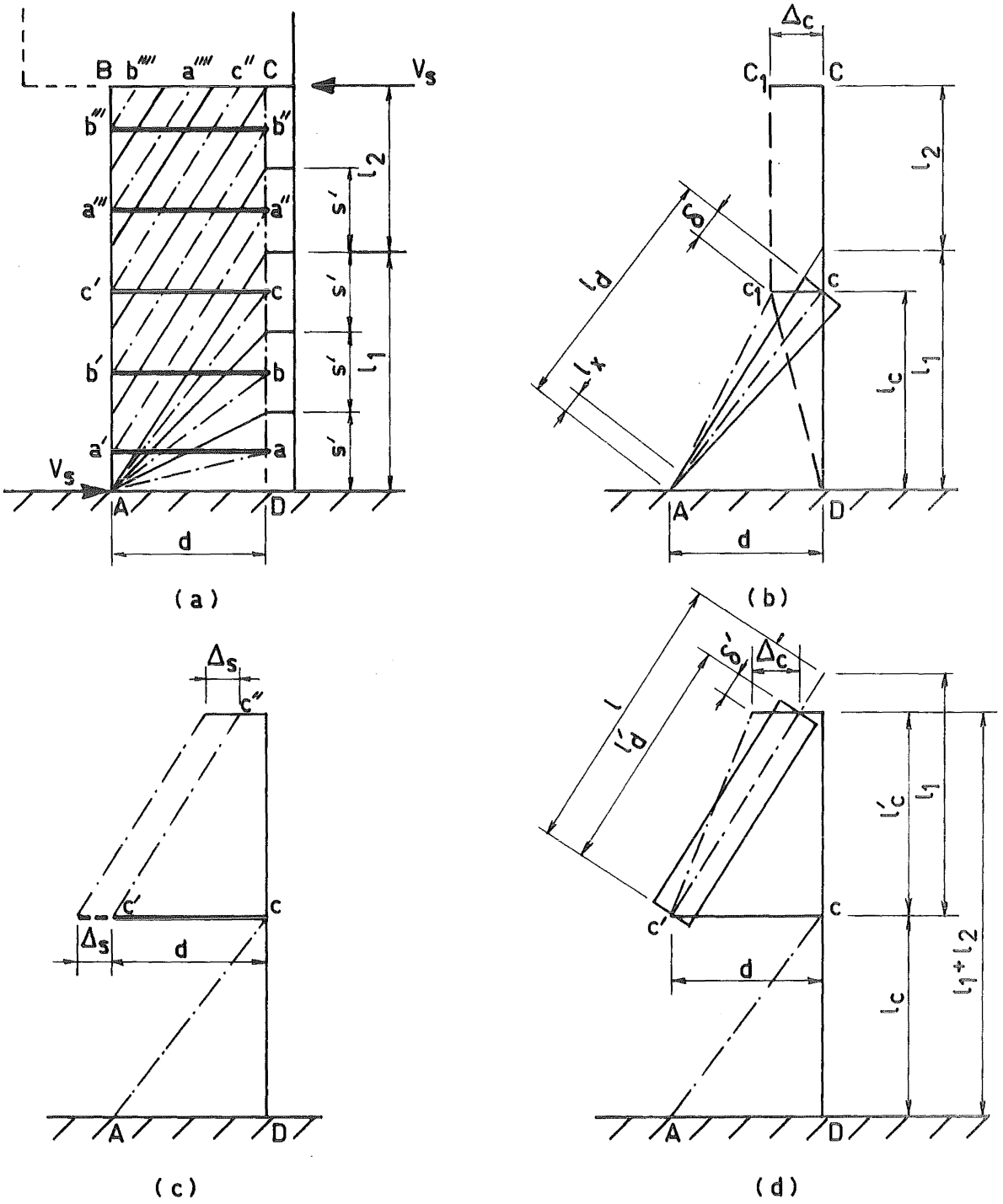

Fig. 8.5 The Analogous Truss

Arbitrary shears are assigned to each path through the truss so that the sum of these shears equals the total applied shear. The deflections of the truss at C are then calculated for each path and compared. Adjustments are made to the arbitrarily chosen shears so that the truss deflections from each path are equal.

Further assumptions made to enable the truss mechanism to be solved are:

(i) The stirrups are uniformly stressed over their entire length.

(ii) There is no shear transfer between the compression struts by aggregate interlock or dowel action.

(iii) The crack spacing at the level of the tension reinforcement is uniform.

In the analogous truss shown in fig. 8.5 (a) there are three paths by which the shear applied at C is transferred to A. These are denoted by Aa..a"", Ab..b"" and Ac..c". The crack spacing s' is given by

$$s' = l_1/3 \qquad (8.9)$$

The stirrups in the test beams can be replaced by equivalent stirrups spaced at s'. The cross sectional area of each being

$$A_{ev} = A_v \frac{s'}{s} \qquad (8.10)$$

Depending on the relative lengths of l_1 and l_2, and on s', one or two stirrups may be required along the paths through the truss.

The condition imposed by Eq. (8.9) merely effects the accuracy of the results. If more struts are taken radiating from A little refinement of the results is obtained and this refinement is not warranted because of other assumptions made. Three struts were originally chosen because this was the most representative number of struts observed in the test beams.

8.4.1.1 Deformation of Individual Members

Deflection of the whole truss is the sum of deformations of three types of members. A representative example of each is Ac, cc' and c'c".

The tapered concrete strut Ac is shown in fig. 8.5 (b). Let the proportion of the shear carried by the path Acc'c" be V_{sc}. The component along the tapered strut centre line is

$$P = \frac{l_d}{d} V_{sc}$$

It can be shown that the shortening of this concrete strut over the length from l_x to l_d under the applied load P is

$$\delta_c = \frac{P l_d^2}{E_c s' d b} \log\left(\frac{l_d}{l_x}\right) \qquad (8.11)$$

The cross sectional area of the strut at c is:

$$\frac{s'db}{l_d}$$

From Eqs.(8.9) and (8.11) and putting P in terms of V_{sc}, the transverse deflection at C is:

$$\Delta_c = \frac{3l_d^4 V_{sc}}{E_c l_1 bd^3} \log\left(\frac{l_d}{l_x}\right) \qquad (8.12)$$

The deflection at C attributed to stirrup extension, shown in fig. 8.5 (c), is given by:

$$\Delta_s = \frac{V_{sc} d}{E_s A_{ev}}$$

and from Eq. (8.10)

$$\Delta_s = \frac{3V_{sc} sd}{E_s A_v l_1} \qquad (8.13)$$

If the extension of two stirrups is involved the deflection would be double that given by Eq. (8.13), i.e., if $l_c < l_2$

$$\Delta_s = \frac{6V_{sc} sd}{E_s A_v l_1} \qquad (8.14)$$

The deformation of the truss mechanism from the contribution of the concrete strut c'c" is shown in fig. 8.5 (d). The component of load along the strut centre line is

$$P' = \frac{l}{d} V_{sc}$$

where $l = \sqrt{l_1^2 + d^2}$

The cross sectional area is

$$\frac{s'db}{l}$$

The length of the strut is given by

$$l'_d = l'_c \frac{l}{l_1} \tag{8.15}$$

where $$l'_c = (l_1 + l_2) - l_c \tag{8.16}$$

The shortening of the strut is

$$\delta'_c = \frac{P'l'_d l}{E_c s'db}$$

The deflection due to the shortening of the strut after substitution for P', l'_d and s', is given by

$$\Delta'_c = \frac{3V_{sc} l^4 l'_c}{E_c l_1^2 bd^3} \tag{8.17}$$

The total deflection of the truss mechanism Acc'c" is found from Eqs. (8.12), (8.13) or (8.14), and (8.17) thus

$$\Delta = \Delta_c + \Delta_s + \Delta'_c \tag{8.18}$$

To find Δ_c from Eq. (8.12) the value of l_x (see fig. 8.5 (b)) must be known. It cannot be equal to zero. From study of the photographs of the beams when diagonal cracking was well developed a representative value of 1 inch was taken for l_x, i.e., there was negligible diagonal compression within a 1 inch radius of the reentry corner A. This can be justified by the assumpt-

ion that the compression in the concrete struts converging at A is carried to the end block of the beam by the compression reinforcement and surrounding compression zone concrete. This would be stiff enough to support the diagonal compression from the struts.

8.4.2 Comparison of Calculated and Derived Stirrup Extensions

Observed stirrup extension over 12 inches of the stirrups in beam N1-S63 at .858 P_u^* are shown in fig. 8.6. Also shown are the calculated extensions in the equivalent stirrups derived from the theory discussed in section 8.4.1. The load used was 90% of theoretical yield load which is approximately equal to .858 P_u^*. As can be seen in the figure the agreement is only fair. This is attributed to the assumption of the proportion of shear taken by the stirrups after diagonal cracking (see Eq. (8.2) and compare with figs. 7.1 to 7.7 parts (b)). However, the general shapes of the two distributions are not too different except for the sharp rise obtained from theory at the right hand end of the diagram. The small observed stirrup extension in this region is due to the diagonal cracks having not propagated right to the critical section of the beam.

Included in fig. 8.6 is the beam expansion over 89% of the total depth. The difference between the

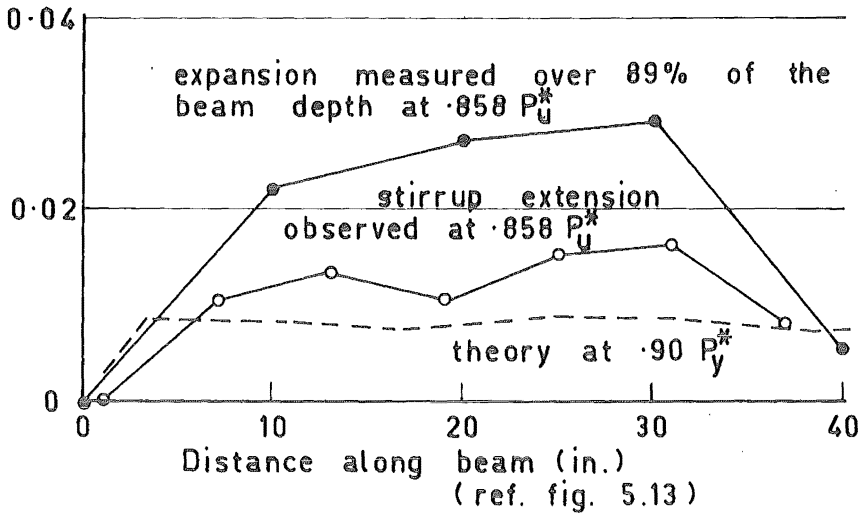

Fig. 8.6 Theoretical and Observed Stirrup Extension in Beam N1–S63

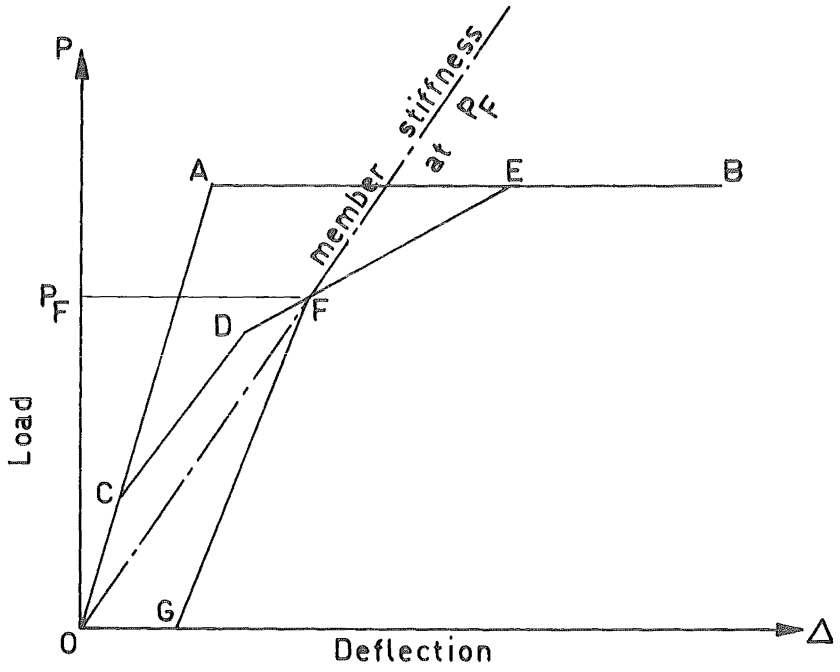

Fig. 8.7 Idealised Load – Deflection Relationship of Reinforced Concrete Members

expansions measured on the stirrups and the total expansion is attributed to stirrup anchorage slip. This is discussed in section 8.7.4.

8.5 Member Stiffness

Before the member stiffness of a beam as it is used in this chapter is defined it is convenient to consider linear elastic behaviour. A series of idealised load deflection curves are shown in fig. 8.7. Line OAB is a bilinear relationship. The branch OA of the curve represents linear elastic behaviour. If the load is taken up to point A and then reduced to zero the beam deflection would follow the same path back to O.

The idealised load deflection curve for a reinforced concrete member is the curve OCDEB. The four straight portions represent:

(i) no cracking, OC

(ii) flexural cracking, CD

(iii) diagonal cracking, DE and

(iv) yield of the longitudinal reinforcement, EB.

If the load is reduced to zero from a point such as F the load deflection curve follows the line FG to zero load. The deflection OG is referred to as permanent set. This is caused by irreversible elastic deformation in the concrete, anchorage slip in longitudinal steel and web reinforcement, and cracks not closing.

If the load is increased again from the point G the load deflection curve follows the path GFEB. It should be noted that this discussion is very artificial.

The term "member stiffness" as it is used in this chapter is defined as; the oblique load required to produce unit deflection at the assumed free end of the 40 inch long cantilever if the load deflection relationship is assumed linear and passes through the origin. The member stiffness at load P_F is the slope of the linear load deflection relationship OF.

The definition does not take the permanent set OG into account as this is not known at any particular load.

8.5.1 Types of Member Stiffness

In the deflection of beams subjected to flexure and shear there are two types of member stiffnesses involved. These are:

(i) Flexural member stiffness. This refers to deflections resulting from flexural stresses only. These stresses give rise to curvatures which when summed along a finite length of beam produce a deflection of one end with respect to the tangent at the other end of the beam length.

(ii) Shear member stiffness arising from shear deformations in the web of a member. Shear deflections do not result from rotations but rather from relative length changes in web members.

The total member stiffness of a beam is not the sum of two stiffnesses, but rather the reciprocal of the sum of the reciprocals of the flexural and shear stiffnesses.

8.6 Theoretical Beam Deflections

The theoretical deflections of the test beams are calculated at the following three stages of crack development:

(i) uncracked

(ii) flexurally cracked

(iii) diagonally cracked

It should be noted that there is no clear demarcation between flexural and diagonal cracking in the shear span of a reinforced concrete beam. For the purposes of this discussion, however, flexural cracks are assumed to propagate normal to the longitudinal axis of the beam, i.e., they do not influence the stresses at any other section than the one which contains the flexural crack. On the other hand diagonal cracks do influence the stresses over a significant length of the beam as shown in section 8.2.

8.6.1 The Uncracked Beam

When finding the theoretical deflection of the uncracked beams both flexural and shear deformations were considered. For the flexural deformations the following assumptions were made:

(i) Plane sections before bending remained plane after bending.

(ii) The modulus of elasticity of the reinforcement was 29×10^6 lb/in^2.

(iii) The modulus of elasticity of the concrete was the 50% secant modulus measured on a 6" x 12" cylinder.

(iv) The effective moment of inertia was that of the transformed concrete section.

The assumptions made to find the shear deformation of the test beams were:

(i) The built in end of the cantilever was free to deform.

(ii) Poissons ratio of concrete is 0.18.

(iii) The effect of the reinforcement on the shear stress distribution was ignored.

8.6.2 The Flexurally Cracked Beam

Only theoretical flexural deflections were found for beams with flexural cracks. Two assumptions used in the calculation of the flexural

deflections were:

(i) Plane sections before bending remain plane after bending.

(ii) The concrete does not sustain tensile stresses caused by bending.

The first assumption ignores the effect of diagonal cracking. The second assumption enables the curvatures of the sections to be calculated directly from the tension reinforcement strains and the neutral axis heights found from the conventional elastic analysis summarised in appendix C. These curvatures are summed by the method discussed in chapter 3 to give the flexural deflections of the flexurally cracked beams. It should be noted that the beams were cracked over their entire lengths.

Several methods of calculating flexural deflections in reinforced beams have been proposed [4]. One of these due to Yu and Winter [50] involves using a modified second moment of area given by

$$I_{eff} = \frac{I_{cr}}{\left(1 - b\frac{M_1}{M_{max}}\right)} \qquad (8.19)$$

where I_{cr} = second moment of area of the cracked transformed section at the maximum moment section

$M_1 = 0.1(f'_c)^{\frac{2}{3}}t(t - kd)$

k being found at the section of maximum moment

M_{max} = maximum moment in the beam under working load.

From Eq. (8.19) it is apparent that the beam deflection calculated using I_{eff} is less than it would be if I_{cr} is used. Because of the effect of the eccentricity of the axial load in the test beams the effective second moment of area decreases away from the section of maximum moment. Thus the test beams deflect more than if the deflection was calculated using I_{cr}. It will be shown in section 8.7.2 that the flexural deflections of the test beams were even greater than calculated using the second moment of area of the cracked beam at each section as discussed at the beginning of this section. Therefore I_{eff} given by Eq. (8.19), and similar such relationships [4], is not suitable for beams subjected to axial tension as well as flexure.

8.6.3 Diagonally Cracked Beam

The deflections of the diagonally cracked beams are calculated from the theory developed in sections 8.3 and 8.4. From Eqs. (8.8) and (8.18) the total theoretical deflection from flexure and shear deformations can be found for the test beams with web reinforcement.

8.7 Comparison of Theoretical and Observed Deflections

8.7.1 The Uncracked Beams

Deflection measurements were made on only three beams at sufficiently low load intensities to enable the deflections of the uncracked beams to be observed. These load deflection relationships have been plotted in figs. 5.19 (b), 5.40 (b) and 5.56 (b). From the three figures it can be seen that at very low load intensities the beams were less stiff than theoretically predicted. As was discussed in chapter 3 shrinkage cracking is the cause of this.

8.7.2 Flexural Deflections of Flexurally and Diagonally Cracked Beams

The observed flexural deflections of the test beams have been found from equivalent curvatures derived from measured longitudinal reinforcement strains. These are shown by the dashed lines in the respective load deflection relationships shown in chapters 4 and 5. Also shown are the theoretical deflections of the flexurally cracked beams. The agreement for all the beams is seen to be very good even when the beams are close to yield. The theoretical flexural deflections are always less than those observed in the tests because of the influence

of diagonal cracking on the strains in the tension reinforcement.

Fig. 8.8 gives the observed and conventional theoretical flexural member stiffnesses of the beams with web reinforcement at 90% of their theoretical yield loads. Also shown are the theoretical flexural member stiffnesses based on the diagonally cracked model beam at the same load intensity. Fair agreement is obtained between the observed and the theoretical flexural member stiffnesses of the diagonally cracked beams. The discrepancies are due to the assumed equivalent neutral axis in the model beam after diagonal cracking. The observed equivalent curvatures in the low moment end of the cantilevers were smaller than those theoretically derived.

The observed flexural member stiffnesses are seen to vary between 56% and 68% of the member stiffness of the corresponding uncracked beam.

8.7.3 Total Member Stiffness of Diagonally Cracked Beams

The theoretical member stiffnesses of all but one of the diagonally cracked beams with web reinforcement were calculated at 90% of their theoretical yield loads. These member stiffnesses, along with the observed member stiffnesses at the corresponding load

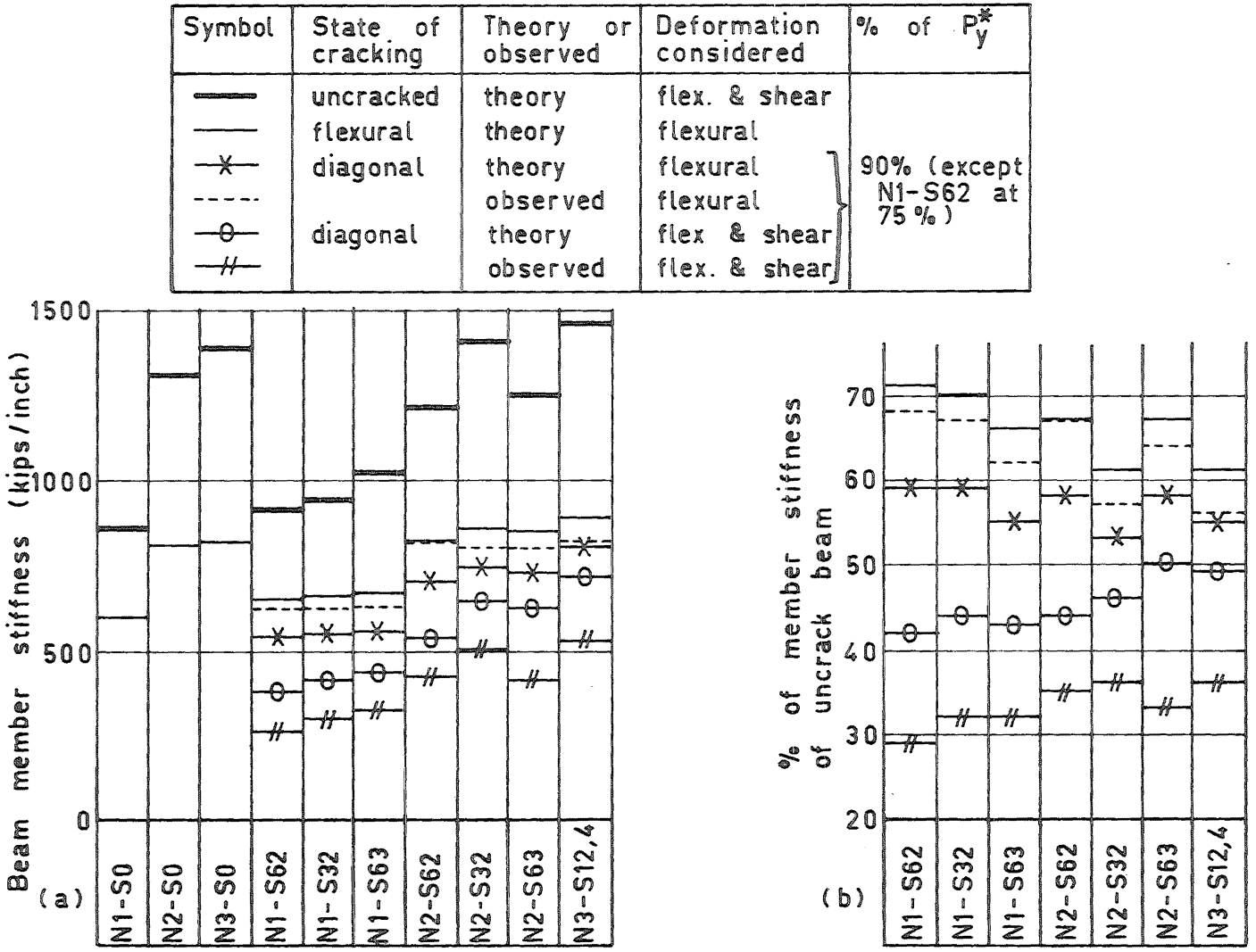

Fig. 8.8 Comparison of Member Stiffnesses of the Test Beams

intensity are presented in fig. 8.8. It can be seen that the agreement between theory and experiment is not very good. In all cases the measured member stiffnesses being less than those predicted by the theory developed in this chapter. The reason for this is believed to be slip at the anchorage of the stirrups. This will be discussed in the next section.

The observed member stiffnesses of all the beams with web reinforcement lie between 29 and 36% of that of the corresponding uncracked beam. Near yield approximately half of the total deflection is due to shear deformation in the webs of the beams.

Conventional deflection theories [4] for reinforced concrete flexural members do not take account of shear deformations. As the span to depth ratio in a beam becomes smaller the discrepancy between these theories and observation becomes more pronounced. This is because shear deflections vary approximately linearly with span whereas flexural deflections vary with the cube of the span.

8.7.4 Slip of Stirrups

Mayer [36] in 1967 qualitatively discussed the slip of stirrup hooks and the resulting transverse expansion. He proposed that the stiffness of the reinforcing cage in a beam depends on the bond properties

of the stirrups used.

A quantitative assessment of the anchorage slip in reinforcement bars is in progress at the Technische Hochschule Munchen, Germany [7]. Tests carried out by H. H. Muller were designed to investigate useable anchorages associated with tolerable slip in reinforcement, rather than anchorages to develop the ultimate strength of the bars. Tolerable slip at service load is a design criterion of anchorage because of the crack widths associated with the slip. In this project slip of 0.3 mm was considered the maximum acceptable. This gives a crack width of approximately 0.01 inches.

The tests included the position of the bars and anchorage hooks with respect to the direction of placement of the concrete. The observations made included the load deflection relationship of the anchorage. Fig. 8.9 (a) shows a typical test set up and part (b) shows a typical load deflection relationship for a test.

The relationship between stress and concrete cube strength for a slip of .1 mm for 180 degree hooks was approximated by:

$$f_s = k_s f_{cu} \qquad (8.20)$$

The values of the constant k_s are summarised in table 8.1. These values include 95% of the experimental results.

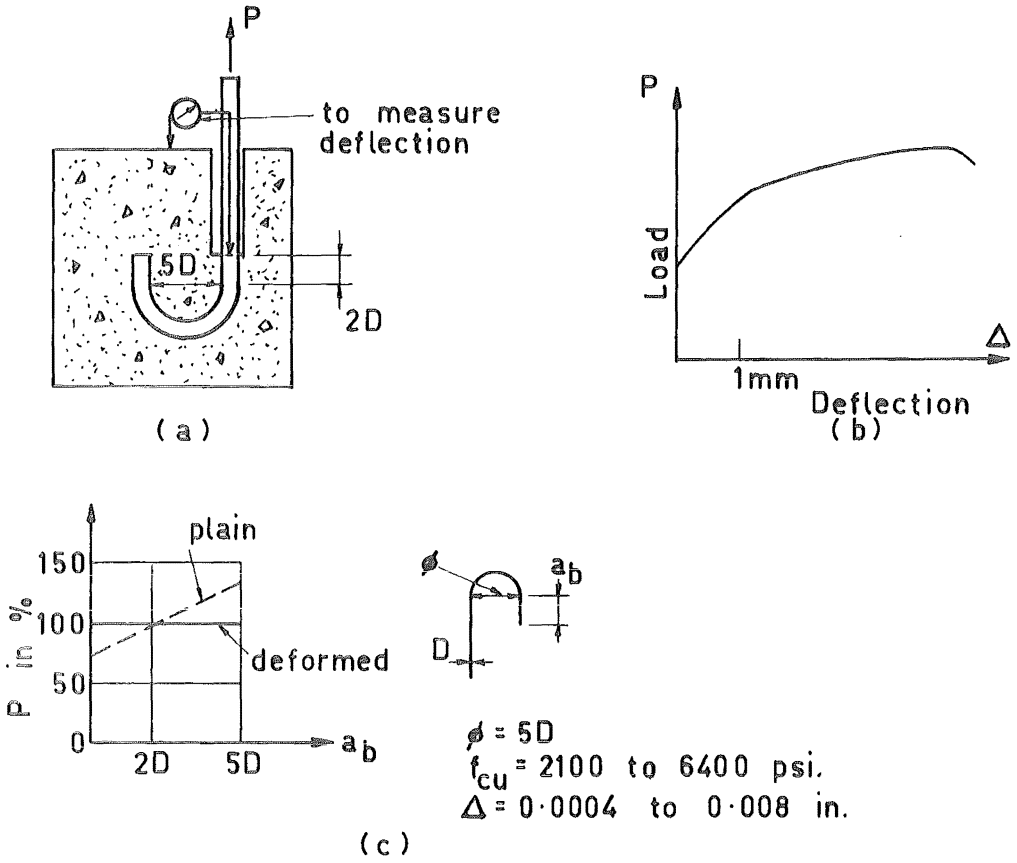

Fig. 8.9 Anchorage Slip (Müller [7])

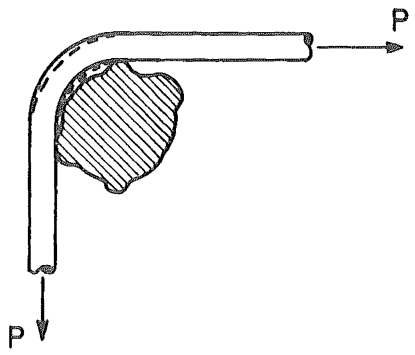

Fig. 8.10 Slip Around a Deformed Bar

Table 8.1 Values of k_s

		Plain	Deformed
Bottom hooks	J ⊂	1.70	3.75
Top hooks	⅂ ⊂	1.20	2.00

It has also been shown in the tests that the bond length of a deformed bar past the hook has little influence on the stirrup anchorage slip. A diagram showing this is reproduced in fig. 8.9 (c). The influence of bond length on plain bars has some effect but the increase in load seems likely to decrease as the bond length increases past the 5D shown.

From these tests of Muller's the following points with reference to the beams tested in this project are relevant.

The contact between the longitudinal reinforcement and the stirrups could not be guaranteed because the stirrups were tied rather than spot welded. Any concrete between the stirrups and longitudinal steel would be very weak indeed and hence the resistance to bearing and slip would be reduced (see the values of k_s for top compared to bottom bars).

Even if there was direct contact of the main reinforcement with the stirrups the position of the ribs of the main steel would be important. Fig. 8.10 shows a typical anchorage of a stirrup around a deformed

bar. It can be seen that when the stirrup is stressed it tends to straighten as shown by the broken lines. Some additional slip could result from this especially with the weak cement paste which is likely to accumulate between the two bars.

From fig. 8.9 (c) it can be concluded that the slip associated with stirrups in the form of closed hoops as in the test beams, is little different from that of stirrups hooked around the longitudinal reinforcement. The entire slip of deformed stirrups and much of that of plain stirrups is governed by the portion of the stirrup in the bend around the longitudinal steel.

8.7.4.1 Beam Deflection Associated With Stirrup Slip

A quantitative assessment of the slip at stirrup anchorage in the test beams was attempted from the data shown in fig. 8.9 (b) and from Eq. (8.20). It was found that the theoretical stirrup stresses were all well in excess of those given by Eq. (8.20) for a slip of 0.1 mm. Some of the stirrups were near yield and all were stressed to approximately twice the value of f_s from Eq. (8.20). It was considered that a slip of 0.3 mm. at each end of a stirrup was more likely to be of the correct order. If two stirrups are included in calculating the deflection of the analogues truss

(see fig. 8.5) the deflection owing to slip of these stirrups is 0.047 inches. If only one stirrup is included in the particular path through the truss the deflection is half of this. However the proportion of the shear attracted to this path would be increased. The modifications to the member stiffnesses of the beams with web reinforcement taking stirrup slip into account are summarised in table 8.2. These stiffnesses have been calculated assuming a total slip along every path through the analogues truss of 0.047 inches. Consideration of the few paths which include only one stirrup is not warranted because of the approximations already made.

It can be seen from table 8.2 that a slip of 0.3 mm can account for the low observed member stiffnesses compared with those theoretically derived. To find the shear deflections of the test beams more accurately it would be necessary to know the load slip relationship for the stirrups. The determination of this was not attempted in this project.

8.8 The Effect of Axial Tension On Beam Member Stiffness

8.8.1 Flexural Deflections

It has been shown that the flexural deflection of a beam subjected to axial tension as well as bending can be adequately calculated by summing the curvatures obtained from the elastic analysis described in appendix C. The axial tension applied at the geometric centre of the beam modifies the strain profile of a section by increasing the tension reinforcement strain and decreasing the depth of the compression zone. The effects of these two responses have opposite influence on the curvature at a section. The increased curvature caused by increased tension reinforcement strain predominates. For the beams tested the flexural deflection owing to the axial load at a constant eccentricity of d/2 would be approximately 25% of the total flexural deflection. For a constant eccentricity of 2d the deflection owing to the axial tension would be approximately 10% of the total flexural deflection.

8.8.2 Shear Deformations

The shear deformations are not directly influenced by the axial tension applied to the beams. In the theoretical analysis of the shear deflections it can be seen that the stirrup stresses and the stresses in the compression struts depend on the shear carried by the stirrups only. Except for the possible slight

increase of shear carried by the stirrups as a result of a slightly lower diagonal cracking load in beams subjected to axial tension, the axial tension has no influence on the shear deformations of the beam.

Table 8.2 Deflections Associated With Stirrup Slip

(1)	Observed member stiffness K_{test} Kips/inch	Theory-no slip		Theory-slip=.3mm	
		Member stiffness K_o Kips/inch	$\frac{K_{test}}{K_o}$	Member stiffness $K_{.3mm}$ Kips/inch	$\frac{K_{test}}{K_{.3mm}}$
N1-S62	262	386	0.68	280	0.94
N1-S32	304	413	0.74	306	0.99
N1-S63	327	435	0.75	318	1.03
N2-S62	422	543	0.78	402	1.05
N2-S32	503	645	0.78	454	1.11
N2-S63	413	625	0.66	446	0.93
N3-S12,4	523	719	0.73	502	1.04

(1) All beams at 90% P_y^* except N1-S62 at 75% P_y^*

CHAPTER 9

CONCLUSIONS AND RECOMMENDATIONS FOR FUTURE RESEARCH

9.1 Conclusions

From the investigation of the behaviour of reinforced concrete members subjected to shear, flexure and axial tension the following conclusions have been drawn.

9.1.1 Method of Testing

The loading frame used for the beam tests reproduced the likely conditions of stress in columns of single curvature subjected to axial tension. In two of the beams tested without web reinforcement arch action was able to develop because of the way in which the transverse loads were applied to the beams. It is believed that the axial tension was applied to the test lengths of the beams at a sufficient distance to ensure that St. Venant's principle was satisfied.

The accuracy of the demec gauges used was adequate. The method of finding the beam deflections gave consistent results throughout the tests although it was based on an assumption known not to be accurate.

9.1.2 Cracking

It was found that the crack patterns of the beams tested in this project were similar to those in the shear span of members not subjected to axial load and of similar a/d ratio. Separation did not occur along diagonal cracks at an inclination to the beam axis of greater than 45^{o}. Such cracks did develop but only under the load point as in normal flexural members.

The shear at diagonal cracking was found to be independent of the axial tension to shear force ratio of the applied load, and to show no appreciable variation from the diagonal cracking shear of similar beams without axial tension.

9.1.3 Flexural Behaviour

Prior to diagonal cracking the conventional elastic theory describes beam flexural behaviour satisfactorily. Once diagonal cracking has been initiated allowance for the redistribution of internal forces must be taken into account.

Ultimate flexural capacity can be accurately determined if account is taken of possible strain hardening of the tension reinforcement and spalling of the unbound compression zone concrete. Concrete strength had relatively little influence on the ultimate flexural capacity of the test beams. Shear and diagonal

cracking does not substantially reduce the ultimate flexural strength of members subjected to axial tension.

9.1.4 Shear Resistance

The current ACI Code recommendations for provision against shear failure in members subjected to axial tension is adequate and has been found to be conservative for a number of the beams tested. This conclusion does not apply to members in double curvature where it is thought that the ACI recommendations may not be adequate. It has been found that

(i) Stirrup spacing had little influence on the shear resistance of the test beams provided more than one stirrup crossed the critical potential separation crack. In beam N3-S12,4 the shear resistance designed to be provided by stirrups across the critical diagonal crack was not obtained because the stirrup spacing was too large, viz., (4/5)d.

(ii) Dowel action is an effective means of resisting shear both before and after yield of the tension reinforcement provided that the dowel is supported by stirrups.

9.1.5 Deflection Characteristics of Flexural Members Subjected to Axial Tension

(i) The flexural member stiffnesses of the test beams in the elastic range were not significantly influenced by concrete strength or diagonal cracking. The flexural stiffnesses were approximately constant throughout the elastic range of loading and were of the order of 60% of the theoretical stiffness of the uncracked beams. Axial tension decreases the flexural stiffness and hence current methods [4, 50] of calculating flexural deflections in normal reinforced concrete beams do not apply to beams subjected to significant axial tension. Flexural deflections can be conveniently calculated from curvatures derived from the conventional elastic analysis.

(ii) Shear deflections prior to diagonal cracking were small but once diagonal cracking was initiated the shear deflections in beams with stirrups increased approximately linearly with the additional applied shear after diagonal cracking. Without knowledge of stirrup anchorage

slip-load relationships it was found impossible to predict shear deflections adequately from analysis of the analogous truss. At 90% of the yield load the member stiffnesses of the test beams were approximately $\frac{1}{3}$ of the theoretical member stiffness of the corresponding uncracked beams.

(iii) The region of plastic deformation in the test beams extended a distance of between d and 2d along the tension reinforcement from the section of maximum moment. The member ductility can be large provided a separation failure is prevented by sufficient web reinforcement, and buckling in the compression reinforcement is suppressed. Cantilever deflections of up to 20 times the deflection at yield were obtained in the test beams.

9.1.6 Failure

It was reaffirmed that shear failure is sudden when no web reinforcement is present. All the beams tested which contained web reinforcement gave warning of imminent failure in the form of opening of diagonal and/or flexural cracks.

9.2 Suggestions for Future Research

During the course of this project some topics related to the topic being studied were found to require further investigation. These are listed below.

(i) The stirrup anchorage slip-load relationship for various stirrup sizes, surface properties and types of anchorage.

(ii) The shear resistance at the point of contra-flexure in columns in double curvature subjected to axial tension.

(iii) The dowel shear resistance of more than one layer of reinforcement supported by stirrups, and the effect of axial forces in the dowel.

(iv) Detailed study of the kink effect.

(v) The behaviour of members subjected to cycles of applied shear and axial tension followed by shear of the opposite sense and axial compression, as would be encountered during seismic loading. Two points of interest are; the degradation of stiffness as a result of repeated cycles of such loading, and any possible reduction in the ability of the web reinforcement to carry the applied shear. Further considerations should include the modes of failure of the members, and the participation of

dowel action and aggregate interlock action in shear resistance after the concrete is heavily cracked.

APPENDIX A

DOWEL TEST LOAD SEQUENCE TABLES

Table A.1 Load Sequence for Dowel Test Specimens.

Increment	Maximum Dowel Shear lbs.	Time When Load Applied	Shear at Start of Reading Gauges lbs.	Time at Start of Reading Gauges	Shear at End of Reading Gauges lbs.	Time at End of Reading Gauges
a	b	c(2)	d	e(2)	f	g(2)
			Specimen 77-21			
1	157	0	139	3	113	7
2	319	9	315	10	284	15
3	526	16	477	17	455	23
4	697	23	643	25	626	30
5	904	31	850	33	833	38
6	1152	39	1066	42	1053	47
7	1314	49	1219	52	1206	57
8	1485	59	1417	63	1404	68
9	1759	68	1651	72	1634	77
10	2065	78	1903	82	1886	88
11	2515	107	2407	110	2381	115
12	3109	116	2970	119	2939	125
13	3658	125	3505	129	3470	135
14	3946	136	3676	140	3641	145
15	4126	145	3762	150	3731	155
16	4252	156	3955	162	3920	167
			Specimen 77-22			
1	175	0	175	0	153	6
2	337	8	315	11	302	15
3	499	17	472	19	450	24
4	652	27	616	30	590	35
5	823	36	760	40	743	46
6	1035	47	981	52	959	57
7	1291	58	1219	65	1197	71
8	1579	72	1498	75	1467	81
9	1930	101	1849	104	1823	110
10	2349	111	2236	114	2205	120
11	2812	121	2637	125	2606	131
12	2925	134	2758	136	2723	142
13	3145	143	2961	147	2930	153
14	3289	154	3064	157	3038	162
			Specimen 77-23 (1)			
1	194	0	194	3	185	10
2	396	11	396	14	387	21
3	599	22	599	26	590	33
4	801	34	801	40	781	46
5	1004	47	1004	53	988	59
6	1206	76	1206	80	1193	87
7	1409	88	1409	92	1391	98
8	1611	99	1611	103	1593	109
9	1814	110	1814	111	1790	117
10	1868	118	1868	123	1846	129
			Specimen 77-23 (ii)			
1	175	0	166	2	144	9
2	355	11	337	14	311	21
3	549	22	481	30	473	36
4	760	38	711	44	684	50
5	1003	52	855	78	846	84
6	1215	87	1143	93	1130	100
7	1435	102	1363	104	1341	111
8	1678	112	1597	117	1580	123
9	1903	124	1795	129	1791	135
			Specimen 77-24 (1)			
1	194	0	194	2	194	11
2	396	12	396	15	396	23
3	599	24	599	27	599	33
4	801	34	801	38	786	43
			(Sudden formation of crack)			
5	1004	65	1004	69	986	75
6	1206	76	1206	80	1182	86
7	1292	87	1292	90	1272	97
			Specimen 77-25			
1	162	0	139	5	117	11
2	346	12	310	16	257	21
3	535	22	472	25	441	31
4	724	32	666	36	639	42
5	814	43				
			(Sudden formation of crack)			
			504	57	504	63
6	526	63	481	70	464	77
7	643	79	598	84	594	90
8	760	115	720	118	707	122
9	904	125	832	127	815	133
10	985	134	940	136	923	142
11	1084	142	1030	145	1008	151
12	1147	152	1084	154	1067	160
13	1192					
			Specimen 77-26 (1)			
1	194	0	194	1	190	8
2	396	9	396	11	390	17
3	599	18	599	19	590	25
4	801	26	801	31	790	36
5	940	37				
			(Sudden formation of crack)			
			131	43	129	49
6	198	50	198	54	192	59
			Specimen 79-21			
1	265	0	247	2	162	8
2	535	9	499	13	468	19
3	801	22	796	25	725	32
4	1098	34	1012	39	977	44
5	1561	47	1453	51	1431	57
6	2038	57	1921	61	1895	69
7	2556	69	2425	71	2399	78
8	3069	79	2898	105	2885	110
9	3537	112	3379	118	3362	124
10	4045	127	3739	130	3704	137
11	4198	139	3726	146	3713	152

Table A.1 (cont.)

a	b	c	d	e	f	g
			Specimen 79-22			
1	162	0	157	1	122	7
2	355	7	319	9	293	14
3	553	15	522	22	509	28
4	747	29	706	31	680	37
5	931	38	873	44	864	50
6	1228	51	1125	60	1116	66
7	1521	67	1444	71	1422	77
8	1822	77	1723	82	1715	88
9	2092	108	2002	111	1976	116
10	2389	117	2286	119	2259	125
11	2664	126	2533	129	2516	134
12	2983	135	2862	138	2831	143
13	3289	144	3127	148	3101	153
14	3469	154	3253	162	3231	168
15	3564	169	3316	174	3299	180
			Specimen 79-23			
1	220	0	202	3	131	9
2	445	9	409	21	378	29
3	724	31	670	35	648	41
4	931	42	850	44	837	49
5	1147	51	1066	55	1049	62
6	1597	63	1489	70	1467	77
7	1984	79	1858	91	1850	98
8	2407	99	2245	125	2241	131
9	2826	131	2592	136	2570	142
			Specimen 79-24			
1	157	0	112	4	117	9
2	328	10	265	14	252	21
3	513	22	445	24	432	30
4	693	31	625	34	603	40
5	868	42	783	46	761	52
6	922	53				
	(Sudden formation of crack)					
			702	64	702	69
7	994	70	900	76	891	82
8	1210	103	1111	106	1098	111
9	1390	112	1300	115	1274	120
10	1602	120	1476	124	1449	130
11	1831	130	1692	139	1679	144
12	2074	145	1921	150	1904	155
13	2083	156	1944	159	1922	165

a	b	c	d	e	f	g
			Specimen 79-26			
1	157	0	157	5	117	11
2	328	12	292	15	270	20
3	499	21	463	25	441	31
4	679	32	616	34	608	40
5	742	40				
	(Sudden formation of crack)					
			275	52	275	58
6	301	58	265	62	257	68
7	315	68	283	73	275	79
8	382	79	342	86	338	92
9	454	110	427	113	410	118
10	540	124	499	128	482	135
11	571	136	508	142	500	147
			Specimen 77-00			
1	184	0	175	1	158	5
2	346	7	310	8	293	12
3	508	13	-	13	450	16
4	625	19	571	22	563	28
5	760	29	702	31	689	34
6	891	36				
	(Sudden formation of crack)					
			292	38	279	41
7	139	44	126	45		
			Specimen 77-00 (ii)			
1	171	0	153	2	144	5
2	328	6	274	7	266	10
3	468	11	396	14	383	17
4	598	20	549	25	545	29
5	697	30				
	(Sudden formation of crack)					
			567	32	563	35
6	697	37				
	(Sudden formation of crack)					
			166	38	162	42
			Specimen 79-00			
1	202	0	184	2	176	7
2	351	9	319	10	311	13
3	517	14	468	15	455	18
4	679	19	616	21	608	24

a	b	c	d	e	f	g
5	841	25	751	27	734	31
6	864	32				
	(Sudden formation of crack)					
			184	33	176	37

(1) These specimens had the displacement on the jack adjusted before reading the gauges so that the shear at the start of reading the gauges equalled the maximum dowel shear.

(2) Time in minutes from start of test.

APPENDIX B

BEAM TEST LOAD SEQUENCE TABLES

Table B.1 Load Sequence for Beam N1-SO*

1	2	3	4	5	6	7	8	9	10	11
Increment	Date of Test	When Load Applied		At Start of Gauge Readings		At End of Gauge Readings		P/P_u*	N/V	e' inches
		Load Kips	Time	Load Kips	Time	Load Kips	Time			
0	30/7/68	0	9.22 a.m.	0	9.27 a.m.	0	9.58 a.m.	0	0.98	38.30
1		6.02	10.03 "	5.92	10.13 "	5.88	10.38 "	0.088	0.985	38.30
2		12.00	10.41 "	11.92	11.12 "	11.88	11.35 "	0.179	0.985	38.31
3		18.07	11.38 "	17.91	1.29 p.m.	17.94	1.59 p.m.	0.270	0.986	38.32
4		0	2.06 p.m.	0	2.11 "	0	2.34 "	0	0.984	38.30
5	31/7/68	0	8.35 a.m.	0	8.40 a.m.	0	9.48 a.m.	0	0.984	38.30
6		6.02	9.53 "	6.02	9.57 "	5.93	10.26 "	0.089	0.985	38.31
7		12.00	10.28 "	11.92	10.48 "	11.87	11.17 "	0.179	0.986	38.31
8		18.09	11.18 "	18.08	11.25 "	18.00	11.57 "	0.271	0.986	38.32
9		24.11	12.01 p.m.	23.98	1.28 p.m.	23.95	2.05 p.m.	0.360	0.987	38.33
Fail.		30.05	2.07 "						0.987	38.33

* Constant load type loading was used throughout this test.

(3) Load attained on jack = $N^2 + V^2$.

(5) Load on jack before any of the dial or demec gauges on the beam were read.

(7) Load on jack after all dial and demec gauges were read.

(9) Ratio of load on jack from column 7 to load on jack required for beam to reach ultimate flexural capacity by traditional ultimate theory.

(10) Axial tension to shear force ratio.

(11) Eccentricity from centroid of tension reinforcement at critical flexural section.

Table B .2 Load Sequence for Beam N2-SO*

+1	2	3	4	5	6	7	8	9	10	11
Increment	Date of Test	When Load Applied		At Start of Gauge Readings		At End of Gauge Readings		P / P_u^*	N / V	e' inches
		Load Kips	Time	Load Kips	Time	Load Kips	Time			
0	1/7/68	0	9.27 a.m.	0	9.28 a.m.	0	10.25 a.m.	0	2.08	18.33
1		7.50	11.00 "	7.50	11.29 "	7.50	11.46 "	0.087	2.094	18.33
2		15.00	11.50	15.00	12.10 p.m.	14.86	12.26 p.m.	0.173	2.091	18.34
3		22.50	1.40 p.m.	22.45	1.45 "	22.30	2.03 "	0.260	2.089	18.36
4		30.05	2.07 "	30.05	2.43 "	29.85	2.58 "	0.348	2.089	18.37
5		0	3.21 "	0	3.32 "	0	3.48 "	0	2.095	18.33
6	2/7/68	0.07	8.48 a.m.	0.07	8.48 a.m.	0.04	9.41 a.m.	0	2.095	18.33
7		7.52	9.45 "	7.52	9.56 "	7.46	10.19 "	0.087	2.094	18.34
8		15.53	10.22 "	15.52	10.55 "	15.44	11.20 "	0.180	2.091	18.35
9		22.50	11.23 "	22.50	11.32 "	22.40	11.56 "	0.261	2.090	18.36
10		30.05	11.59 "	30.00	12.07 p.m.	29.95	12.28 p.m.	0.349	2.089	18.37
11		35.05	12.33 p.m.	35.00	1.46 "	34.95	2.12 "	0.406	2.089	18.38
12		40.05	2.16 "	40.05	2.40 "	40.05	3.06 "	0.466	2.089	18.38
13		44.00	3.10 "	44.15	3.34 "	44.10	4.03 "	0.514	2.088	18.39
14		48.00	4.05 "	48.05	4.31 "	48.10	4.55 "	0.560	2.088	18.39
15	3/7/68	52.00	8.45 a.m.	52.00	9.05 a.m.	51.90	9.36 a.m.	0.604	2.088	18.40
16		56.00	9.39 "	55.90	9.57 "	55.85	10.22 "	0.650	2.088	18.40
17		59.80	10.27 "	60.05	11.10 "	60.00	11.38 "	0.699	2.083	18.41
18		63.70	11.44 "	63.90	11.57 "	63.90	12.22 p.m.	0.744	2.080	18.42
19		67.75	12.28 p.m.	67.80	1.43 p.m.	67.75	2.11 "	0.789	2.077	18.43
20		71.45	2.15 "	71.60	2.30 "	71.55	2.55 "	0.831	2.076	18.44
21		75.35	2.57 "	75.55	3.28 "	75.50	3.58 "	0.877	2.074	18.45
22		79.10	4.02 "	77.00	4.23 "	75.55	4.51 "	0.875	2.058	18.46
Fail.		78.45	4.54 "						2.058	18.46

* Constant load type loading except increment 22.

\+ For notes on cols. 1-11 see table B .1.

Table B.3 Load Sequence for Beam N3-SO*

+1	2	3	4	5	6	7	8	9	10	11
Increment	Date of Test	When Load Applied		At Start of Gauge Readings		At End of Gauge Readings		P / P_u^*	N / V	e' inches
		Load Kips	Time	Load Kips	Time	Load Kips	Time			
0	13/5/68	0	10.51 a.m.	0	10.51 a.m.	0	12.07 p.m.	0	3.16	14.31
1		5.00	12.19 p.m.	5.00	12.23 p.m.	4.72	12.45 "	0.051	3.16	14.33
2		10.00	1.47 "	9.84	1.53 "	9.82	2.13 "	0.107	3.16	14.34
3		15.00	2.37 "	14.90	2.45 "	14.86	3.04 "	0.161	3.18	14.34
4		20.05	3.07 "	19.95	3.39 "	19.90	3.51 "	0.216	3.17	14.34
5		25.10	4.00 "	25.00	4.11 "	25.00	4.30 "	0.272	3.18	14.34
6	14/5/68	0	1.38 "	0	1.38 "	3.40	2.41 "	0.037	3.13	14.34
7		25.05	2.50 "	24.80	3.15 "	24.65	3.44 "	0.268	3.18	14.34
8		29.10	3.46 "	29.05	4.05 "	28.95	4.38 "	0.314	3.18	14.34
9		33.10	8.42 "	33.10	9.15 a.m.	33.00	9.43 a.m.	0.358	3.18	14.34
10		36.00	9.45 "	36.05	10.05 "	35.80	10.32 "	0.388	3.18	14.34
11		39.05	10.36 "	39.05	11.03 "	38.85	11.31 "	0.422	3.18	14.35
12		42.00	11.33 "	41.90	11.57 "	41.95	12.23 p.m.	0.456	3.19	14.35
13	15/5/68	46.00	1.06 p.m.	46.00	1.36 p.m.	45.70	2.03 "	0.497	3.19	14.35
14		50.00	2.06 "	50.00	2.29 "	49.85	2.59 "	0.542	3.19	14.35
15		53.95	3.00 "	53.95	3.32 "	53.70	4.03 "	0.584	3.19	14.35
16		57.95	4.06 "	57.85	4.24 "	57.75	4.47 "	0.628	3.19	14.35
17		61.80	8.37 a.m.	61.85	9.06 a.m.	61.55	9.34 a.m.	0.669	3.19	14.35
18		65.70	9.38 "	65.70	10.10 "	65.75	10.32 "	0.715	3.19	14.36
19		69.55	10.34 "	69.50	11.01 "	69.40	11.23 "	0.754	3.18	14.36
20	16/5/68	73.40	11.25 "	73.35	11.54 "	73.30	12.20 p.m.	0.796	3.20	14.36
21		77.25	1.17 p.m.	77.35	1.40 p.m.	77.25	2.09 "	0.840	3.19	14.36
22		81.05	2.13 "	81.05	2.22 "	80.40	2.46 "	0.874	3.19	14.37
23		84.85	3.00 "	84.85	3.29 "	84.80	3.55 "	0.920	3.19	14.37
24		88.70	3.59 "	88.85	4.07 "	88.80	4.34 "	0.965	3.20	14.37
25	17/5/68	92.45	8.55 a.m.	92.20	9.10 a.m.	91.90	9.38 a.m.	0.999	3.19	14.38
Fail.		100.10	9.58 "						3.19	14.38

* Constant load type loading was used throughout.

\+ For notes on cols. 1-11, see table B.1.

Table B. 4 Load Sequence for Beam N1-S62

+1	2	3	4	5	6	7	8	9	10	11	12
Increment	Date of Test	When Load Applied		Time in mins. constant load.	At Start of Gauge Readings		At End of Gauge Readings		P / P_u^*	N / V	e' inches
		Load Kips	Time		Load Kips	Time	Load Kips	Time			
0	1/10/68	0	9.30 a.m.	-	0	9.30 a.m.	0	10.34 a.m.	0	0.98	38.37
1		6.01	11.10 "	5.00	5.14	11.36 "	4.04	11.53 "	0.059	0.984	38.37
2		12.00	12.01 p.m.	"	11.48	1.34 p.m.	11.41	1.53 p.m.	0.166	0.985	38.38
3		18.06	1.56 "	5.45	17.56	2.34 "	17.37	2.54 "	0.253	0.985	38.39
4		0	2.58 "	-	0	3.22 "	0	3.41 "	0	0.983	38.37
5	2/10/68	0	8.44 a.m.	-	0	8.47 a.m.	0	9.34 a.m.	0	0.983	38.37
6		6.00	9.34 "	5.00	5.88	9.44 "	5.78	10.10 "	0.084	0.984	38.38
7		12.00	10.14 "	"	11.79	10.37 "	11.68	11.00 "	0.170	0.985	38.38
8		18.06	11.02 "	"	17.93	11.12 "	17.66	11.37 "	0.258	0.986	38.39
9		24.05	11.39 "	"	23.55	12.04 p.m.	23.30	12.29 p.m.	0.340	0.986	38.40
10		30.10	12.34 p.m.	"	28.90	1.46 "	28.65	2.15 "	0.423	0.987	38.41
11		35.20	2.18 "	"	34.25	2.38 "	33.60	3.08 "	0.490	0.988	38.42
12		40.25	3.12 "	"	38.55	3.39 "	38.05	4.04 "	0.554	0.989	38.43
13		45.30	4.08 "	"	43.85	4.34 "	43.35	4.58 "	0.632	0.989	38.45
14	3/10/68	50.20	8.40 a.m.	"	48.80	9.08 a.m.	48.40	9.27 a.m.	0.706	0.990	38.46
15		54.90	9.40 "	1.00	48.45	9.55 "	48.10	10.13 "	0.701	0.987	38.48
Fail.		54.90	9.40 "							0.987	38.48

+ For notes on cols. 1-4 and 6-12, see table B.1

(5) Time that the load shown in column 3 was applied to the beam. After this time interval the valve to the hydraulic pump was closed and the load was of the constant displacement type.

Table B.5 Load Sequence for Beam N1-S32

+1	2	3	4	5	6	7	8	9	10	11	12
Increment	Date of Test	When Load Applied		Time in mins constant load	At Start of Gauge Readings		At End of Gauge Readings		P / P_u^*	N / V	e' inches
		Load Kips	Time		Load Kips	Time	Load Kips	Time			
0	19/3/69	0	8.30 a.m.	-	0	8.49 a.m.	0	9.46 a.m.	0	0.99	38.22
0i		1.10	9.53 "	2.00	1.09	9.57 "	1.08	10.03 "			
0ii		2.08	10.04 "	"	2.04	10.08 "	2.00	10.12 "			
0iii		2.99	10.13 "	"	2.96	10.16 "	2.91	10.20 "			
0iv		4.66	10.21 "	"	4.62	10.24 "	4.52	10.27 "			
0v		6.09	10.47 "	"	5.96	10.53 "	5.89	10.57 "			
0vi		8.14	10.58 "	"	8.02	11.02 "	7.94	11.05 "			
0vii		10.10	11.07 "	"	10.02	11.10 "	9.89	11.14 "			
1		12.14	11.16 "	5.00	11.65	11.43 "	11.45	12.05 p.m.	0.171	0.986	38.24
1i		18.08	12.08 p.m.	2.00	17.91	12.11 p.m.	17.68	12.15 "			
2		24.05	12.17 "	5.00	23.00	1.34 "	22.90	1.54 "	0.343	0.987	38.26
3		0	1.57 "	-	0	2.14 "	0	2.33 . "	0	0.986	38.22
4	20/3/69	0	8.30 a.m.	-	0	8.40 a.m.	0	9.29 a.m.	0	0.986	38.22
4i		6.06	9.32 "	2.00	6.00	9.35 "	5.90	9.38 "			
5		12.24	9.41 "	5.00	11.99	9.49 "	11.75	10.14 "	0.176	0.987	38.25
5i		18.10	10.17 "	2.00	17.95	10.21 "	17.86	10.28 "			
6		24.20	10.26 "	5.00	23.75	10.55 "	23.60	11.22 "	0.353	0.987	38.26
7		32.25	11.23 "	"	31.30	11.48 "	31.05	12.13 p.m.	0.465	0.988	38.27
8		40.35	12.15 p.m.	"	38.90	1.50 p.m.	38.65	2.19 "	0.579	0.988	38.29
9		46.25	2.20 "	"	45.20	2.43 "	44.75	3.08 "	0.671	0.989	38.30
10		52.25	3.09 "	"	50.20	3.43 "	49.35	4.10 "	0.740	0.989	38.33
11‡	21/3/69	58.15	8.47 a.m.	"	52.95	9.14 a.m.	49.25	9.41 a.m.	0.738	0.989	38.34
12		58.25	10.06 "	"	57.80	10.14 "	57.00	10.37 "	0.855	0.990	38.35
13		64.20	10.56 "	"	61.50	11.35 "	61.20	12.01 p.m.	0.919	0.991	38.37
14		68.10	12.03 p.m.	0.30	63.35	12.12 p.m.	62.65	12.34 "	0.950	1.014	38.37
15		69.40	2.28 "	0.05	60.25	2.35 "	59.45	2.52 "	0.906	1.024	38.37
16		64.50	2.55 "	0.00	52.70	3.23 "					
Fail.		69.40								1.024	38.37

\+ For notes on cols 1-12, see tables B.1 and B.4

‡ Load increment was not used as leak occurred in jack during constant displacement type of loading.

Table B.6 Load Sequence for Beam N1-S32

+1	2	3	4	5	6	7	8	9	10	11	12
Increment	Date of Test	When Load Applied		Time in mins. constant load	At Start of Gauge Readings		At End of Gauge Readings		P/P_u^*	N/V	e' inches
		Load Kips	Time		Load Kips	Time	Load Kips	Time			
0	21/1/69	0	8.30 a.m.	-	0	9.06 a.m.	0	9.47 a.m.	0	0.97	38.55
1		8.16	9.58 "	6.00	7.78	10.44 "	7.69	11.01 "	0.115	0.977	38.56
2		16.12	11.03 "	5.00	15.52	11.37 "	15.38	11.53 "	0.230	0.978	38.57
3		24.35	11.56 "	"	23.10	1.38 p.m.	22.90	2.00 p.m.	0.341	0.979	38.58
4		0	2.03 p.m.	-	0	2.10 "	0	2.26 "	0	0.976	38.55
5	22/1/69	0	8.16 a.m.	-	0	8.33 a.m.	0	9.20 a.m.	0	0.976	38.55
6		8.60	9.22 "	5.00	8.50	9.33 "	8.36	9.57 "	0.125	0.978	38.56
7		16.79	10.00 "	"	16.69	10.10 "	16.49	10.31 "	0.246	0.978	38.58
8		25.50	10.35 "	"	25.00	11.05 "	24.80	11.28 "	0.370	0.979	38.58
9		34.00	11.30 "	"	33.25	11.56 "	33.00	12.17 p.m.	0.493	0.980	38.60
10		42.90	12.20 p.m.	"	41.40	1.41 p.m.	41.20	2.05 "	0.616	0.981	38.63
11		50.90	2.16 "	"	49.90	2.40 "	49.45	3.04 "	0.740	0.982	38.66
12		58.45	4.16 "	"	57.75	4.34 "	57.30	4.58 "	0.858	0.983	38.68
13	23/1/69	64.55	8.44 a.m.	"	62.50	9.02 a.m.	61.90	9.32 a.m.	0.926	0.985	38.70
14		71.00	9.36 "	1.00	65.55	9.53 "	65.00	10.17 "	0.989	1.015	38.67
Fail.		73.6								1.015	38.67

+ For notes on cols. 1-12, see table B.1 and B.4.

Table B.7 Load Sequence for Beam N2-S62*

1	2	3	4	5	6	7	8	9	10	11
Increment	Date of Test	When Load Applied		At Start of Gauge Readings		At End of Gauge Readings		P / P_u*	N / V	e' inches
		Load Kips	Time	Load Kips	Time	Load Kips	Time			
0	26/8/68	0	10.00 a.m.	0	10.00 a.m.	0	11.45 a.m.	0	2.10	18.36
1		7.48	12.14 p.m.	7.42	1.41 p.m.	7.40	2.05 p.m.	0.086	2.110	18.42
2		14.96	2.08 "	14.96	2.31 "	14.94	2.55 "	0.174	2.109	18.43
3		22.60	3.06 "	22.60	3.26 "	22.60	3.49 "	0.264	2.109	18.44
4		29.95	3.51 "	29.90	4.04 "	29.85	4.27 "	0.348	2.109	18.44
5		0	4.32 "	0	4.34 "	0	4.54 "	0	2.114	18.36
6	27/8/68	0	8.40 a.m.	0	8.48 a.m.	0	9.32 a.m.	0	2.114	18.36
7		7.49	9.35 "	7.46	9.43 "	7.40	10.12 "	0.086	2.110	18.42
8		14.94	10.15 "	15.02	10.49 "	14.96	11.14 "	0.175	2.110	18.43
9		22.60	11.17 "	22.50	11.28 "	22.40	11.55 "	0.262	2.110	18.44
10		30.00	11.57 "	29.95	12.05 p.m.	29.85	12.33 p.m.	0.348	2.109	18.45
11		37.50	12.37 p.m.	37.45	1.59 "	37.45	2.28 "	0.438	2.109	18.45
12		44.95	2.31 "	44.90	3.20 "	44.90	3.48 "	0.525	2.110	18.46
13		52.45	3.51 "	52.50	4.06 "	52.45	4.37 "	0.612	2.111	18.46
14	28/8/68	59.90	8.26 a.m.	59.90	8.52 a.m.	59.70	9.21 a.m.	0.696	2.110	18.47
15		67.50	9.25 "	67.60	9.50 "	67.55	10.17 "	0.788	2.105	18.51
16		74.40	10.50 "	74.70	11.21 "	74.65	11.41 "	0.870	2.102	18.53
17		81.45	11.48 "	81.70	12.01 p.m.	81.70	12.30 p.m.	0.953	2.100	18.55
18		85.80	1.40 p.m.	80.30	2.03 "	79.50	2.36 "	0.936	2.219	18.53
Fail.		87.50							2.219	18.53

* Constant load type loading except increment 18

\+ For notes on cols 1-11, see table B.1

Table B.8 Load Sequence for Beam N2-S32

+1	2	3	4	5	6	7	8	9	10	11	12
Increment	Date of Test	When Load Applied		Time in mins. constant load	At Start of Gauge Readings		At End of Gauge Readings		P / P_u^*	N / V	e' inches
		Load Kips	Time		Load Kips	Time	Load Kips	Time			
0	18/2/69	0	8.38 a.m.	-	0	9.11 a.m.	0	10.19 a.m.	0	2.16	18.20
0i		1.00	10.51 "	0.00	0.91	11.03 "	0.90	11.06 "			
0ii		2.07	11.08 "	1.00	2.04	11.11 "	1.99	11.14 "			
0iii		3.09	11.15 "	"	3.06	11.17 "	3.01	11.20 "			
0iv		4.06	11.21 "	"	3.98	11.24 "	3.95	11.27 "			
0v		5.05	11.28 "	"	4.95	11.32 "	4.90	11.35 "			
0vi		7.02	11.36 "	"	6.96	11.38 "	6.86	11.41 "			
0vii		9.03	11.42 "	"	8.95	11.44 "	8.84	11.47 "			
0viii		12.14	11.48 "	"	12.04	11.50 "	11.90	11.52 "			
0ix		15.06	11.54 "	"	14.92	11.57 "	14.74	12.01 p.m.			
1		18.10	12.03 p.m.	5.00	17.01	1.54 p.m.	16.75	2.19 "	0.201	2.159	18.23
1i		27.10	2.23 "	"	26.90	2.33 "	26.80	2.37 "			
2		36.40	2.40 "	5.00	35.40	3.33 "	35.20	3.51 "	0.423	2.156	18.25
3		0	3.55 "	-	0	4.08 "	0	4.24 "	0	2.166	18.21
4	19/2/69	0	8.34 a.m.	-	0	8.36 a.m.	0	9.18 a.m.	0	2.166	18.20
4i		9.05	9.24 "	5.00	8.96	9.34 "	8.91	9.39 "			
5		18.20	9.41 "	"	18.11	9.51 "	17.89	10.17 "	0.215	2.160	18.24
5i		27.20	10.19 "	"	27.15	10.26 "	27.10	10.29 "			
6		36.35	10.52 "	"	36.15	11.04 "	35.85	11.32 "	0.430	2.156	18.26
7		45.45	11.36 "	"	44.90	11.57 "	44.60	12.21 p.m.	0.536	2.155	18.27
8		54.35	12.23 p.m.	"	52.95	1.52 p.m.	52.75	2.23 "	0.634	2.153	18.28
9		62.25	2.27 "	"	61.85	2.38 "	61.25	3.03 "	0.736	2.152	18.29
10		69.70	3.17 "	"	68.60	3.45 "	68.20	4.07 "	0.819	2.151	18.30
11		77.55	4.10 "	"	76.25	4.34 "	75.65	4.58 "	0.909	2.149	18.32
12	20/2/69	83.50	8.44 a.m.	"	81.05	9.02 a.m.	80.15	9.28 a.m.	0.962	2.149	18.33
13		87.70	9.32 "	"	83.90	9.52 "	83.05	10.20 "	1.002	2.212	18.35
14		92.70	11.37 "	1.00	88.70	11.45 "	87.70	12.01 p.m.	1.061	2.243	18.37
15		95.65	12.09 p.m.	"	92.05	12.14 p.m.	90.95	12.27 "	1.102	2.278	18.38
16		99.45	1.47 "	"	94.20	1.57 "	93.55	2.05 "	1.136	2.308	18.40
17		101.20	2.15 "	0.00	95.65	2.18 "	94.70	2.22 "			18.42
18		99.45	2.52 "	"	92.0*	2.56 "	91.5*	-			
19		96.35	3.06 "	"	85.00	3.11 "	84.50	3.16 p.m.			
Fail.		101.20								2.32	18.42

+ For notes on cols 1-12, see tables B.1 and B.4

* Estimated.

Table B.9 Load Sequence for Beam N2-S63

+1	2	3	4	5	6	7	8	9	10	11	12
Increment	Date of Test	When Load Applied		Time in mins. constant load	At Start of Gauge Readings		At End of Gauge Readings		P / P_u^*	N / V	e' inches
		Load Kips	Time		Load Kips	Time	Load Kips	Time			
0		0	9.00 a.m.	-	0	9.02 a.m.	0	10.08 a.m.	0	2.06	18.42
1	6/11/68	10.02	10.23 "	5.00	9.36	11.38 "	9.28	12.03 p.m.	0.108	2.080	18.42
2		20.00	12.05 p.m.	"	19.00	1.36 p.m.	18.85	2.00 "	0.220	2.078	18.44
3		30.15	2.03 "	"	29.50	2.33 "	29.25	2.53 "	0.341	2.077	18.45
4		0	2.57 "	-	0	3.33 "	0	3.54 "	0	2.077	18.41
5	7/11/68	0.15	8.37 a.m.	-	0.16	8.45 a.m.	0.22	9.30 a.m.	0	2.077	18.41
6		10.03	9.42 "	5.00	9.89	9.53 "	9.72	10.21 "	0.114	2.080	18.43
7		20.20	10.23 "	"	19.85	10.50 "	19.70	11.22 "	0.230	2.078	18.44
8		30.10	11.24 "	"	29.85	11.39 "	29.60	12.04 p.m.	0.346	2.077	18.45
9		40.25	12.07 p.m.	"	39.00	1.37 p.m.	38.80	2.08 "	0.453	2.076	18.46
10		50.20	2.10 "	"	49.50	2.35 "	49.10	3.00 "	0.573	2.074	18.47
11		60.25	3.03 "	"	59.30	3.29 "	58.90	3.54 "	0.688	2.072	18.49
12		69.70	3.57 "	"	68.75	4.16 "	68.20	4.42 "	0.795	2.070	18.51
13	8/11/68	79.80	8.43 a.m.	"	78.70	9.03 a.m.	78.10	9.33 a.m.	0.910	2.068	18.54
14		85.75	9.36 "	"	80.95	10.02 "	80.50	10.31 "	0.945	2.133	18.55
15		89.75	10.55 "	"	86.40	11.10 "	85.50	11.39 "	1.004	2.151	18.58
Fail.		93.25									

+ For notes on cols. 1-12, see tables B.1 and B.4

Table B.10 Load Sequence for Beam N3-S12,4

+1	2	3	4	5	6	7	8	9	10	11	12
Increment	Date of Test	When Load Applied		Time in mins. constant load	At Start of Gauge Readings		At End of Gauge Readings		P / P_u^*	N / V	e' inches
		Load Kips	Time		Load Kips	Time	Load Kips	Time			
0	15/4/69	0	8.43 a.m.	-	0	8.57 a.m.	0	9.50 a.m.	0	3.29	14.02
Oi		1.51	9.52 "	1.00	1.49	9.56 "	1.42	10.00 "			
Oii		3.11	10.02 "	2.00	3.07	10.05 "	2.98	10.08 "			
Oiii		4.55	10.09 "	"	4.47	10.12 "	4.38	10.15 "			
Oiv		6.07	10.16 "	"	6.03	10.19 "	5.90	10.22 "			
Ov		8.09	10.23 "	"	8.05	10.26 "	7.93	10.29 "			
Ovi		11.17	10.52 "	"	11.11	10.55 "	10.99	10.58 "			
Ovii		14.12	10.58 "	"	14.04	11.02 "	13.93	11.04 "			
Oviii		17.08	11.06 "	"	17.01	11.08 "	16.89	11.12 "			
1		20.13	11.13 "	5.00	19.69	11.41 "	19.55	11.59 "	0.216	3.278	14.05
1i		30.20	12.02 p.m.	2.00	30.10	12.05 p.m.	29.85	12.10 p.m.			
2		40.20	1.32 "	5.00	39.75	2.00 "	39.65	2.17 "	0.437	3.272	14.07
3		0	2.22 "	-	0	2.31 "	0	2.49 "	0	3.292	14.03
4	16/4/69	0	8.30 a.m.	-	0	8.38 a.m.	0	9.24 a.m.	0	3.293	14.02
4i		6.12	9.27 "	2.10	6.05	9.30 "	5.97	9.34 "			
4ii		12.11	9.36 "	2.00	12.02	9.40 "	11.95	9.43 "			
5		20.12	9.45 "	5.00	20.03	9.52 "	19.90	10.12 "	0.220	3.278	14.06
5i		30.00	10.15 "	2.00	29.85	10.19 "	29.70	10.23 "			
6		40.30	10.34 "	5.00	40.00	10.59 "	39.95	11.20 "	0.440	3.272	14.07
7		54.40	11.22 "	"	53.90	11.53 "	53.80	12.13 p.m.	0.593	3.269	14.08
8		64.52	12.15 p.m.	"	63.55	2.10 p.m.	63.50	2.31 "	0.700	3.268	14.09
9		74.27	2.33 "	"	73.20	3.21 "	73.05	3.46 "	0.805	3.267	14.10
10		82.15	3.49 "	"	81.10	4.18 "	80.80	4.40 "	0.890	3.265	14.11
11	17/4/69	89.70	8.47 a.m.	"	86.10	9.28 a.m.	85.85	9.52 a.m.	0.947	3.266	14.12
12		96.00	9.56 "	1.00	90.70	10.14 "	90.30	10.37 "	0.999	3.375	14.10
13		104.40	11.43 "	"	99.50	11.50 "	98.20	12.14 p.m.	1.087		
14		110.20	12.22 p.m.	0.03	104.55	12.25 p.m.	104.10	12.27 "			
15		117.85	1.48 "	0.00	100.10	1.53 "	98.30	2.04 "			
Fail.		117.85								3.375	14.10

+ For notes on cols. 1-12, see tables B.1 and B.4

APPENDIC C

ELASTIC AND ULTIMATE FLEXURAL ANALYSIS OF BEAMS SUBJECTED TO ECCENTRIC AXIAL TENSION

C.1 Analysis of a Cracked Elastic Section

Fig. C.1 shows a doubly reinforced concrete section subjected to an eccentric axial force. The concrete at the section is assumed to carry no flexural tensile forces, i.e., it is cracked to the height of the neutral axis. Resolving forces in part (c) of the figure

$$N = T - C' - C'' \tag{C.1}$$

Taking moments about the tension reinforcement

$$Ne' = C'jd + C''(d - d') \tag{C.2}$$

The forces C', C'' and T are given by

$$C' = \tfrac{1}{2}\varepsilon_c E_c bkd \tag{C.3}$$

$$C'' = E_c \varepsilon'_s A'_s (n' - 1) \tag{C.4}$$

$$T = \varepsilon_s E_s A_s \tag{C.5}$$

From part (b) of the figure

$$\varepsilon_c = \frac{\varepsilon_s k}{1 - k}$$

$$\varepsilon'_s = \frac{\varepsilon_s (kd - d')}{(1 - k)d}$$

Putting the forces in terms of ε_s, substituting

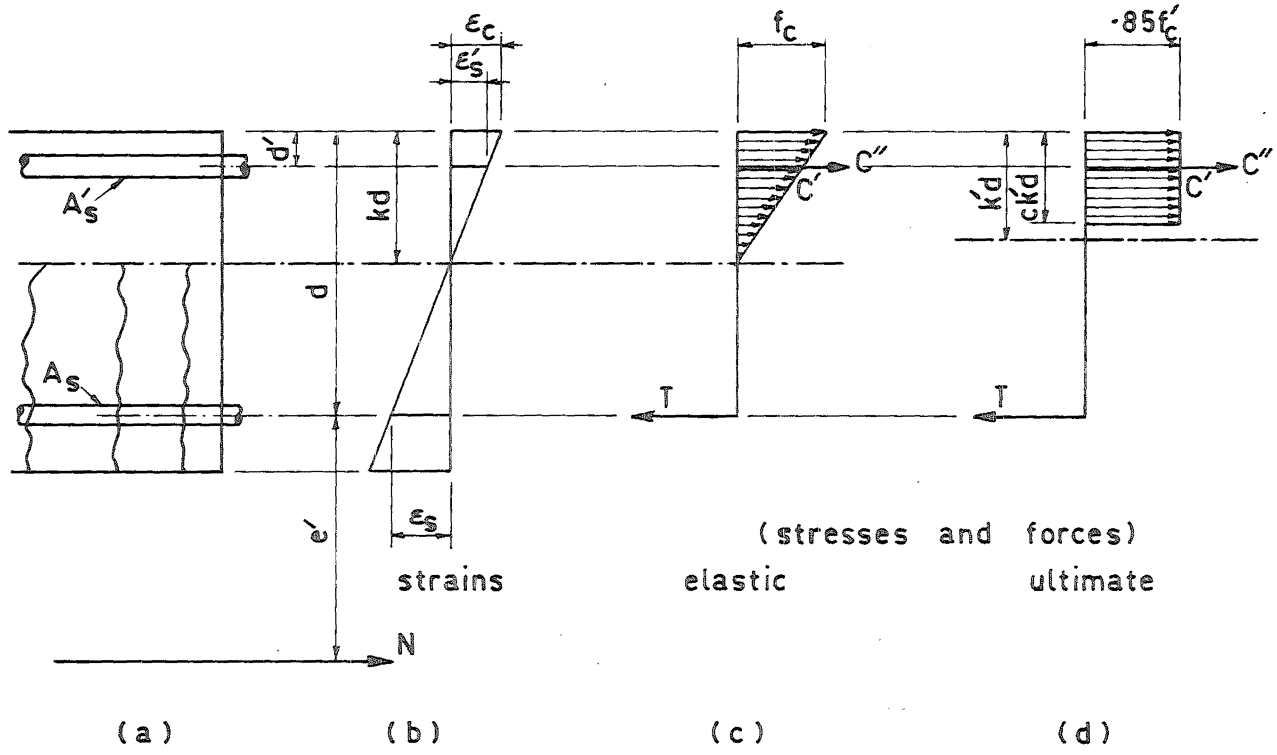

Fig. C.1 Conventional Analysis of a Section Subjected to Flexure and Axial Tension

in Eqs. (C.1) and (C.2), and eliminating N gives the following:

$$\frac{1}{6}k^3bd^3 - \frac{1}{2}k^2bd^3 + e'\left((1-k)nA_sd - \frac{1}{2}k^2bd^2\right) - A_s'(n'-1)(kd-d')(d-d'+e') = 0 \qquad (C.6)$$

Solution of Eq. (C.6) gives k from which C', C" and T can be found in terms of ε_s from Eqs. (C.3), (C.4) and (C.5). Substituting for these in Eq. (C.1) gives ε_s for any chosen value of axial tension.

$$\varepsilon_s = \frac{N}{E_c}\left(\frac{1}{nA_s - \frac{bdk^2}{2(1-k)} - \frac{A_s'(n'-1)(kd-d')}{(1-k)d}}\right) \qquad (C.7)$$

C.2 Ultimate Flexural Strength

Whitneys[49] equivalent stress block is used to approximate the concrete compression force. Strain hardening of the reinforcement is ignored.

Consider fig. C.1 parts (b) and (d). The tension reinforcement is assumed to have yielded, i.e., the section is under-reinforced. The forces are given by

$$T = A_sf_y \qquad (C.8)$$

$$C' = .85f_c'ck'db \qquad (C.9)$$

$$C'' = A_s'(\varepsilon_s'E_s' - .85f_c') \qquad (C.10)$$

where $\varepsilon_s'E_s' \leqslant f_y'$

c is defined in the ACI Code[5] section 1503.

$$\varepsilon'_s = \varepsilon_{cu} \frac{(k'd - d')}{k'd}$$

where ε_{cu} = the ultimate concrete strain.

From Eq. (C.10)

$$C'' = A'_s\left(\varepsilon_{cu} \frac{(k'd - d')}{k'd} E'_s - .85f'_c\right) \qquad (C.11)$$

At ultimate load Eq. (C.1) remains unchanged but Eq. (C.2) becomes

$$N = \frac{1}{e'}\left(C'(d - \frac{ck'd}{2}) + C''(d - d')\right) \qquad (C.12)$$

The method of solution involves the following steps.

Step 1 : find T from Eq. (C.8)

Step 2 : choose a value of k'

Step 3 : find C' and C" from Eqs. (C.9) and (C.11)

Step 4 : find N from both Eqs. (C.1) and (C.12)

Step 5 : compare the values of N obtained in Step 4.

(i) If both are equal they are the values of the ultimate eccentric axial tension.

(ii) If N from Eq. (C.1) is greater than from Eq. (C.12), k' is increased and the solution restarts at step 3.

(iii) If N from Eq. (C.1) is smaller than from Eq. (C.12), k' is decreased and the solution restarts at step 3.

An alternate method of solution involves a direct method of kinding k'. It is given in terms of the section properties by a cubic equation. A trial and

error method is required to solve the equation.

A typical interaction curve for a beam subjected to varying intensity of axial tension is shown in fig. C.2. It can be seen that the interaction is almost linear and can, therefore, be approximated to linear for the purposes of design.

THE LIBRARY
UNIVERSITY OF CANTERBURY

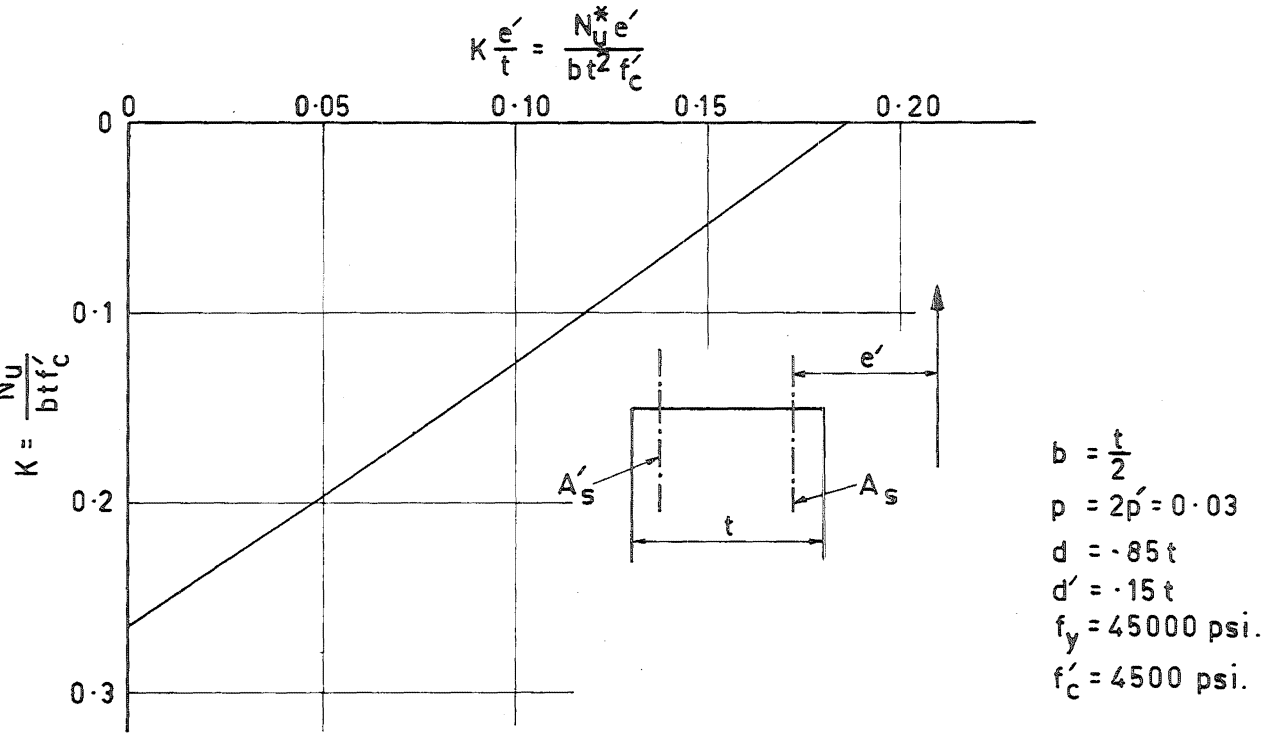

Fig. C.2 Typical Interaction Curve for Flexure and Axial Tension